NOTICE

The quality of this microform is heavily dependent upon the quality of the original thesis submitted for microfilming. Every effort has been made to ensure the highest quality of reproduction possible.

If pages are missing, contact the university which granted the degree.

Some pages may have indistinct print especially if the original pages were typed with a poor typewriter ribbon or if the university sent us an inferior photocopy.

Previously copyrighted materials (journal articles, published tests, etc.) are not filmed.

Reproduction in full or in part of this microform is governed by the Canadian Copyright Act, R.S.C. 1970, c. C-30.

AVIS

La qualité de cette microforme dépend grandement de la qualité de la thèse soumise au microfilmage. Nous avons tout fait pour assurer une qualité supérieure de reproduction.

S'il manque des pages, veuillez communiquer avec l'université qui a conféré le grade.

La qualité d'impression de certaines pages peut laisser à désirer, surtout si les pages originales ont été dactylographiées à l'aide d'un ruban usé ou si l'université nous a fait parvenir une photocopie de qualité inférieure.

Les documents qui font déjà l'objet d'un droit d'auteur (articles de revue, tests publiés, etc.) ne sont pas microfilmés.

La reproduction, même partielle, de cette microforme est soumise à la Loi canadienne sur le droit d'auteur, SRC 1970, c. C-30.

Canada

EXPERIMENTS ON THE STRUCTURE OF TURBULENCE AND THE DIFFUSION OF HEAT FROM A LINE SOURCE IN UNIFORMLY SHEARED FLOWS

by

UMESH KARNIK

A thesis
presented to the University of Ottawa
on 12th May, 1988
in partial fulfillment of the
requirement for the degree of
DOCTOR of PHILOSOPHY
in
MECHANICAL ENGINEERING

ISBN 0-315-46785-1

UNIVERSITÉ D'OTTAWA
UNIVERSITY OF OTTAWA

PREVIEW

The development of turbulence structure under the influence of a uniform shear, the reduction of the mean shear with the use of uniform screens and grids and the dispersion of scalar contaminants (heat in this case) in uniformly sheared flows are the three problems examined in this thesis.

Part A presents a study of (a) the evolution of turbulent stresses and scales in a uniformly sheared flow and (b) the generation and manipulation of shear with the use of screens. A detailed documentation of the study of diffusion from a continuous line source in a uniformly sheared flow is presented in Part B.

AKNOWLEDGEMENTS

I express gratitude to Professor Stavros Tavoularis for his motivating guidance; for providing constant encouragement and a comfortable and friendly working atmosphere; and for always being available for discussions. His careful editing and numerous comments have helped immensely in the compilation of this dissertation.

Thanks are due to Don Seaman, our administrative officer, for his unwavering support and to the machine shop for providing assistance when needed. I would also like to thank my colleague Gordon Holloway for his *"turbulent"* discussions.

The financial support provided by N.S.E.R.C. is greatly appreciated.

Finally, I am indebted to my wife, Padmaja, for her support especially during the *"diffusive"* and *"dissipative"* periods.

TABLE OF CONTENTS

PART A

PART B

ABSTRACT

Part A

(a) Measurements of the reduction of mean shear in a flow crossing transverse grids and gauzes with uniform solidities are reported. For small flow disturbances i.e. small relative screen element thickness, d/h, the shear reduction factor, A, was found comparable to predictions, A_p. However, for $d/h > 0.01$, the ratio A/A_p decreased rapidly with increasing d/h. Results on the effect of screen insertion on the upstream shear and the combined effects of multiple screens are briefly discussed.

(b)Measurements of the Reynolds stresses, integral length scales and Taylor microscales are reported for several cases of uniformly sheared turbulent flows with shear values in a range substantially wider than those of previous measurements. It is shown that such flows demonstrate a self-preserving structure, in which the dimensionless Reynolds stress ratios and the dissipation over production ratio remain essentially constant. Flows with sufficiently large $k_s = (1/\overline{U_c})d\overline{U_1}/dx_2$ have exponentially growing stresses and $\epsilon/P \approx 0.68$; a linear relationship between the coefficient in the exponential law and k_s is shown to be compatible with measurements. The possibility of a self-preserving structure with asymptotically constant stresses and $\epsilon/P \approx 1.0$ is also compatible with measurements, corresponding to

flows with small values of k_s. The integral length scales appear to grow according to a power law with an exponent of about 0.8, independent of the mean shear, while the Taylor microscales, in general, approach constant values. Various attempts to scale the stresses and to predict their evolution are discussed and the applicability of Hasen's theory is scrutinized.

Part B

The diffusion of a passive scalar (heat) from a continuous line source placed in a uniformly sheared, nearly homogeneous, turbulent shear flow is examined. Measurements near the source indicate that the mean temperature profile is nearly Gaussian and not very different from that observed in isotropic turbulence. However, further downstream, the mean shear has a marked effect on the diffusion process, causing the mean temperature profile to become asymmetric and to shift towards the region of lower velocity. The r.m.s. temperature fluctuation profile is double peaked close to the source, single peaked at intermediate distances and demonstrates a re-appearence of double peaks which grow in relative magnitude far away from the source. Double peaking is explained by focussing attention on the local mean temperature gradient and the local scale of turbulence. In comparison to similar experiments in isotropic turbulence, the centerline mean temperature appears to have a comparable decay rate, whereas the centerline mean square temperature fluctuation appears to decay at a faster rate . The spread of the plume far away from the source is faster than that in isotropic turbulence.

The measured turbulent heat fluxes and triple temperature-velocity correlations demonstrate self preserving features. The development of temperature integral length scales and microscales is comparable to that in other heated, uniformly sheared flows, while the temperature probability density function (pdf) and the temperature-velocity joint pdf are distinctly non-Gaussian, especially away from the centerline. The relative magnitudes of the two measured components of the turbulent diffusivity tensor are in agreement with earlier measurements.

Lagrangian scales in a uniformly sheared flow are estimated from dispersion measurements behind a line source using techniques similar to those adopted in grid- generated turbulence. In conformity with earlier projections, the Lagrangian scales are larger than their Eulerian counterparts measured in a convected frame.

NOMENCLATURE

Part A

A	measured shear reduction factor
A_p	predicted shear reduction factor
$A_{p\infty}$	predicted shear reduction factor at large Reynolds numbers
A_{prod}	product of individual grid reduction factors
d	rod diameter; screen element thickness
h	height of test section
k	exponent in kinetic energy growth law
k_L	exponent in length scale exponential growth law
k_s	wind tunnel shear constant
K	pressure loss coefficient
K_∞	pressure loss coefficient at large Reynolds numbers
K_{ij}	dimensionless Reynolds stress tensor
l_H	characteristic length of the disturbances
L_{11}	streamwise velocity integral length scale
L_r	reference value of length scale

l_p	length of sensor
M	screen spacing; mesh size
n_L	power in length scale power growth law
P	kinetic energy production
P_{ij}	production tensor
ΔP	pressure drop across screen
$\frac{1}{2}\overline{q^2}$	mean turbulent kinetic energy
$\frac{1}{2}\overline{q_r^2}$	reference turbulent kinetic energy
R_H	Reynolds number based on U_H and l_H
R	Reynolds number based on screen element thickness
T_{ij}	mean transport tensor
$\overline{u_i u_j}$	Reynolds stress tensor
U_1	far upstream mean velocity
U_1^*	far downstream mean velocity
$\overline{U_{1c}}$	centerline mean velocity
U_H	Hasen's barrier velocity
x_i	co-ordinate axes; i=1,2,3
x_r	reference position for turbulent kinetic energy
x_{rL}	reference position for length scale

Greek Symbols

α	deflection coefficient
β	shear parameter
ϵ	turbulent dissipation
ϵ_{ij}	turbulent dissipation tensor
η_K	Kolmogoroff length scale
λ_{11}	streamwise Taylor microscale
ν	kinematic viscosity of fluid
ρ	fluid density
σ	screen solidity
τ	dimensionless time or total strain
τ_e	turnover time of a typical turbulent eddy
τ_g	total strain measured upto position of last grid
τ_K	Kolmogoroff time microscale
τ_s	characteristic straining time of the flow
τ_T	characteristic time for transport of $\overline{q^2}$
τ_u	lifetime of the energy containing eddies
ϕ_{ij}	pressure-strain rate tensor

Part B

d	diameter of line source
D_{ij}	turbulent diffusivity tensor
g	gravitational acceleration
h	height of test section
k_u	exponent in temporal growth law for Reynolds stresses
$L_{ij,k}$	velocity integral length scale
$L_{\theta\theta,k}$	temperature integral length scale
M	height of individual channel in shear generator
n	power in the mean temperature decrease law
n_θ	power in temperature fluctuation decrease law
R_f	flux Richardson number
R_L	Lagrangian autocorrelation function
S	half-width of the mean temperature profile
S_θ	skewness factor for temperature
S_{u_i}	skewness factor for velocity
T_E	Eulerian integral time scale
T_L	Lagrangian integral time scale
t	diffusion time
t_s	local time scale
$\Delta\overline{T}$	mean temperature rise

$\Delta\overline{T_c}$	mean temperature rise on centerline
$\Delta\overline{T_p}$	peak mean temperature rise
$\overline{U}_{1c}$	centerline mean velocity
u_i'	Eulerian r.m.s. turbulent velocities
v_i'	Lagrangian r.m.s. turbulent velocities
X_i	Lagrangian co-ordinate axes; i=1,2,3
$\overline{X_i^2}$	mean square particle displacement
x_i	co-ordinate axes; i=1,2,3
x_1	distance from flow separator
x_θ	distance from line source
x_{2P}	location of peak mean temperature

Greek Symbols

η	dimensionless time scale
θ	instantaneous temperature fluctuation
$\overline{\theta^2}$	mean square temperature fluctuation
λ_{ij}	Taylor microscale
$\lambda_{\theta i}$	Corrsin microscale
$\rho_{u_1\theta}$	velocity-temperature correlation coefficient
τ_L	Lagrangian temporal Taylor microscale

LIST OF TABLES

LIST OF FIGURES

Part A

Part B

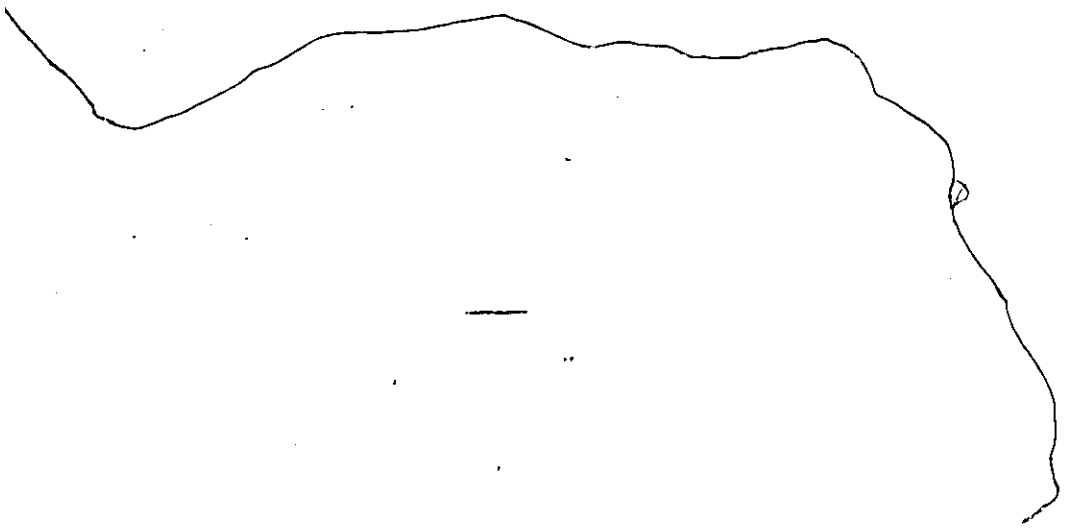

Part A

STRUCTURE OF UNIFORMLY SHEARED TURBULENT FLOWS

Chapter 1

INTRODUCTION

1.1 A Review of the Study of Turbulence

Turbulent flows and their effects are encountered in nature and in almost every case where fluid motion is involved. The boundary layers in the the earth's atmosphere and on aircraft wings, the flow of natural gas and oil through pipelines, the flow of rivers and the wakes of ships, cars and submarines are some examples where turbulent motion is encountered.

Since the first detailed experiments of Hagen (1839) and Reynolds (1883), the study of turbulence has been directed towards understanding its occurrence and structure and formulating practical procedures for its prediction. The random nature of turbulence necessitates the use of a statistical approach for its study. Reynolds (1894) introduced statistical methods in the description of turbulence by decomposing the instantaneous quantities into mean and fluctuating parts. However, such a statistical study of the equation of motion results in the well known "closure problem" of turbulence theory viz. a system of equations in which there are more unknowns than equations. Approximate techniques used to overcome this problem rely heavily on ad hoc assumptions and on the use of semi-empirical relations between various turbulent quantities.

Although analytical and computational methods have also been employed, experimental techniques have provided the most reliable results in the study of turbulent flows. A number of measurements have been obtained in flows with "simple" geometries, where the various effects can, presumably, be isolated and examined separately. The simplest case is grid generated, nearly isotropic turbulence, which has been studied in great detail. This flow, however, does not possess a mechanism for the production of turbulence and its energy decays. Turbulence can be generated and maintained by a mean velocity gradient (shear) as is the case in nearly all flows with practical interest. Therefore, it is worthwhile to investigate the structure of a turbulent flow in the presence of a mean shear. The simplest possible flow for such a study is one with a uniform value of the mean shear. A literature survey of such flows is provided in the following section.

1.2 Uniformly Sheared Turbulent Flows

The idea that a transversely homogeneous shear flow (i.e. a unidirectional flow which, in the presence of a uniform mean velocity gradient, exhibits homogeneity of the variances of the fluctuating velocity components in the plane perpendicular to the direction of the mean flow) could be generated in the laboratory was introduced by Corrsin (1963). Subsequently, flows subjected to an approximate uniform mean shear resulting in near transverse homogeneity, have been studied experimentally among others by Rose (1966,1970), Robertson and Johnson (1970), Champagne et al. (1970), Hwang (1971), Mulhearn and Luxton (1975), Harris et al. (1977), Tavoularis and Corrsin (1981 a,b), Karnik (1983), Karnik and Tavoularis (1983), Sreenivasan (1985) and Rohr et al. (1988).

Analyses and computations concerning various aspects of such flows have also been published by many investigators, including Reis (1952), Burgers and Mitchner (1953), Tchen (1953), Craya (1958), Deissler (1961,1965,1970), Fox (1964), Hasen (1967), Shaanan et al. (1975), Corrsin and Kollman (1977), Gence et al. (1978), Courseau and Loiseau (1978), Rogallo (1981), Cambon et al. (1981), Feiereisen et al. (1982), Rogallo and Moin (1984), Moin et al. (1985) and Tavoularis (1985).

In general, these experiments and analyses have contributed, to a certain degree, to our understanding of the influence of a mean shear on the structure of turbulence. However, a few questions remain unresolved e.g.

(i) In the case of the "low shear" experiments the Reynolds stresses reached constant asymptotic values whereas in the case of the "high shear" these stresses grew exponentially. Are these two cases distinct or would the low shear case exhibit the features of the high shear, viz. an exponential growth of stresses, if it were allowed a larger development time (e.g. an increase in wind tunnel length) as claimed by Harris et al. (1977) ?

(ii) If indeed the two cases are distinct, then what are the criteria that would distinguish the two classes of flows ?

Although the present author had made an attempt to answer the above questions in his master's thesis (Karnik, 1983), the results were inconclusive due to lack of sufficient number of cases. The objective of the present study is to provide new measurements and to re-evaluate earlier results on uniformly sheared turbulence, in an attempt to answer the above questions conclusively and also to provide

further insight into the structure of the flow.

1.3 Shear Reduction with the use of Screens

The design of several independent shear generators to produce mean shear values spanning a wide range would be expensive and time consuming. Consequently, an improvisation, viz. the generation of transversely homogeneous flows with a wide range of mean shear values and initial conditions by passing a uniformly sheared flow through various screens was considered. A literature review of flow through screens is provided in the following text.

A screen is defined here as a relatively thin, periodic obstruction such as an array of parallel rods (grid) or a plain rectangular mesh (gauze), placed transversely to a fluid stream. Screens have been used extensively in wind tunnels, water channels and other fluid apparatus. Uniform screens are used most commonly for reducing the free stream turbulence level and the mean velocity non-uniformity and, in some cases, for producing nearly isotropic turbulence. Non-uniform screens have been used for producing non-uniform velocity fields. A review of flow through screens has been compiled by Laws and Livesey (1978).

Simplified theories of flow behind screens have been developed, among others, by Prandtl (1933), Collar (1939), Taylor and Batchelor (1949) and Elder (1959). In particular, the generation of non-uniform mean velocity profiles by passing a stream through a properly designed screen has been explored theoretically and experimentally by Owen and Zienkiewicz (1957), Elder (1959), McCarthy (1964), Livesey and Turner (1964), Cockrell and Lee (1966), Rose (1966) and Kotansky

(1966).

Nearly all earlier theories were based on the assumption that the degree of mean flow non-uniformity, both upstream and downstream of the screen, was small. Most relevant experiments were designed to satisfy this assumption, although occasional non-systematic and probably unintentional violations can be discovered. Screens have figured prominently in the design of shear generators (to generate a uniform shear) used by experimenters e.g. the non-uniform plane screens (Rose, 1966; Mulhearn and Luxton, 1975), curved screens (Maul and Young, 1973), tapered honeycombs (Kotansky, 1966; Rose, 1970; Richards and Morton, 1976) and merging channel flows, where the flow in each channel was adjusted to the desired level by screens (Champagne et al., 1970; Harris et al., 1977; Tavoularis and Corrsin, 1981; Karnik, 1983; Karnik and Tavoularis, 1983).

The only earlier measurements that are relevant to the problem of passing uniformly sheared streams through highly perturbing screens are those of Rose(1970), whose main concern was to study the effect of the screen on the turbulence development and not on the mean shear.

Chapter 2

ANALYTICAL CONSIDERATIONS

2.1 The General Governing Equations

The velocity field for an incompressible fluid flow with negligible body forces and constant viscosity is described by the Navier-Stokes equations, which in the Cartesian co-ordinate system (x_1, x_2, x_3) have the form

$$\frac{\partial U_i}{\partial t} + U_j \frac{\partial U_i}{\partial x_j} = \frac{-1}{\rho}\frac{\partial P}{\partial x_i} + \nu \frac{\partial^2 U_i}{\partial x_j \partial x_j} \qquad (Momentum) \tag{2.1}$$

$$\frac{\partial U_i}{\partial x_i} = 0 \qquad (Continuity) \tag{2.2}$$

where $i = 1, 2, 3$ and repeated indices are summed.

In the following analysis, the Reynolds decomposition procedure (Reynolds, 1894) has been used, i.e. the instantaneous velocity and pressure have been decomposed into mean (designated by overbars) and fluctuating (designated by lower case letters) components as follows

$$U_i = \overline{U_i} + u_i \tag{2.3}$$

and

$$P = \overline{P} + p \tag{2.4}$$

where $\overline{u_i} = 0$ and $\overline{p} = 0$ by definition.

Thus, the *mean continuity equation* is

$$\frac{\partial \overline{U_i}}{\partial x_i} = 0 \tag{2.5}$$

and the *mean momentum equation* is

$$\frac{\partial \overline{U_i}}{\partial t} + \overline{U_j}\frac{\partial \overline{U_i}}{\partial x_j} = \frac{-1}{\rho}\frac{\partial \overline{P}}{\partial x_i} + \nu\frac{\partial^2 \overline{U_i}}{\partial x_j \partial x_j} - \frac{\partial \overline{u_i u_j}}{\partial x_j} \tag{2.6}$$

where $\overline{u_i u_j}$ is the Reynolds stress tensor.

By further manipulating the instantaneous flow equations, one can derive the equation for the *Reynolds stresses* as

$$\begin{aligned}\frac{\partial \overline{u_i u_j}}{\partial t} + \overline{U_k}\frac{\partial \overline{u_i u_j}}{\partial x_k} = \quad & -\overline{u_j u_k}\frac{\partial \overline{U_i}}{\partial x_k} - \overline{u_i u_k}\frac{\partial \overline{U_i}}{\partial x_k} \\ & -\tfrac{1}{\rho}\left(\overline{u_i \frac{\partial p}{\partial x_j}} + \overline{u_j \frac{\partial p}{\partial x_i}}\right) - \frac{\partial \overline{u_i u_j u_k}}{\partial x_k} \\ & +\nu\left(\overline{u_i \frac{\partial^2 u_j}{\partial x_k \partial x_k}} + \overline{u_j \frac{\partial^2 u_i}{\partial x_k \partial x_k}}\right)\end{aligned} \tag{2.7}$$

and the equation for the *mean turbulent kinetic energy*, $\frac{\overline{q^2}}{2} = \frac{1}{2}\overline{u_i u_i}$, as

$$\frac{\partial \frac{\overline{q^2}}{2}}{\partial t} + \overline{U_k}\frac{\partial \frac{\overline{q^2}}{2}}{\partial x_k} = -\overline{u_i u_k}\frac{\partial \overline{U_i}}{\partial x_k} - \frac{1}{\rho}\frac{\partial \overline{u_k p}}{\partial x_k} - \frac{1}{2}\frac{\partial \overline{u_k u_i u_i}}{\partial x_k}$$
$$+\nu\left(\frac{\partial^2 \frac{\overline{q^2}}{2}}{\partial x_k \partial x_k} + \frac{\partial^2 \overline{u_i u_k}}{\partial x_i \partial x_k}\right) - \frac{1}{2}\nu\overline{\left(\frac{\partial u_i}{\partial x_k} + \frac{\partial u_k}{\partial x_i}\right)\left(\frac{\partial u_i}{\partial x_k} + \frac{\partial u_k}{\partial x_i}\right)} \qquad (2.8)$$

A common physical interpretation of the various terms in Equation (2.8) is as follows :

(a) the terms on the left hand side of the equation represent the total rate of change of the turbulent kinetic energy;

(b) the first term on the right hand side being usually positive, represents the production of turbulent kinetic energy;

(c) the second term represents work done due to pressure fluctuation gradients;

(d) the third term symbolizes turbulent diffusion of kinetic energy;

(e) the fourth term could be considered as molecular diffusion of kinetic energy;

(f) the final term, being always negative, represents dissipation of turbulent kinetic energy by viscous forces.

2.2 Equations for Uniformly Sheared Turbulent Flows

Assume that the flow has the following properties :

(a) it is a rectilinear mean flow, parallel to the x_1-axis imposed with a constant mean velocity gradient in the x_2-direction. Hence

$$\overline{U_2} = \overline{U_3} = 0, \qquad \frac{\partial \overline{U_1}}{\partial x_2} = constant, \qquad \frac{\partial \overline{U_1}}{\partial x_3} = 0; \qquad (2.9)$$

(b) all turbulence moments are transversely homogeneous, i.e.

$$\frac{\partial\overline{(\ )}}{\partial x_2} = \frac{\partial\overline{(\ )}}{\partial x_3} = 0; \tag{2.10}$$

(c) the flow is stationary, i.e.

$$\frac{\partial\overline{(\ )}}{\partial t} = 0. \tag{2.11}$$

2.2.1 The Mean Continuity and Momentum Equations

As a result of the above assumptions, the *mean continuity equation* reduces to

$$\frac{\partial\overline{U_1}}{\partial x_1} = 0 \tag{2.12}$$

whereas the *mean momentum equation* becomes

$$\frac{\partial\overline{P}}{\partial x_i} = -\rho\frac{\partial\overline{u_i u_2}}{\partial x_1} \tag{2.13}$$

2.2.2 Equation for the Reynolds Stresses

The equation for the Reynolds stresses is simplified to

$$\begin{aligned}\overline{U_1}\frac{d\overline{u_i u_j}}{dx_2} &= -\overline{u_1 u_j}\frac{d\overline{U_1}}{dx_2} - \overline{u_2 u_i}\frac{d\overline{U_1}}{dx_2}\delta_{j1} \\ &+\frac{1}{\rho}\overline{p\left(\frac{\partial u_i}{\partial x_j} + \frac{\partial u_j}{\partial x_i}\right)} - 2\nu\overline{\frac{\partial u_i}{\partial x_i}\frac{\partial u_j}{\partial x_k}}\end{aligned} \tag{2.14}$$

which in condensed form becomes

$$T_{ij} = P_{ij} + \phi_{ij} - 2\epsilon_{ij} \tag{2.15}$$

where T_{ij} represents the transport of the stresses, P_{ij} is the production due to the mean shear, ϕ_{ij} is the pressure-strain correlation rate and ϵ_{ij} represents viscous actions including energy dissipation.

2.2.3 The Turbulent Kinetic Energy Equation

The simplified form of the turbulent kinetic energy equation is

$$\overline{U_1}\frac{d(\frac{\overline{q^2}}{2})}{dx_1} = -\overline{u_1 u_2}\frac{d\overline{U_1}}{dx_2} - \nu\overline{\frac{\partial u_i}{\partial x_j}\frac{\partial u_i}{\partial x_j}} \tag{2.16}$$

In equation (2.16) the first term represents transport (T), the second term production (P) and the third term viscous dissipation (ϵ) of kinetic energy.

Assuming that there exists an asymptotic state in which the dimensionless Reynolds stress tensor K_{ij} is constant (as indicated by previous measurements)

$$K_{ij} = \frac{\overline{u_i u_j}}{\overline{q^2}} = constant \tag{2.17}$$

and the ratio $\epsilon : P$ is also constant (based on earlier experimental evidence), equation (2.16) can be further simplified (Tavoularis, 1985) as

$$\frac{d\overline{q^2}}{dx_1} = k\overline{q^2} \tag{2.18}$$

where the coefficient k is defined as

$$k = \frac{-2K_{12}}{\overline{U_1}} \frac{d\overline{U_1}}{dx_2}(1 - \frac{\epsilon}{P}) \tag{2.19}$$

Then, Equation (2.18) has the solution

$$\overline{q^2}(x_1) = \overline{q_r^2} e^{k(x_1 - x_r)} \tag{2.20}$$

where $\overline{q_r^2}$ is the turbulent kinetic energy at a reference location $x_1 = x_r$ in the asymptotic region.

2.3 Estimates of Shear Reduction by Uniform Screens

Consider a bounded, unidirectional flow stream $\overline{U_1(x_2)}$, with a constant transverse mean gradient $d\overline{U_1}/dx_2$, passing through a screen, normal to the flow direction as shown in Figure 2.1. The screen is characterized by the element thickness, d, the element spacing, M, the solidity (i.e. the ratio of the projected blocked area over the total area), σ, and the geometrical shape and arrangement of the elements. Far downstream of the screen, a new unidirectional velocity field, $\overline{U_1^*}(x_2)$, is achieved. We shall assume, as all earlier analytical and experimental evidence indicates, that the downstream velocity also has a constant transverse mean gradient $d\overline{U_1^*}/dx_2$. Thus a shear reduction factor A can be defined as

$$\frac{d\overline{U_1^*}}{dx_2} = A \frac{d\overline{U_1}}{dx_2} \tag{2.21}$$

Neglecting wall effects, one would expect that A should, in general, depend on the oncoming shear, $d\overline{U_1}/dx_2$, the screen spacing, M, the screen solidity, σ, the

screen geometry and a Reynolds number based on the mean centerline velocity, $\overline{U_{1c}}$, and the screen element thickness i.e. $R = \overline{U_{1c}}d/\nu$.

Crude estimates of A in terms of the pressure loss coefficient

$$K = \frac{\Delta\overline{P}}{\frac{\rho\overline{U_{1c}^2}}{2}} \tag{2.22}$$

across the screen can be based on the theories of Prandtl (1933) and Collar (1939). Taylor and Batchelor (1949) refined these theories by including the effect of the deflection coefficient, α, defined as the ratio of the local incidence angles, immediately downstream and immediately upstream of the screen, for the limiting case of extremely small angles. Their theory results in the following estimate

$$A = \frac{1+\alpha-\alpha K}{1+\alpha+\alpha K} \tag{2.23}$$

Equation (2.23) can be derived as a special case of Elder's (1959) theory, which provided a general relationship between an arbitrary upstream velocity profile and a downstream velocity profile, in terms of the shape of the screen and the variation of K over the screen.

Among the various semi-empirical estimates of α, the following expression by Gibbings (1973)

$$\alpha = \left[\left(\frac{K}{4}\right)^2 + 1\right]^{\frac{1}{2}} - \left(\frac{K}{4}\right) \tag{2.24}$$

appears to be in good agreement with experimental results having $0.7 < K < 5.2$

and incidence angles up to 45 degrees.

Substituting equation(2.24) into equation(2.23) one can derive an expression for A in terms of K alone and verify the expectation that the shear reduction factor decreases with increasing pressure loss as seen in Figure 2.2. Estimates of A, based on different expressions for $\alpha(K)$, are only slightly different from values based on equation(2.24) especially for $K < 2$ (see Gibbings, 1973).

The pressure loss coefficient, K, is generally a function of screen geometry and spacing as well as of Reynolds number. Although several independent measurements of K have been performed, there seems to be no general agreement on its variation. The measurements of Annand (1953) and Pinker and Herbert (1967) for square mesh gauzes are generally compatible with the expression

$$K = 0.52\frac{\sigma(2-\sigma)}{(1-\sigma)^2} \tag{2.25}$$

at least for $R > 400$. This expression can be modified to include Annand's low Reynolds number ($20 < R < 400$) results, as

$$K = (0.52 + \frac{17}{R})\frac{\sigma(2-\sigma)}{(1-\sigma)^2} \tag{2.26}$$

Harris' (1958) measurements with parallel rods having $0.125 < \sigma < 0.625$ and $R > 1000$ can be represented by

$$K = 0.12 + \frac{1.51\sigma^2}{(1-\sigma)^2} \tag{2.27}$$

Finally, Davis (1957; quoted by Elder, 1957) recommends the expression

$$K = [\frac{1 - 0.95(1-\sigma)}{0.95(1-\sigma)}]^2 + \frac{88\sigma}{R} \tag{2.28}$$

for all screen geometries with sufficiently small mesh size. The above expressions result in substantially distinct estimates of K, as seen in Figure 2.3.

Substitution of expressions (2.25), (2.26), (2.27), (2.28) into (2.24) and, in turn, into (2.23) would provide expressions for the deflection angle, α, and for the predicted shear reduction factor, A_p, in terms of the screen solidity alone at sufficiently high Reynolds numbers. Such expressions are plotted in Figure 2.4, while Figures 2.5 and 2.6 illustrate the effect of R on K and A_p. It is clear, however, that as the relative size of the screen elements d/h (h is the flow height) increases, these expressions would become inaccurate, due to the breakdown of the small disturbance assumption. The aim of the present study is to provide an empirical relationship between A and d/h valid for small as well as large d/h.

Chapter 3

EXPERIMENTAL APPARATUS AND MEASUREMENT PROCEDURES

The wind tunnel and related apparatus that were used in the present experiments have been described in detail by Karnik (1983). The following sections provide salient features of the same.

3.1 The Flow Facility

The wind tunnel (Figure 3.1) used in the present experiments was designed and constructed at the University of Ottawa. The flow was produced by two centrifugal blowers and passed through a filter, a honeycomb, a settling chamber with several turbulence reducing screens and a 16:1 contraction before entering the final test section (Figure 3.2) which was 305mm high, 457mm wide and 5180mm long. The vertical walls of the downstream end were adjustable to compensate for boundary layer growth. The test section was also provided with four slots for inserting screens or other flow obstructions.

The desired mean velocity profile was produced with the use of a shear gener-

ator inserted in the flow immediately after the contraction. The shear generator (Figure 3.3) consisted of a set of 12 parallel aluminium plates, about 150mm wide and 254mm apart, which separated the flow into 12 channels, and a system of interchangeable screens stretched across up to four positions in each channel, which provided the desired channel pressure drop. A flow separator (Figure 3.4), consisting of 12 parallel aluminium plates 610mm long and aligned with those in the shear generator, was inserted into the flow in order to produce transverse uniformity of scales.

The screens used in the present experiments consisted of grids and gauzes of varying spacing and solidities. Specifications for these have been tabulated with the results in Table 1. The probes were mounted on a traversing mechanism which provided the necessary longitudinal, transverse and cross-stream motions.

3.2 Velocity Measurement Technique

3.2.1 Instrumentation

Hot-wire anemometry was used extensively throughout the present study. The velocity components and shear stress were measured with a commercial cross-wire probe (TSI model 1248BJTI5). The wires were operated in a constant temperature mode with the use of two TSI 1050 constant temperature anemometer modules which were powered by a TSI 1051 2D monitor and power supply.

3.2.2 Calibration

A hot-wire anemometer measures flow velocity through its relationship to the heat transfer rate from a heated body immersed in a flowing fluid. An expression,

relating the heat transfer to the fluid velocity commonly known as King's law is

$$\frac{Q}{T_{op} - T_f} = A' + B'U^n \tag{3.1}$$

where $Q = E^2/R_w$ is the heat transfer rate, E is the voltage across the wire, R_w is the operating resistance of the wire, $T_{op} - T_f$ is the difference between the operating temperature of the sensor and the fluid temperature, U is the velocity normal to the sensor and A_1, B_1, n are empirical constants determined by calibration.

The modified version of King's law can be expressed as,

$$\frac{E^2}{T_{op} - T_f} = A + BU^n \tag{3.2}$$

Each of the wires was individually calibrated versus the flow velocity measured with a pitot tube in a smooth flow in the wind tunnel. The operating resistance of the wires was set such that the operating temperature was $250°C$. The fluid temperature was monitored regularly and was found to be essentially constant over the duration of the calibration. Also, it did not change by more than 2°C during each experiment. It has been shown (Tavoularis, 1978) that mean temperature changes of 5°C would result in only 0.06% errors in the measurement of $\overline{u_1^2}$ and $\overline{u_2^2}$. The wire frequency response was optimized using the standard square wave test under typical flow conditions. Typical calibration curves are shown in Figure 3.5.

3.2.3 Measurement Procedure

The use of a modified King's law for a slanted wire is appropriate if an effective cooling velocity that would produce the same cooling effect as the velocity normal

to the sensor is considered. Assuming that each of the wires is inclined at 45° to the flow and is perpendicular to the other, the effective cooling velocities normal to the two wires (Figure 3.6) could be written as,

$$U_{eff1} = (\overline{U_1} + u_1 + \overline{U_2} + u_2)cos45 \tag{3.3}$$

$$U_{eff2} = (\overline{U_1} + u_1 - \overline{U_2} - u_2)cos45 \tag{3.4}$$

where overbars denote averages and lower case symbols denote fluctuations.

Thus the modified King's law for the two wires can be written as,

$$\frac{E_1^2}{T_{op} - T_f} = A_{11} + B_{11}U_{eff1}^{n_1} \tag{3.5}$$

$$\frac{E_2^2}{T_{op} - T_f} = A_{22} + B_{22}U_{eff2}^{n_2} \tag{3.6}$$

Further assuming that the temperature of the fluid is constant, the above equations can be simplified to

$$E_1^2 = A_1 + B_1U_{eff1}^{n_1} \tag{3.7}$$

$$E_2^2 = A_2 + B_2U_{eff2}^{n_2} \tag{3.8}$$

Thus the components of velocity in the x_1 and x_2 directions can be obtained as

$$\overline{U_1} = (\overline{U}_{eff1} + \overline{U}_{eff2})/2 \tag{3.9}$$

$$\overline{U_2} = (\overline{U}_{eff1} - \overline{U}_{eff2})/2 \tag{3.10}$$

$$u_1 = \frac{(U_{eff1} + U_{eff2})}{2} - \overline{U}_1 \tag{3.11}$$

$$u_2 = \frac{(U_{eff1} - U_{eff2})}{2} - \overline{U}_2 \tag{3.12}$$

where the effective cooling velocities are evaluated by inverting equations 3.7 and 3.8.

Proper orientation of the cross-wire in the $x_1 - x_3$ plane would provide the x_1 and x_3 components of velocity.

3.3 Analog Signal Processing and Data Acquisition

The anemometer output signals were observed on a Tektronix model 5113 dual beam storage oscilloscope. The oscilloscope was equipped with two differential amplifiers (Tektronix 5A22N) with gains ranging from 0.1 to 50,000 and built-in high pass and low pass filters with a 3 db drop off per octave.

The amplified, conditioned signals were discretized and processed using a LSI 11/23 micro-computer with a 64 K byte memory. The computer was equipped with an ADAC model 1601 GPT programmable 16 bit general purpose timer and a 12 bit analog to digital converter (ADAC model 1012) with a 16 channel multiplexer.

The input voltage range of the analog to digital converter was programmable and usually set between -1.0 and +1.0 volt. Signals outside this range had to be attenuated or offset, while low level signals had to be amplified in order to utilize the full capacity of the system. The digital output ranged between 0 and 4095 which produced a digitizing uncertainty of 0.5 mV.

The minimum conversion time with direct memory access was 40μs. This introduced a delay between consecutive samples, thus producing appreciable errors in cross-wire measurements. As a remedy, one of the signals was delayed by passing it through a home-made analog delay line with a frequency response which was good to 5 kHz (-3 db point).

Other peripheral units were RX02 diskettes, Winchester drive, LA50 printer and a VT100 CRT display monitor. Sampling was accomplished using assembly language software and all computations were performed in FORTRAN language.

3.4 Computational Procedures

The evaluation of the various turbulent parameters consisted of firstly obtaining a discrete time history for the three components of velocity u^j_{1k}, u^j_{2k}, u^j_{3k}, where $j = 1, 2, ...M$(M is the number of records between 15 and 20) and $k = 1, 2, ...N$(N is the number of points per record between 1600 to 2000). The number of points per record was adjusted depending on the number of records chosen for the discretization process so that the memory storage capacity of the micro-computer would not be exceeded.

3.4.1 One Point Moments

For each component of velocity e.g the u_1 - component, the one point moments were easily calculated from the discrete time history as

$$\overline{u_1^n} = \frac{\sum_{j=1}^{M} \sum_{k=1}^{N} u_{1k}^{nj}}{N \times M} \tag{3.13}$$

The shear stress, $\overline{u_1 u_2}$ was evaluated as,

$$\overline{u_1 u_2} = \frac{\sum_{j=1}^{M} \sum_{k=1}^{N} u_{1k}^{j} u_{2k}^{j}}{N \times M} \tag{3.14}$$

3.4.2 Two-Point Correlations

The components of a general two-point correlation tensor in the cartesian co-ordinate system (x_1, x_2, x_3) are defined as

$$R_{ij}(r_1, r_2, r_3; \tau) = \frac{\overline{u_i(x_k; t) u_j(x_k + r_k; t + \tau)}}{u_i'(x_k) u_j'(x_k + r_k)} \tag{3.15}$$

where $i, j, k = 1, 2, 3$.

Spatial correlations are obtained when τ is fixed, temporal correlations when r_1, r_2, and r_3 are fixed and space-time correlations when τ as well as r_1, r_2 and r_3 vary. R_{ij} is called the autocorrelation coefficient when $i = j$ and cross-correlation when $i \neq j$.

In the present investigation, only the component $R_{11}(\tau) = R_{11}(0, 0, 0; \tau)$ is measured. $R_{11}(r) = R_{11}(r, 0, 0; 0)$ is evaluated from $R_{11}(\tau)$ by employing Taylor's "frozen flow" approximation, namely the assumption that the flow structure

remains unchanged while being convected by the mean speed past the measuring probe. Taylor's approximation is accurate only when the turbulence intensity u'/U is relatively small (typically below 10%), a condition satisfied in the present investigation. Therefore,

$$R_{11}(r) = R_{11}(\tau) \quad with \quad r = \overline{U_1}\tau \tag{3.16}$$

Thus from the discretized data, $R_{11}(\tau)$ can be evaluated for each record, j, as

$$R^j_{u_1}(\tau) = \frac{\sum_{k=1}^{N-i} u^j_{1k} u^j_{1k+i}}{\sum_{k=1}^{N} u^j_{1k} u^j_{1k}} \left(\frac{N}{N-i}\right) \tag{3.17}$$

where the separation time $\tau = i \times \Delta t$.

The ensemble average was then computed as

$$R_{u_1}(\tau) = \frac{1}{M} \sum_{j=1}^{M} R^j_{u_1}(\tau) \tag{3.18}$$

3.4.3 Integral Length Scales

The integral length scale is a measure of the typical size of the energy containing eddies of the flow. The Eulerian integral length scale of the streamwise velocity component, along the streamwise direction is defined as,

$$L_{11} = \int_0^\infty R_{11}(r) dr \tag{3.19}$$

Using Taylor's hypothesis, the Eulerian integral length scale, L_{11}, can be determined from the Eulerian integral time scale,

$$T_{11} = \int_0^\infty R_{11}(\tau) d\tau \tag{3.20}$$

as

$$L_{11} = \overline{U_1} T_{11} \tag{3.21}$$

In the present measurements, the autocorrelation coefficient, $R_{11}(\tau)$, evaluated from the discrete data, was numerically integrated up to the first zero to obtain the integral time scale. The integral length scale was obtained by using Taylor's hypothesis.

3.4.4 Taylor Microscales

The Taylor microscales can be estimated according to the definition,

$$\lambda_{ii} = \left[\frac{\overline{u_i^2}}{(\frac{\partial u_i}{\partial x_i})^2} \right]^{0.5} \tag{3.22}$$

$$\lambda_{ij} = \left[\frac{2\overline{u_i^2}}{(\frac{\partial u_i}{\partial x_j})^2} \right]^{0.5}, \quad i \neq j \tag{3.23}$$

where repeated indices are not summed.

Using Taylor's approximation, the streamwise microscale, λ_{11}, can be estimated as

$$\lambda_{11} = \overline{U_1} \left[\frac{\overline{u_1^2}}{(\frac{\partial u_1}{\partial t})^2} \right]^{0.5} \tag{3.24}$$

The derivative in the above expression is obtained from the discrete data as

$$\overline{(\frac{\partial u_1}{\partial t})^2} = \frac{1}{(N-1)\times M}\sum_{j=1}^{M}\sum_{k=1}^{N-1}\frac{u_{1k+1}^j - u_{1k}^j}{\Delta t} \tag{3.25}$$

3.5 Measuring Accuracies

3.5.1 Temporal Resolution

The fastest relevant events in a turbulent flow can be measured accurately only if the characteristic times associated with the response of the hot-wire and the analog to digital conversion system are smaller than the convection time of the smallest relative motions which are usually associated with viscous dissipation (Corrsin, 1963).

In the present experiment the convection Kolmogoroff time was equal to

$$\tau_k = \frac{1}{\overline{U}_{1c}}(\frac{\nu^3}{\epsilon})^{1/4} \approx 8.0\mu s \tag{3.26}$$

while the convection time of the energy containing eddies was

$$\frac{L_{11}}{\overline{U}_{1c}} \approx 3.5ms. \tag{3.27}$$

The characteristic time of the hot wire was

$$\tau_1 = \frac{d}{\overline{U}_{1c}} \approx 0.38\mu s, \tag{3.28}$$

where $d = 5\mu m$ is the diameter of the sensor, and the sampling time of the analog to digital converter was $40\mu s$.

Therefore it can be concluded that although the quantities associated with large scale motions e.g. $\overline{U_1}$, $\overline{u_i^2}$ and L_{11} could be measured accurately those associated with dissipation e.g. $\overline{(\partial u_i/\partial t)^2}$ and λ_{11} would be subject to considerable inaccuracy.

3.5.2 Spatial Resolution

The spatial resolution of a hot-wire is limited by its length and, in the case of a cross-wire, also by the spacing between the two sensors. In order to obtain accurate estimates these quantities should be small in comparison to the characteristic length scales of the flow. In the present experiments the Eulerian integral length scale , L_{11}, was typically 50mm, the Taylor microscale, λ_{11}, was 8mm and the Kolmogoroff microscale, η_K was typically 0.3mm. For a probe with length $l_p \approx 1.75mm$

$$\frac{l_p}{L_{11}} \approx 0.035 \quad \frac{l_p}{\lambda_{11}} \approx 0.22 \quad \frac{l_p}{\eta_K} \approx 5.8. \tag{3.29}$$

From these ratios it is possible to estimate the measurement error, for example, in $\overline{u_1^2}$ (Corrsin, 1963) as

$$\frac{\overline{u_{1meas}^2}}{\overline{u_1^2}} = \frac{2\int_0^{l_p}(l_p - t)R(t)dt}{l_p^2}. \tag{3.30}$$

Using the relation

$$R(t) = 1 - \frac{t^2}{2\lambda_{11}^2} \tag{3.31}$$

we obtain

$$\frac{\overline{u_{1meas}^2}}{\overline{u_1^2}} = 1 - \frac{l_p^2}{24\lambda_{11}^2} \approx 0.998 \tag{3.32}$$

indicating that the error is negligible.

It could be concluded that the spatial resolution is adequate for measuring the phenomena which are dominated by the energy containing range of the energy spectrum and that considerable inaccuracy would be introduced in the measurement of the fine structure parameters.

Chapter 4

MEASUREMENTS

4.1 Free Stream Measurements

Measurements in a free stream (i.e. without the shear generator and flow separator and with the vertical walls of the test section adjusted to compensate for the boundary layer growth), shown in Figure 4.1, indicated that along the centerline, the mean velocity was nearly constant and that the turbulent intensity (at all measuring positions) was less than 0.4 % at a reference speed of 14 m/s. Typical transverse profiles indicate that away from the walls, the mean velocity profiles were uniform. In conclusion, experimental evidence indicates that the wind tunnel was capable of producing a stable uniform free stream with a moderately low free stream turbulence level.

4.2 The Mean Velocity Field

4.2.1 Unobstructed Mean Shear

The maximum possible shear was achieved behind the shear generator when no other obstruction was inserted in the test section. The shear parameter

$$\beta = \frac{h}{\overline{U_{1c}}} \frac{d\overline{U_1}}{dx_2} \tag{4.1}$$

was about 2.0 and decreased slightly (Figure 4.2) with increasing mean tunnel speed in the range 5 to 15 m/s. Typical transverse profiles of the mean velocity, shown in Figure 4.3, demonstrate the near uniformity and downstream constancy of the mean shear in the tunnel core. The mean shear also exhibited a reasonable spanwise uniformity (Figure 4.4). Mean velocities, measured at spanwise distances up to 0.45 h on either side of the centerplane, differed by less than 5% from the corresponding centerline values.

4.2.2 Shear Reduction by a Single Screen

In all cases examined, the mean velocity downstream of the screen was found to be unidirectional, with a uniform transverse gradient $d\overline{U_1}/dx_2$, which was preserved in the entire test section. Typical mean velocity profiles downstream ($x_1/h = 7.5$) of the various screens used in the present experiments are shown in Figure 4.5. It appears that the uniformity of the shear behind screens was usually better than that in the undisturbed flow. Screens which were not uniform or not stretched tautly did not exhibit this behaviour and these results were discarded. Specifications for the tested screens as well as the corresponding measured and predicted shear reduction factors are presented in Table 1. This table also includes the results of Rosé (1970), which appear relevant to the present study. The predicted values of A in Table 1 do not include corrections at low Reynolds numbers, since it was discovered that such corrections worsened rather than improved the consistency of measurements for similar geometries.

4.2.3 Shear Reduction by Multiple Screens

A few tests were performed with two or three grids inserted in separate slots of the test section. In all cases, the far downstream shear was also found to be uniform as seen in Figure 4.6. The results, summarized in Table 2, demonstrate that the total shear reduction factor was not significantly different from the product of the shear reduction factors of the individual grids.

4.2.4 Shear Upstream of Screens

The flow disturbance introduced by a screen is expressed by a distortion of the streamline pattern and by changes in the pressure field. It is obvious that there must be a region in the neighborhood of the screen, where the mean shear is adjusted from its far upstream value to its far downstream value. Furthermore, the possibility of flow changes within the flow generator due to increased pressure upstream of the grid also deserves attention. In order to test these results, we conducted measurements at a station 1.5 h upstream of screens inserted in slot D ($x_1/h = 4.5$). The mean shear at that station was found to decrease slightly (by 4 to 7 %, Figure 4.7) after a screen insertion, but not sufficiently to indicate that screen insertion introduced any significant change in the wind tunnel operation.

4.3 Development of the Reynolds Stresses

As shown in Figure 4.8, for a few typical cases, the r.m.s. turbulent velocities presented a degree of variation that was comparable to those in earlier experiments. The development of the four dominant Reynolds stresses and the turbulent kinetic energy $\overline{q^2} = \overline{u_i u_i}$ along the wind tunnel axis is shown in Figure 4.9 for some repre-

sentative conditions; semi-logarithmic co-ordinates were used for convenient comparison with Tavoularis's (1985) predictions. In all cases, the plots demonstrated linear ranges with either positive or nearly zero slopes, corresponding to either exponential growth or constancy of the Reynolds stresses. For each set of conditions, the rates of growth of all stresses away from the origin were essentially the same. The magnitudes of the stresses were always ordered as $\overline{u_1^2} > \overline{u_3^2} > \overline{u_2^2} > \overline{u_1 u_2}$. The same ordering has been observed by others in uniformly sheared flows as well as in heterogeneous flows with a fixed dominant mean shear direction. The first inequality reflects the fact that the streamwise normal stress receives energy directly from the mean shear while the other two normal stresses are maintained by means of their coupling to the streamwise stress through pressure-velocity correlations (Champagne et al., 1970). Another observation that can be made is that the ratios $\overline{u_i u_i}/\overline{U_{1c}}^2$ appear to depend only slightly on the wind tunnel speed for a given flow generating apparatus. On this issue, Rohr et al.(1988) point out that plots of these ratios collapse when plotted versus the total strain

$$\tau = (\frac{x_1}{\overline{U_{1c}}})(\frac{d\overline{U_1}}{dx_2}) \tag{4.2}$$

All present and some previous measurements of the turbulent kinetic energy are summarized in Figure 4.10 Each set of data away from the origin was fitted by the relation (Tavoularis, 1985)

$$\overline{q^2} = \overline{q_r^2} e^{k(x_1 - x_r)} \tag{4.3}$$

where $x_r, \overline{q_r^2}$ are reference values, corresponding to a location near the end of the

wind tunnel and k has dimensions of a wave number. Based on the least-squares-fitted values of k (Table 4), it is possible to distinguish two subclasses of flows: those with k close to zero, i.e. flows with roughly constant Reynolds stresses, and those with a clearly positive k, i.e. flows with exponentially growing Reynolds stresses. A detailed discussion on the classification of such flows will be provided in Chapter 5.

The effect of crossing a grid or screen on the turbulence was manifested by a nearly stepwise jump of $\overline{q^2}$ across the obstruction; near the grid, turbulence is produced by the small scale shear between consecutive jets and wakes of the rods or wires. Grid generated turbulence decays rapidly downstream, so that it seems reasonable to assume that, away from the grids, turbulence production was almost entirely due to the constant mean shear. A closer look at the results reveals that the region of exponential growth of turbulent stresses is approached within a distance that is shorter for the parallel-rod grids than for the square-mesh screens.

Figure 4.11 contains the measurements of the dominant components of the dimensionless Reynolds stress tensor

$$K_{ij} = \overline{u_i u_j}/\overline{q^2} \tag{4.4}$$

In all cases, the values of K_{ij} in the downstream part of the tunnel were practically constant. Deviations between the fully developed values of each K_{ij} for different sets of conditions were relatively small. It is interesting to notice that values of K_{11}, K_{22} and K_{33} near the flow origin were closer to each other than they were away from it. When the flow crossed a screen, the Reynolds stress

tensor was reoriented tending towards its isotropic form, but away from the grid K_{ij} resumed an anisotropic form that is typical for uniformly sheared flows. This form, averaged over all experiments, was

$$K_{ij} = \begin{bmatrix} 0.51 \pm 0.04 & -0.16 \pm 0.01 & 0 \\ -0.16 \pm 0.01 & 0.22 \pm 0.02 & 0 \\ 0 & 0 & 0.27 \pm 0.03 \end{bmatrix} \tag{4.5}$$

4.4 Integral Length Scales

The streamwise integral length scale L_{11} of the streamwise velocity fluctuation was measured by integrating the corresponding autocorrelation coefficient to its first zero and using Taylor's "frozen flow" approximation. The accuracy of this technique has been demonstrated by Comte-Bellot and Corrsin (1971) and has been found to be satisfactory by Champagne et al. (1970) and by Tavoularis and Corrsin (1981a) in the case of uniformly sheared flows.

All present and previous measurements of L_{11} have been plotted versus streamwise distance in Figure 4.12a using logarithmic co-ordinates. Within the experimental uncertainty, one can represent all data using power laws of the type

$$\frac{L_{11}(x_1)}{L_r} = \left[\frac{x_1}{x_{rL}}\right]^{n_L} \tag{4.6}$$

where L_r and x_{rL} are reference values. The least-squares fitted values of the exponent n_L were on the average 0.8 with a standard deviation of about 0.1 (Table 4). Considering the relatively large uncertainty in the length scales measurement

(random experimental error was of the order of 7%), a linear growth of L_{11} might also be possible as suggested by Harris et al.(1977), Tavoularis and Corrsin(1981 a) and Rohr et al.(1988). It is interesting to observe that the growth rate of L_{11} is essentially independent of the shear or any other parameter and that it is substantially higher than the growth rate in nearly isotropic, grid turbulence, where integral length scales appear to grow according to a power law with an exponent of about 0.4 (see, for instance, Sreenivasan et al., 1980). For a given flow generating apparatus, L_{11} was found essentially independent of the wind tunnel speed, which is another indication that the integral length scales are not affected by changes of the shear value.

In order to test the possibility of exponential growth, the same scales have been plotted in Figure 4.12b using semi-logarithmic coordinates. Although the expression

$$\frac{L_{11}}{L_r} = e^{k_L(x_1 - x_r)} \tag{4.7}$$

may be roughly fitted to the data in the range $5 < x_1/h < 12$, it is clear that a power law is more successful in describing the entire range of measurements. The average value of k_L was about $0.33m^{-1}$ (Table 4).

4.5 Taylor Microscales

The streamwise Taylor microscale was measured as

$$\lambda_{11} = \left[\frac{\overline{u_1^2}}{\overline{(\partial u_1/\partial x_1)^2}} \right]^{1/2} \tag{4.8}$$

where the streamwise derivative was estimated from the time derivative using Taylor's "frozen flow" approximation. Measurements shown in Figure 4.13 demonstrate that λ_{11} was roughly constant along the centerline, at least for $x_1/h > 5$. Constancy of λ_{11} was a central assumption in Tavoularis's (1985) predictions of exponential growth of Reynolds stresses and self-preservation of turbulence structure.

Chapter 5

ANALYSIS AND DISCUSSION OF RESULTS

5.1 The Reduction of Shear with Screens

As discussed earlier, the shear reduction coefficient is fairly sensitive to changes in the screen solidity, all other factors being constant. Accurate measurements have revealed a significant variation of the wire diameter, especially for the fine mesh screens. In one case, our measured average solidity was nearly 10% different from its estimate based on screen manufacturer's specifications (this being the result of merely a 0.025 mm difference in wire diameter values); such differences could result in up to 8% error in the estimate of A. Considering this effect, as well as possible imperfections in the manufacturing and mounting of fine screens, one might anticipate slight discrepancies among results of different investigators.

Figure 5.1 presents a comparison between the present and Rose's (1970) measurements of A with estimates based on three semi-empirical expressions. To avoid influence of disturbance size, only results with small d/h (less than 0.01) are included. All measurements and estimates demonstrate the same trend and span the same overall range of A. Furthermore, results within each set of experiments appear to be consistent. Nevertheless, neither measurements nor estimates can be fitted to a universal relation, not surprisingly so, if one takes into account differ-

ences in screen geometries and experimental uncertainties. In fact, a closer study of the measurements together with the corresponding experimental conditions has revealed that our measurements of A with square-mesh gauzes are close to the predictions based on Eq. (2.25), which was developed from K-measurements behind square-mesh gauzes. Similarly, our results with the parallel-rod grid appear close to predictions based on Eq. (2.27), which corresponds to parallel-rod grids. Rose's results with square-mesh grids appear to be close to predictions based on Eq. (2.28) (without the Reynolds number correction) for reasons we have not been able to explain.

At this point, we return to the discussion of the relative screen spacing effect. In order to correlate the disturbance and the shear reduction factor, both M/h and d/h appear suitable as independent variables. However, we have discovered that the results correlate better with relative element thickness d/h. Figure 5.2a and b show that for $d/h < 0.01$, A appears to be independent of d/h and compatible with predictions for the particular values of solidity. However, Fig. 5.2c, which corresponds to grids with similar geometries but different d/h, demonstrates a significant, monotonic decrease of A, for d/h increasing beyond about 0.01. All available results (Figure 5.3) appear compatible with an empirical expression of the type

$$\frac{A}{A_p} = \frac{1}{(1 + (\frac{d/h}{0.065})^2)^{1/2}} \qquad (5.1)$$

where A_p is the small d/h prediction of A for the corresponding screen geometry and solidity. This expression corresponds to solidities of about 0.378, which are

comparable to values commonly encountered in wind-tunnel facilities.

5.2 The Evolution of Turbulent Stresses and Scales

5.2.1 Definition of Scaling Parameters

In an unbounded uniformly sheared flow, the sole externally imposed parameter is the value of the mean shear, which represents the mean vorticity and the mean strain rate. This value imposes the characteristic "straining" time

$$\tau_s = (d\overline{U}_1/dx_2)^{-1} \tag{5.2}$$

In the hypothetical case of unbounded, transversely homogeneous shear flow there is neither an external length scale nor a velocity scale and further non-dimensionalization becomes impossible, unless one assigns an arbitrary value to one of these parameters. In laboratory generated flows, it has been demonstrated (see also Rohr et al., 1988), that, for a fixed flow generating set-up but changing mean-velocity, the Reynolds stresses can be scaled with the centreline velocity. Then it is possible to define a wind-tunnel (or water-channel) shear constant, k_s, as

$$k_s = \frac{1}{\overline{U}_c}\frac{d\overline{U}_1}{dx_2} \tag{5.3}$$

which has dimensions of a wavenumber. The dimensionless total strain imposed upon the turbulence at a particular station is simply

$$\tau = k_s x_1 \tag{5.4}$$

One might anticipate that the value of k_s, which is constant for a given flow, could have a qualitative effect on the turbulence structure, while the value of τ, which grows downstream, should not affect a self-preserving structure.

The development and interaction of turbulent motions are characterized by internal scales, which, although the results of external conditions, are best identified by direct measurement. A measure of turbulent activity is the turbulent kinetic energy which for an incompressible flow is characterized by the r.m.s. value of a component of velocity, e.g. u_1'. The average size of turbulent eddies which contain most of the activity is characterized by integral length scales, for example the streamwise one, L_{11}. Such scales generally grow downstream from an initial value, which is set by the spacing of the flow generating elements. In the case of an unobstructed flow, this spacing is clearly the width of the individual channels of the shear generator and flow separator. When one or more grids or screens are inserted, the initial scale appears to be a complicated function of upstream flow characteristics, grid mesh size and solidity. In a crude way one might infer from the present results that the initial length scale is comparable to the larger of either the channel width or grid mesh size. A corresponding time scale, which can be interpreted as the "turnover time" of a typical turbulent eddy (Compte-Bellot and Corrsin, 1971) is

$$\tau_e = L_{11}/u_1' \tag{5.5}$$

Another time scale that is commonly used in turbulence modeling is the typical "lifetime" of the energy containing eddies

$$\tau_u = \overline{q^2}/\epsilon \tag{5.6}$$

where ϵ is the turbulent kinetic energy dissipation rate. If one further defines a characteristic time for transport of $\overline{q^2}$ by the mean flow as

$$\tau_T = (k\overline{U_c})^{-1}, \tag{5.7}$$

where k is the exponent in the stress growth law, it is possible, with the use of the simplified kinetic energy equation (Tavoularis, 1985), to derive a relation between the two latter time scales and τ_s as

$$\frac{1}{\tau_u} = \frac{-K_{12}}{\tau_s} - \frac{1}{2\tau_T} \tag{5.8}$$

Finally, the fine structure of turbulence, including energy dissipation phenomena, is characterized by the Kolmogoroff length and time micro-scales, respectively defined as

$$\eta_K = (\nu^3/\epsilon)^{1/4} \qquad \tau_K = (\nu/\epsilon)^{1/2} \tag{5.9}$$

5.2.2 Tests of Self-Preservation

"The hypothesis of self-preserving development of a turbulent flow assumes that all aspects of the motion except those directly influenced by viscosity have

similar forms at all stages, the differences being described wholly by changes of velocity and length scales which are functions of time (in decaying turbulence) or of the position in the flow direction" (Townsend, 1976, pp. 60-61). The mean velocity field, $\overline{U}_1(x_2)$, obviously meets the criteria of self-preservation, since it is essentially invariant. Second-order turbulent moments are also self-preserving in the bulk of the flow, since their relative magnitudes remain constant, as demonstrated by the constancy of all components of K_{ij}. This was true for all cases, both those with constant and those with growing moments. Integral length scales appear to follow a well-defined growth pattern, which is independent of the kinetic energy evolution. Also, relative magnitudes of integral scales in different directions appear to be roughly constant for both "low shear" (Champagne et al. 1970) and the "high shear" (Tavoularis and Corrsin, 1981a) cases.

In conclusion, all existing evidence supports the hypothesis that uniformly sheared turbulence in wind-tunnels achieves an approximately self-preserving state in which turbulent velocity and length scales follow fixed laws of downstream evolution and properly non-dimensionalized quantities remain invariant.

5.2.3 Criteria for the Evolution of Turbulent Kinetic Energy

As discussed earlier, it has been possible to identify two subclasses of uniformly sheared turbulence, namely flows with growing stresses and flows with roughly constant stresses. One might then speculate on the existence of a third subclass of flows with decaying stresses which has actually been predicted theoretically for "extremely weak" turbulence (e.g. by Deissler, 1961, 1965). The experimental confirmation of the third subclass is inconclusive. The few cases in

Rose's (1970) experiments that he interprets as decaying sheared turbulence are subject to extremely low signal-to-noise ratio and also contradicted by his Figure 6. Our experiments have not yielded any case having a negative value of k which deviated from zero by an amount larger than the measuring uncertainty. The limiting case $d\overline{U}_1/dx_2 = 0$ can, of course, be represented by grid-generated unsheared turbulence, whose second moments decay. However, the unsheared case is a singular limit since it does not satisfy the assumption $\epsilon/\overline{q^2} = constant$, which was the basis for the derivation of an exponential law.

We now proceed to identify parameters which possibly affect the balance between production and dissipation and thus the evolution law of the turbulent stresses and the turbulent kinetic energy. The mean shear is certainly a relevant parameter, because, all other external conditions being the same, an increase of mean shear leads from a constant- $\overline{q^2}$ flow (Champagne et al., 1970) to a growing-$\overline{q^2}$ flow (Harris et al., 1977; Tavoularis and Corrsin, 1981a). However, the value of $d\overline{U}_1/dx_2$ alone is not sufficient to determine the energy law; this can be seen by comparing cases with about the same shear but different centerline velocities, for example cases M and K versus case F and case L versus case E in Table 1.

Harris et al. (1977) have suggested that it is the value of the total strain τ that determines whether a state of growing stresses has been achieved and that, if "low shear" flows were permitted to achieve a sufficiently large τ by extending the wind-tunnel length, they would also exhibit growing stresses. Rohr et al. (1988) further suggest a "threshold" of $\tau \approx 4$ above which turbulence grows. Some of the present measurements contradict these hypotheses. As Figure 5.4 demonstrates, the kinetic energy in case L was practically constant in the range $4 < \tau - \tau_g < 8$

(τ_g was the total strain measured from the flow separator to the position of the last grid, when applicable). Such persistence is unlikely to be attributed to the presence of a grid; it is furthermore reminded that case L has a self-preserving turbulence structure and that, although case L has relatively large length scales, the fact that these scales continue growing at a constant rate precludes a total suppression of kinetic energy production by the wind-tunnel walls.

Following Tavoularis (1985), the kinetic energy exponent coefficient can be expressed as

$$k = -2K_{12}(1 - \epsilon/P)k_s \tag{5.10}$$

where the kinetic energy production is

$$P = -\overline{u_1 u_2} d\overline{U}_1/dx_2 \tag{5.11}$$

The values of the ratio ϵ/P, computed from measurements of k and K_{12} using equation 5.10, are plotted in Figure 5.5a versus k_s. Once more, it is possible to identify two subclasses of flows, since

$$\epsilon/P \approx 1 \quad for "small" k_s \tag{5.12}$$

$$\epsilon/P < 1 \quad for "large" k_s \tag{5.13}$$

The scatter of ϵ/P in the second subclass about a constant value 0.68 ± 0.06 seems to be non-systematic. Using the average values $\epsilon/P = 0.68$ and $K_{12} =$

−0.16, one can derive the relation

$$k \approx 0.1\, k_s \tag{5.14}$$

which, as shown in Figure 5.5b, is compatible with all measurements at sufficiently large k_s. The implication is that the asymptotic evolution of $\overline{q^2}$ in wind-tunnel confined, uniformly sheared turbulence depends on wind-tunnel shear constant k_s. For small k_s, $\overline{q^2}$ may be constant, while for large k_s it grows exponentially; in the latter case the exponent is proportional to k_s, although the ratio ϵ/P is independent of k_s. Independent estimates of the ratio ϵ/P, based on the measured Taylor microscale, are compatible with the existence of two distinct subclasses.

The present experiments cover a range of k_s that is substantially wider than those in previous ones. Although, in our opinion, the large-k_s range has been adequately described by equations (2.20) and (5.14), it would have been desired to further scrutinize the low-k_s range. Unfortunately, our attempts to decrease k_s by using high-solidity screens led to inhomogeneous flows. It is also clear that the uncertainty in the determination of k and ϵ/P increases dramatically as k_s decreases.

In addition to the above, we have tested several other possible criteria for the evolution of kinetic energy. For instance, a relevant parameter might be the quantity $(L/\overline{U}_c)\,(d\overline{U}_1/dx_2)$ where L is some scale characteristic of turbulent eddy size, i.e. the shear generator spacing, grid mesh size, L_{11} etc. None of these quantities was successful in separating the two subclasses of flows identified above, as can be seen by considering, for example, cases O and A, which have roughly

the same values of the above parameters but different energy laws.

5.2.4 On Hasen's Stability Theory

In her non-linear stability analysis of uniformly sheared flows, Hasen (1967) concluded that two-dimensional disturbances would decay if their amplitude were smaller than a "barrier" velocity and that they would not decay otherwise. She also found that the barrier velocity was bounded upwards and downwards by two quantities, which were proportional to the velocity

$$U_H = (l_H d\overline{U_1}/dx_2)/R_H^{2/3} \tag{5.15}$$

where l_H is the characteristic length of the disturbances and the Reynolds number was defined as

$$R_H = (d\overline{U_1}/dx_2)l_H^2/\nu \tag{5.16}$$

Substituting equation (5.16) into equation (5.15), one gets

$$U_H = \left[\frac{1}{l_H}\frac{d\overline{U}_1}{dx_2}\right]^{1/3} \nu^{2/3} \tag{5.17}$$

According to this theory, no finite-amplitude, two-dimensional disturbances would decay if $U_H \rightarrow 0$, which can occur either when $d\overline{U_1}/dx_2 = 0$ or when $l_H \rightarrow \infty$. Consequently, one might speculate that the lower U_H for a flow is, the "more unstable" the flow would be. This appears to contradict the intuitive expectation that for given l_H and ν, a flow should become "more stable" as $d\overline{U_1}/dx_2$

decreases. On the other hand, the implication of increased stability as l_H grows is compatible with intuition. Rose's (1970) attempt to correlate his results with Hasen's theory, is not conclusive in our opinion, first because, as indicated earlier, his few cases of alleged decaying turbulence are questionable, and second, because his study addresses only the effect of length scale and does not take into account the amplitude of disturbances. In grid turbulence, amplitudes and scales are inherently coupled, as demonstrated by the fact that the energy decay law is a function of grid mesh size; a large-mesh grid causes a large-amplitude disturbance. A proper test of Hasen's theory should involve a laminar shear flow and disturbances whose amplitudes and wavelengths should be independently controlled. In any case, calculations of U_H based on maximum apparatus spacing (Table 4) show that, in general, large values of U_H correspond to growing (unstable?) turbulence, in contrast to implications of Hasen's theory. In view of this discussion, the apparent success of using U_H as a criterion for the evolution of $\overline{q^2}$ (Karnik and Tavoularis, 1983) might be coincidental. The present discussion is consistent with the discussion by Rohr et al. (1988).

5.2.5 Scaling of the Turbulent Stresses

A general feature of self-preserving turbulent shear flows such as two- and three-dimensional wakes, jets, plumes etc. is that the "effective Reynolds number"

$$R_T = \frac{\Delta U \, l}{\nu_T} \tag{5.18}$$

(ΔU is a characteristic mean velocity difference, l is a transverse length characteristic of the mean flow extent and $\nu_T = -\overline{u_1 u_2}/(\partial \overline{U_1}/\partial x_2)$ is the "eddy viscosity")

shows small variation within each class of flows and has values comparable to the lower critical Reynolds number for laminar instability (Corrsin, 1957). The applicability of such a postulate to uniformly sheared flows is quite plausible, in view of their reasonable transverse homogeneity.

The parameters ΔU and l are, most likely, related to the imposed time scale τ_s as

$$\frac{\Delta U}{l} = \frac{d\overline{U_1}}{dx_2} = \tau_s^{-1} \tag{5.19}$$

which leads to the following expression for R_T

$$R_T = \frac{(d\overline{U_1}/dx_2)^2\, l^2}{-K_{12}\overline{q^2}} \tag{5.20}$$

containing l as the sole unspecified quantity. By analogy to other self-preserving shear flows, where l corresponds to a transverse width, one is tempted to use the wind-tunnel height, h, as the transverse scale l. Nevertheless, the resulting Reynolds number has too wide a range to be useful. Another length scale that might be appropriate as l is the integral length scale, L_{11}. Figure 5.6 shows that the corresponding Reynolds number, R_{TL}, generally increases with total strain but only mildly for the cases with growing stresses, reflecting the fact that the growth rates of stresses and L_{11} in such cases are not very different. A proposition that is equivalent to the universality of R_{TL} has been made by Harris et al. (1977). We note, however, that their Figure 5 appears to contain a numerical error reducing the difference between "low shear" and "high shear" results. Although the possibility

of such a universality cannot be discounted if the results were extrapolated to higher τ, Figure 5.6 does not provide such evidence.

L_{11} is not an externally imposed scale; however, as mentioned earlier, its starting value is related to the spacing of the flow generator(s). When measurements of L_{11} are not available, it would be useful to define R_T based on clearly defined external length. Among other choices, it seems that variation of R_T is reduced if the maximum among the spacings between the elements in the shear generator and/or grids or screens is used as l. The so computed R_{TM} (Table 4) presents a variation between 3.2 and 10.7 for the constant-stress cases, which is quite small, considering that the stresses themselves range over four orders of magnitude. In the cases with growing stresses, R_{TM} decreases monotonically downstream but its variation among different cases is also relatively small.

A related quantity, the ratio of eddy turnover time over the straining time,

$$\frac{\tau_e}{\tau_s} = \frac{L_{11}}{u_1'} \frac{d\overline{U}_1}{dx_2} \tag{5.21}$$

also has a relatively narrow range (Table 4), taking values between 1.9 and 3.7. The ratio of eddy lifetime over the straining time

$$\frac{\tau_u}{\tau_s} = \frac{1}{(\epsilon/P)\,(-K_{12})} \tag{5.22}$$

has nearly constant values, which are different for the two subclasses of flows, in contrast to Sreenivasan's (1985) conclusions based on earlier available data.

Chapter 6

CONCLUSIONS

The main conclusions of the present study can be summarized as follows:

6.1 On the Reduction of Shear with Screens

(1) A uniformly sheared flow remains uniformly sheared (with a reduced gradient), when it crosses a uniform screen, even at relatively large values of shear and flow disturbances.

(2) Predictions of the shear reduction factor based on earlier studies are accurate as long as the relative element thickness of the screen is small and an appropriate expression for K is utilized. For $d/h > 0.01$, the small disturbance assumption broke down and a shear reduction stronger than its prediction, occurs. Thus, large spacing screens are more effective in reducing mean flow non-uniformities than small spacing screens of the same solidity and shape.

(3) As a corollary of the above conclusion, one may deduce that any non-uniformity in the mean velocity of a stream crossing a uniform screen will be reduced in amplitude but, most likely, preserve its shape. This would apply to cases where the screen mesh size is small compared with the characteristic length of the non-uniformity.

(4) A low Reynolds number correction for the pressure loss coefficient seems to worsen rather than improve predictions of the shear reduction factor.

6.2 On the Turbulent Structure

(1) Uniformly sheared turbulent flows demonstrate a self-preserving structure, in which the dimensionless Reynolds stress ratios K_{ij} and the ϵ/P ratio remain essentially constant.

(2) Flows with sufficiently large shear parameter, k_s, have $\epsilon/P \approx 0.68$ and exhibit an exponential growth of the turbulent stresses. A linear relationship appears to exist between the coefficient in the exponential law and k_s.

(3) The existence of another class of flows with asymptotically constant stresses and $\epsilon/P \approx 1.0$ also seems to be compatible with measurements in flows with small values of k_s.

(4) The integral length scales grow according to a power law with an exponent of about 0.8, independent of the mean shear while the Taylor microscales, in general, approach constant values.

(5) The success of using a barrier velocity, U_H (Hasen, 1967), as a criterion for the evolution of $\overline{q^2}$ (Karnik and Tavoularis, 1983) might be coincidental considering that the present class of flows is not an ideal test of Hasen's stability theory.

Part B

DIFFUSION OF HEAT FROM A CONTINUOUS LINE SOURCE IN UNIFORMLY SHEARED FLOWS

Chapter 7

INTRODUCTION

7.1 Motivation

The ability of turbulence to mix and transport scalars such as heat, moisture, chemical reactants and pollutants has provided the motivation for much turbulence research. The study of diffusion is important in understanding the natural phenomena in the field of environmental engineering and in industrial processes which involve mixing and transport of scalars. Most research on scalar diffusion has been conducted in simplified turbulent flows, whose flow characteristics were known. Of course, it is presumed that the information so obtained would also be applicable to more complex flows which are of technological interest.

It has been documented that velocity shear plays a vital role in the mixing of contaminants in lakes, seas, rivers and the atmosphere. Although some theories and experiments have been reported on related topics, the mechanism of diffusion in the presence of a velocity shear has not been entirely understood. This provides the motivation to study the diffusion of contaminants from concentrated sources in turbulent flows subjected to a uniform shear.

7.2 Literature Survey

7.2.1 Diffusion in Isotropic Turbulence

The study of turbulent diffusion probably originated with the pioneering work of Taylor (1921). Since then Corrsin (1951, 1952) and Durbin (1982), among others, have provided further theoretical insight to the decay of temperature fluctuations in isotropic turbulence.

The lateral spread of heat from a fixed line source in nearly-isotropic (grid generated) turbulence has been studied experimentally most notably by Schubauer (1935), Collis (1948), Frenkiel (1950), Townsend (1951, 1954), Uberoi & Corrsin (1952), Schlien and Corrsin (1974), Warhaft (1984) and Stapountzis (1986). Numerical simulations which are consistent with experimental realizations have been presented by Libby & Scragg (1972), Sullivan (1976), Lumley (1978), Anand & Pope (1983), Pope (1981, 1983), Lumley & Van Cruyningen (1984) and Shih and Lumley (1986). Dispersion of heat from two fixed line sources in grid turbulence has been studied by Kistler (1956; an unpublished report) and Warhaft (1981, 1984).

Heat diffusion in nearly isotropic turbulence has also been studied by introducing a distributed temperature field with the use of electrically heated grids, screens and other devices. Experiments with a uniform mean temperature profile have been performed by Kistler, O'Brien & Corrsin (1956), Mills et al. (1958), Mills & Corrsin (1959), Yeh & Van Atta (1973), Lin & Lin (1973) and Sepri (1976),

Newman et al. (1977), Warhaft & Lumley (1978) and Sreenivasan et al. (1980) whereas cases with a uniform mean temperature gradient have been studied by Wiskind (1962), Alexopoulous & Keffer (1971), Venkataramani & Chervay (1978), Sirivat & Warhaft (1982), and Budwig et al. (1985). Sreenivasan et al (1981) have used a related experiment to assess the applicability of gradient transport models. Finally, studies of thermal mixing layers in isotropic turbulence have been conducted by Watt & Baines (1973), Keffer (1977) and La Rue (1981 a & b).

7.2.2 Diffusion in uniformly sheared turbulence

Corrsin (1952) was probably the first to examine diffusion in homogeneous shear flows. Discussion on the theory of dispersion in turbulent shear flow has been reviewed by Hinze (1961) and Monin & Yaglom (1973).

A number of the available analyses and experiments have considered the case of a uniform temperature gradient superimposed on the uniformly sheared velocity field. Analyses of such flows have been presented, among others, by Deissler (1962), Fox (1964) and Tavoularis & Corrsin (1985). The experiments of Tavoularis and Corrsin (1981, a & b) provide a detailed documentation of such a flow. Sreenivasan et al. (1981) focus their attention on evaluating the performance of gradient transport models whereas Tavoularis and Corrsin (1985) investigate the effect of mean shear on the diffusivity tensor. Riley & Corrsin (1974) have attempted to relate the turbulent diffusivities to the Lagrangian velocity statistics, whereas Riley & Corrsin (1976) and Jones and Musonge (1983) have presented numerical analyses for scalar transport in uniformly sheared turbulent flows.

There have been various attempts to study diffusion from a point source in

a uniformly sheared flow. These include, most notably, the analyses of Novikov (1958), Elrick (1962), Okubo & Karweit (1969), Huang (1979) and Hwang (1979) and the recent experiments of Nakamura et al (1986) and Sakai et al (1986).

Although Okubo & Karweit (1969) have presented a model for the diffusion of a passive scalar emanating from a fixed line source in a uniform shear flow, only recently, Stapountzis and Britter (1987) and Kyong and Chung (1987) have attempted to study this problem experimentally. Apart from these studies and the preliminary results of Tavoularis and Corrsin (1981a), using a single heating rod in their shear generator, there does not appear to be any literature available on the problem.

7.2.3 Diffusion in Boundary Layers

Related investigations include the study of diffusion in turbulent boundary layers and atmospheric turbulence. The theories of Batchelor (1964) and Yaglom (1976), the experiments of Poreh and Cermak (1964), Shlien and Corrsin (1976), Sreenivasan et al. (1976) and Antonia and Danh (1977, 1978) and the numerical simulations of Sullivan (1971) and Durbin and Hunt (1980) provide an insight to the problem of diffusion in boundary layers. The effect of wind shear on the diffusivity tensor has been studied , among others, by Saffman (1964), Gee & Davies (1963, 1964), Tyldesley & Wallington (1965) and Gee (1967).

7.2.4 Scalar Dispersion and Lagrangian Characteristics

Turbulent dispersion is inherently related to the material or Lagrangian velocity field. The direct measurement of the Lagrangian velocity, through observation of the motion of tagged particles, is cumbersome and the sparsely available

measurements are subject to considerable inaccuracies. A general theory of turbulent diffusion has not yet been developed, although several studies have been published, whose object were the "simple" cases of homogeneous turbulence and self-preserving flows such as decaying grid turbulence and two-dimensional or axisymmetric jets and wakes. A thorough exposition of previous findings can be found in the book by Monin and Yaglom (1973).

The study of diffusion was initiated by Taylor (1921), who derived a relationship between the dispersion of a scalar in homogeneous turbulence and the Lagrangian velocity statistics. This study was extended to decaying isotropic turbulence by Townsend (1954), who introduced the assumption of self-preservation of the Lagrangian velocity correlations. Further analytical and experimental results applicable to decaying, grid-generated turbulence have been reported by Corrsin (1952,1962), Uberoi and Corrsin (1953), Saffman (1963), Snyder and Lumley (1971), Shlien and Corrsin (1974) and Sato and Yamamoto (1987).

Among the few studies relating Lagrangian characteristics and turbulent dispersion in uniformly sheared turbulence are those by Corrsin (1953), O'Brien (1962), Riley and Corrsin (1971,1974) and Tavoularis and Corrsin (1985). All these studies utilize an unconventional decomposition of the Lagrangian velocity, which introduces some uncertainty into the estimates.

7.3 Objectives of Present Research

7.3.1 Diffusion from a Line Source

The computations of Okubo and Karweit (1969) predict that the mean tem-

perature profiles, which are Gaussian in isotropic turbulence, would be skewed towards the region of lower velocity when a continuous line source is placed in a uniformly sheared turbulent flow field. Measurements of diffusion from a point source by Nakamura et al. (1986) also indicate skewed profiles but with the locus of the peak mean temperature shifting towards the region of lower velocity contrary to the predictions of Okubo and Karweit (1969). The measurements of Stapountzis and Britter (1987), for a line source, revealed a symmetric temperature profile with the peak shifted to the side of the higher velocity. The results of Kyong and Chung (1987) will not be considered any further because they correspond to a case with extremely weak shear and a prominent effect of the heated source wake. The preliminary results of Tavoularis and Corrsin (1981 a) indicate a shift in the mean temperature peak towards the lower velocity region.

In the present experiments, the diffusion of heat from a line source in the presence of a uniform mean shear is studied. Although it is well known that exact transverse homogeneity is incompatible with the preservation of uniform shear (Harris et al., 1977), the present flow field exhibits improved transverse homogeneity compared to those in previous studies. The velocity field as well as the mean and fluctuating temperature fields are documented in detail. Having already established the fact that the velocity field attains a self preserving structure asymptotically (part A), it seemed worthwhile to investigate whether the temperature field is also self-preserving. Furthermore, the present study provides, for the first time, temperature-velocity statistics such as heat fluxes and higher correlations as well as probability density functions with the purpose not only to describe in-depth the diffusion process but also to generate a reliable database for testing

theoretical and computational models.

7.3.2 Estimate of Lagrangian Characteristics

The present study attempts to utilize the assumption of self-preservation of the Lagrangian correlations and scales for the specific case of uniformly sheared turbulence with stresses and scales that grow exponentially. The objective is to derive a relationship between scalar dispersion and the Lagrangian autocorrelation, which can be used to evaluate the latter from measurements of the temperature field behind a line source.

Chapter 8

MATHEMATICAL ANALYSIS

8.1 The Heat Diffusion Equation

The governing equation for the transport of a passive scalar in a turbulent flow viz. the diffusion equation can be written as

$$\frac{\partial T}{\partial t} + U_j \frac{\partial T}{\partial x_j} = \gamma \frac{\partial^2 T}{\partial x_j \partial x_j} \tag{8.1}$$

where T is a passive scalar (temperature) and γ is the thermal molecular diffusivity. Applying Reynolds decomposition to equation (8.1) we obtain

$$\frac{\partial \overline{T}}{\partial t} + \frac{\partial \theta}{\partial t} + (\overline{U_j} + u_j)(\frac{\partial \overline{T}}{\partial x_j} + \frac{\partial \theta}{\partial x_j}) = \gamma \frac{\partial^2 \overline{T}}{\partial x_j \partial x_j} + \gamma \frac{\partial^2 \theta}{\partial x_j \partial x_j} \tag{8.2}$$

where $\overline{U}$ and $\overline{T}$ are the ensemble mean components and u and θ are the fluctuating components of velocity and temperature respectively.

8.2 Balance Equation for the Mean Temperature

Averaging equation (8.2) we obtain a balance equation for the mean viz.

$$\frac{\partial \overline{T}}{\partial t} + \overline{U_j}\frac{\partial \overline{T}}{\partial x_j} = \gamma \frac{\partial^2 \overline{T}}{\partial x_j \partial x_j} - \frac{\partial \overline{u_j \theta}}{\partial x_j} \tag{8.3}$$

where

(a) the terms on the left hand side represent transport of the mean temperature,

(b) the first term on the right hand side represents molecular diffusion and

(c) the last term represents turbulent diffusion

In order to close the above equation, it is common to model the heat flux $\overline{u_j \theta}$ as a first order term using the gradient transport model of the form

$$\overline{u_i \theta} = -D_{ij}\frac{\partial T}{\partial x_j} \tag{8.4}$$

where D_{ij} is the *turbulent* or *eddy diffusivity.*

Although in the case of isotropic turbulent flows, D_{ij} is diagonal, this is not true for other flows as proved by Calder (1965) and observed experimentally by Tavoularis and Corrsin (1985).

Assuming stationarity, the balance equation for the mean temperature in the case of a continuous line source placed along the $x_3 - axis$ in a uniformly sheared flow with transversely homogeneous turbulent characteristics simplifies to

$$\overline{U}_1 \frac{\partial \overline{T}}{\partial x_1} = \gamma\left(\frac{\partial^2 \overline{T}}{\partial x_1^2} + \frac{\partial^2 \overline{T}}{\partial x_2^2}\right) - \left(\frac{\partial \overline{u_1 \theta}}{\partial x_1} + \frac{\partial \overline{u_2 \theta}}{\partial x_2}\right) \tag{8.5}$$

8.3 Balance Equation for the Mean Square Temperature Fluctuations

Subtracting equation (8.3) from equation (8.2) we obtain a balance equation for the fluctuating temperature as

$$\frac{\partial \theta}{\partial t} + \overline{U}_j \frac{\partial \theta}{\partial x_j} + u_j \frac{\partial \overline{T}}{\partial x_j} + \frac{\partial u_j \theta}{\partial x_j} - \frac{\partial \overline{\theta u_j}}{\partial x_j} = \gamma \frac{\partial^2 \theta}{\partial x_j \partial x_j} \tag{8.6}$$

Multiplying the above equation by θ and averaging, we obtain the balance equation for the mean square temperature fluctuations $\overline{\theta^2}$ as

$$\frac{\partial \overline{\theta^2}}{\partial t} + \overline{U}_j \frac{\partial \overline{\theta^2}}{\partial x_j} = -2\overline{\theta u_j} \frac{\partial \overline{T}}{\partial x_j} - \frac{\partial \overline{\theta^2 u_j}}{\partial x_j} + \gamma \frac{\partial^2 \overline{\theta^2}}{\partial x_j \partial x_j} - 2\gamma \overline{\frac{\partial \theta}{\partial x_j} \frac{\partial \theta}{\partial x_j}} \tag{8.7}$$

where the various terms in the above equation can be interpreted as follows :

(a) the terms on the left hand side represent the total rate of change of the temperature fluctuations.

On the right hand side,

(b) the first term represents the rate of production of the temperature fluctuations,

(c) the second term represents the transport of temperature fluctuations by turbulent velocity fluctuations,

(d) the third term represents the molecular diffusion of $\overline{\theta^2}$ and

(e) the final term, generally denoted as $-2\epsilon_\theta$, represents dissipation of the temperature fluctuations.

In the case of a continuous line source placed in a stationary uniformly sheared flow, the above equation simplifies to

$$\overline{U_1}\frac{\partial\overline{\theta^2}}{\partial x_1} = -2\overline{\theta u_1}\frac{\partial\overline{T}}{\partial x_1} - 2\overline{\theta u_1}\frac{\partial\overline{T}}{\partial x_2} - \frac{\partial\overline{\theta^2 u_1}}{\partial x_1} - \frac{\partial\overline{\theta^2 u_2}}{\partial x_2} + \gamma(\frac{\partial^2\overline{\theta^2}}{\partial x_1^2} + \frac{\partial^2\overline{\theta^2}}{\partial x_2^2}) - 2\epsilon_\theta \quad (8.8)$$

8.4 Derivation of a Relationship between Scalar Dispersion and Lagrangian Velocity Statistics

8.4.1. Background Analysis

Consider an incompressible turbulent flow that has a zero mean velocity along the direction x_i. Then, the displacement, X_i, of a fluid particle, occupying the origin at time t=0 is, by definition, the integral of its Lagrangian velocity fluctuation v_i. In general, the Lagrangian displacement is a function the initial position $X_{i0}(t_0)$ and current time, t. However, in the present analysis all particles will be assumed to originate at the same position and for simplification in the notation, the dependence upon X_{i0} will not be shown in the following. Therefore,

$$X_i(t) = \int_0^t v_i(t_1)dt_1. \quad (8.9)$$

For homogeneous turbulence, Taylor (1921) demonstrated that the mean square particle displacement can be expressed as

$$\overline{X_i^2}(t) = 2\int_0^t v_i'(t_1)\int_0^{t_1} v_i'(t_1-\tau)R_L(t_1,\tau)d\tau dt_1 \tag{8.10}$$

where repeated indices are not summed and the Lagrangian autocorrelation coefficient is defined as

$$R_L(t,\tau) = \frac{\overline{v_i(t)v_i(t-\tau)}}{v_i'(t)v_i'(t-\tau)} \tag{8.11}$$

If the flow is also stationary, $(v_i'(t) = v_i'(t-\tau) = v_i')$ then R_L becomes a function of the time delay τ alone, and Equation (8.10) is simplified into

$$\overline{X_i^2}(t) = 2v_i'\int_0^t\int_0^{t_1} R_L(\tau)d\tau dt_1 \tag{8.12}$$

which, after double differentiation, leads to the simple relationship

$$R_L(\tau) = \frac{1}{2\overline{v_i^2}}\left[\frac{d^2\overline{X_i^2}}{dt^2}\right]_{t=\tau} \tag{8.13}$$

In the absence of heat conduction by molecular motions, the particle dispersion $\overline{X_i^2}$ is equal to the second moment of the mean temperature field resulting from a continuous heating source at the origin (Townsend, 1954), so that $R_L(\tau)$ can be estimated from measurements of heat diffusion.

In non-stationary flows, Equation (8.10) cannot, in general, be simplified. However, following Townsend (1954), one may derive relationships similar to Equation (8.13) for classes of flows in which the Lagrangian velocity field is self-preserving. According to this procedure, the dimensionless velocity $v_i(t)/u_i'(t)$ is assumed to

be a stationary random variable of a dimensionless time, η, defined as

$$\eta(t) = \int_0^t \frac{dt}{t_s(t)} \tag{8.14}$$

where the local time scale $t_s(t)$ is the ratio of a characteristic length scale and a characteristic Eulerian r.m.s. velocity $u_i'(t)$. (Note: the analysis of Sato and Yamamoto (1987) normalizes velocity and time using the Lagrangian r.m.s. velocity). After further replacing v_i' by u_i' in the definition of R_L (Equation 8.11), the assumption of self preservation implies that $R_L(t,\tau)$ is a function of the dimensionless time difference

$$\Delta\eta(t,\tau) = \eta(t) - \eta(t-\tau) = \int_{t-\tau}^{t} \frac{dt_1}{t_s(t_1)} \tag{8.15}$$

With proper expressions for $u_i'(t)$ and $t_s(t)$ introduced into Equation(8.10), one may derive an integral equation for $R_L(\Delta\eta)$, which, if solved, would provide the desired relationship between R_L and $\overline{X_i^2}$.

8.4.2. An Analysis Applicable to Uniformly Sheared Flows

The first step in the analysis would be to define laws for the temporal evolution of the r.m.s. velocity fluctuation and of the dimensionless time η. The present class of flows is stationary and transversely homogeneous with essentially zero mean velocity in the x_2-direction, but they evolve in the x_1-direction, which is the direction of the mean speed. Since the turbulent intensity is generally small, it is possible to approximate the diffusion time t by the quantity $x_1/\overline{U_1}$ (see, for example, Uberoi and Corrsin, 1953), thus replacing spatial inhomogeneity with

non-stationarity in a frame convected with the local mean field. The transverse variation of $\overline{U_1}$ should have only a small effect on the analysis for relatively narrow ranges of X_2.

The exponential growth of $u_2'(x_1)$ has been well documented. However, the growth rate of the integral length scales has not been entirely clarified, although exponential laws could be fitted to the measurements within limited ranges. An analysis based on the different growth rates for the velocity and length scales was carried out but resulted in an integral equation that could not be solved. For simplicity, the present study will focus on the particular case when u_2' and L_{22} grow exponentially at identical rates. This case corresponds closely to measurements in the unobstructed flow (part A) and to the measurements by Harris et al. (1977) and by Tavoularis and Corrsin (1985).

In this case, the local time scale, $t_s(t)$, which is proportional to the ratio L_{22}/u_2', is a constant. Then, the dimensionless time η is proportional to the diffusion time t and the autocorrelation R_L becomes stationary in the variable t. The physical explanation for this result is that, although the size of the turbulent eddies (which represent typical distances that fluid particles must travel) grows downstream, the kinetic energy of these particles also grows at such a rate that the time for completing one mean path remains unaltered. Substituting $u_2'(t) = u_{20}'e^{k_u t}$ instead of $v_2'(t)$ in Equation (8.10) one gets

$$\overline{X_2^2}(t) = 2\overline{u_{20}^2}\int_0^t e^{2k_u t_1}\int_0^{t_1} e^{-k_u \tau} R_L(\tau)\, d\tau\, dt_1. \qquad (8.16)$$

After differentiation w.r.t. t, Equation (8.16) becomes

$$\frac{1}{2\overline{u_{20}^2}e^{2k_u t}}\frac{d\overline{X_2^2}(t)}{dt} = \int_0^t e^{-k_u \tau} R_L(\tau) d\tau \tag{8.17}$$

and after one more differentiation, one gets the following expression for the Lagrangian autocorrelation coefficient

$$R_L(t) = \frac{e^{-k_u t}}{2\overline{u_{20}^2}}\left[\frac{d^2\overline{X_2^2}}{dt^2} - 2k_u\frac{d\overline{X_2^2}}{dt}\right] \tag{8.18}$$

If the function $\overline{X_2^2}(t)$ is known through measurement or analysis, then the function $R_L(t)$ can be integrated to provide the Lagrangian integral scale, $\mathcal{L}$, and expanded in a Taylor series to provide the Lagrangian microscale, λ_L.

Chapter 9

EXPERIMENTAL APPARATUS AND MEASUREMENT PROCEDURES

The flow facility used to study the diffusion of a passive scalar in uniformly sheared turbulent flows was the same as that used in part A. A detailed description of this facility along with particulars of the velocity measuring techniques has been presented in Chapter 3. Improvements or additions to the instrumentation are described in the following sections.

9.1 The Heating System

The heating system shown in Figure 9.1 consists of a wooden frame which could be inserted into slots provided in the wind tunnel test section. The vertical walls of the frame were fitted with rectangular metal blocks which supported conductive pins. The heating element, which was stretched across the vertical walls of this wooden frame, was fixed to a conductive pin at one end and after being passed around a similar pin at the other end it was threaded through the frame. The free end of the element supported weights to prevent it from sagging at elevated temperatures. The metallic blocks were connected to a variable voltage source

(Powerstat, The Superior Electric Co., USA) with a full scale output of 100 volts, so as to produce the desired amount of heat. The heating system was inserted in the wind tunnel test section at $x_1/h = 4.6$ (as shown in Figure 9.2) since experimental evidence showed that, at this position, the flow had reached an asymptotic state and was not contaminated with initial shear generator non-uniformities.

For measurements close to the source, a nichrome wire with diameter d=0.051mm and supplied with approximately 7 W/m power was used. At a mean centerline velocity $U_{1c} = 13.0$m/s , the Reynolds number, based on the kinematic viscosity of the air in the vicinity of the heated wire, was estimated to be 22. This estimate was lower than the critical value of 40, above which vortex shedding might occur. It was found that in order to obtain measurable signals further downstream, it would be necessary to release more heat than a single cylindrical wire could withstand in the low Reynolds number regime. Thus, a heating ribbon (toaster element) with a thickness t=0.13mm and a width of 0.528mm, provided with approximately 70 W/m was used as a source; it was expected that the temperature field of this source would approximate that of a line source at a sufficient downstream distance. The Reynolds number based on the thickness of the element and at the mean speed of 7.8 m/s used for these tests was approximately 67 at ambient temperature and approximately 15 at the film temperature of about 700°C.

The possibility of vortex shedding with the ribbon considered as a bluff body could be ruled out on the basis of the low Re. The possibility of unsteady flow separation due to random incidence caused by turbulence was also remote, because the maximum instantaneous angle of attack of the effective velocity (corresponding

to a typical maximum transverse velocity fluctuation) for the present flow was about 2.5degrees, much less than the stall angle for symmetrical airfoils.

In order to test for the presence of buoyancy effects the flux Richardson number

$$R_f = \frac{g}{\overline{T}} \frac{\overline{\theta u_2}}{\overline{u_1 u_2} \frac{d\overline{U_1}}{dx_2}} \tag{9.1}$$

was evaluated in a region where the transverse temperature gradient was dominant. In the region of lower velocity R_f varied, with downstream distance, from 0.03 to 0.01 in the range $4 < x_\theta/M < 84$. In the region of higher velocity R_f had similar values but changed sign. In conclusion, values of R_f were found to be lower than the critical value of 0.2.

9.2 The Calibration Tunnel

The calibration tunnel shown in Figure 9.3 was specially designed and constructed at the University of Ottawa. The flow, produced by a centrifugal blower, was passed through various turbulence reducing screens, a settling chamber and then through a 24:1 converging section with a 22.5mm exit diameter to generate a uniform jet. The flow was heated with the use of heaters, located immediately following the fan, to facilitate the calibration of temperature probes. The probes could be mounted on a swivelling mechanism so that they could be positioned at any desired angle w.r.t the axis of the jet.

9.3 Temperature Measuring Instrumentation

The mean temperature was measured with glass coated thermistor miniprobes (Fenwal Electronics, 2000 Ω beads). These beads were mounted on slender sup-

ports (2mm diameter, 185mm long) in order to reduce probe interference. The mini-probes were operated with a home-made, linear response electronic circuit, shown in Figure 9.4. The circuit, which could operate up to two thermistors, provided the analog difference between the response of the two thermistors in addition to their individual outputs.

The fluctuating temperature was measured with a 1.3μm platinum wire (Dantec type 55P31) operating at a constant current of 0.32mA supplied by an active bridge (Tavoularis, 1978). A diagram of this constant temperature circuit is shown in Figure 9.5. The circuit consists of (a) an adjustable voltage source, consisting of a low-drift battery (mercury cell) connected to a voltage follower through a variable resistor and (b) a voltage to current converter which supplies the cold wire with a constant current. The frequency response of the system is determined mainly by the cold wire thermal inertia. Although a test of the dynamic responce of the cold wire was not performed, Hojstrup et al. (1976) have found that the 3-dB cut off frequency of the response of temperature fluctuations for platinum wires in the range between 0.2μm and 1.0μm was between 2 and 5 kHz.

9.4 Analog Signal Conditioning

The temperature signals were conditioned with the use of Tektronix 5A22N instrumentation amplifiers with built-in low pass filters described in section 3.3. The cross-wire signals were processed with two home-made signal conditioning circuits. The circuit diagram shown in Figure 9.6 was the same for both circuits. The circuit consisted of a cascade of two 2-pole Butterworth filters with 3-dB cut off frequency settings of 1,3,5,10 KHz and provided amplification factors of

0.5,1.0,2.0,5.0,10.0 and 50.0. In order to obtain DC output values within the range of the analog-to-digital converter (±10V), the circuit was provided with a voltage source which could superimpose a positive or negative offset on the input signal. The frequency response of the system, obtained by using a sine wave with a typical voltage signal as an input, is shown in Figure 9.7.

9.5 Data Acquisition System

The conditioned signals from the sensors were digitized with the use of a PC-controlled data acquisition system. The data acquisition system consisted of a DT2828 high speed analog and digital input/output board (Data Translation Inc.) mounted on a IBM-PC-AT compatible personal computer (System 1800). The A/D board featured a 5mV resolution (12bit, ±10V input range), four simultaneous sample and hold input channels and a maximum throughput rate of 100KHz. The PC supported a hard disk with a 20MB storage capacity and a 1MB Random Access Memory (RAM). The signals, suitably amplified to use the resolution of the system to advantage, were stored on high capacity (1.2MB) 5.25in. diskettes and subsequently processed with user written software (FORTRAN). Other peripheral units were a TTL 720/350 monochrome monitor and a Star SG10 dot matrix printer.

9.6 Measurement Procedures

9.6.1 Measurement of Velocity

The measurement procedure for velocity has been described in detail in Chapter 3. In the present case, due to the presence of the heated source, the fluid

temperature could no longer be assumed to be constant and corrections to the hot-wire signal for temperature contamination were necessary. As presented earlier, the effective cooling velocities for the two wires can be written as

$$U_{eff1} = \left[\frac{(\frac{E_1^2}{T_{op1} - T_f}) - A_1}{B_1} \right]^{1/n_1} \tag{9.2}$$

$$U_{eff2} = \left[\frac{(\frac{E_2^2}{T_{op2} - T_f}) - A_2}{B_2} \right]^{1/n_2} \tag{9.3}$$

The instantaneous measurement of temperature from the cold wire was used in the evaluation of these effective cooling velocities. Then, the various components of velocity were evaluated following the procedure outlined in section 3.2.

9.6.2 Mean Temperature

The thermistors were calibrated in the heated jet of the calibration tunnel versus a mercury thermometer with a 0.1°C resolution. The thermistor circuits were adjusted such that the individual calibration curves (Figure 9.8) had the same slopes. This facilitated the direct measurement of the difference in the output of the two thermistors. To account for the drift in ambient temperature, the temperature rise above the ambient was measured. The ambient temperature was monitored upstream of the heating source.

The thermistor signals were amplified so as to obtain a sensitivity of 0.455 V/°C. Thus with the 0.5mV resolution of the ADAC 1012 and the 5mV resolution of the DT2828, temperatures as low as 0.001°C and 0.01°C respectively were measurable. The signals were low-pass filtered to eliminate contamination due to noise.

9.6.3 Fluctuating Temperature

The "cold" wire was calibrated in the heated jet of the calibration tunnel using a previously calibrated thermistor probe as a reeference. Due to the low level of the temperature signal, an amplification of 5000 was necessary. However, for the purpose of calibration, the cold wire signal was amplified by a factor of 1000 since higher gains resulted in a considerable drift of the DC output of the amplifier. A typical calibration equation for the cold wire is shown in Figure 9.9; its sensitivity to temperature was 0.04V/°C at a gain of 1000.

The temperature fluctuations were recorded using a gain of 5000. The signal was low-pass filtered to eliminate the high frequency noise. A typical power spectrum of a cold wire signal in a similar configuration (Tavoularis, 1978) indicates that more than 95% of the temperature signal is contained in the part of the spectrum below 500Hz. Consequently, the cold wire signal was filtered at 3kHz (3dB cut off).

Although it has been established that for currents less than 0.4mA the cold wire is practically insensitive to velocity changes (Tavoularis, 1978), this fact was confirmed by traversing the wire in the unheated shear flow. Apart from random scatter, the cold wire response remained unchanged. The rms output of the cold wire in the unheated flow, $\sqrt{\overline{e_n^2}}$ (frequently termed as noise), was equivalent to a rms temperature fluctuation of 0.013°C. The signal to noise ratio, defined as $(\overline{e_\theta^2} - \overline{e_n^2})/\overline{e_\theta^2}$, where $\overline{e_\theta^2}$ is the mean square cold wire signal in a heated flow, was at worst 60%. Assuming that the noise was statistically independent of the temperature fluctuations, simple corrections were applied to the cold wire signal to eliminate

noise contamination.

9.7 Computational Procedures

A discretized time history of the cross-wire signals and the temperature signal u_{1k}, u_{2k}, and θ_k, $k = 1, 2, ...N$ was acquired. The number of points, N, for each signal was 96,000 and the time interval ΔT between consecutive values was 0.3msec. The total sample time was 28.8sec which was at least 5000 times the largest integral time scale of the flow.

The one-point moments, two-point correlations, length scales and microscales for u_1, u_2 and θ were evaluated as outlined in section 3.4. The following sub-section provides the computational procedure for the probability density functions which is limited by measuring resolution and computer capacity.

9.7.1 Evaluation of Probabilities

The discrete time history was transformed into a normalized time history

$$s_k = \frac{\theta_k}{\sigma_\theta} \tag{9.4}$$

by dividing it by the standard deviation σ_θ. The probability density $P_s(\eta)$ of the normalized signal was then computed as

$$P_s(\eta) = \frac{P(\eta - \frac{w}{2} \leq s_k \leq \eta + \frac{w}{2})}{w} \tag{9.5}$$

where the numerator on the right hand side of equation (9.5) represents the number of data points in the interval $\left[\eta - \frac{w}{2}, \eta + \frac{w}{2}\right]$ divided by the total number of points

N. The window w was chosen depending on the value of η (wider windows were used for larger η). By definition,

$$\int_{-\infty}^{\infty} P_s(\eta)d\eta = 1 \qquad (9.6)$$

The joint probability density function of two simultaneously sampled discrete time histories e.g. velocity fluctuation u_{ik} and temperature fluctuations θ_k, $k = 1, 2, ...N$, were calculated by normalizing the two time histories as

$$s_k = \frac{u_{ik}}{\sigma_{u_i}} \qquad (9.7)$$

and

$$r_k = \frac{\theta_k}{\sigma_\theta} \qquad (9.8)$$

The joint probability was then computed as,

$$P_{s,r}(\eta, \zeta) = \frac{P(\eta - \frac{w}{2} \leq s_k \leq \eta - \frac{w}{2}, \zeta - \frac{w}{2} \leq r_k \leq \zeta - \frac{w}{2})}{w^2} \qquad (9.9)$$

By definition,

$$\int_{-\infty}^{\infty}\int_{-\infty}^{\infty} P_{s,r}(\eta, \zeta)d\eta d\zeta = 1 \qquad (9.10)$$

Chapter 10

MEASUREMENTS

10.1 The Velocity Field

Detailed measurements presented in part A of this thesis have established the downstream constancy and the spanwise uniformity of the mean shear. A study of the turbulent characteristics has also been documented in part A.

Although, as mentioned earlier, exact transverse homogeneity is not possible in unbounded uniformly sheared flows, it was desirable to have the least possible inhomogeneity within the region of interest in order to isolate the effect of mean shear on diffusion. Further improvement of the homogeneity level reported earlier (part A) was accomplished by finely adjusting the screens in the shear generator. Although, as expected, the mean shear was sensitive to such changes, Figure 10.1 shows that a clearly improved transverse homogeneity was achieved with only a slight distortion of the mean shear, which remained reasonably uniform and maintained a near downstream constancy. Confirmation of the exponential growth (part A) of the Reynolds stresses is documented in Figure 10.2 in which x_θ is the distance downstream from the source. Figures 10.1 and 10.2 also illustrate that, except in the vicinity of the source, the velocity field was unaltered by the addition of heat to the flow, thus emphasizing the passivity of the scalar.

Figures 10.3 and 10.4 respectively present the transverse mean and rms velocity profiles in the shear flow downstream of the ribbon and the nichrome wire . In both cases, the velocity deficit is visible near the source but not further downstream.

10.2 The Mean Temperature Field

The mean temperature field near the line source was studied with the use of the 0.051mm diameter wire as a heating source whereas the field further downstream was studied with the use of the ribbon. Transverse mean temperature profiles near the source at various stations downstream of the 0.051mm diameter wire are presented in Figure 10.5a. The profiles appear to be nearly Gaussian in conformity with the findings of Stapountzis and Britter (1987); the peaks are on the axis except very close to the wire, where a slight buoyancy effect is manifested by a shift of the peak towards positions of higher velocity. Transverse mean temperature profiles downstream of the ribbon are shown in Figure 10.5b. Near the source, except for the slight buoyancy effect, the profiles are also nearly Gaussian. However, further downstream the profiles appear to be shifted towards the region of lower velocity with the position, x_{2P}, of the peak mean temperature also shifting in the same direction (Figure 10.6). A similar observation was made by Nakamura et al. (1986) for diffusion from a point source in a uniform shear flow. The observation of symmetric profiles by Stapountzis and Britter (1987) is compatible with the present results, if one considers that their measurements did not extend sufficiently far from the source, where the effect of shear on diffusion would be measurable. Their observation of a shift of the peak temperature towards the region of higher velocity could possibly be due to buoyancy rather than to shear.

The growth of the half-width, S, of the mean temperature profile, defined as half the distance between points having a temperature rise which is 50% of the centerline value, $\Delta\overline{T_c}$, is shown in Figure 10.7. The growth rate appears to be nearly linear and near the source it seems to be comparable to that observed in isotropic turbulence; further downstream, this growth rate remains roughly constant but it is faster than that in isotropic turbulence. Figure 10.8 presents the loci of points with mean temperature at a particular fraction of $\Delta\overline{T_c}$ whereas Figure 10.9 shows some mean iso-therms on the wind tunnel centerplane. Both these figures provide further evidence of the shift of the mean temperature profiles.

Measurements of the downstream decrease of the centerline mean temperature rise are presented in Figure 10.10 along with measurements in isotropic turbulence (Warhaft, 1984; Stapountzis et al., 1986) and in uniformly sheared flows (Tavoularis and Corrsin, 1981a). It should be noted that, since the peak mean temperature rise, $\Delta\overline{T_p}$, was not appreciably different from $\Delta\overline{T_c}$, the decrease of $\Delta\overline{T_p}$ can also be deduced from Figure 10.10. The decay rate of $\Delta\overline{T_p}$ in the shear flow could be fitted, within limited ranges, by power laws of the type

$$\Delta\overline{T_p} \propto (x_\theta/M)^{-n} \tag{10.1}$$

Two distinct patterns of decay could be observed; one near the thin wire source with $n \approx 1.0$ and the other downstream of the ribbon with $n \approx 0.75$. These exponent values are not very different from the ones observed in isotropic turbulence. In the latter case these values were found to be in the range $n \approx 1.0$ to 1.2 near the source and $n \approx 0.8$ further downstream (see Warhaft, 1984 and Stapountzis

et al., 1986).

10.3 The Fluctuating Temperature Field

The transverse distribution of the mean square temperature fluctuations is shown in Figure 10.11. Close to the source, the profiles exhibit distinct double peaks which are suppressed in an intermediate region but reappear prominently further downstream. The peak on the side of higher velocity is greater than that on the lower side. Double peaks have also been observed in the shear flow experiments of Tavoularis and Corrsin (1981 a) and in the isotropic turbulence experiments of Warhaft (1984). A possible explanation of double peaking will be presented in the discussion.

The downstream development of the centerline mean square fluctuations is presented in Figure 10.12. A simple power law of the type

$$\overline{\theta_c^2} \propto (x_\theta/M)^{-n_\theta} \tag{10.2}$$

cannot be fitted to the entire range. Near the source, a value $n_\theta \approx 1.7$ seems appropriate, whereas further downstream the decay is faster, corresponding to $n_\theta \approx 3.2$. The decay close to the source is not very different from that observed in isotropic turbulence which ranges from 1.5 to 1.8 (see Sreenivasan et al., 1980, Warhaft, 1984 and Stapountzis et al., 1986). Figure 10.13 indicates that the ratio of the centerline values of the rms temperature fluctuation and the mean temperature difference approaches a downstream value of 0.15, substantially lower than the value of 0.7 obtained in isotropic turbulence. The value 0.15 is also

compatible with the preliminary measurements of Tavoularis and Corrsin (1981a).

10.4 Integral Length Scales and Microscales

The velocity and temperature integral length scales were evaluated by integrating respective autocorrelation functions to their first zero and using Taylor's "frozen flow" approximation. The autocorrelation functions for the streamwise velocity fluctuation u_1, the transverse velocity fluctuation u_2 and the temperature fluctuation θ are shown in Figure 10.14 for two typical downstream positions. A typical transverse distribution of the integral scales, presented in Figure 10.15, indicates reasonable uniformity.

The downstream development of the integral length scales along the centerline is presented in Figure 10.16. Near the source, these scales are affected by the wake of the source, but away from it they achieve growth rates comparable with those presented in part A. The growth rate for $L_{22,1}$, is not very different from that for $L_{11,1}$, and the ratio $L_{22,1}/L_{11,1}$, is approximately 0.3. Considering the uncertainty involved in measuring the length scales this ratio is not too far from the value of 0.23 measured by Tavoularis and Corrsin (1981 a). The ratio $L_{\theta\theta,1}/L_{11,1}$ appears to approach an asymptotic value of 0.82 which is not very different from the values of 0.76 and 0.83 observed in the shear flow measurements of Tavoularis and Corrsin (1981 a) and the heated grid experiments reported by Sreenivasan et al. (1980) respectively.

The Taylor microscales and the Corrsin microscale were evaluated according

to the definitions

$$\lambda_{11} = \overline{U_1}\left[\frac{\overline{u_1^2}}{\overline{(\partial u_1/\partial t)^2}}\right]^{0.5} \tag{10.3}$$

$$\lambda_{21} = \overline{U_1}\left[\frac{2\overline{u_2^2}}{\overline{(\partial u_2/\partial t)^2}}\right]^{0.5} \tag{10.4}$$

$$\lambda_{\theta 1} = \overline{U_1}\left[\frac{2\overline{\theta^2}}{\overline{(\partial \theta/\partial t)^2}}\right]^{0.5} \tag{10.5}$$

Figure 10.17(a) shows that the transverse distributions of the microscales λ_{11}, λ_{21} and $\lambda_{\theta 1}$ are fairly uniform although some values appear to increase slightly in the direction of the shear, as also observed by Tavoularis (1985). The downstream development of $\lambda_{11}, \lambda_{21}$ and $\lambda_{\theta 1}$ (Figure 10.17b) indicates the attainment of nearly constant asymptotic values, as observed in previous experiments (Tavoularis and Corrsin, 1981 a). The asymptotic values of the ratios $\lambda_{21}/\lambda_{11}$ and $\lambda_{\theta 1}/\lambda_{11}$ are 0.85 and 1.23, which are comparable to the values 0.68 and 0.87 measured by Tavoularis and Corrsin (1981 a).

10.5 Skewness Factors and Temperature-Velocity Correlations

Skewness factors were evaluated according to their definitions e.g. $S_{u_1} = \overline{u_1^3}/(u_1')^3$, where the third moments were evaluated as outlined in section 3.4.

Measurements of skewness factors for the two components of velocity and the temperature are presented in Figure 10.18. Transverse measurements of the skew-

ness factor for temperature (S_θ) at various downstream positions (Figure 10.18a) indicate that S_θ is positive with a minimum value near the axis of the plume. The downstream decrease in the centerline values of S_θ is shown in Figure 10.18(b) along with the skewness factors for the velocity components (S_{u_1} and S_{u_2}). As expected in homogeneous turbulence, S_{u_1} and S_{u_2} tend to vanish.

Transverse profiles of the correlation coefficients $\rho_{u_1\theta} = \overline{u_1\theta}/u_1'\theta'$ and $\rho_{u_2\theta} = \overline{u_2\theta}/u_2'\theta'$ are presented in Figure 10.19. These coefficients have opposite signs and they reverse signs near the location of the peak mean temperature. $\rho_{u_2\theta}$ is approximately -0.37 on the side of the lower velocity and 0.34 on the side of the higher velocity. A similar behavior has been observed in a related experiment performed by Sreenivasan et al.(1981) where the values changed from -0.5 to 0.35. Complementing this behaviour, $\rho_{u_1\theta}$ changes from about 0.44 on the side of lower velocity to -0.46 on the side of higher velocity.

Figures 10.20 presents transverse distributions of the triple correlation coefficients $\overline{\theta^2 u_1}/\overline{\theta^2}u_1'$ and $\overline{\theta^2 u_2}/\overline{\theta^2}u_2'$. As in the case of $\rho_{\theta u_1}$ the correlation coefficient $\overline{\theta^2 u_1}/\overline{\theta^2}u_1'$ (Figure 10.20a) changes sign from positive values in the region of lower velocity to negative values in the region of higher velocity. However, the values in each region grow in magnitude away from the centerline and there appears to be a region of near constancy coinciding with the region having a small mean temperature gradient, before the change in sign occurs. Qualitatively, the transverse profile for $\overline{\theta^2 u_2}/\overline{\theta^2}u_2'$ (Figure 10.20b) shows similar trends but is of opposite sign to the $\overline{\theta^2 u_1}/\overline{\theta}u_1'$ profile.

Transverse profiles for $\overline{u_1^2\theta}/\overline{u_1^2}\theta'$ and $\overline{u_2^2\theta}/\overline{u_2^2}\theta'$ are presented in Figure 10.21.

These profiles are very similar to each other and indicate a change in sign twice; once in the region of lower velocity and again in the region of higher velocity. Finally, the profiles of $\overline{u_1 u_2 \theta}/u_1' u_2' \theta'$, shown in Figure 10.22, appear to be mirror images of the profiles in Figure 10.21.

It is interesting to note that the transverse profiles of all the above correlations measured at three downstream stations nearly collapse when plotted versus the normalized distance x_2/S, indicating that the structure of the temperature field demonstrates self-preserving features. Exact self-preservation is, of course, not attained, as, for example, evidenced by the developing skewness in the mean temperature profile and the growth of double peaks of θ'.

Downstream measurements of the temperature-velocity correlations (shown in Figures 10.23a,b,c) reveal that at large diffusion times the heat fluxes $\overline{u_i \theta}$ and the triple correlations $\overline{u_i^2 \theta}$, $\overline{u_i u_j \theta}$ and $\overline{\theta^2 u_i}$, normalized by appropriate local values, seem to reach constant asymptotic values.

10.6 Probability Density Functions

The probability density functions (pdf) of the two velocity components u_1 and u_2, shown in Figure 10.24, closely match the standard normal distribution function also represented in the Figure. Such a behaviour has also been observed by Tavoularis and Corrsin (1981a). On the other hand, the pdf of the temperature fluctuation on the centerline shows a measurable deviation from Gaussianity and a skewness that increases with distance from the centerline (Figure 10.25). The pdf of θ at positions with the same fraction of $\Delta \overline{T_p}$ appear to be very close to each

other.

The joint pdf of the two velocity components, shown in Figure 10.26, corroborates the observation of Tavoularis and Corrsin (1981 a) that this quantity is not very different from a jointly normal pdf with the same correlation coefficient. The joint pdf of each of the velocity components and the temperature fluctuations, shown in Figure 10.27, indicate increasing deviation from Gaussianity with increasing distance from the centerline.

Chapter 11

ANALYSIS AND DISCUSSION OF RESULTS

11.1 Mean Temperature Profiles

As mentioned earlier, the computations of Okubo and Karweit (1969) predicted that, in the presence of a mean shear, the mean temperature profiles would be skewed towards the region of lower velocity and that the location of the peak mean temperature would shift towards the region of higher velocity. Physically this was explained by noting that, at a given distance from the source, diffusion in eddies convected at a high mean speed would have occurred for less time than that in eddies with low mean speed.

A close examination of Figures 10.8 and 10.9 reveals that, at a given x_0, the spread of the isotherms w.r.t the position of the peak mean temperature is greater in the region of low velocity than in the region of high velocity. The asymmetry of the mean temperature profile is illustrated more clearly in Figure 11.1, showing the transverse mean temperature gradient distribution. Not only is the magnitude of this gradient generally higher on the high-speed side, but its asymmetry increases downstream, as evidenced, for example, by the increase of the ratio of maximum gradient magnitudes of the high-speed and low-speed sides from 1.13 at $x_0/M = 48$ to 1.33 at $x_0/M = 84$. A similar asymmetry in the mean temperature profiles has also been observed in the experiments of Nakamura et al. (1986) and

Tavoularis and Corrsin (1981a), while the reported symmetry in the profiles measured by Stapountzis and Britter (1987) was possibly due to the fact that their measurements were in a region where the effect of the mean shear was not measurable. The observed higher spread of isotherms towards the low-velocity region is consistent with the physical explanation provided earlier. The same consideration of the convection over diffusion ratio alone would imply that the location of the peak mean temperature should move towards the high-velocity region. However, the present experiments, as well as those of Nakamura et al. (1986) and Tavoularis and Corrsin (1981 a), indicate that the locus of the peak mean temperature shifts monotonically towards the region of lower velocity. A clear explanation for this shift has not yet been found.

11.2 Temperature Fluctuations

The phenomenon of the occurrence, suppression and subsequent re-appearance of the double peaks in the r.m.s. temperature fluctuation profiles deserves further attention. Temperature fluctuations are produced "locally" in regions of non-zero mean temperature gradient as well as transported from neighbouring regions by turbulent motions.

The ratio between the rms temperature fluctuations and the magnitude of the local mean temperature gradient, $\mid \partial\overline{T}/\partial x_2 \mid$, shown in Figure 11.2, is fairly constant away from the position of mean temperature peak, although θ' varies considerably across the flow, with generally higher values in the high velocity region. This observation is in perfect agreement with the concept of gradient transport in a transversely homogeneous turbulent field,

If local production were the only source of temperature fluctuations (and if one neglects production by the weak streamwise gradient), then θ' should vanish at locations of peak mean temperature. However, temperature fluctuations are also transported by turbulent eddies originating in regions where θ is produced. Therefore, the size of these eddies becomes an important parameter.

If the size of these eddies is small w.r.t the distance over which $\partial T/\partial x_2$ changes appreciably, local conditions prevail; if, however, the size of energy containing eddies is relatively large, turbulent transport dominates over local production and the profile of θ' would tend to be more uniform than that in the previous case. A measure of the relative eddy size is the ratio $L_{11}/2S$, plotted in Figure 11.3 versus distance from the source. The fact that this ratio generally decreases away from the source is consistent with the increasing eminence of double peaks in the θ' profiles (Figure 11.4). The observation of double peaks very close to the source can be explained by the same reasoning; in this case, however, the relevant scale for transport should be related to the molecular free length, since diffusion takes place mostly by molecular diffusion (notice also that $L_{11}/2S$ is small in the wake of the source).

11.3 Temperature-Velocity Correlations

Physical reasoning, based on the gradient transport concept, can be used to interpret, at least qualitatively, the variation of all measured temperature-velocity correlations. It has already been demonstrated by several investigators that $\overline{u_2\theta}$ has a sign opposite to that of $\partial\overline{T}/\partial x_2$ in flows where this gradient is dominating; in conformity with the negative correlation $\overline{u_1u_2}$ in the present flow, $\overline{u_1\theta}$ is generally

found to have the same sign as $\partial\overline{T}/\partial x_2$. A generalization of this concept to any transported quantity, 'a' , leads to the general rule that the covariance $\overline{u_2 a}$ must have the opposite sign and the covariance $\overline{u_1 a}$ the same sign as the mean gradient $\partial\overline{a}/\partial x_2$. This rule is adequate for explaining all present results. For example, the measured covariance $\overline{u_2^2\theta}$ is positive in regions with $\partial\overline{\theta u_2}/\partial x_2 < 0$, vanishes near the stationary points of $\overline{\theta u_2}$ (nearly coinciding with the inflection points of the mean temperature profile) and is negative in regions with $\partial\overline{\theta u_2}/\partial x_2 > 0$ (e.g. around the centerline). Similar explanations can be devised for the variations of $\overline{u_1\theta^2}$, $\overline{u_2\theta^2}$, $\overline{u_1^2\theta}$, and $\overline{u_1 u_2\theta}$.

On the other hand, the positive sign of the triple moment $\overline{\theta^3}$ (and, thus, of the temperature fluctuation skewness, S_θ) is due to an entirely different reason. At first, one may observe that positive skewness of a random variable corresponds to a non-Gaussian distribution in which negative peaks of the variable occur with smaller amplitude but longer total duration than the positive peaks. In the present situation, the fluctuating temperature is bounded between the unheated, ambient fluid temperature and the heating source temperature, although fluid with intermediate temperatures is produced at different positions in the thermal plume of the source as a result of molecular diffusion and mixing. The observed positive skewness of θ is attributed to the occurrence of low-amplitude negative peaks in the θ-signal, corresponding to the "cold" fluid. This also explains why S_θ increases dramatically from the centerline towards the edges of the plume. The fact that S_θ decreases monotonically downstream is due to the smearing out of hot-fluid,

positive temperature peaks by molecular diffusion.

11.4 Turbulent Diffusivities

The applicability of a turbulent diffusivity tensor, D_{ij}, defined as

$$\overline{\theta u_i} = -D_{ij}\frac{\partial \overline{T}}{\partial x_j} \tag{11.1}$$

to nearly homogeneous, shear flows has been established by the experiments of Sreenivasan et al. (1981) and Tavoularis and Corrsin (1981a, 1985). Estimates of the components of D_{ij} (Tavoularis and Corrsin, 1985) indicate that the tensor is neither diagonal nor symmetric.

Although, in the present flow, both $\partial\overline{T}/\partial x_2$ and $\partial\overline{T}/\partial x_1$ are generally non-zero, the former gradient is much larger than the latter, except within a narrow region around the peak of the mean temperature profile. With this consideration and in view of the appreciable turbulent transport into regions with small $\partial\overline{T}/\partial x_2$, estimates of D_{11} and D_{21} are subjected to large errors and will not be presented here.

The transverse variation of the measured D_{12} and D_{22} components, shown in Figure 11.5a, is comparable to the combined magnitudes of measuring uncertainty and transverse inhomogeneity (the latter being of the order of 10%); the ratio D_{12}/D_{22} is remarkably close to the value 2.1, measured by Tavoularis and Corrsin (1985), throughout the heated region (Figures 11.5b and 11.5c).

Turbulent diffusivities in homogeneous flows can be expressed as products of a Lagrangian characteristic velocity and a Lagrangian characteristic length (Corrsin,

1957). Rough estimates of D_{22} can be obtained from the product of the Eulerian scales $u_2' L_{11}$. Figure 11.6 illustrates that the ratio $D_{22}/(u_2' L_{11})$ was about 0.1, in close agreement with the measurements of Sreenivasan et al. (1981) and Tavoularis and Corrsin (1981 a).

Following the success of our earlier (section 11.3) qualitative rationalization of the signs of the third-order temperature-velocity correlations one could further explore the accuracy of simple gradient transport models for the third moments. Since the transporting mechanism is the same for all quantities, one is tempted to consider the use of identical diffusivities for the corresponding second and third-order covariances, as

$$\overline{u_i u_k \theta} = -D_{ij} \frac{\partial \overline{u_k \theta}}{\partial x_j} \tag{11.2}$$

$$\overline{u_i \theta^2} = -D_{ij} \frac{\partial \overline{\theta^2}}{\partial x_j} \tag{11.3}$$

As seen in Table 5, the values of the central diffusivity D_{22}, estimated from the three third-order covariances are not very different from that estimated from the heat flux. Also, the ratio D_{12}/D_{22} of the two measurable components of the turbulent diffusivity tensor is comparable in both cases. Thus it appears that a universal turbulent diffusivity tensor could be used for rough estimates of both second and third-order temperature-velocity corelations.

11.5. Estimates of Lagrangian Autocorrelation and Scales

As mentioned earlier, the particle mean square displacement $\overline{X_2^2}$ can be approx-

imated by the variance of the mean temperature field generated by a line source, provided that molecular conduction is negligible compared to turbulent diffusion. Measurements of the half-width, S, of the mean temperature profile at different downstream distances from the source have been presented in Figure 10.7. In the following it will be assumed that $(\overline{X_2^2})^{1/2} = 0.85S$, as would be the case for a Gaussian distribution, and that the diffusion time $t = x_\theta/\overline{U_{1c}}$. The growth of S is essentially linear for $t > 0.04s$, but it is non-linear for smaller times.

For the latter case, a third order polynomial was fitted to the measurements of $\overline{X_2^2}$ and proper conditions were imposed on the first and second derivatives of $\overline{X_2^2}$ so as to obtain a smooth transition from the region of small diffusion times to that of large diffusion times. The Lagrangian autocorrelation function, $R_L(t)$, resulting from the expressions for $\overline{X_2^2}$ is plotted in Figure 11.7 versus the dimensionless time $\eta = tu'_{20}/L_{220}$. Also plotted alongside are the two-point space-time corelation measurements of Harris et al. (1977) (also reported by Tavoularis and Corrsin, 1985). As is evident from the Figure, the Lagrangian autocorrelation appears to be greater than its Eulerian counterpart. Some discrepancy is to be expected due to differences in the flow structure.

An estimate of the Lagrangian integral time scale, obtained by integrating the Lagrangian autocorrelation coefficient up to its first zero, was $T_L = 0.047s$ corresponding to a ratio $T_L/(L_{220}/u'_{20}) = 1.7$. The latter value is approximately twice as large as the value of $T_E/(L_{220}/u'_{20})$, where the Eulerian integral length scale in a convected frame, T_E, was obtained by integrating the envelope of the corresponding two-point, Eulerian space time correlations (Tavoularis and Corrsin, 1985). In grid turbulence, the ratio $T_L/(L_{220}/u'_{20}) \approx 1.9$, while the ratio $T_L/T_E \approx$

1.3 (Shlien and Corrsin, 1974).

The Lagrangian Taylor temporal microscale, τ_L, was estimated by fitting the relationship

$$R(t) = 1 - \frac{t^2}{\tau_L^2} \tag{11.4}$$

to the initial part of the curve $R(t)$. For this purpose, only the measurements behind the 0.051mm diameter wire were used. The estimated value was $\tau_L \approx 0.044s$, so that the ratio $\tau_L/T_L = 0.94$, slightly larger that its estimate 0.69 in grid turbulence (Shlien and Corrsin, 1974). The ratio $\tau_L/(\lambda_{21}/u'_{20})$ was 2.1, about six times larger than its Eulerian counterpart in a convected frame (Harris et al., 1977). The values of these two ratios in grid turbulence are, respectively, 3.5 and 12 (Shlien and Corrsin, 1974). Finally, the ratio $\tau_L/(\lambda_{21}/\overline{U_{1c}})$ was 69 in the present flow and about 200 in grid turbulence. In interpreting the above results, one must bear in mind that differences in the flow structure, Reynolds number and in measuring techniques in the various experiments could contribute to the variation of all ratios considered above.

Chapter 12

CONCLUSIONS

The main conclusions of the present study could be summarized as follows.

(a) At sufficiently large diffusion times the mean shear causes the mean temperature profile to become asymmetric and its peak to shift towards the region of lower velocity.

(b) The occurrence, suppression and re-appearance of the double peaks in the temperature fluctuation profiles can be explained by considering the relative size of energy containing eddies with respect to the plume width.

(c) The variations of double and triple temperature-velocity correlations are consistent with the gradient transport concept. A universal turbulent diffusivity tensor can be used to model all these quantities.

(d) The positive temperature fluctuation skewness is due to the effect of "cold" fluid negative fluctuations in the signal.

(e) The collapse of the temperature-velocity correlations at various downstream stations indicates an approach to a self-preserved temperature field, although exact self-preservation is precluded by the monotonic development of the mean and r.m.s. temperature profiles.

(f) Consistent with earlier observations in isotropic turbulence, the Lagrangian scales are larger than those obtained from Eulerian measurements in a convected frame.

REFERENCES

PART A

Annand,W.J.D. 1953 The resistance to air flow of wire gauzes. J.R. Aeronaut. Soc. 57, 141.

Baines,W.D. and Peterson,E.G. 1951 An investigation of flow through screens. Tran. ASME 73, 467.

Batchelor,G.K. 1945 On the concept and properties of the idealized hydrodynamic resistance. Australian Council for Aeronautics, Rep. 13.

Burgers,J.M. and Mitchner,M. 1953 On homogeneous non-isotropic turbulence connected with a mean motion having a constant velocity gradient. Konik. Ned. Akad. v. Wet. B 15, 228; part II, 383.

Cambon,C. Jeandel,D. and Mathieu,J. 1981 Spectral modelling of homogeneous non-isotropic turbulence. J. Fluid Mech. 104, 247.

Champagne,F.H., Harris,V.G.,Corrsin,S. 1970 Experiments on nearly homogeneous shear flow. J. Fluid Mech. 41, 81.

Cockrell,D.J. and Lee,B.E. 1966 Production of shear profiles in a wind tunnel by cylindrical rods placed normal to the stream. J. Roy. Aeron. Soc. 70, 724.

Collar,A.R. 1939 The effect of a gauze on velocity distribution in a uniform duct. Aeronaut. Res. Counc. Rep. Memo. No. 1867.

Comte-Bellot,G and Corrsin,S. 1971 Simple Eulerian time correlation of full- and narrow-band velocity signals in grid generated, "isotropic" turbulence. J. Fluid Mech. 48, 273.

Corrsin,S. 1957 Some current problems in turbulent shear flows. Proc. 1st. Naval Hydr. Symp. Nat. Acad. Sci./Nat. Rec. Counc., Washington , DC, publ. no. 515

Corrsin,S. 1963 Turbulence:Experimental Methods. Handbuch der Physik, 8, 523.

Corrsin,S. and Kollman,W. 1977 Preliminary report on sheared cellular motion as

a qualitative model of homogeneous turbulent shear flow. Turbulence in Internal flows, Project SQUID workshop (ed. S.N.B. Murthy), N. Hemisphere Publ. Corp.

Courseau,P.A. and Loiseau,M. 1978 Contribution à l'analyse de la turbulence homogène anisotrope. J.d. Mecanique 17, 245.

Craya,A. 1958 Contribution à l'analyse de la turbulence associée à des vitesses moyennes. Publ. Scien. et Tech. du Ministere de l'Air no. 345.

Davis,G. 1957 Non-uniform flow through wire screens. PhD thesis, University of Cambridge.

Deissler, R.G. 1961 Effects of inhomogeneity and of shear flow in weak turbulent fields. Phys. Fluids 4, 1187.

Deissler, R.G. 1965 Problem of steady state shear flow turbulence. Phys. Fluids 8, 391.

Deissler, R.G. 1970 Effect of initial condition on weak homogeneous turbulence with uniform shear. Phys. Fluids 13, 1868.

Elder,J.W. 1959 Steady flow through non-uniform gauzes of arbitrary shape. J. Fluidf Turbulence, A.Favre, editor, Gordon and Breach, 64.

Feiereisen, W.J., Shirani, E., Ferziger, J.H., and Reynolds, W.C. 1982 Direct simulation of homogeneous turbulent shear flow on Illiac IV computer : Applications to compressible and incompressible modelling. Turb. Shear Flows 3, 309, Springer.

Fox, J. 1964 Velocity correlations in weak turbulent shear flow. Phys. Fluids 7, 562.

Gence, J.N., Angel, Y. and Mathieu, J. 1978 Partie linéaire des corrélations mettant en jeu la pression dans une turbulence à un cisaillement et un effeect de gravité. J. d. Mecanique 17, 329.

Gibbings, J.C., 1973 The pyramid gauze diffuser. Ing. Arch. 42, 225.

Harris, V.G., 1965 The turbulence generated by an array of parallel rods. M.Sc. Thesis, The Johns Hopkins University, Baltimore, U.S.A.

Harris, V.G., Graham, J.A. and Corrsin, S., 1977 Further Experiments in nearly homogeneous turbulent shear flow. J. Fluid Mech. 81, 657.

Hasen, E.M. 1967 A non-linear theory of turbulence onset in a shear flow. J. Fluid Mech 29, 721.

Hwang, W.S. 1971 Experimental investigation of turbulent shear flows. Ph.D.

dissertation, University of Virginia.

Karnik, U.M., 1983 Experiments on uniformly sheared turbulence. M.A.Sc. Thesis, University of Ottawa.

Karnik, U. and Tavoularis, S., 1983 The asymptotic development of nearly homogeneous turbulent shear flow. Proc. 4th Symp. Turb. Shear Flows, Karlsruhe, 14.18.

Kotansky, D.R., 1966 The use of honeycomb for shear flow generation. AIAA Journal 4, 1490.

Launder, B.E., Reece, G.J. and Rodi, W. 1975 Progress in the development of a Reynolds stress turbulence closure. J. Fluid Mech. 68, 537.

Laws, E.M. and Livesey, J.L., 1978 Flow through screens. Ann. Rev. Fluid Mech. 10, 247.

Leslie, D.C. 1980 Analysis of strongly sheared, nearly homogeneous turbulent shear flow. J. Fluid Mech. 98, 435.

Livesey, J.L. and Turner, J.T., 1964 The generation of symmetrical duct velocity profiles of high uniform shear. J. Fluid Mech. 20, 201.

Lumley,J.L. 1978 Computational modelling of turbulent flows. Adv. Appl. Mech. 18, 123.

Lumley,J.L. 1983 Turbulence modelling. ASME E: J. Appl. Mech. 105, 1097.

Maull, D.J. and Young, R.A., 1973 Vortex shedding from bluff bodies in a shear flow. J. Fluid Mech. 60, 401.

McCarthy, J.H., 1964 Steady-flow past non-uniform wire grids. J. Fluid Mech. 19. 491.

Moin, P., Rogers, M.M. and Moser, R.D. 1985 Structure of turbulence in the presence of uniform shear. Proc. 5th Symp. Turb. Shear Flows, Ithaca, 1.

Monin,A.S. and Yaglom,A.M. 1973 Statistical Fluid Mechanics. MIT Press.

Mulhearn, P.J. and Luxton, R.E. 1975 The development of turbulence structure in a uniform shear flow. J. Fluid Mech. 68, 577.

Naot, D., Shavit, A. and Wolfshtein, W. 1973 Two-point correlation model and the redistribution of Reynolds stresses. Phys. Fluids 16, 738.

Pinker, R.A. and Herbert, M.B., 1967 Pressure loss associated with compressible flow through square mesh wire gauzes. J. Mech. Eng. Sci. 9, 11.

Reis, F.B. 1952 Studies of correlation and spectra in homogenoeus turbulence. Ph.d. dissertation, Massachusetts Institute of Technology.

Richards, H.K. and Morton, J.B., 1976 Experimental investigation of turbulent shear flow with quadratic mean-velocity profiles. J. Fluid Mech. 73, 165.

Robertson, J.M. and Johnson, H.F., 1970 Turbulence structure in plane Couette flow. J. Eng. Mech. Div., ASCE, 96, 1171.

Rodi,W. 1976 A new algebraic relation for calculating the Reynolds stresses. Z. Angew. Math. Mech. 56, 219.

Rogallo, R.S., 1981 Numerical experiments in homogeneous turbulence. NASA TM-81315.

Rogallo, R.S. and Moin, P. 1984 Numerical simulation of turbulent shear flows. Ann. Rev. Fluid Mech. 16, 99.

Rohr, J.J., Itsweire, E.C., Helland, K.N. and Van Atta, C.W. 1988 An investigation of the growth of turbulence in a uniform shear flow. J. Fluid Mech. (in press).

Rose, W.G., 1966 Results of an attempt to generate a homogeneous turbulent shear flow. J. Fluid Mech. 25, 97.

Rose, W.G., 1970 Interaction of grid turbulence with a uniform mean shear. J. Fluid Mech. 44, 767.

Rotta, J. 1951 Statistische theorie nichthomogener turbulenz. J. Phys. 129, 547.

Shaanan, S., Ferziger, J.H. and Reynolds, W.C. 1977 Numerical simulation of turbulence in the presence of shear. Dept. Mech. Eng., Stanford University, Rep. TF-6.

Sreenivasan,K.R., Tavoularis,S., Henry,R. and Corrsin,S. 1980 Temperature fluctuations and scales in grid turbulence. J. Fluid Mech. 100, 597.

Sreenivasan,K.R. 1985 The effect of contraction on a homogeneous turbulent shear flow. J. Fluid Mech. 154, 187.

Stillinger, D.C., Head, M.J., Helland, K.N. and Van Atta, C.W., 1983 A closed loop gravity driven water channel for density-stratified shear flows. J. Fluid Mech. 131, 73.

Tavoularis,S. and Corrsin,S. 1981 Experiments in a nearly homogeneous shear flow with a uniform mean temperature gradient, part 1. J. Fluid Mech. 104, 311.

Tavoularis,S. and Corrsin,S. 1981 Experiments in nearly homogeneous turbulent

shear flow with a uniform mean temperature gradient, part2. J. Fluid Mech. 104, 349.

Tavoularis,S. and Corrsin,S. 1985 Effects of shear on the turbulent diffusivity tensor, Int. J. Heat Mass Transfer 28, 265.

Tavoularis,S. 1985 Asymptotic laws for transversely homogeneous turbulent shear flows. Phys. Fluids 28, 999.

Taylor, G.I. and Batchelor, G.K., 1949 The effect of a gauze on small disturbances in a uniform stream. Quart. J. Mech. Appl. Math. 2, 1.

Taylor, G.I. and Davis, R.M., 1944 The aerodynamics of porous sheets. Aeronaut. Res. Counc. Rep. Memo 2237.

Tchen, C.M. 1953 On the spectrum of energy in turbulent shear flow. J. Res. Nat. Bur. Stand. 50, res. Pap. 2388.

Townsend,A.A. 1976 The structure of turbulent shear flow (second edition). Cambridge University Press.

Weinstock, J. and Burk, S. 1985 Theoretical pressure-strain term, experimental comparison, and resistance to large anisotropy. J. Fluid Mech. 154, 429.

PART B

Alexopoulos,C.C. and Keffer,J.F. 1971 Turbulent wake in a passively stratified field. Phys. Fluids 14, 216.

Anand,M.S. and Pope,S.B. 1983 Diffusion behind a line source in grid turbulence. Proc. Fourth Symp. Turb. Shear Flows, Karlsruhe, 17.11.

Antonia,R.A. and Danh,H.Q. 1977 Structure of temperature fluctuations in a turbulent boundary layer. Phys. Fluids 20, 1050.

Antonia,R.A. and Danh,H.Q. 1978 Comments on "Ratio of scalar and velocity dissipation time scales in shear flow turbulence. Phys. Fluids 21, 2378.

Budwig,R., Tavoularis,S. and Corrsin,S. 1985 Temperature fluctuations and heat flux in grid generated isotropic turbulence with streamwise and transverse mean temperature gradients. J. Fluid Mech. 153, 441.

Collis,D.C. 1948 The diffusion process in turbulent flow. Div. Aero. Australian Council Sci. and Indus. Res., Rep. A55.

Corrsin,S. 1952 Heat transfer in isotropic turbulence. J. Appl. Phys. 23, 113.

Corrsin,S. 1953 Remarks on turbulent heat transfer. Proc. Iowa Thermo. Symp. 5, State Univ. of Iowa, Iowa City.

Corrsin,S. 1957 Some current problems in turbulent shear flow, in Naval Hydrodynamics, Proc. First Symp. on Naval Hydrodyn., Publ. No. 515, 373.

Corrsin,S. 1962 Theories of turbulent dispersion, Mécanique de la Turbulence, Paris : C.N.R.S., 27.

Corrsin,S. 1974 Limitations of gradient transport models in random walks and in turbulence. Adv. Geophys. 18A, 25.

Deissler,R.G. 1963 Turbulent heat transfer and temperature fluctuations in a field with uniform velocity and temperature gradients. Int. J. Heat Mass Transfer 6, 257.

Durbin,P.A. 1982 Analysis of the decay of temperature fluctuations in isotropic turbulence. Phys. Fluids 25, 1328.

Durbin,P.A. and Hunt,J.R.C. 1980 Dispersion from elevated sources in turbulent boundary layers. J. de Mecanique 19, 680.

Elrick,D.E. 1962 Source functions for diffusion in uniform shear flow. Australian J. Physics 15, 283.

Fox,J. 1964 Turbulent temperature fluctuations and two dimensional heat transfer in a uniform shear flow. NASA Tech. Note D2511.

Frenkiel,F.N. 1950 On turbulent diffusion. Symp. on Turbulence, Naval Ord. Lab., Rep. 1136, 67.

Hinze,J.O. 1961 Dispersion in turbulent shear flow. The Mechanics of Turbulence, A.Favre, editor, Gordon and Breach, 64.

Huang,C.H. 1979 A theory of dispersion in turbulent shear flow. Atmos. Environ. 13, 453.

Hwang,B.C. et al. 1979 J. Atmos. Sci. 36, 1955.

Jones,W.P. and Musonge,M. 1983 Modelling of scalar transport in homogeneous turbulent flows. Proc. Fourth Symp. on Turbulent Shear Flows, Karlsruhe, 17.18.

Keffer,J.K., Olsen,G.J. and Kawall,J.G. 1977 Intermittency in a thermal mixing layer. J. Fluid Mech. 79, 595.

Kistler,A.L. 1956 Measurement of joint probability in turbulent dispersion of heat from two line sources. PhD dissertation, part II, The Johns Hopkins University, Baltimore, U.S.A.

Kistler,A.L., O'Brien,V. and Corrsin,S. 1956 Double and triple correlations behind a heated grid. J. Aero. Sci. 23, 96.

Kyong,H.N. and Chung,K.M. 1987 Measurements of turbulent diffusion field behind a line heat source in a homogeneous shear flow. Korean Soc. Mech. Eng. Journal 1, 24.

Libby,P. and Scragg,C. 1972 Diffusion of heat from a line source downstream of a turbulence grid. Amer. Inst. Aeron. Astron. Journal, 562.

Lin,S.C. and Lin,S.C. 1973 Study of strong temperature mixing in subsonic grid turbulence, Phys. Fluids 16, 1587.

Lumley,J.L. 1978 Computational modelling of turbulent flows. Adv. Appl. Mech. 18. 123.

Lumley,J.L. 1983 Turbulence modelling. Amer. Soc. Mech. Eng. E: J. Appl.

Mech. 105, 1097.

Lumley,J.L. and Van Cruyningen,I. 1985 Limitations of second order modelling of passive scalar diffusion. In Frontiers in Fluid Mechanics, S.H. Davis and J.L. Lumley (editors), Springer, New York, 199. University.

Mills,R., Kistler,A.L., O'Brien,V. and Corrsin,S. 1958 Turbulence and temperature fluctuations behind a heated grid. NACA Tech. Note 4288.

Mills,R.R. and Corrsin,S. 1959 Effect of contraction on turbulence and temperature fluctuations generated by a warm grid. NASA Memo. 5-5-59W.

Monin,A.S. and Yaglom,A.M. 1973 Statistical Fluid Mechanics. MIT Press.

Nakamura,I.,Sakai,Y.,Miyata,M. and Tsunoda,H. 1986 Diffusion of matter from a continuous point source in uniform mean shear flows. Bull. Japan. Soc. Mech. Eng. 29, 1141.

Newman,G.R., Warhaft,Z. and Lumley,J.L. 1977 The decay of temperature fluctuations in isotropic turbulence. Proc. 6th Australasian Hydraulics and Fluid Mech. Conf., Adelaide.

Novikov,E.A. 1958 Turbulent diffusion in a shear flow. Prikl. Matem. Mekh. 22, 412.

O'Brien, E.E. 1962 Turbulent transport of a passive scalar with a variable mean gradient. Phys. Fluids 5, 656.

Okubo,A. and Karweit,M.J. 1969 Diffusion from a continuous source in a uniform shear flow. Limnol. and Oceanogr. 14, 514.

Pope,S.B. 1981 Transport equation for the joint probability density function of velocity and scalars in turbulent flow. Phys. Fluids 24, 588.

Pope,S.B. 1983 Consistent modelling of scalars in turbulent flows. Phys. Fluids 26, 404.

Poreh,M. and Cermak,J.E. 1964 Study of diffusion from a line source in a turbulent boundary layer. J. Heat Mass Transfer 7, 1083.

Riley,J. and Corrsin,S. 1971 Simulation and computation of dispersion in turbulent shear flow. Proc. Conf. on Air Pollut. Met., Amer. Met. Soc., 16.

Riley,J. and Corrsin,S. 1974 The relation of turbulent diffusivities to Lagrangian statistics for the simplest shear flow. J. Geophys. Res. 79, 1768.

Saffman,P.G. 1963 An approximate calculation of the Lagrangian autocorrelation

coefficient for stationary homogeneous turbulence. Appl. Sci. Res. A11, 245.

Sakai,Y.,Nakamura,I.,Miyata,M. and Tsunoda,H. 1986 Diffusion of matter from a continuous point source in uniform mean shear flows (2nd report). Bull. Japan. Soc. Mech. Eng. Journal 29, 1149.

Sato,Y. and Yamamoto,K. 1987 Lagrangian measurement of fluid.particle motion in an isotropic turbulent field. J. Fluid Mech. 175, 183.

Schubauer,G.B. 1935 A turbulence indicator utilizing the diffusion of heat. NACA Rep. 524.

Sepri.P. 1976 Two-point turbulence measurements downstream of a heated grid. Phys. Fluids 19, 1876.

Shih,T.H. and Lumley,J.L. 1986 Influence of timescale ratio on scalar flux relaxation: modelling Sirivat and Warhaft's homogeneous passive scalar fluctuations. J. Fluid Mech. 162, 211.

Shlien,D.J. and Corrsin,S. 1974 A measurement of Lagrangian velocity autocorrelation in approximately isotropic turbulence. J. Fluid Mech. 62, 255.

Sirivat,A. and Warhaft,Z. 1983 The effect of a passive cross stream temperature gradient on the evolution of temperature variance and heat flux in grid turbulence. J. Fluid Mech. 128, 323.

Snyder,W.H. and Lumley,J.L. 1971 Some measurements of particle velocity autocorrelation functions in a turbulent flow. J.Fluid Mech. 48, 41.

Sreenivasan,K.R., Danh,H.Q. and Antonia,R.A. 1976 Diffusion from a heated wall cylinder immersed in a turbulent boundary layer. Thermofluids Conference, Hobart, Australia.

Sreenivasan,K.R.,Tavoularis,S.,Henry,R. and Corrsin,S. 1980 Temperature fluctuations and scales in grid turbulence. J. Fluid Mech. 100, 597.

Sreenivasan,K.R.,Tavoularis,S. and Corrsin,S. 1981 A test of gradient transport and its generalizations. Turbulent Shear Flows 3, 96.

Stapountzis,H.,Sawford,B.L.,Hunt,J.C.R. and Britter,R.E. 1986 Structure of the temperature field downwind of a line source in grid turbulence. J. Fluid Mech. 165, 401.

Stapountzis,H. and Britter,R.E. 1987 Turbulent diffusion behind a heated line source in a nearly homogeneous turbulent shear flow. Proc. Sixth Symp. on Turbulent Shear Flows, Toulouse, 9.2.1.

Sullivan,P. 1976 Dispersion of a line source in grid turbulence. Phys. Fluids 19, 159.

Tavoularis, S. 1978a A circuit for the measurement of instantaneous temperature in heated turbulent flows. J. Sci. Instrum. 11, 21.

Tavoularis,S. and Corrsin,S. 1981a Experiments in a nearly homogeneous shear flow with a uniform mean temperature gradient, part 1. J. Fluid Mech. 104, 311.

Tavoularis,S. and Corrsin,S. 1981b Experiments in nearly homogeneous turbulent shear flow with a uniform mean temperature gradient, part2 : the fine structure. J. Fluid Mech. 104, 349.

Tavoularis,S. and Corrsin,S. 1985 Effects of shear on the turbulent diffusivity tensor, Int. J. Heat Mass Transfer 28, 265.

Tavoularis,S. and Karnik,U. 1987 Further experiments on the evolution of turbulent stresses and scales in uniformly sheared turbulence. Submitted to J. Fluid Mech.

Taylor,G.I. 1921 Diffusion by continuous movements. Proc. Lond. Math. Soc. A20, 196.

Townsend,A.A. 1951 The diffusion of heat spots in isotropic turbulence. Proc. Roy. Soc. London A209, 418.

Townsend,A.A. 1954 The diffusion behind a line source in homogeneous turbulence. Proc. Roy. Soc. London A224, 487.

Uberoi,M.S. and Corrsin,S. 1952 Diffusion from a line source in isotropic turbulence. NACA Tech. Note 2710 (also NACA Rep. 1142).

Venkataramani,K.S. and Chervay,R. 1978 Statistical features of heat transfer in grid generated turbulence : constant gradient case. J. Fluid Mech. 86, 513.

Warhaft,Z. 1981 The use of dual injection to infer scalar covariance decay in grid turbulence. J. Fluid Mech. 104, 93.

Warhaft,Z. 1984 The interference of thermal fields from line sources in grid turbulence, J. Fluid Mech. 144, 363.

Warhaft,Z. and Lumley,J.L. 1978 An experimental study of the decay of temperature fluctuations in grid generated turbulence. J. Fluid Mech. 88, 659.

Wiskind,H.K. 1962 A uniform gradient turbulent transport experiment. J. Geoph. Res. 67, 3033.

Yeh,T.T. and Van Atta,C.W. 1973 Spectral transfer of scalar and velocity fields in heated grid turbulence. J. Fluid Mech. 58, 233.

Screen type	M (mm)	d/h	σ	$d\overline{U_1}/dx_2$ (s^{-1})	R_c	A	A_p		
							eq.(5)	eq.(7)	eq.(8)*
square	1.59	0.00083	0.294	77	219	0.61	0.59	0.68	0.79
mesh	1.81	0.00135	0.4	77	356	0.44	0.39	0.45	0.56
(present)	12.7	0.0058	0.26	77	1533	0.64	0.65	0.74	0.84
	3.18	0.0027	0.446	77	714	0.28	0.30	0.32	0.44
	3.18	0.0017	0.294	77	449	0.58	0.59	0.68	0.79
	1.81	0.0014	0.42	77	370	0.39	0.35	0.4	0.51
	3.18	0.0023	0.388	77	6083	0.38	0.41	0.48	0.59
	1.27	0.0012	0.482	77	317	0.25	0.23	0.22	0.34
square	1.06	0.00032	0.344	12.2	145	0.68	0.50	0.58	0.69
mesh	2.12	0.000737	0.377	12.2	330	0.68	0.44	0.51	0.62
(Rose,'70)	4.23	0.00129	0.338	12.2	580	0.66	0.51	0.60	0.71
	8.47	0.00262	0.342	12.2	1180	0.72	0.50	0.59	0.70
	12.7	0.00399	0.347	12.2	1800	0.73	0.49	0.58	0.69
	25.4	0.00802	0.348	12.2	3610	0.72	0.49	0.57	0.68
	50.8	0.01604	0.347	12.2	7220	0.68	0.49	0.57	0.68
Parallel	12.7	0.016	0.378	60	2880	0.52	0.43	0.50	0.62
rods	12.7	0.016	0.378	84	4160	0.52	0.43	0.50	0.62
(present)	12.7	0.016	0.189	84	4160	0.80	0.76	0.82	0.92
	25.4	0.032	0.378	43.5	3840	0.43	0.43	0.50	0.62
	25.4	0.032	0.378	60	5760	0.46	0.43	0.50	0.62
	25.4	0.032	0.378	84	8320	0.46	0.43	0.50	0.62
	25.4	0.032	0.189	84	8320	0.80	0.76	0.82	0.92
	50.8	0.064	0.378	43.5	7680	0.33	0.43	0.50	0.62
	50.8	0.064	0.378	60	11,520	0.35	0.43	0.50	0.62
	50.8	0.064	0.378	84	16,640	0.35	0.43	0.50	0.62
	50.8	0.064	0.189	84	16,640	0.70	0.76	0.82	0.92
Parallel	50.8	0.026	0.312	12.2	11,700	0.58	0.56	0.65	0.75
rods									
(Rose, '70)									

* excluding the Reynolds number correction term

Table 1. Shear reduction by a single screen.

Grid insertion slot				U_c	A	A_{prod}
A	B	C	D	m/s		
-	12.7	-	25.4	13	0.24	0.24
-	25.4	-	50.8	13	0.20	0.16
-	50.8	-	12.7	13	0.19	0.19
-	50.8	-	25.4	6	0.15	0.14
-	50.8	-	25.4	13	0.18	0.16
-	50.8	25.4	12.7	13	0.101	0.084
-	12.7	50.8	25.4	13	0.096	0.084

Table 2. Shear reduction factor behind multiple grids with parallel rods with σ=0.378. Last column indicates the product of individual grid reduction factors.

Case& *Symbol*	M_{sh} *mm*	M_g *mm*	σ_g -	x_g/h -	x_1/h -	$\overline{U_c}$ *m/s*	$d\overline{U_1}/dx_2$ s^{-1}	$\overline{q^2}$ m^2/s^2	K_{11} -	K_{22} -	K_{33} -	$-K_{12}$ -	L_{11} *mm*	λ_{11} *mm*	$R_{\lambda 1}$ -
A ○	25.4	-	-	-	10	13	84	1.714	.55	.20	.25	.165	38	4.9	310
B ◐	25.4	-	-	-	10	9	60	.912	.56	.20	.24	.165	37	-	-
C ●	25.4	-	-	-	10	6	43.5	.490	.59	.19	.22	.165	42	-	-
D □	25.4	25.4	.378	4.5	10	13	38.4	1.422	.53	.20	.27	.170	50	6.4	360
E ◧	25.4	25.4	.378	4.5	10	9	28	.684	.55	.20	.25	.170	48	-	-
F ■	25.4	25.4	.378	4.5	10	6	18.4	.264	.58	.19	.23	.170	41	-	-
G △	25.4	12.7	.378	1.1	10	13	39.9	.997	.49	.22	.29	.148	50	5.8	270
H ◭	25.4	12.7	.294	1.1	10	13	50.3	.446	.49	.21	.30	.148	30	3.9	120
I ◹	25.4	3.18	.294	1.1	10	13	43.7	.344	.49	.22	.29	.158	26	5.1	140
J ◢	25.4	1.59	.294	1.1	10	13	48.8	.419	.49	.23	.28	.154	26	5.2	160
K *	25.4	1.59	.294	1.1	10	13	20.9	.687	.48	.24	.28	.149	-	-	-
		25.4	.378	4.5											
L ▽	25.4	50.8	.378	1.1	10	13	29	2.230	.52	.22	.26	.155	92	6.1	440
M ▼	25.4	50.8	.378	1.1	10	9	20	.978	.55	.21	.24	.155	87	-	-
N ▼	25.4	50.8	.378	1.1	10	6	13.4	.388	.57	.19	.24	.155	87	-	-
O ×	25.4	50.8	.378	1.1	10	13	13.6	.914	.45	.24	.31	.148	-	-	-
		25.4	.378	4.5											
P +	25.4	50.8	.378	1.1	10	13	9.0	.437	.45	.27	.28	.178	-	-	-
		25.4	.378	2.5											
		25.4	.378	4.5											

Table 3. Summary of measurements

Case& Symbol	M_{sh} mm	M_g mm	σ_g -	x_g/h -	x_1/h -	$\overline{U_c}$ m/s	$d\overline{U_1}/dx_2$ s^{-1}	$\overline{q^2}$ m^2/s^2	K_{11} -	K_{22} -	K_{33} -	$-K_{12}$ -	L_{11} mm	λ_{11} mm	$R_{\lambda 1}$ -
RO ®	var.	-	-	-	10	15.4	13.7	.065	.44	.26	.30	.16	38	10.5	120
R1 ®	6.4	-	-	-	9	15.2	12.2	.0046	-	-	-	-	-	-	-
R2 ®	6.4	8.5	.342	.25	9	15.2	8.8	.011	-	-	-	-	-	-	-
R3 ®	6.4	12.7	.347	.25	9	15.2	8.9	.023	-	-	-	-	-	-	-
R4 ®	6.4	25.4	.348	.25	9	15.2	8.8	.043	-	-	-	-	-	-	-
R5 ®	6.4	50.8	.348	.25	9	15.2	9.3	.13	-	-	-	-	-	-	-
CHC ©	25.4	-	-	-	10	12.2	12.9	.098	.47	.25	.28	.165	48	10.9	155
ML Ⓜ	var.	6.4	hon.	-	9	4.6	5.5	.045	.48	.22	.30	.18	22	16.0	155
TC Ⓣ	30.5	-	-	-	10	12.4	46.8	.765	.53	.19	.28	.14	51	5.8	245
S1 Ⓢ1	30.5	15.2	.31	0.10	10	0.20	1.23	.00060	-	-	-	-	50	10.0	101
S2 Ⓢ2	30.5	15.2	.31	0.10	10	0.20	0.96	.00036	-	-	-	-	50	10.0	124
S3 Ⓢ3	30.5	15.2	.31	0.10	10	0.26	1.29	.00060	-	-	-	-	-	-	-
S4 Ⓢ4	30.5	-	.31	0.10	10	0.20	1.13	.00066	-	-	-	-	-	-	-
S5 Ⓢ5	15.2	38.1	.31	0.03	10	0.28	1.30	.00133	-	-	-	-	-	-	-
S6 Ⓢ6	15.2	38.1	.31	0.30	10	0.28	1.21	.00066	-	-	-	-	-	-	-

References : A-P: present measurements; RO: Rose (1966); R1-R5: Rose (1970); CHC: Champagne et al. (1970); ML: Mulhearn and Luxton (1975); TC: Tavoularis and Corrsin (1981a); S1-S6: Rohr et al. (1987).

Table 3. (continued)

Case	k_s m^{-1}	k m^{-1}	ϵ/P	n_L	k_L m^{-1}	R_{TM}	U_H ms^{-1}	τ_e/τ_s	τ_u/τ_s
A	6.56	.59	.72	.81	.39	16.1	.0091	3.3	8.4
B	6.56	.62	.72	-	-	15.4	.0081	3.1	8.4
C	7.21	.66	.73	-	-	15.1	.0073	3.4	8.3
D	2.95	.39	.61	.94	.39	3.9	.0070	2.2	9.6
E	3.11	.39	.63	-	-	4.3	.0063	2.2	9.3
F	3.05	.33	.69	-	-	4.9	.0055	1.9	8.5
G	3.08	.23	.75	.77	.36	7.0	.0071	2.9	9.0
H	3.87	.36	.68	.75	.30	24.7	.0076	3.2	9.9
I	3.34	.33	.69	.71	.30	22.7	.0073	2.8	9.2
J	3.74	.36	.69	.79	.30	23.8	.0075	2.8	9.4
K	1.61	.13	.73	-	-	5.9	.0057	-	6.7
L	2.23	-.02	1.02	.94	.36	8.2	.0050	2.5	6.5
M	2.23	-.07	1.09	-	-	8.9	.0045	2.4	6.5
N	2.23	-.03	1.04	-	-	10.0	.0040	2.5	6.5
O	1.05	-.01	1.04	-	-	4.6	.0039	-	6.8
P	0.69	.03	.87	-	-	3.57	.0034	-	5.6
CHC	1.05	0	1.0	-	-	9.6	.0046	2.9	6.1
R1	0.80	0	1.0	-	-	8.3	.0075	-	-
R2	0.58	0	1.0	-	-	3.2	.0062	-	-
R3	0.59	0	1.0	-	-	3.5	.0054	-	-
R4	0.58	0	1.0	-	-	7.3	.0043	-	-
R5	0.61	0	1.0	-	-	10.7	.0035	-	-
TC	3.77	.46	.57	.69	.26	20.3	.0070	3.7	12.5
S1	6.12	.55	.72	.54	.31	14.7	.0027	6.1	8.7
S2	4.75	.49	.68	-	-	15.1	.0025	3.9	9.2
S3	4.89	.49	.69	-	-	16.1	.0027	-	9.1
S4	5.54	.49	.72	-	-	11.3	.0021	-	8.7
S5	4.71	.58	.61	.54	.31	11.5	.0020	-	10.2
S6	4.32	.48	.65	-	-	20.2	.0020	-	9.6

Table 4. Summary of relevant experimental parameters.
(conditions as in Table 3.).

$\frac{X_2}{M}$	Estimates of D_{22} (m^2/s)				Estimates of D_{12}/D_{22}			
	$\frac{\overline{u_2\theta}}{\partial\overline{T}/\partial x_2}$	$\frac{\overline{u_2\theta^2}}{\partial\overline{\theta^2}/\partial x_2}$	$\frac{\overline{u_1u_2\theta}}{\partial\overline{u_1\theta}/\partial x_2}$	$\frac{\overline{u_2^2\theta}}{\partial\overline{u_2\theta}/\partial x_2}$	$\frac{\overline{u_1\theta}}{\overline{u_2\theta}}$	$\frac{\overline{u_1\theta^2}}{\overline{u_2\theta^2}}$	$\frac{\overline{u_1^2\theta}}{\overline{u_1u_2\theta}}$	$\frac{\overline{u_1u_2\theta}}{\overline{u_2^2\theta}}$
0	-	-	0.0033	0.0035	-	-	-2.3	-1.3
2.1	0.0016	0.0024	-	-	-2.0	-1.9	-	-
-1.8	0.0025	0.0016	-	-	-2.0	-1.8	-	-

Table 5. Typical estimates of diffusivities at x_θ/M=84.0 and at transverse positions with relatively small measuring uncertainties.

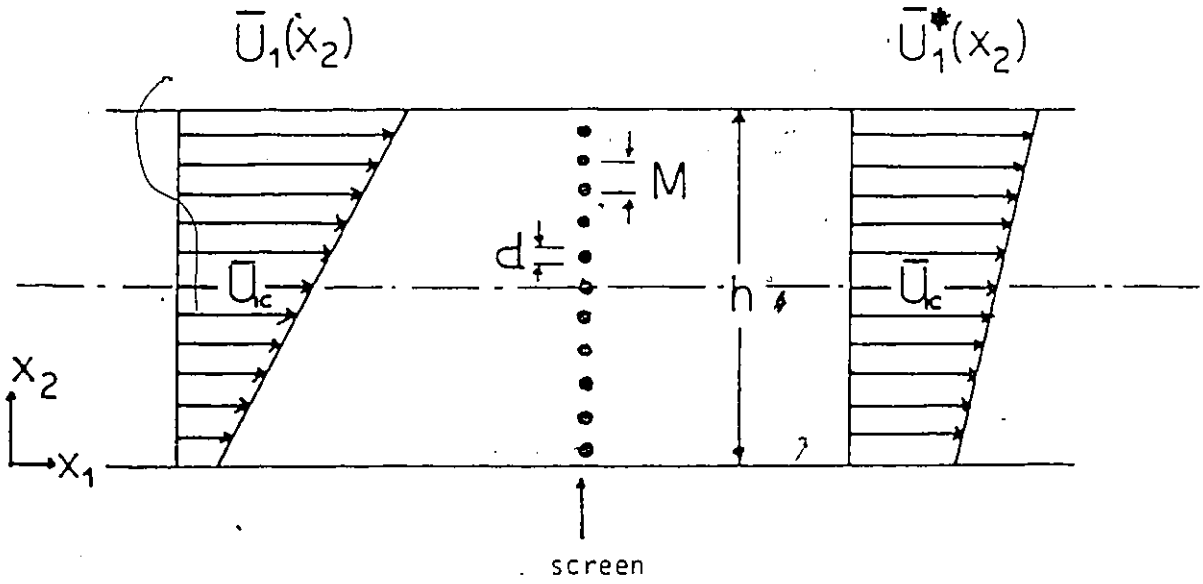

Figure 2.1. Representative velocity profiles upstream and downstream of a screen.

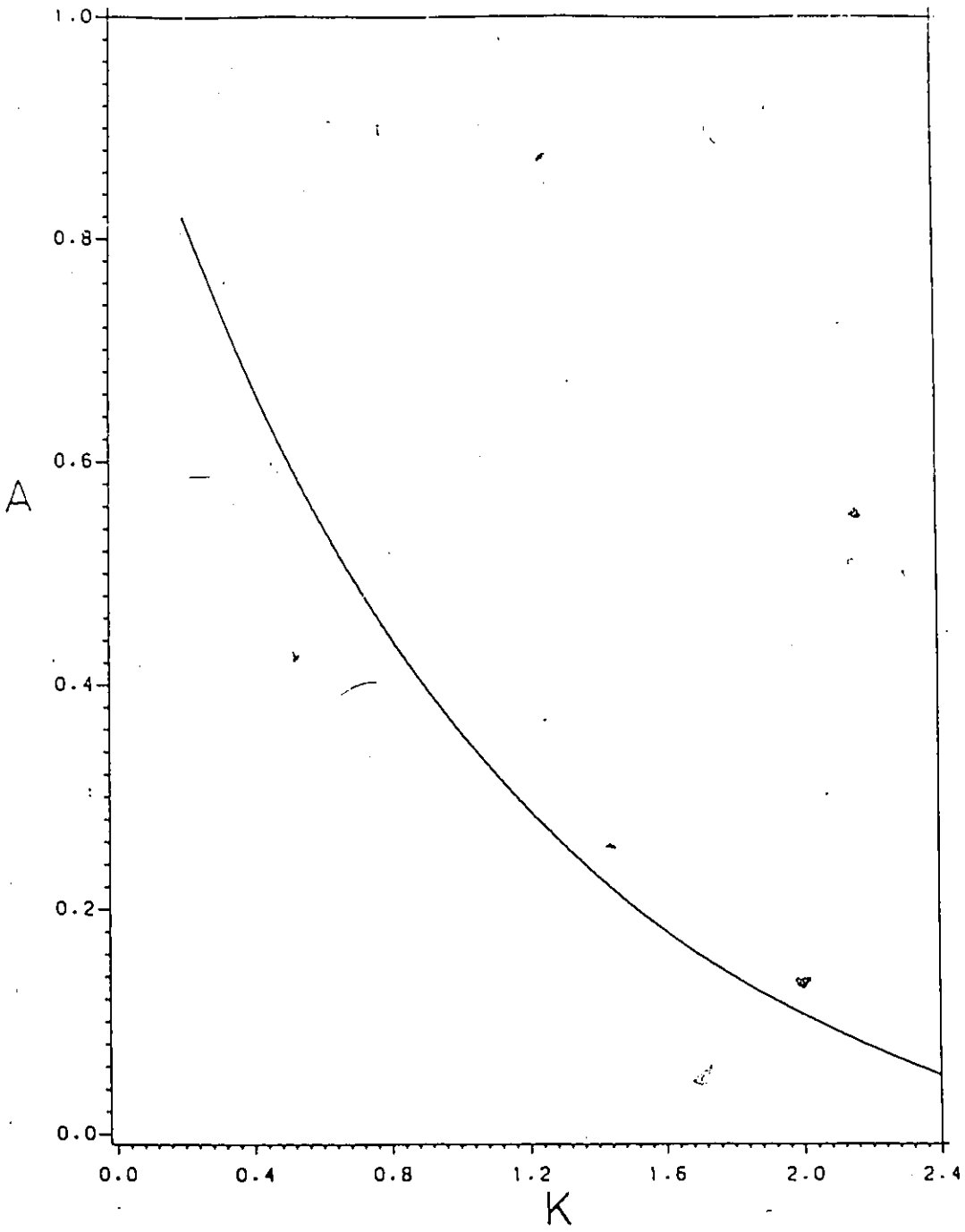

Figure 2.2. Variation of shear reduction factor with pressure loss coefficient.

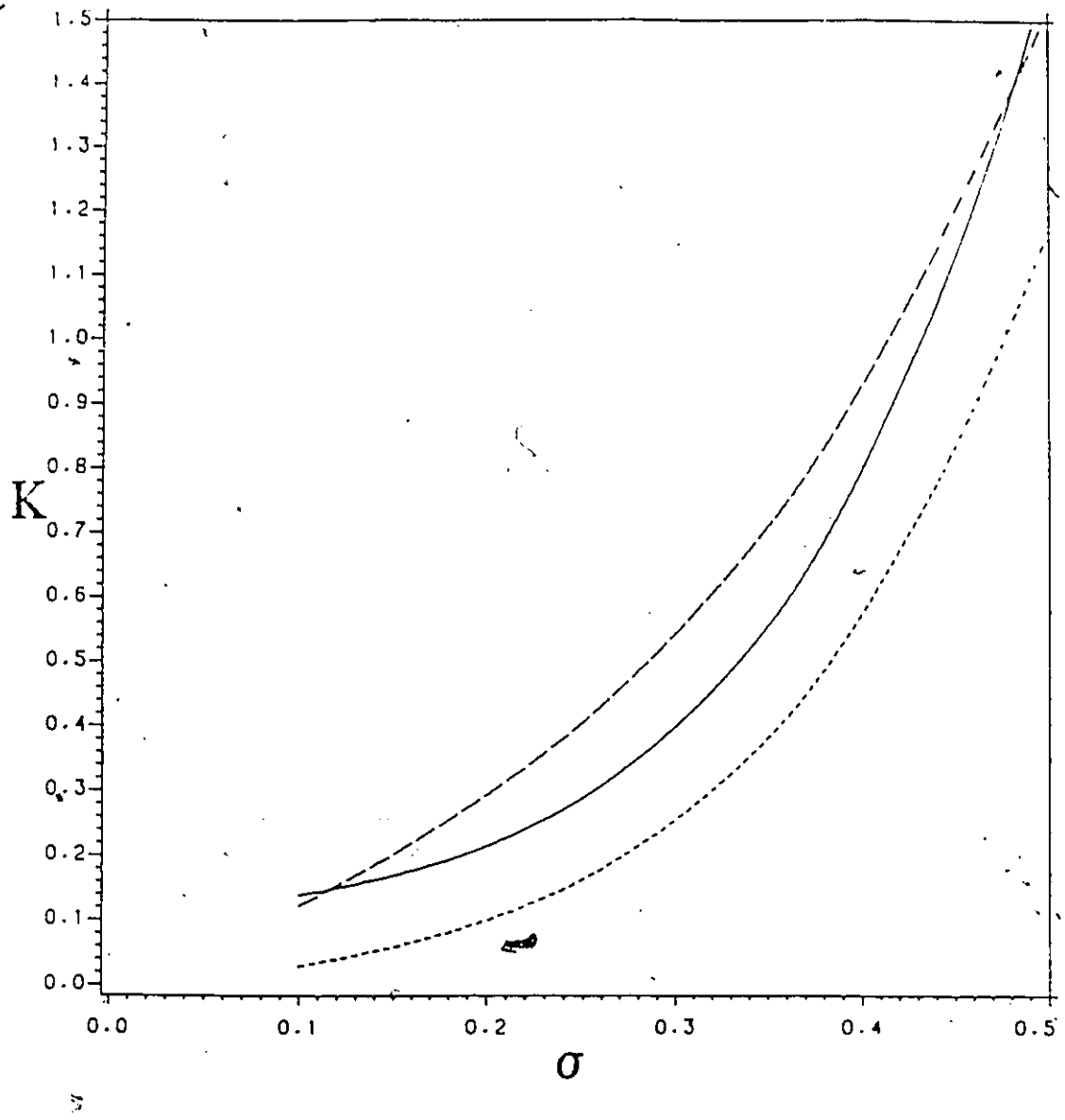

Figure 2.3. Variation of pressure loss coefficient with solidity at large Reynolds numbers; — — based on eq.(2.25), ——— based on eq.(2.27), · · · based on eq.(2.28).

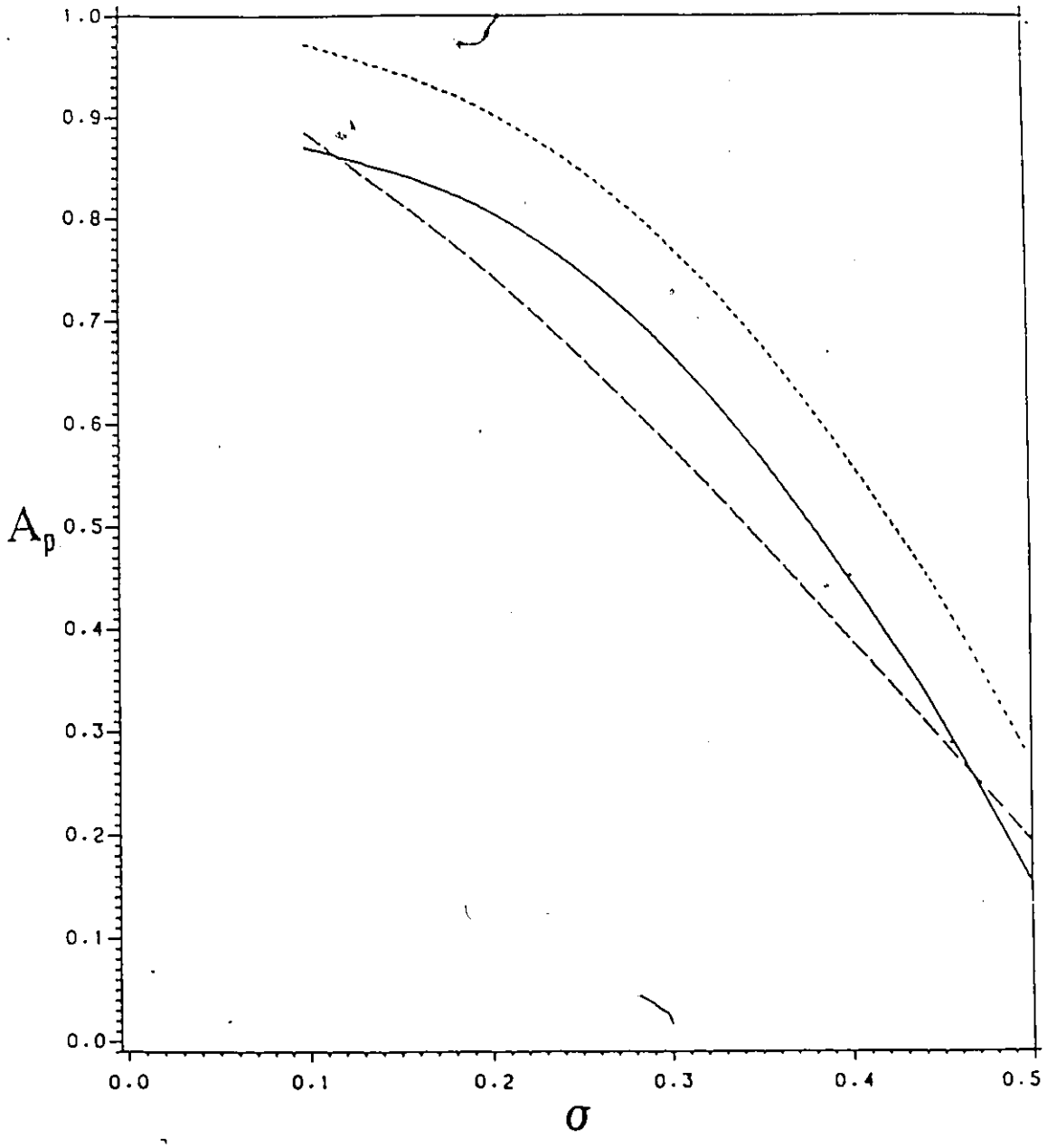

Figure 2.4. Variation of predicted shear reduction factor at large Reynolds numbers. (symbols as in Figure 2.3).

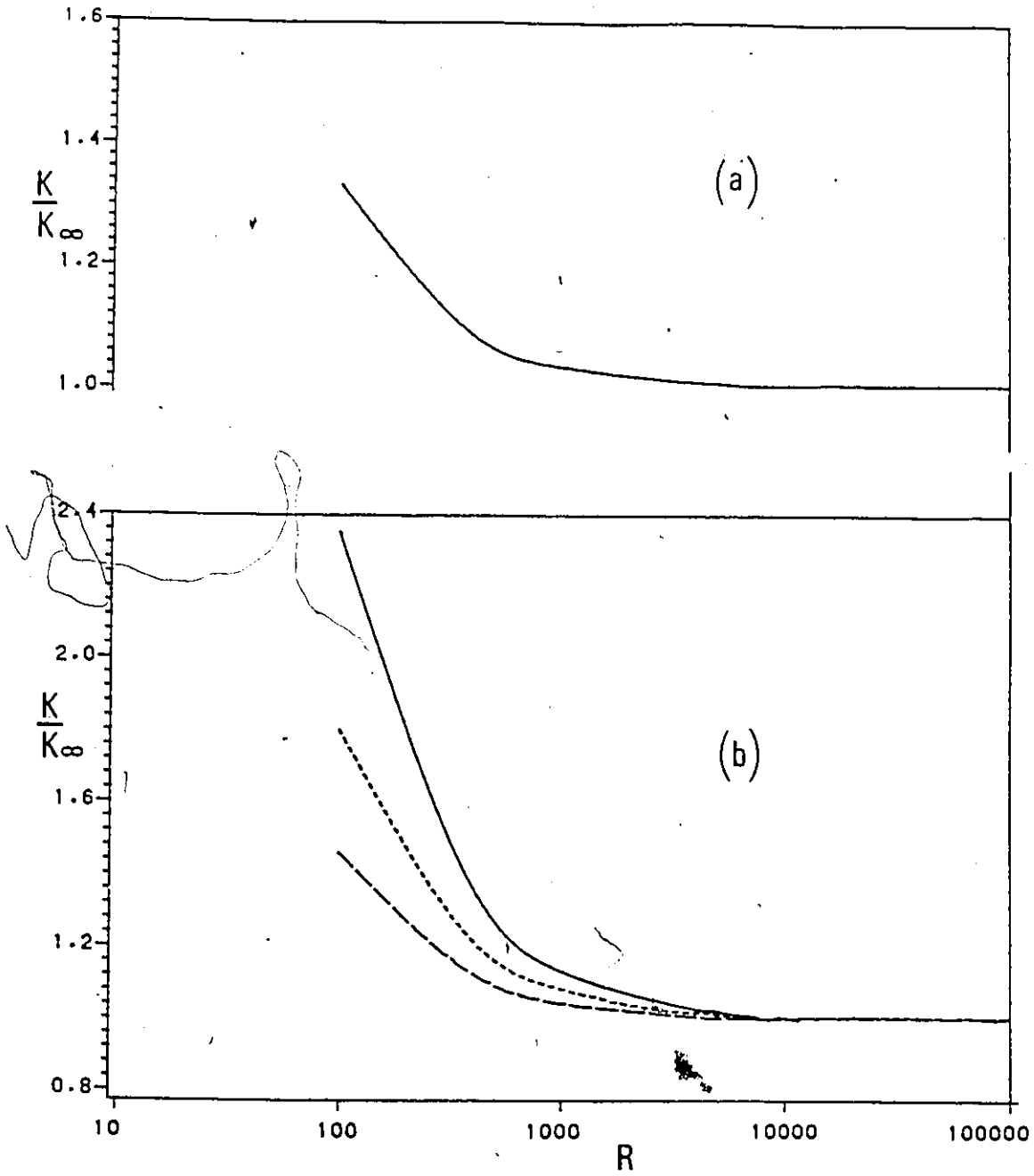

Figure 2.5. Effect of Reynolds number on pressure loss coefficient; (a) based on eq.(2.26), (b) based on eq.(2.28); ——— σ=0.25, - - - σ = 0.35, —— —— σ =0.45. In Figure a, the three curves nearly coincide.

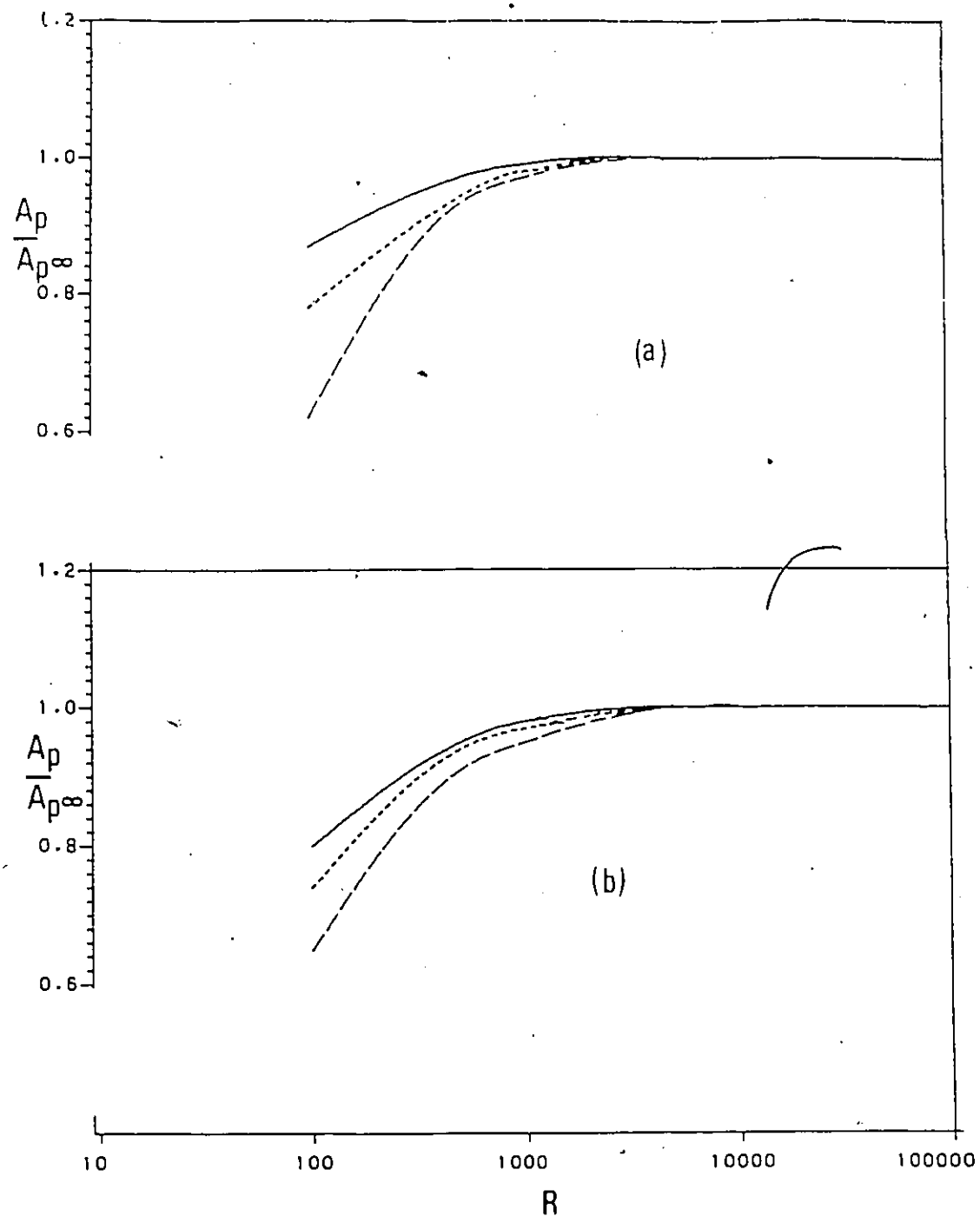

Figure 2.6. Effect of Reynolds number on predicted shear reduction factor; (a) based on eq.(2.26), (b) based on eq.(2.28); ——— σ=0.25, ···· σ = 0.35, — — σ =0.45.

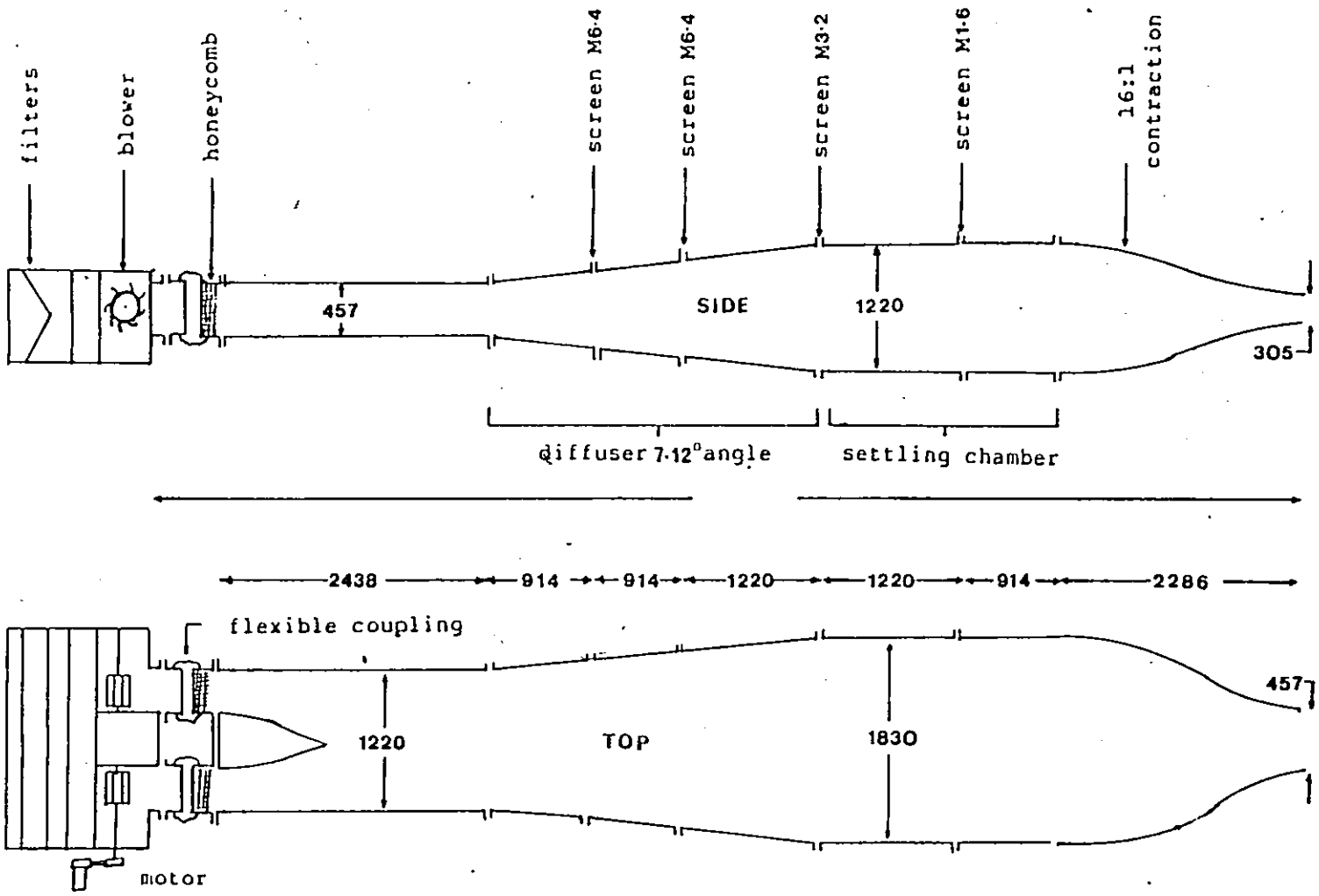

Figure 3.1. Upstream section of the wind tunnel. All dimensions in mm.

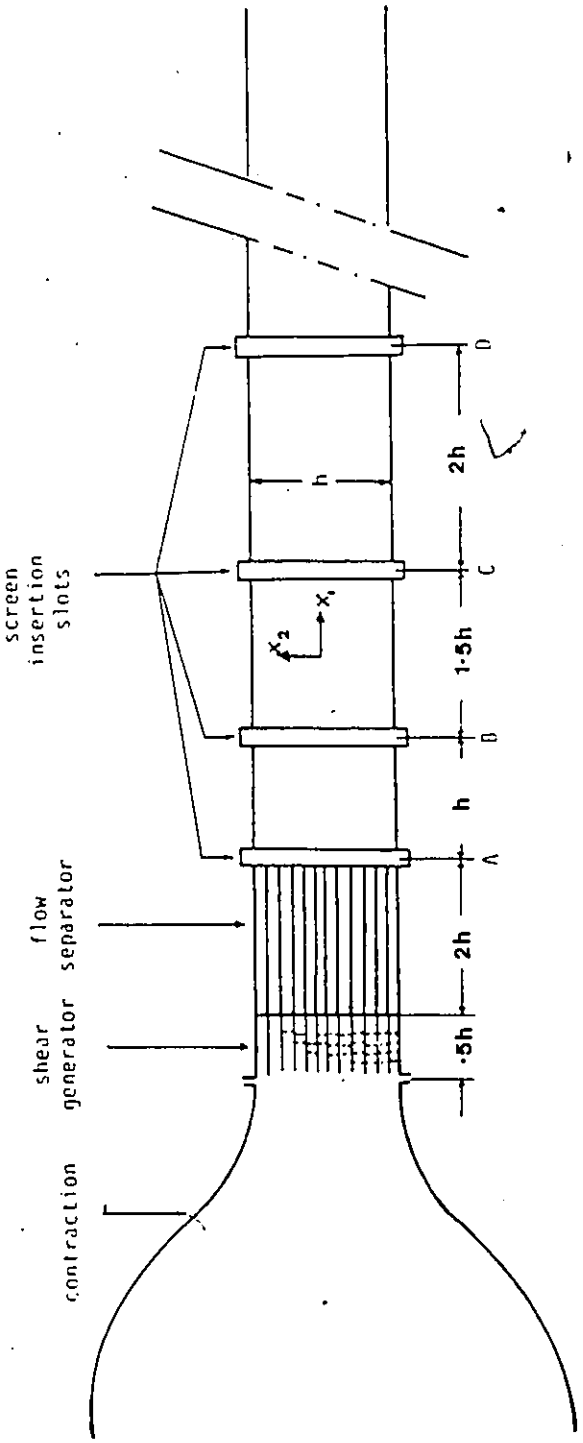

Figure 3.2. Sketch of the test section.

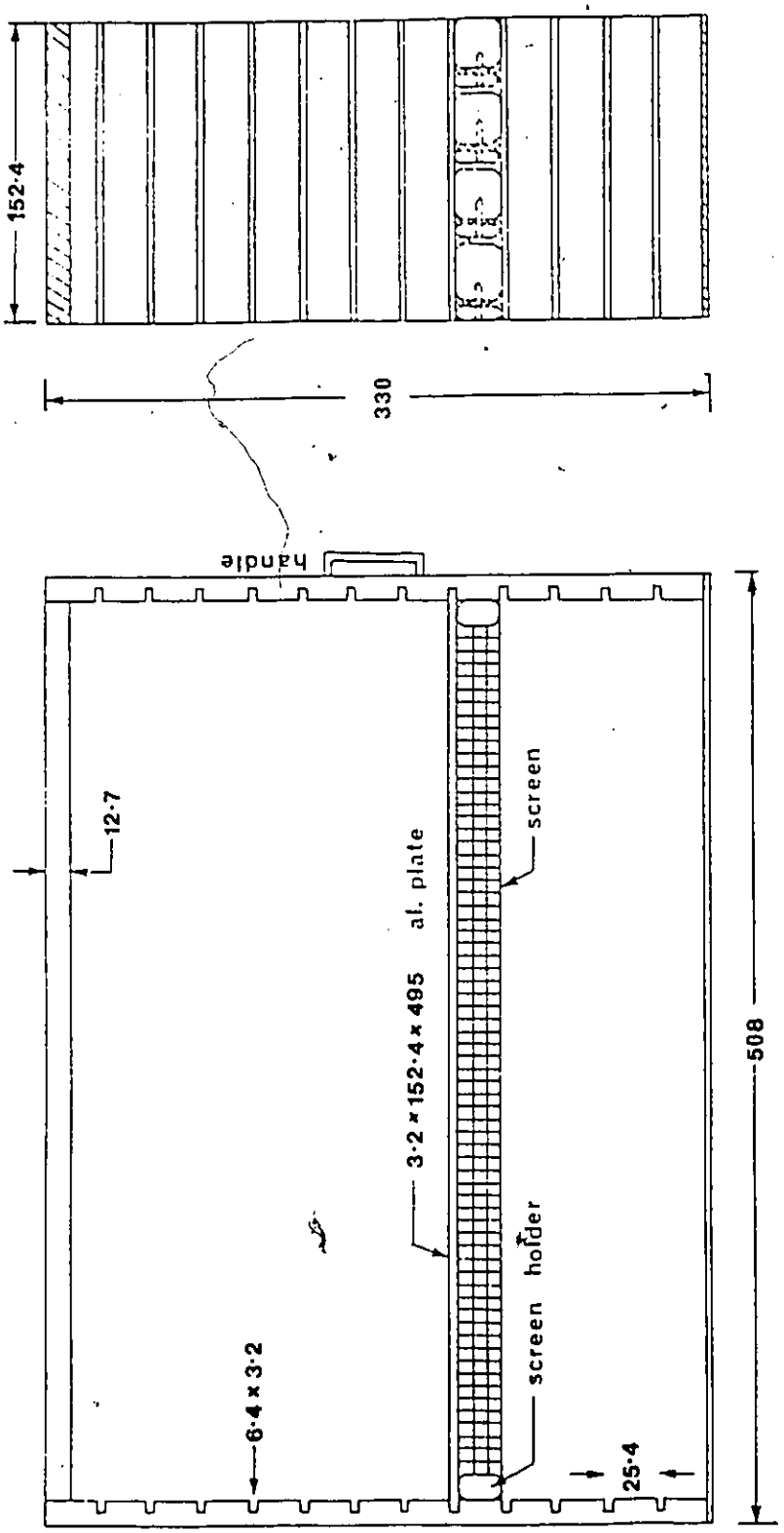

Figure 3.3. Shear generator. All dimensions in mm.

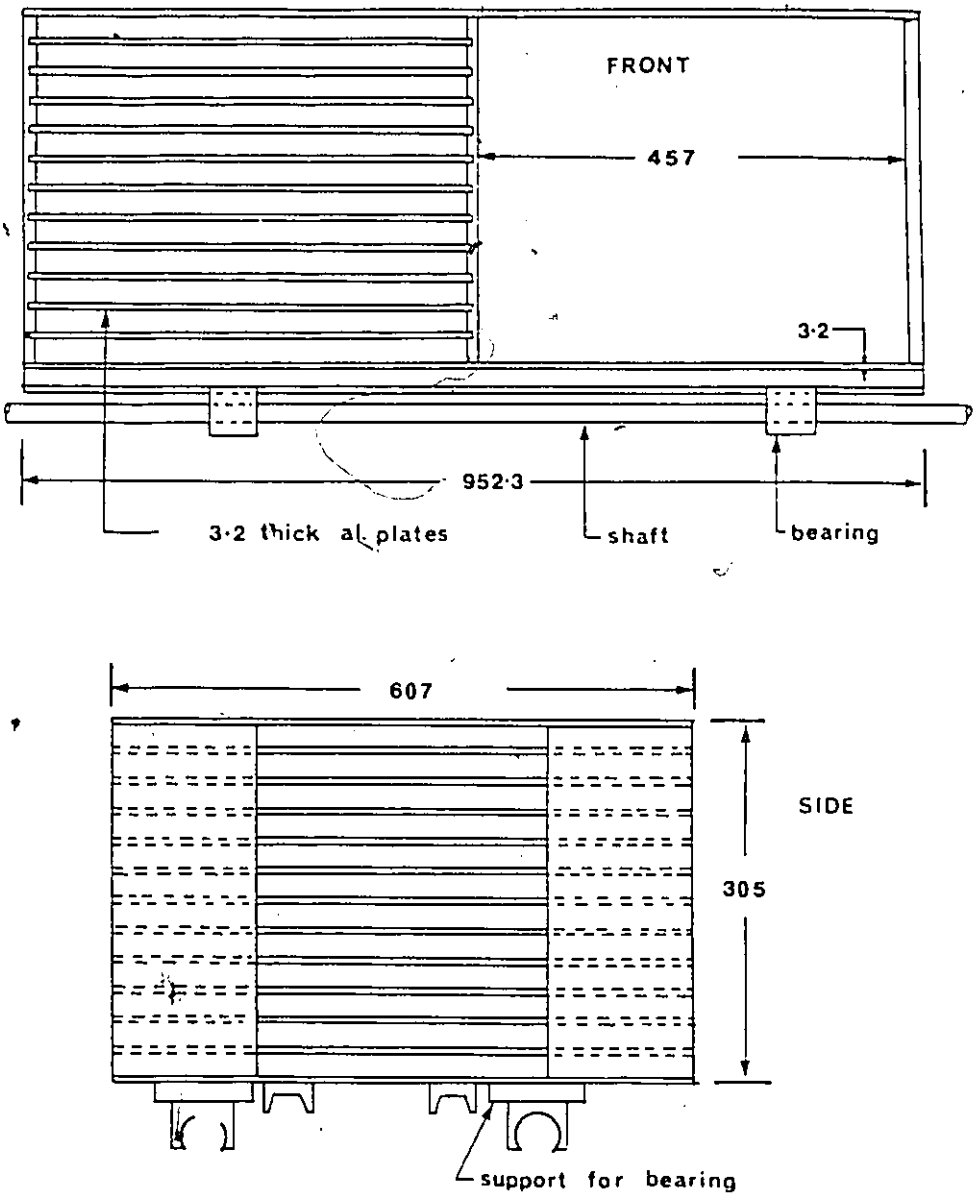

Figure 3.4. Flow separator. All dimensions in mm.

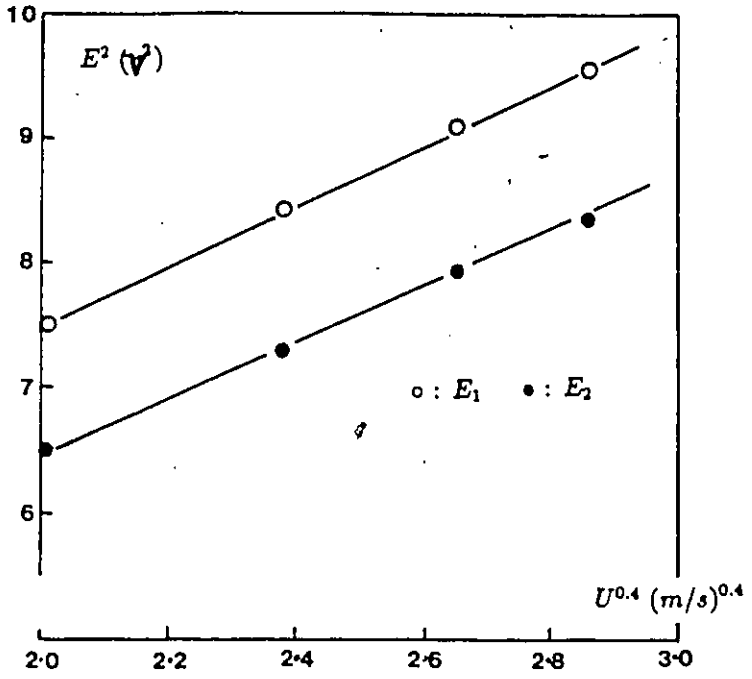

Figure 3.5. Typical calibration curves for a cross-wire.

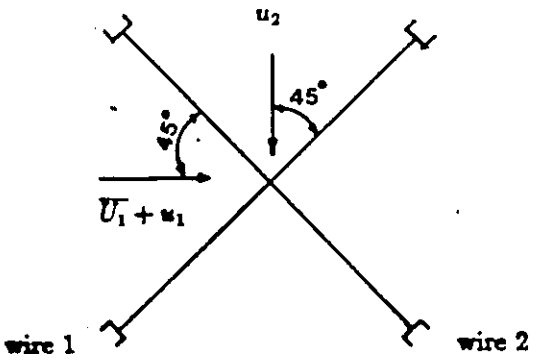

$$U_{eff1} = (\overline{U_1} + u_1 + u_2)cos45$$

$$U_{eff2} = (\overline{U_1} + u_1 - u_2)cos45$$

Figure 3.6. Effective cooling velocities for a cross wire.

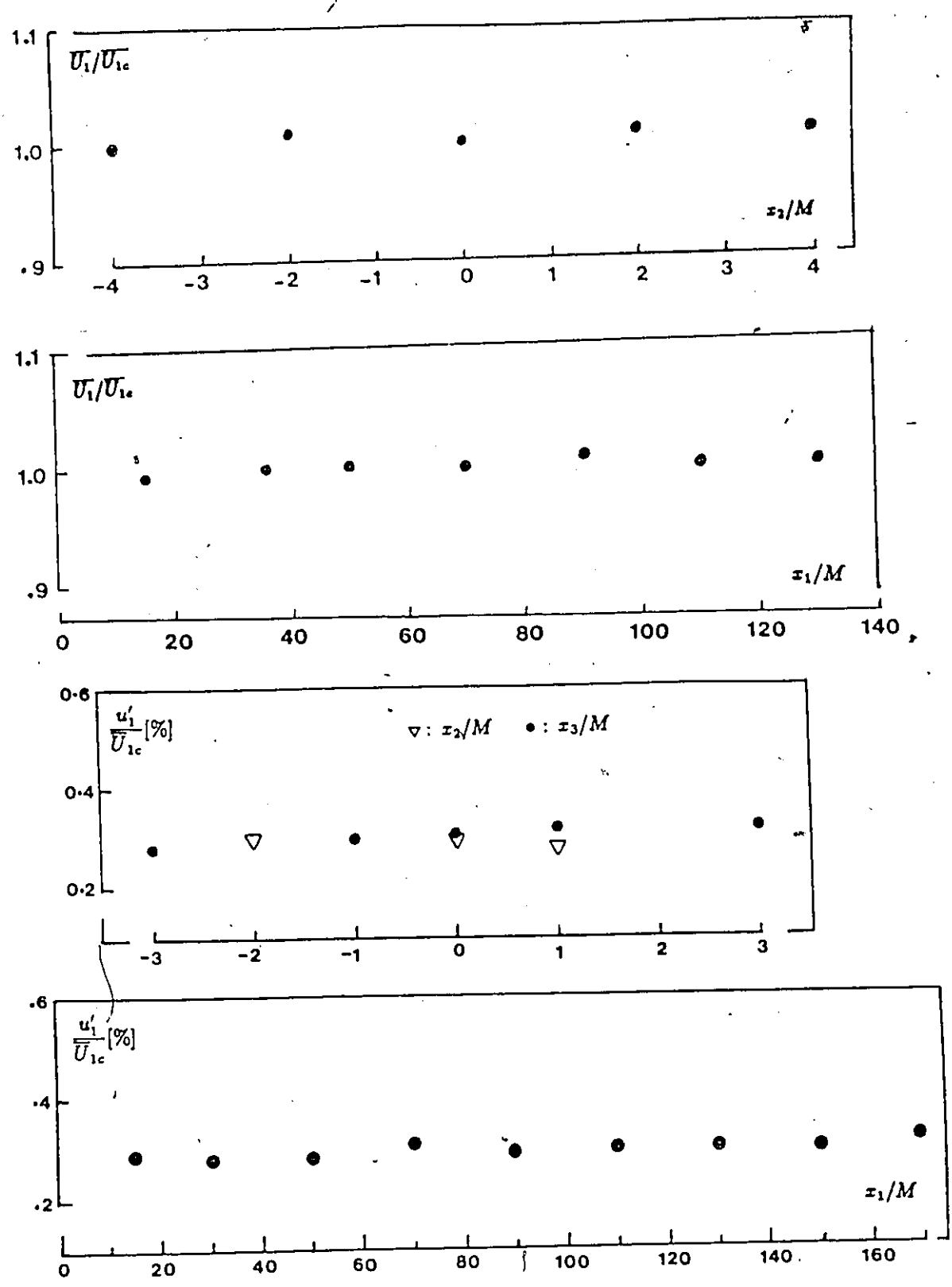

Figure 4.1. Free stream measurements. U_{1c}=14m/s

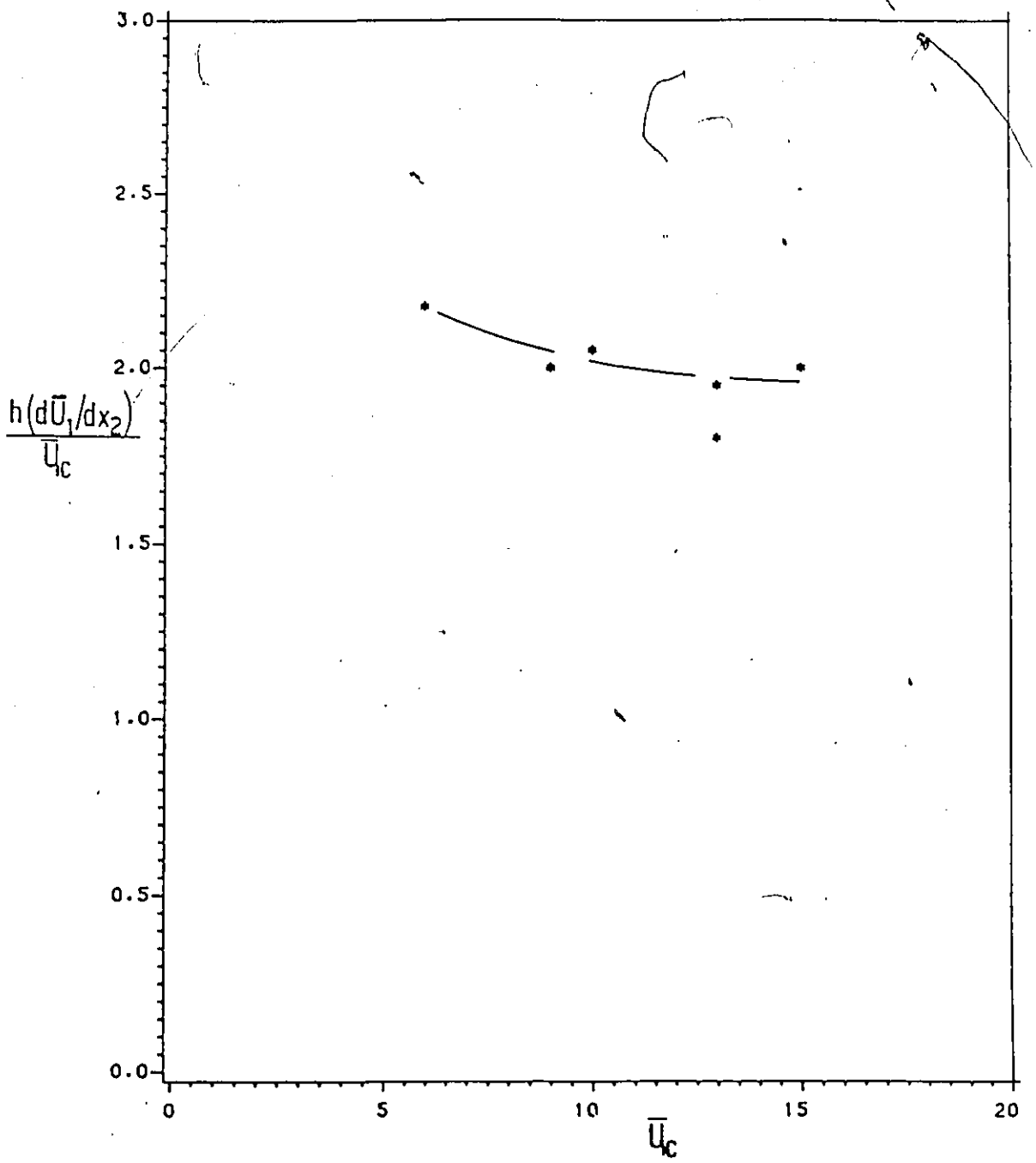

Figure 4.2. Variation of the shear parameter with wind tunnel centerline speed (unobstructed shear).

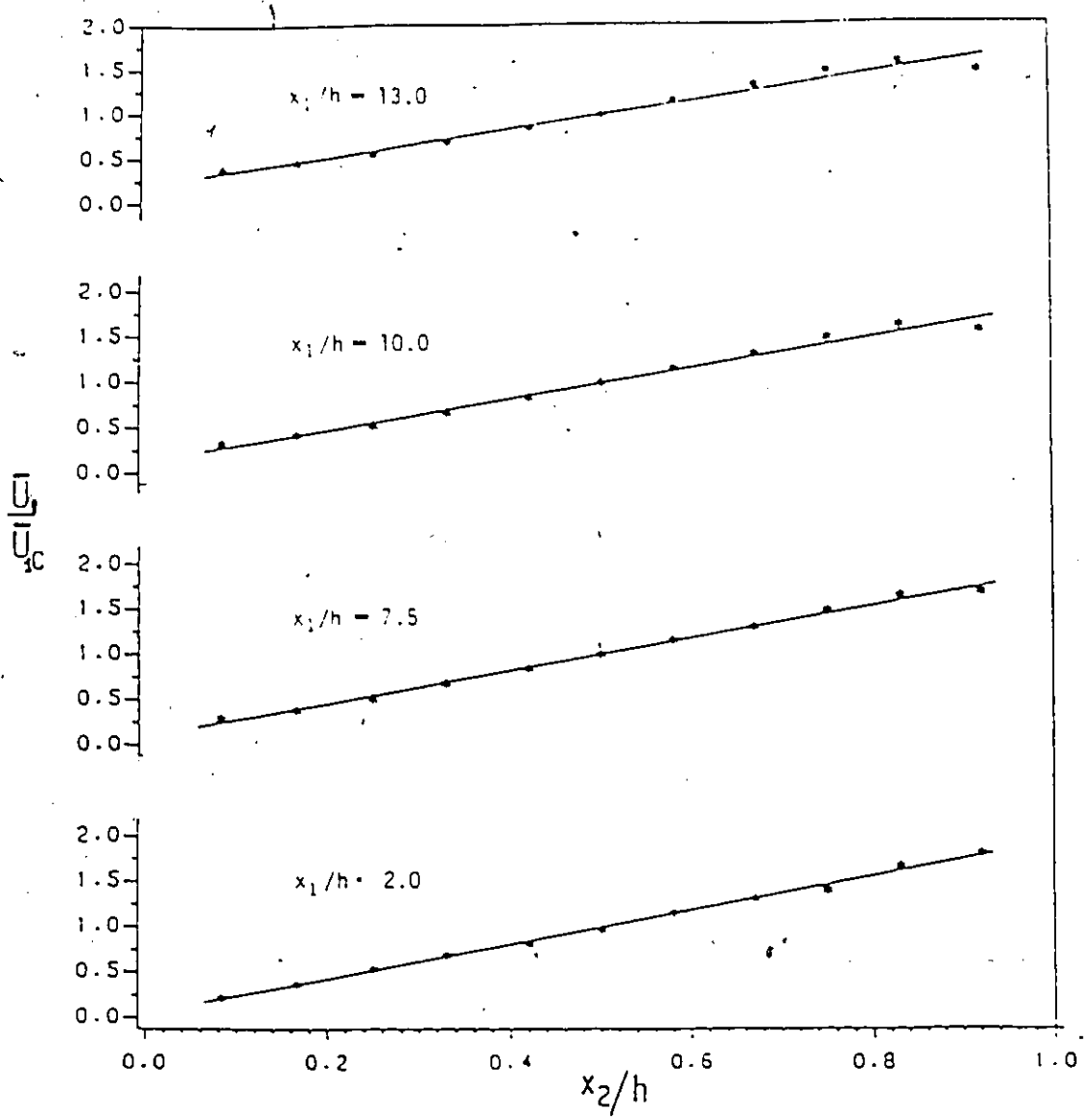

Figure 4.3.Mean velocity profiles; $\overline{U}_{1c} = 13\text{m/s}$.

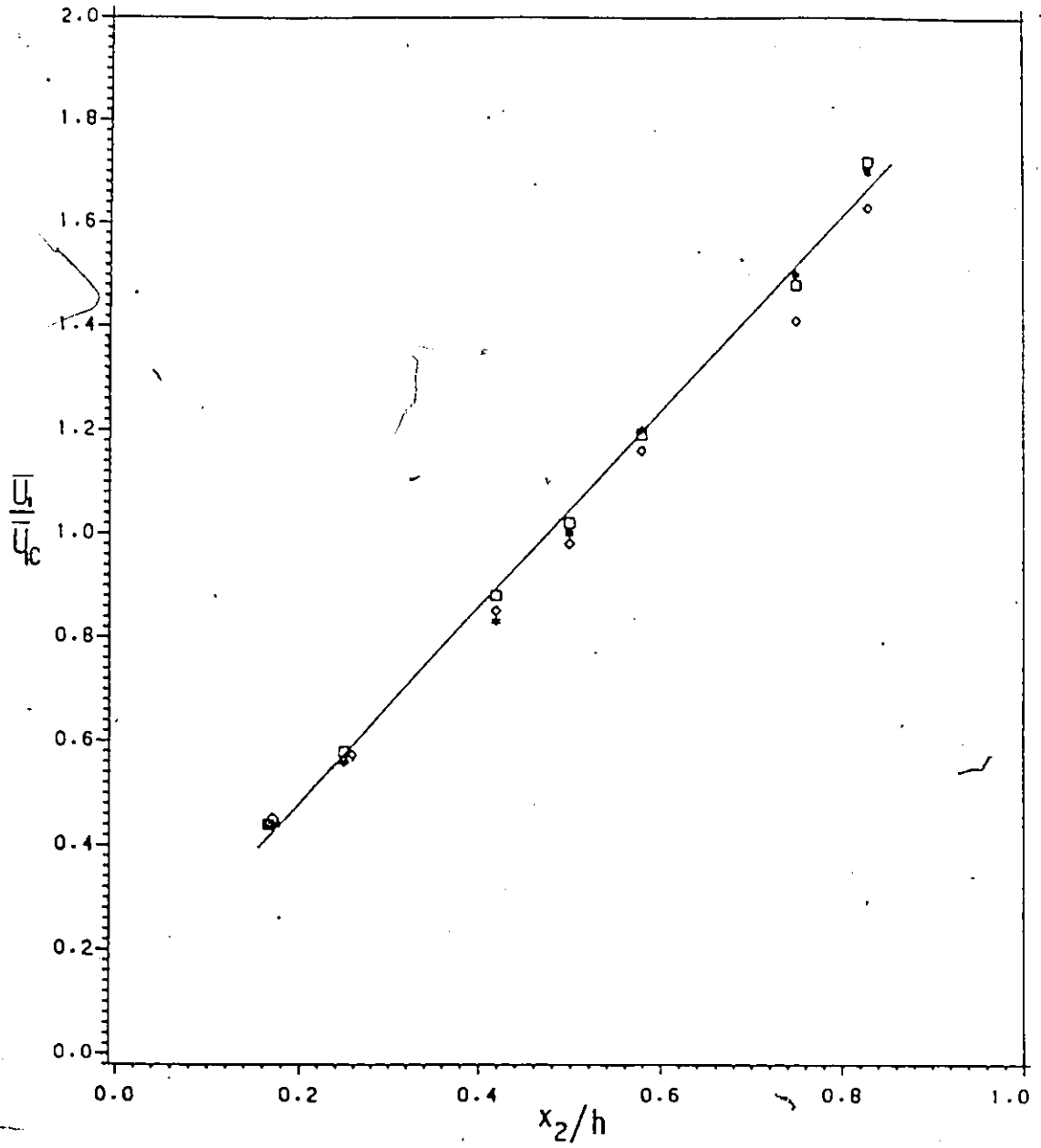

Figure 4.4. Test of spanwise uniformity of mean shear profiles; x_1/h=4.0; $\overline{U}_{1c}$ = 13m/s; x_3/h = -0.451(∗), 0.0(□), +0.451(◇). ——— best fit.

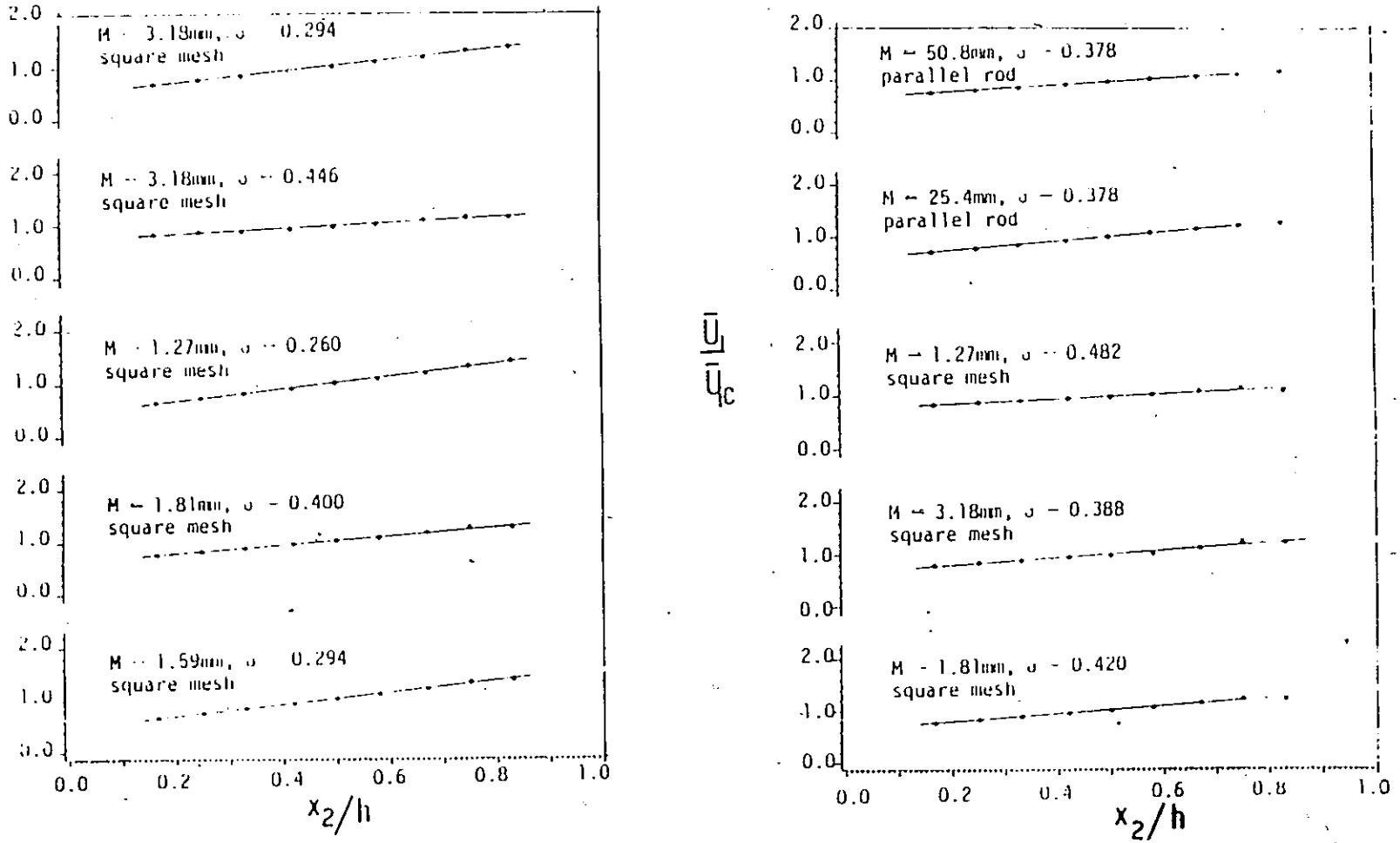

Figure 4.5. Typical mean velocity profiles at $x_1/h = 7.5$ downstream of a single screen inserted at $x_1/h = 1.04$; $\overline{U}_{1c} = 13$in/s.

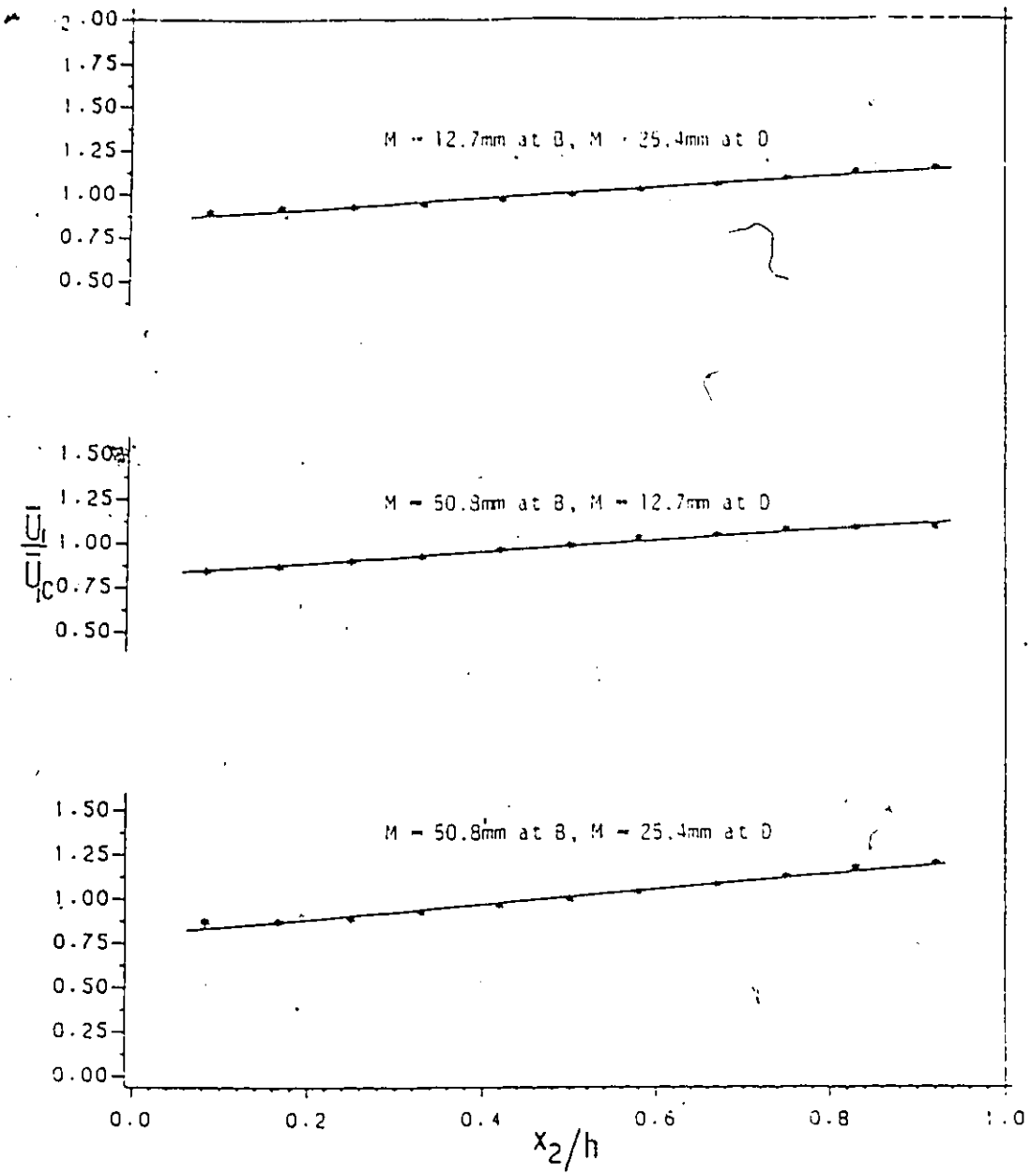

Figure 4.6. Typical mean velocity profiles downstream of multiple grids; $\overline{U}_{1c}$ =13m/s.

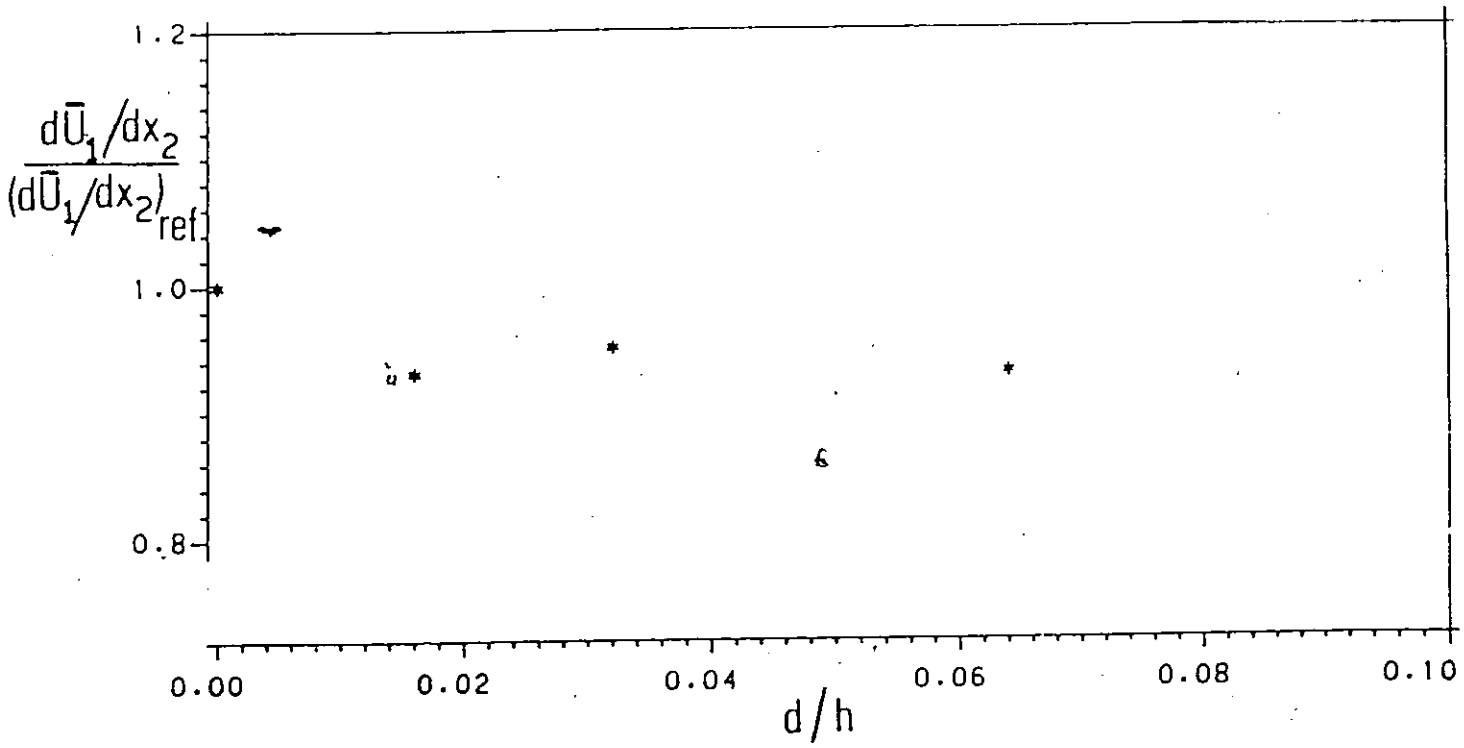

Figure 4.7. Effect of screen insertion at x_1/h=4.5 on the upstream shear at x_1/h=1.5; $(dU_1/dx_2)_{ref}$=84s^{-1}; $\bar{U}_{ic}$=13m/s.

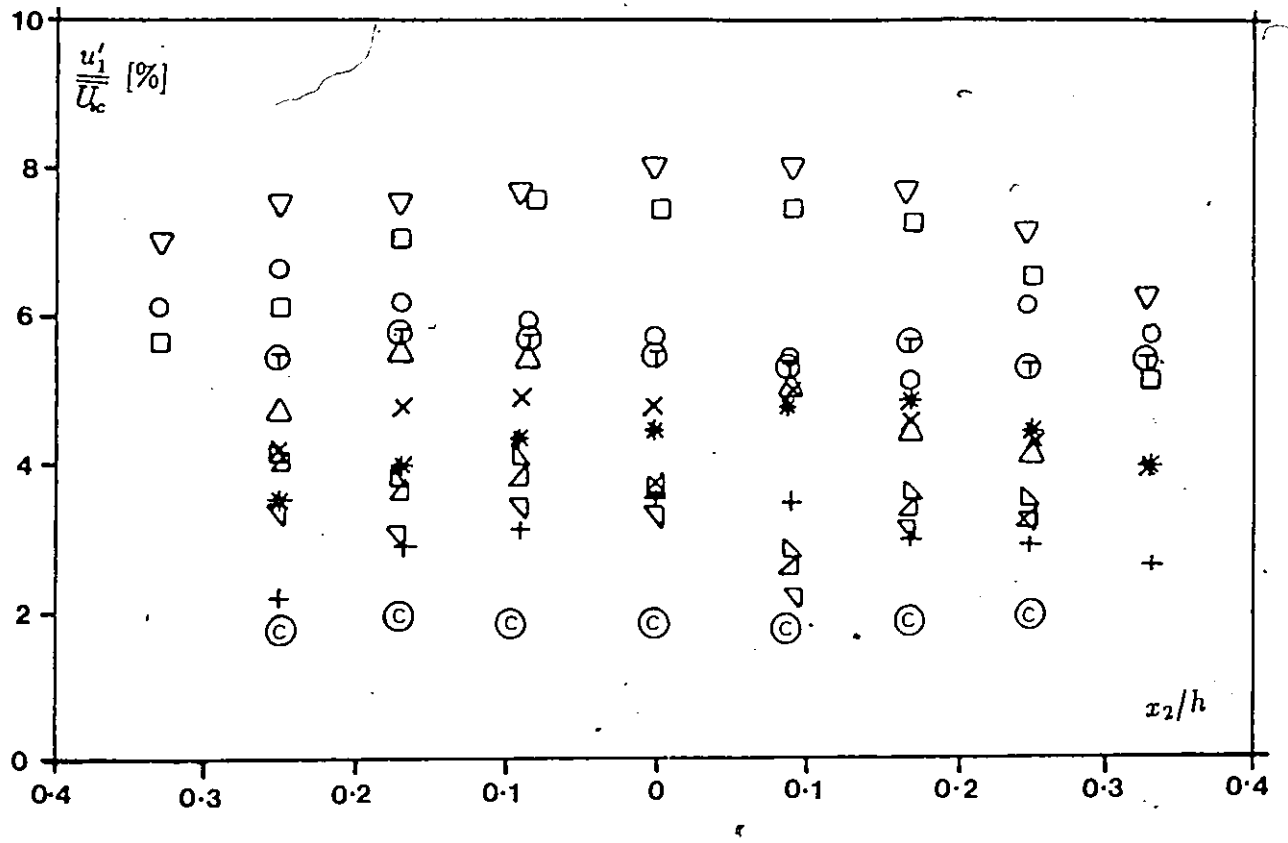

Figure 4.8. Typical transverse variation of the streamwise r.m.s. velocity fluctuations. Symbols as in Table 3; x_1/h=7.5 (o, □, ▽), 8.33 (△,◺,◹,◿). 10.0 (ⓒ), 11.0 (ⓣ), 11.7 (×, +, *).

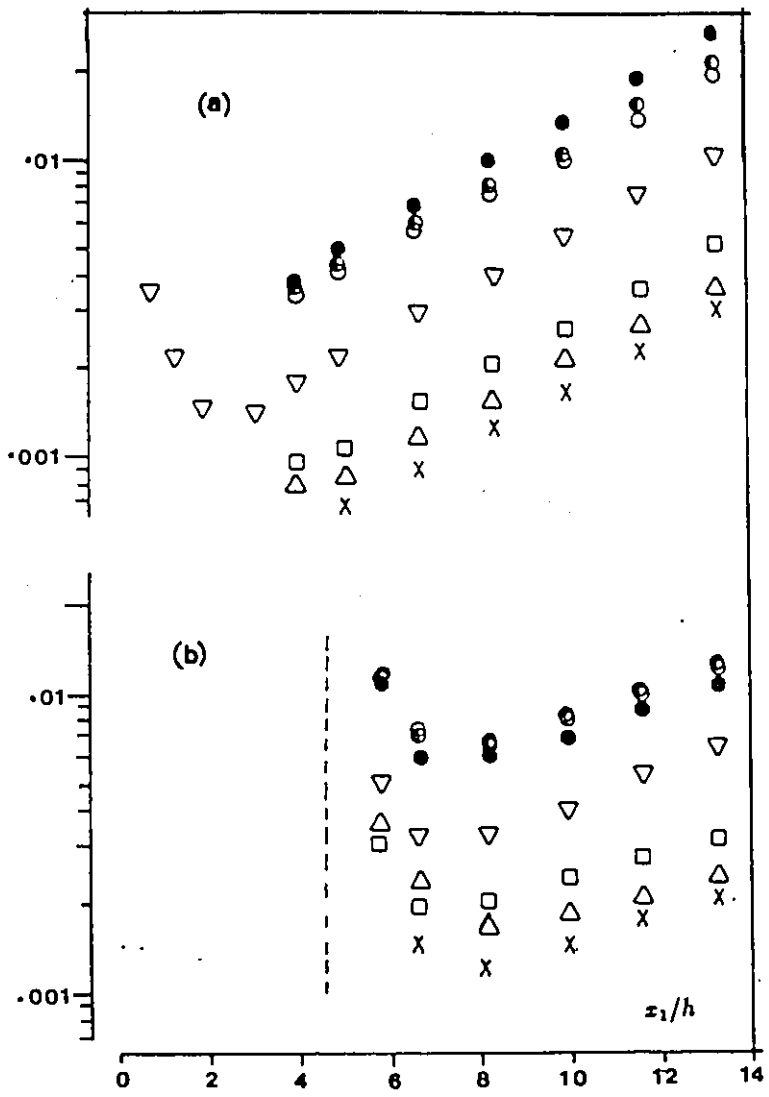

Figure 4.9. Downstream development of the Reynolds stresses and the turbulent kinetic energy. $\nabla \overline{u_1^2}/\overline{U_{1c}^2}$, $\square \overline{u_3^2}/\overline{U_{1c}^2}$, $\times -\overline{u_1 u_2}/\overline{U_{1c}^2}$ ($\overline{U}_{1c}$=13m/s in all cases); $\overline{q^2}/\overline{U_{1c}^2}$: $\circ\, \overline{U}_{1c} = 13m/s$, $\bullet\, \overline{U}_{1c} = 9m/s$, $\bullet\, \overline{U}_{1c} = 6m/s$. Dashed lines indicate position of grids.(a) Cases A, B, C (b) Cases D, E, F (c) Cases L, M, N (d) Case P (Table 3).

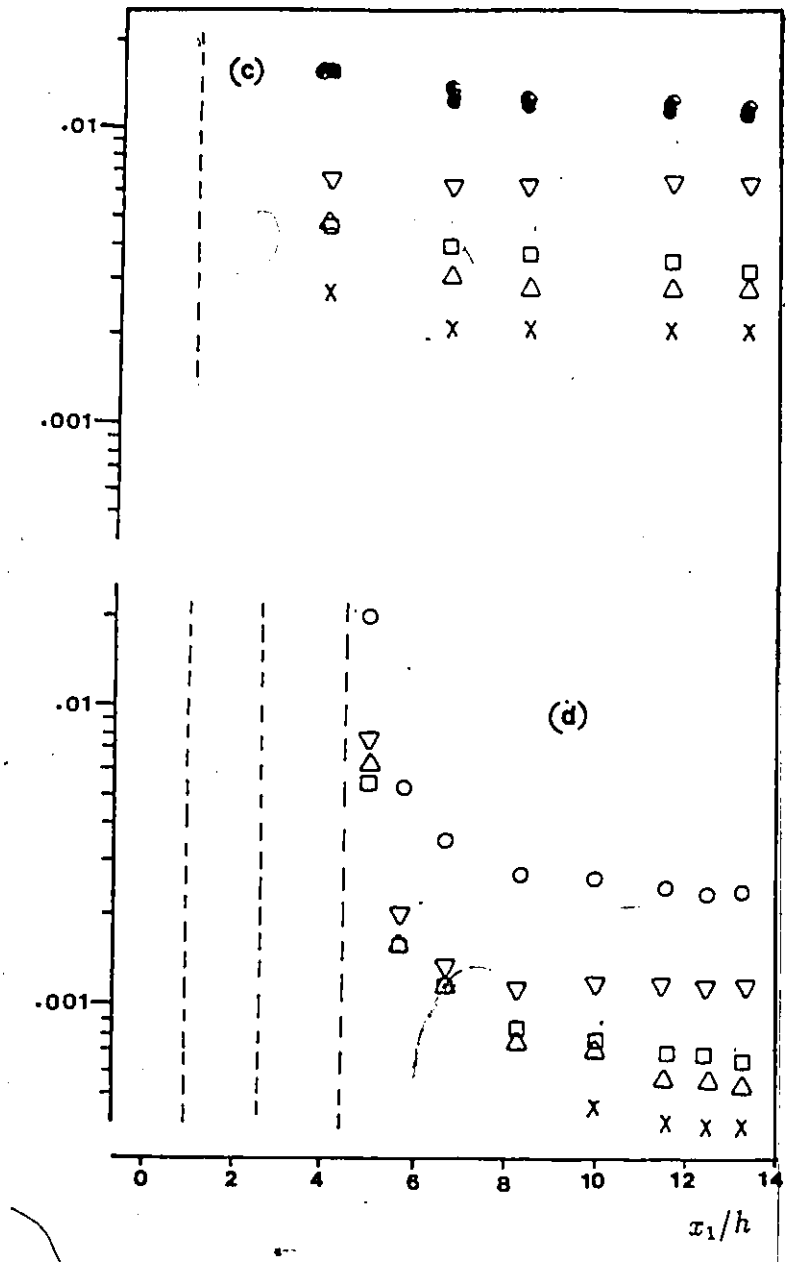

Figure 4.9. continued

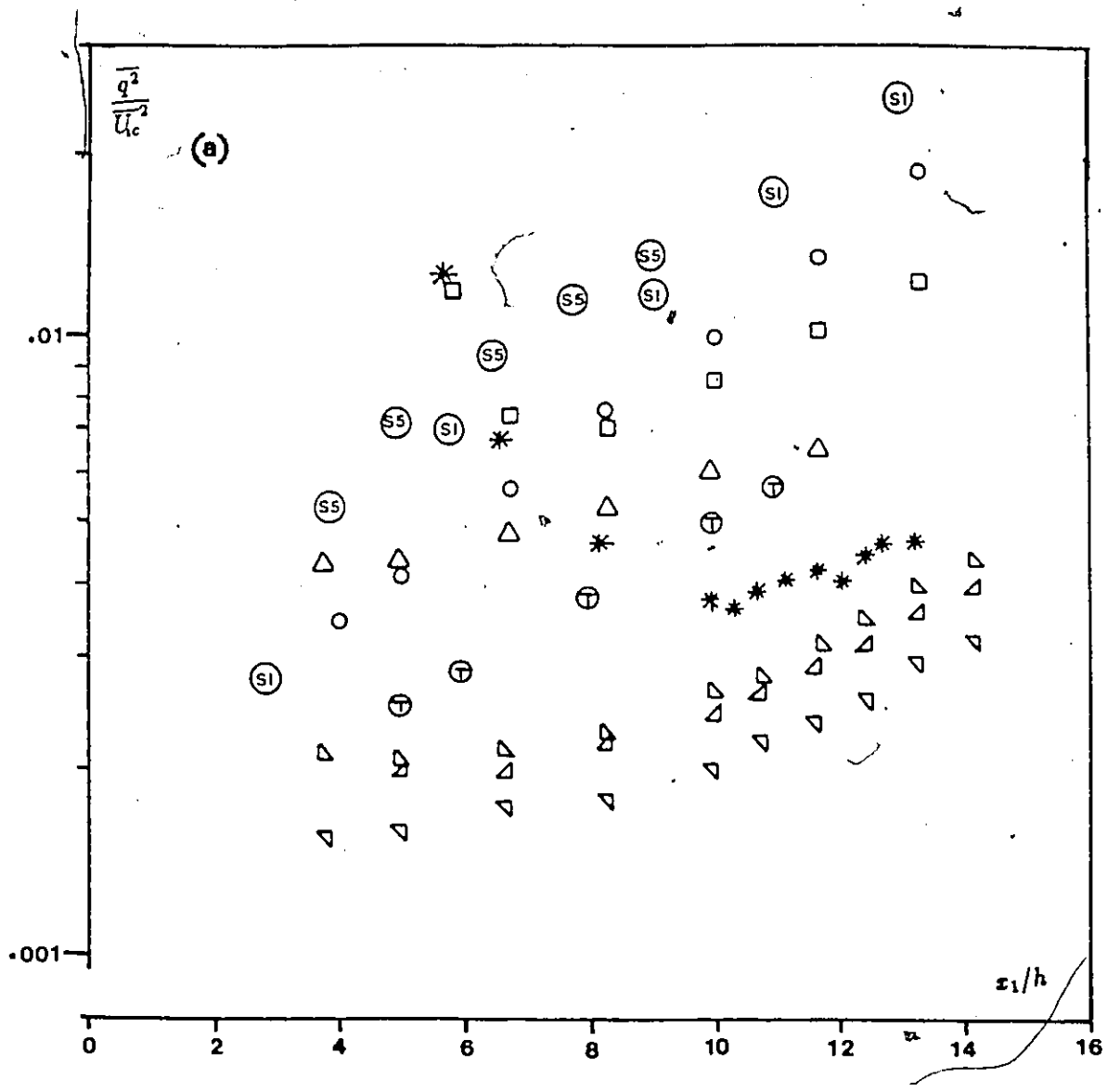

Figure 4.10. Downstream development of $\overline{q^2}/\overline{U_{1c}^2}$. Symbols as in Table 3.

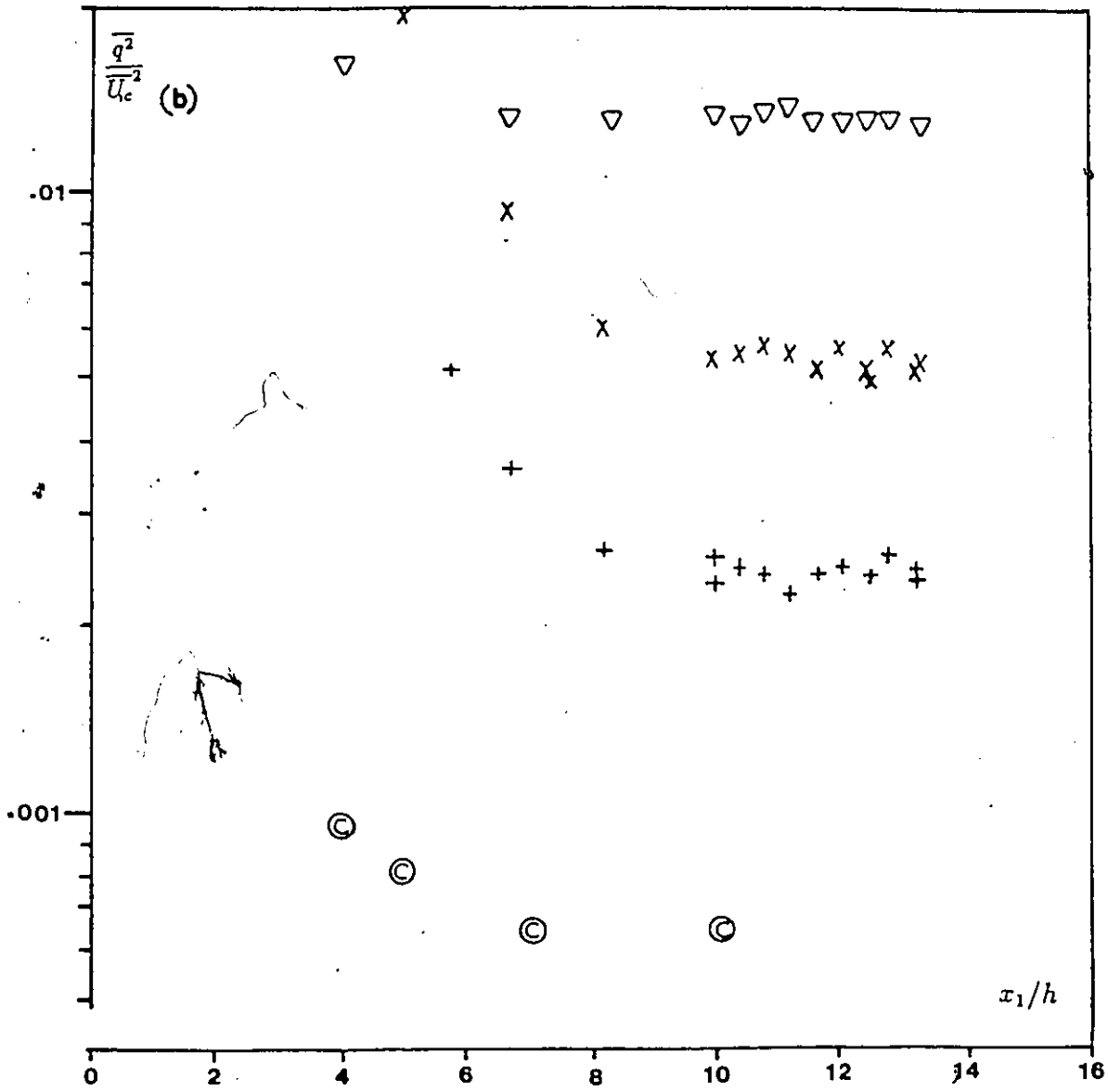

Figure 4.10. continued

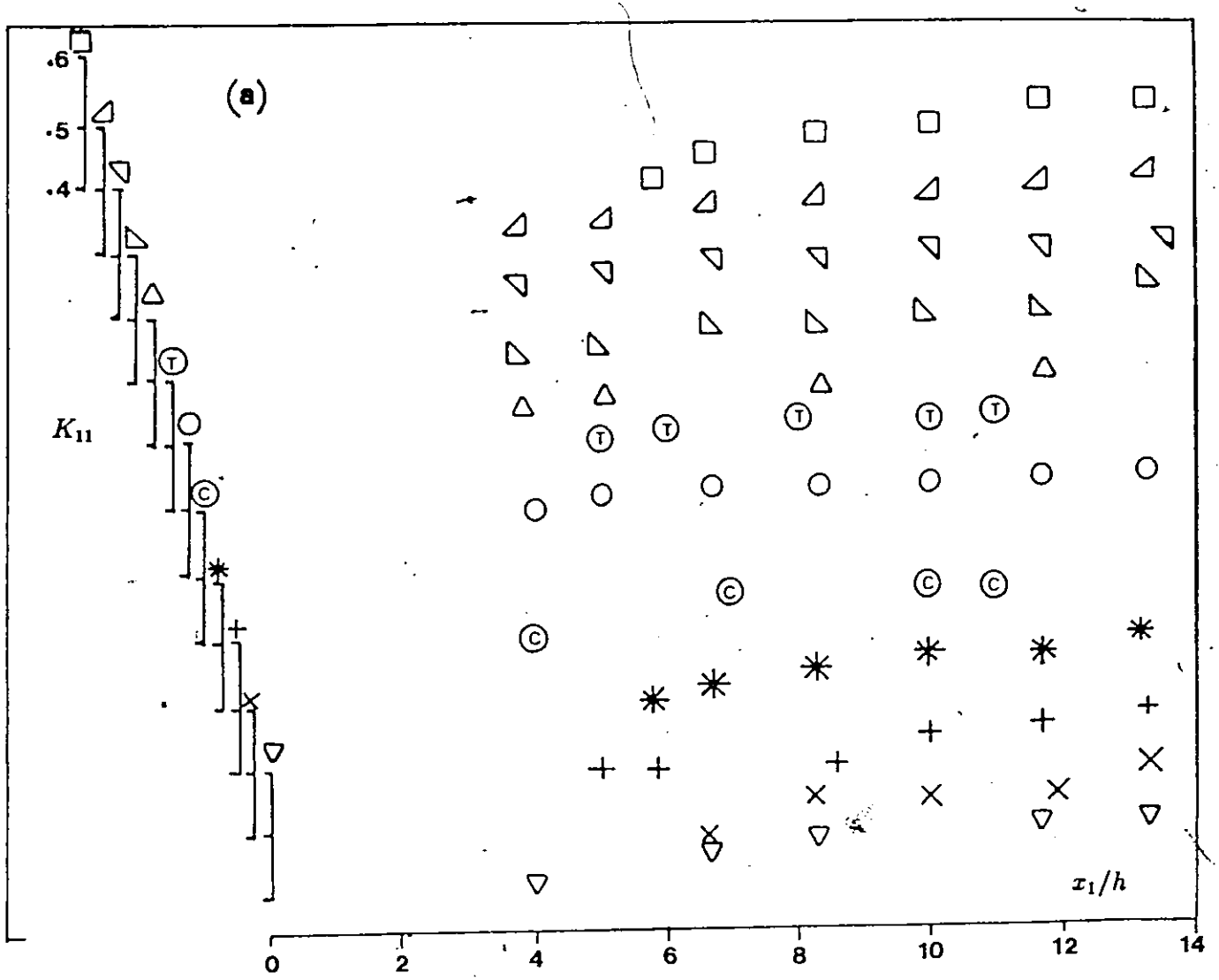

Figure 4.11. Downstream development of the dimensionless Reynolds stresses. Symbols as in Table 3. (a) K_{11} (b) K_{22} (c) K_{33} (d) $-K_{12}$.

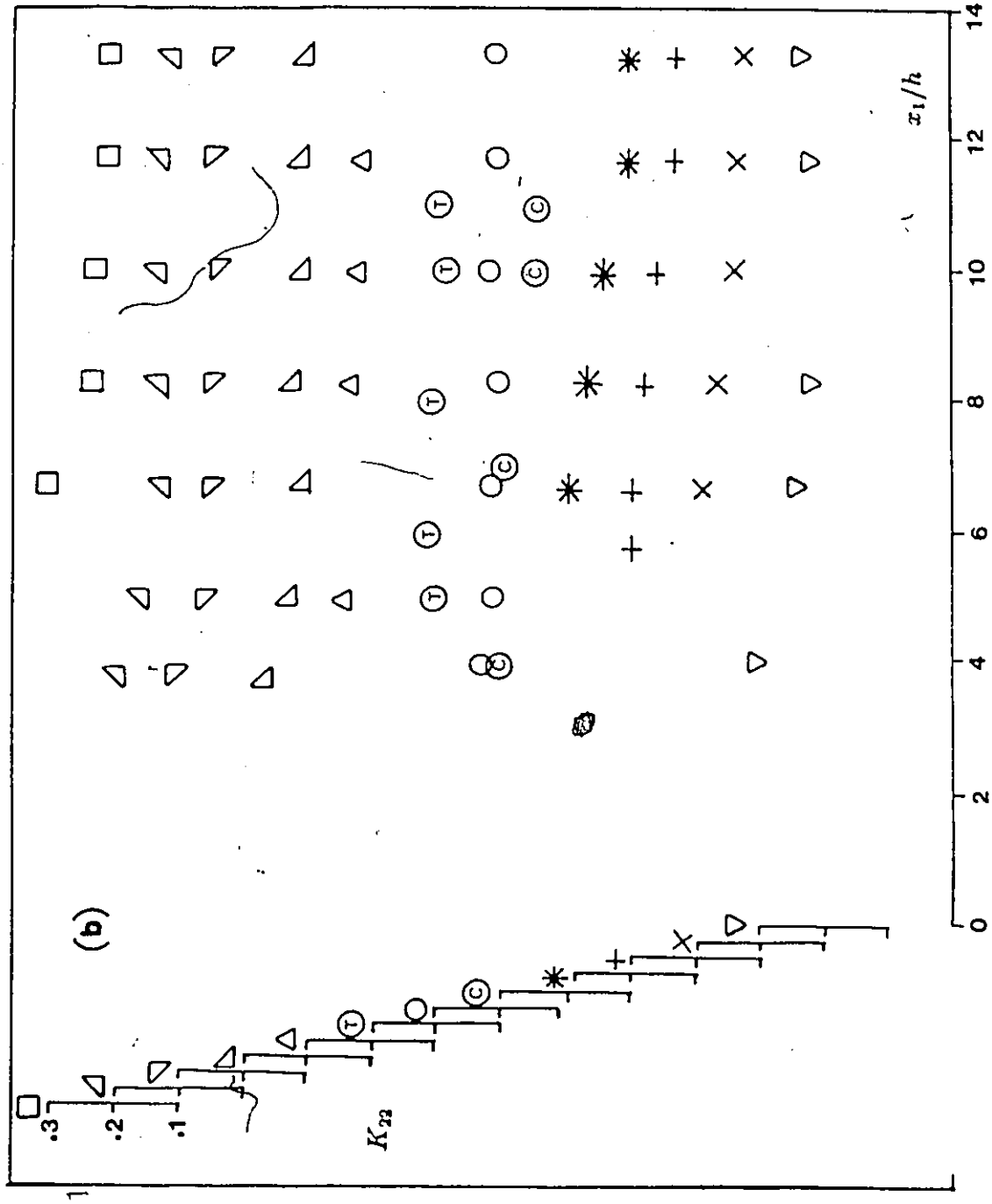

Figure 4.11. continued

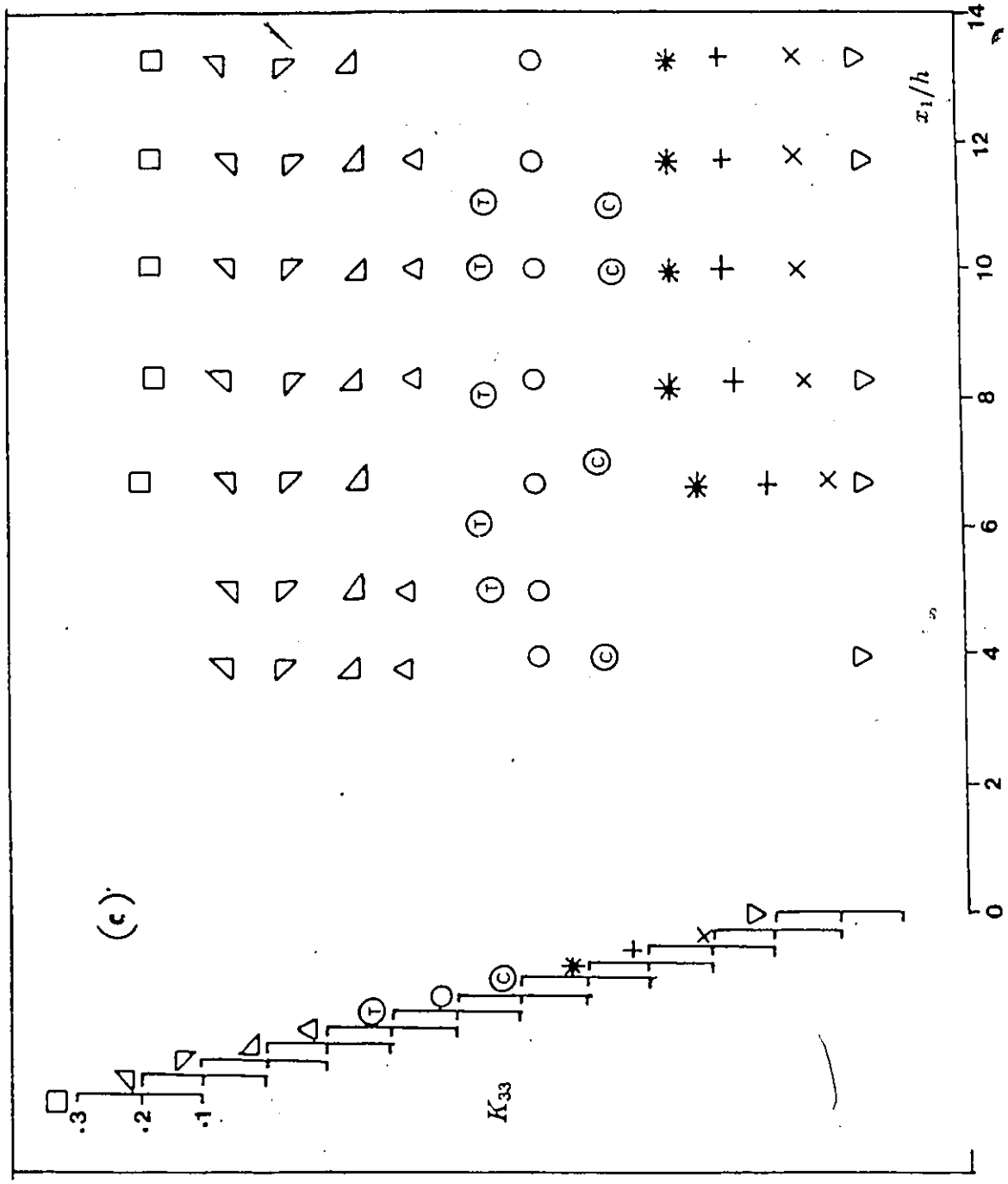

Figure 4.11. continued

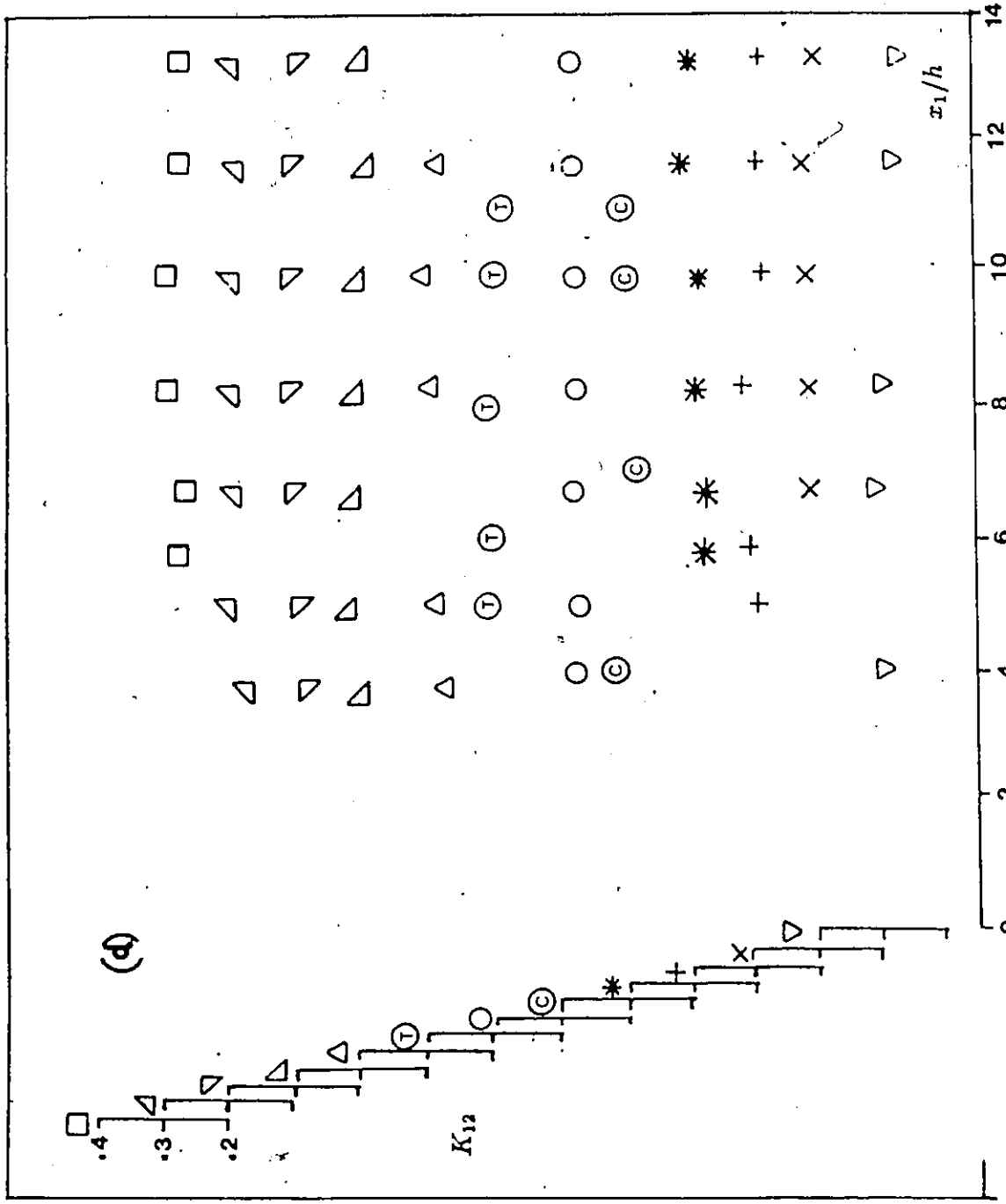

Figure 4.11. continued

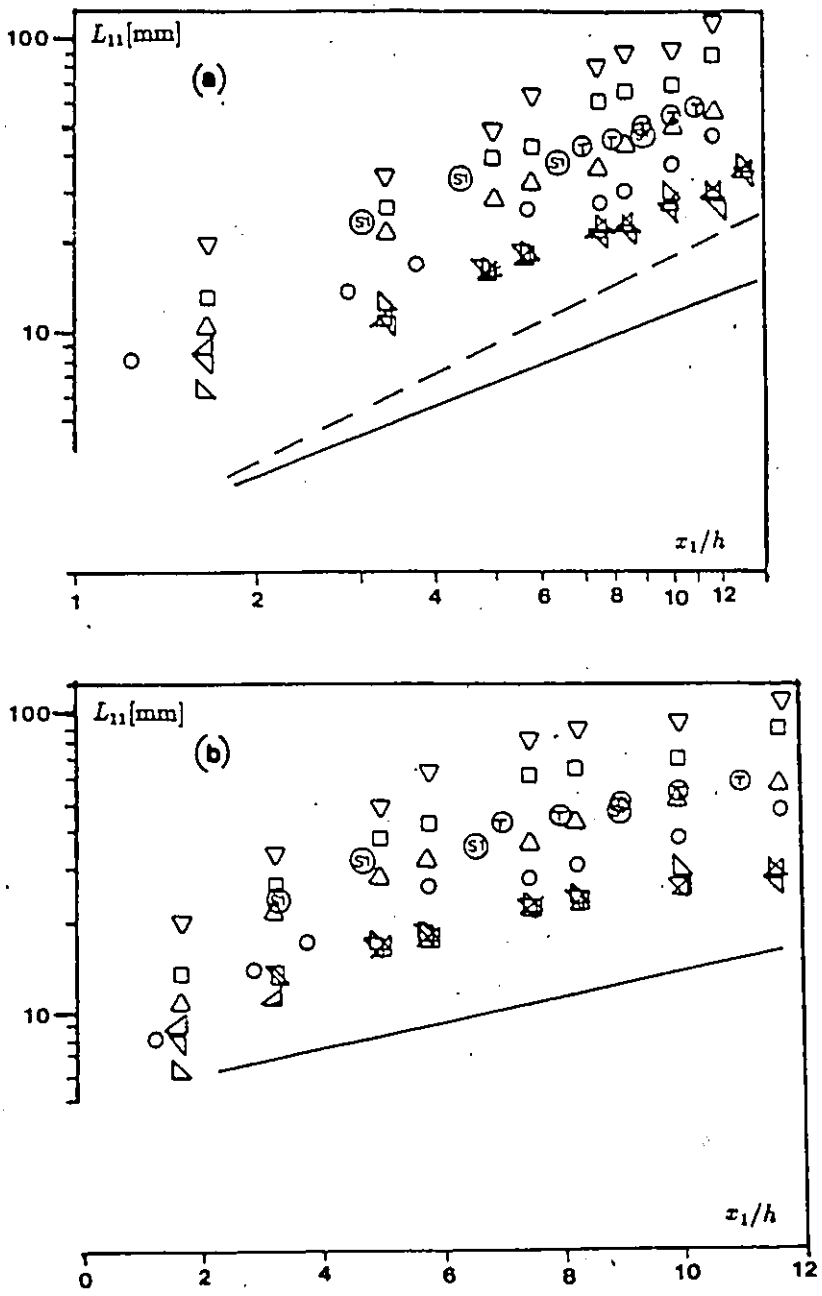

Figure 4.12. Downstream growth of the streamwise integral length scale. Symbols as in Table 3. (a) logarithmic coordinates, ——— n_L=0.8, — — n_L=1.0; (b) semi-logarithmic co-ordinates, ——— k_L=0.33.

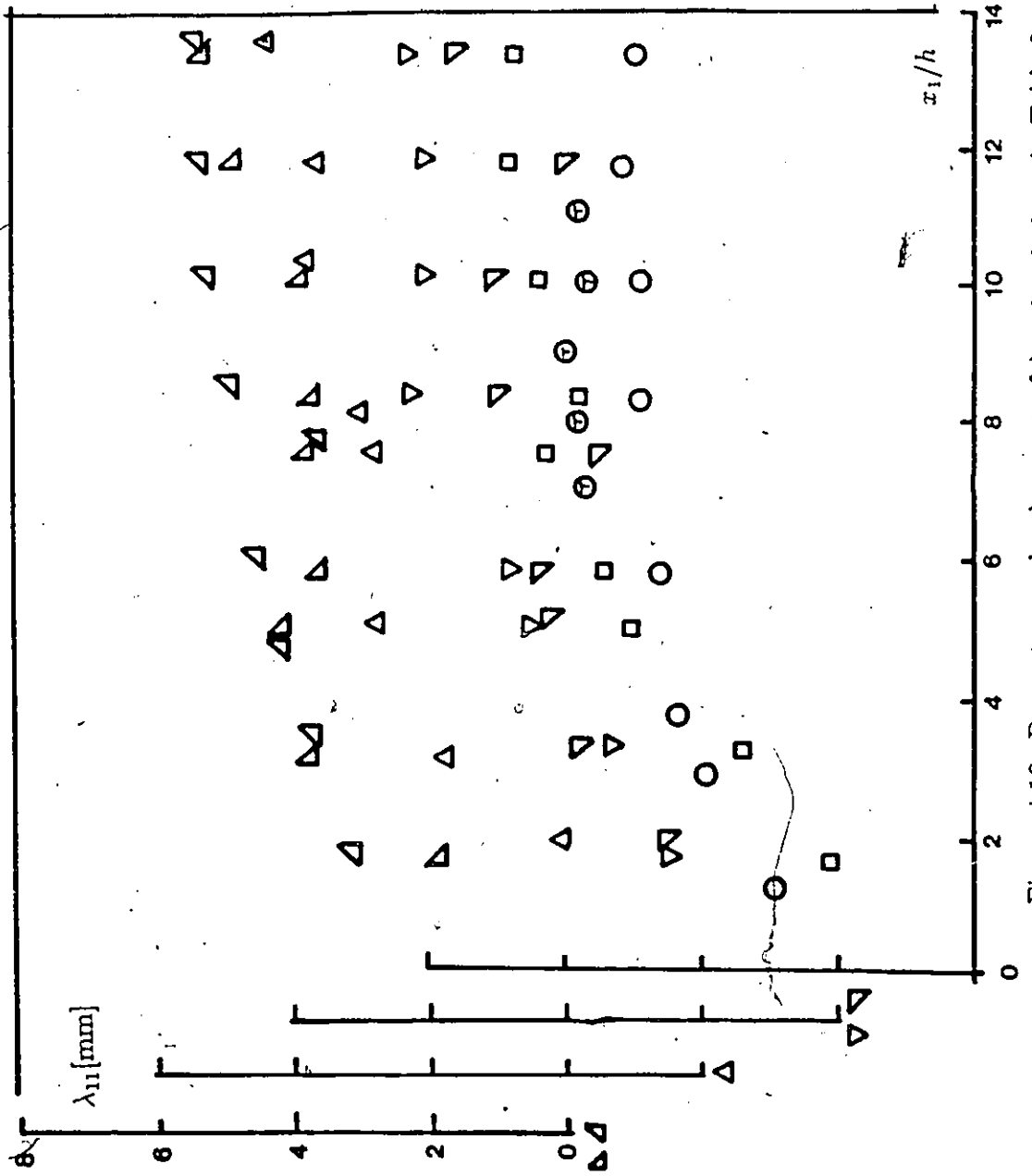

Figure 4.13. Downstream development of λ_{11}. Symbols as in Table 3.

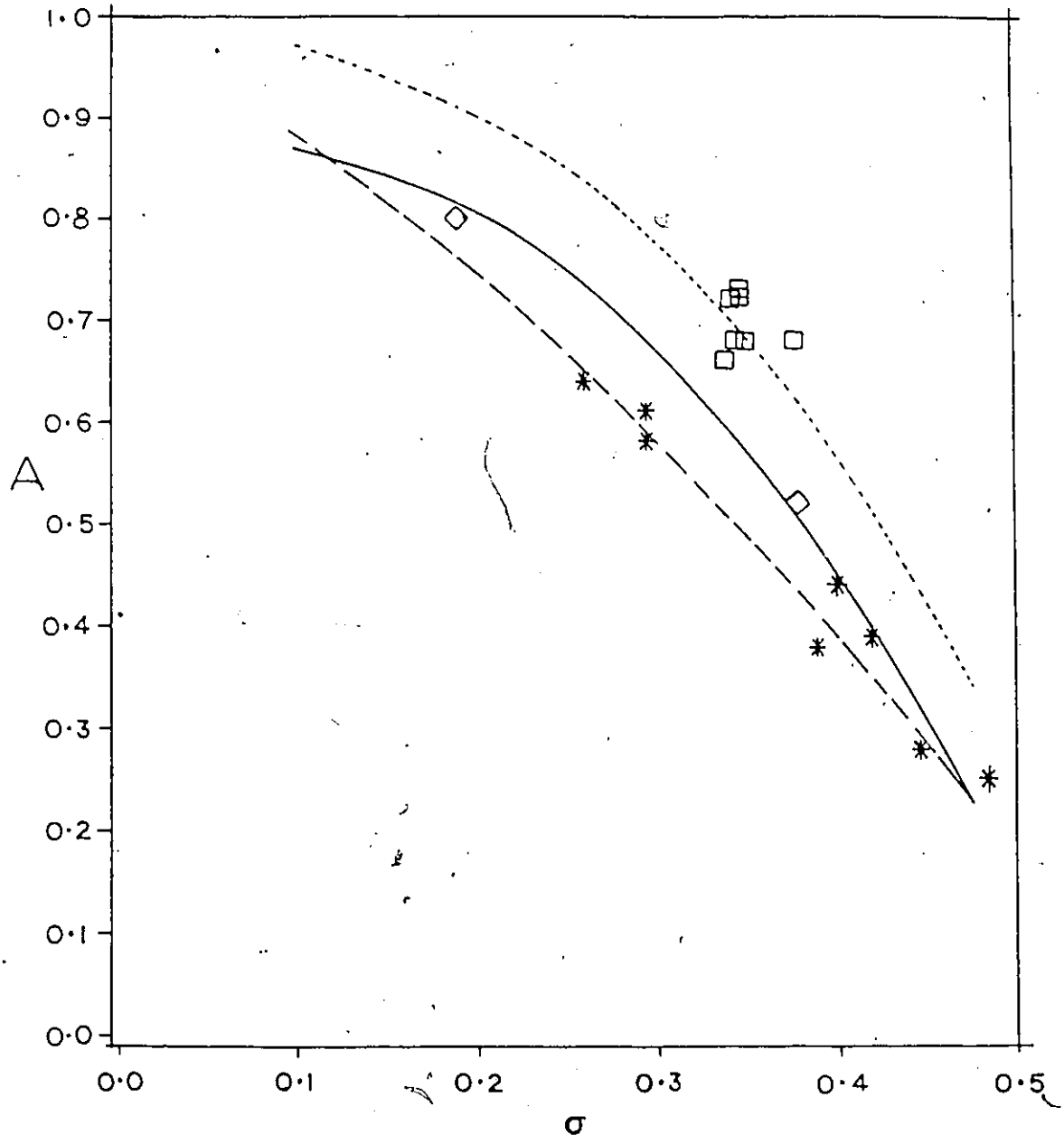

Figure 5.1. Predicted and measured shear reduction factor versus solidity for small d/h; * square mesh (present); □ square mesh (Rose, 1970); ◇ parallel rod (present); —— —— based on eq.(2.25); ——— based on eq.(2.27); - - - based on eq.(2.28).

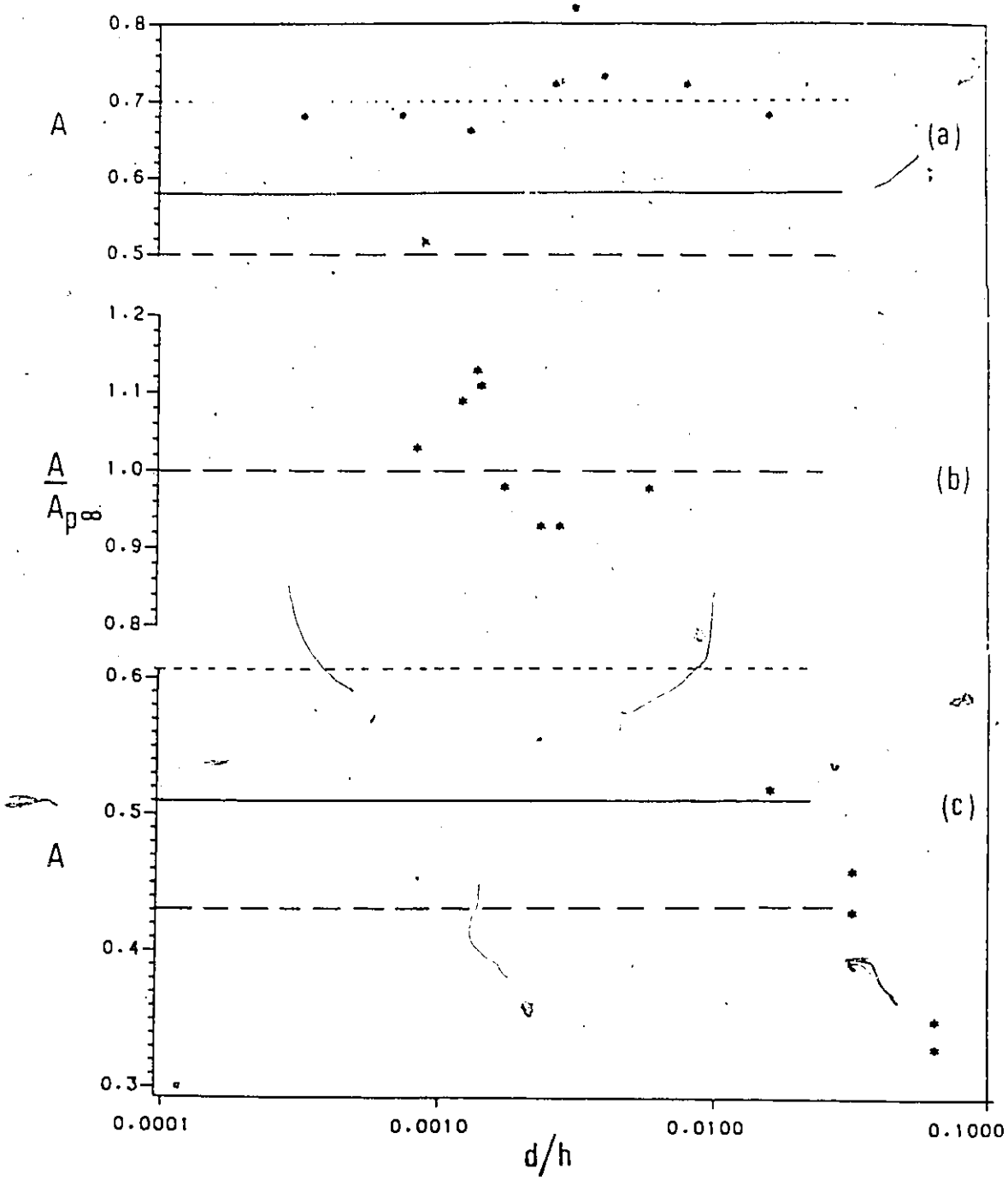

Figure 5.2. Shear reduction factor versus relative-element thickness for different screen configurations. (a) σ=0.35, square mesh (Rose, 1970); (b) square mesh (present) with varying σ, using eq.(2.25) for A_p; (c) σ=0.378, parallel rod (present). —— ——, ————, - - -, based on eqs. (2.25), (2.27), (2.28).

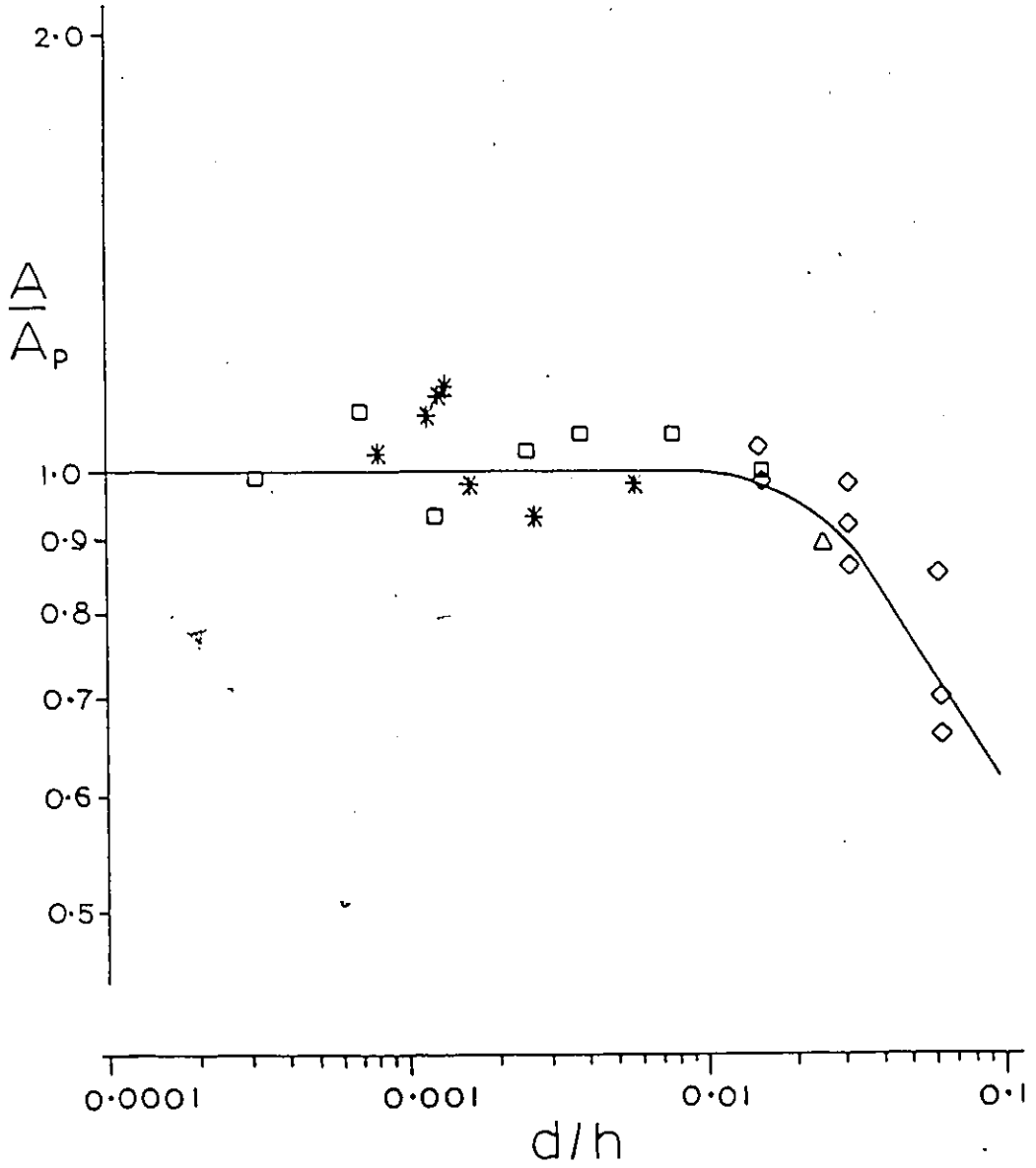

Figure 5.3. Shear reduction factor versus relative element thickness. * square mesh (present), A_p based on eq.(2.25); □ square mesh (Rose, 1970), A_p based on eq.(2.28); ◇ parallel rod (present), A_p based on eq.(2.27); △ parallel rod (Rose, 1970), A_p based on eq.(2.27); ——— empirical fit.

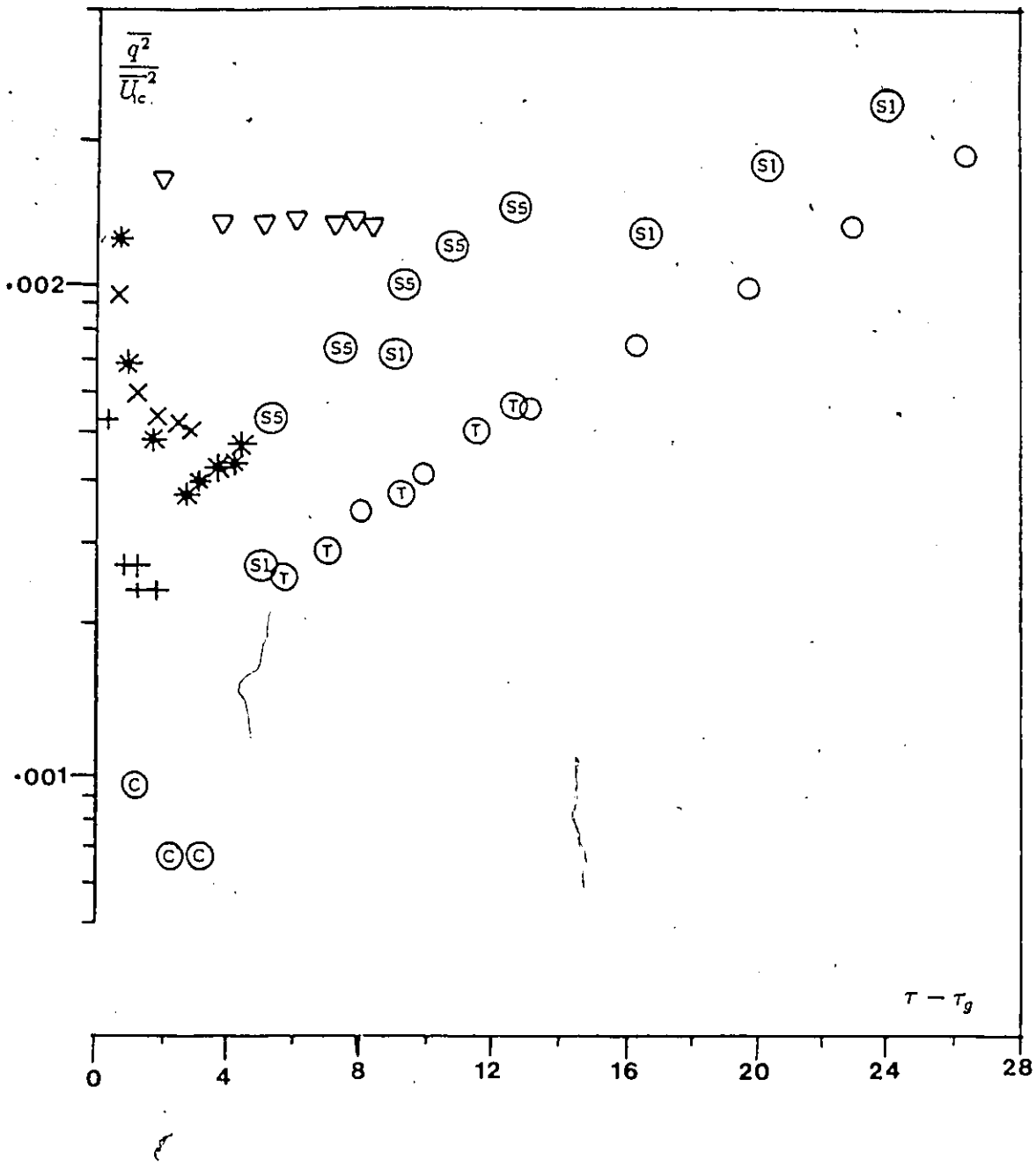

Figure 5.4. Turbulent kinetic energy plotted versus total strain. Symbols as in Table 3.

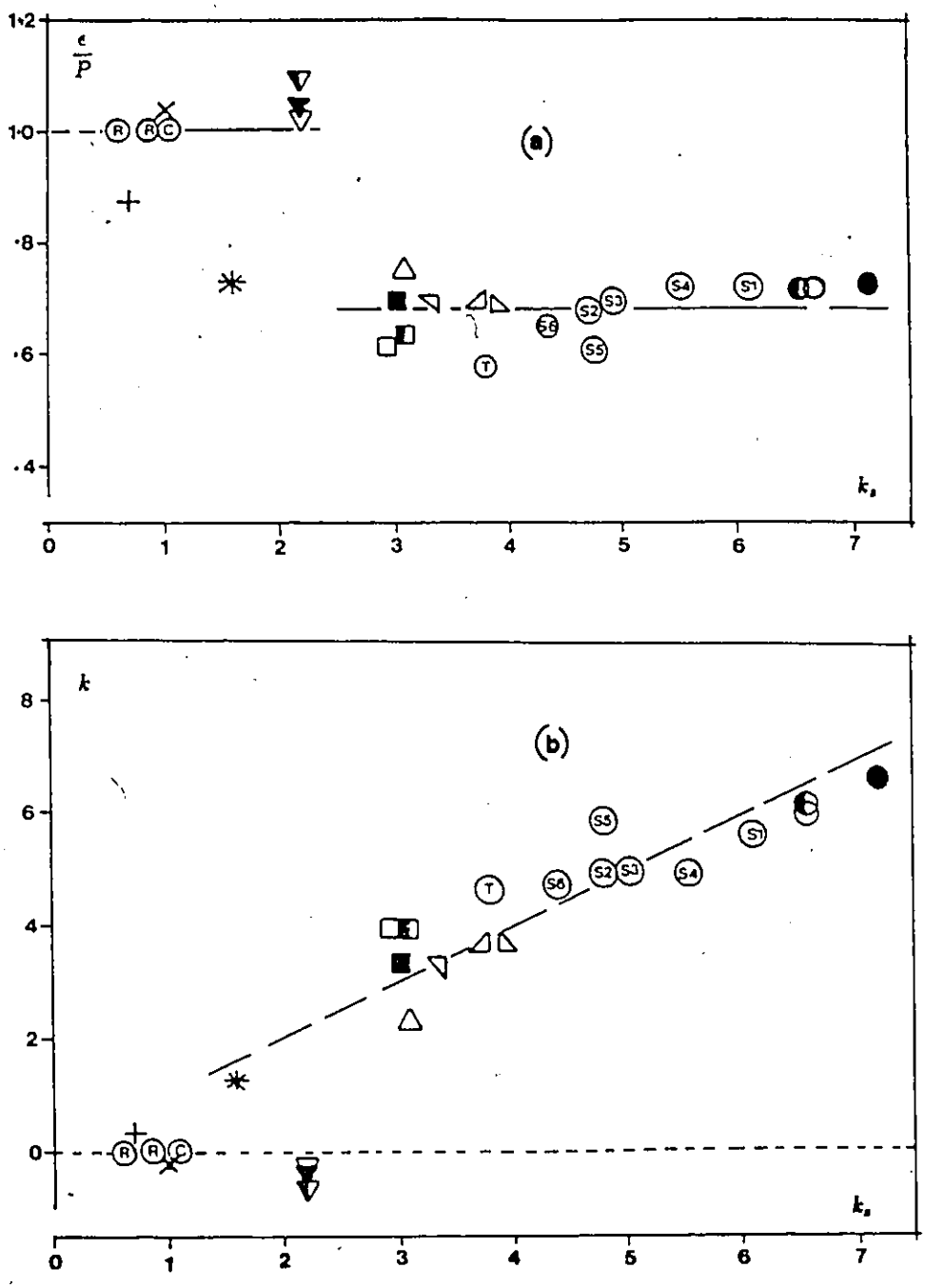

Figure 5.5. (a) The ratio ϵ/P (b) the exponent coefficient k plotted versus k_s. Symbols as in Table 3.

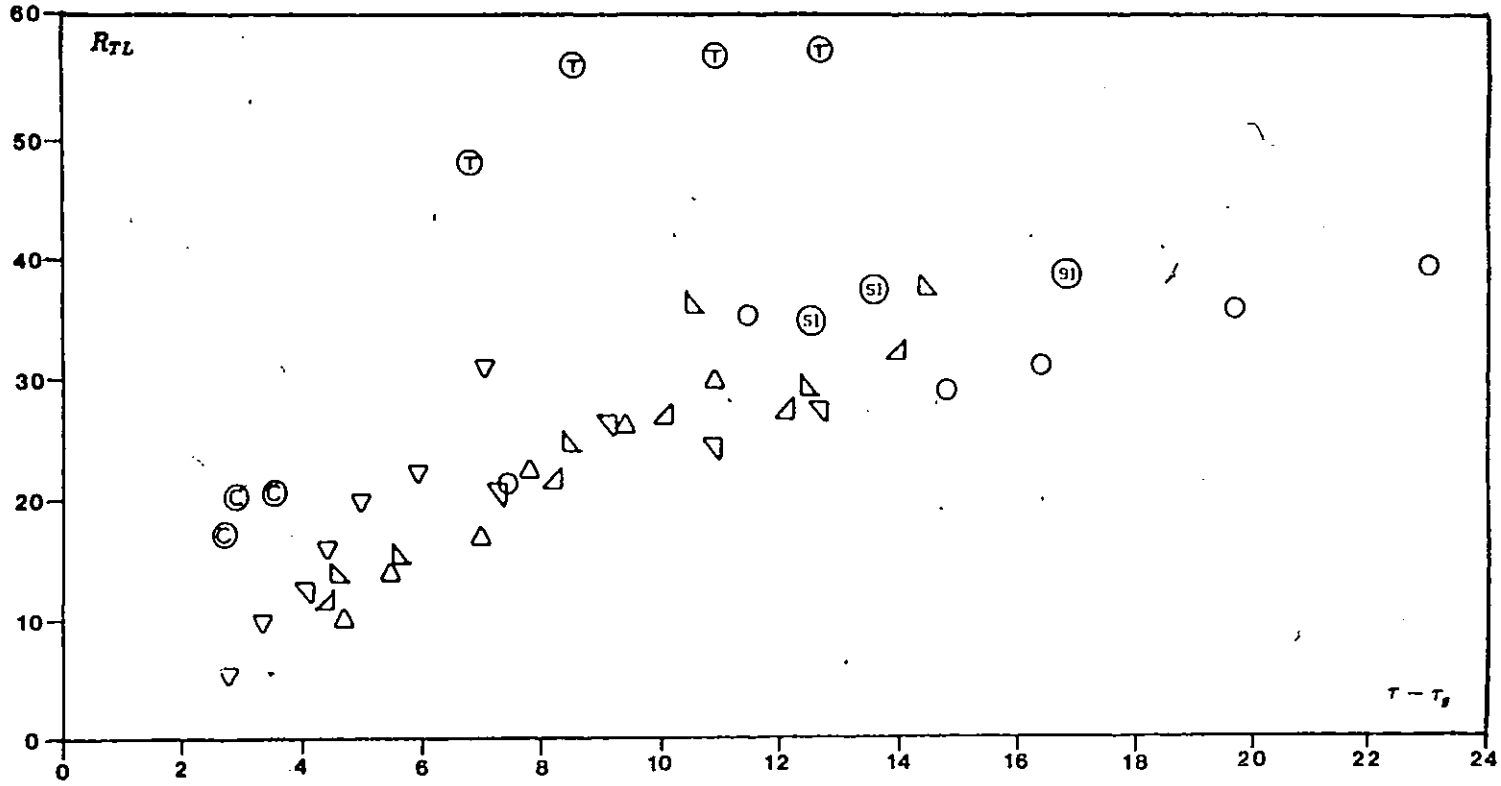

Figure 5.6. Variation of the effective Reynolds number based on L_{11}. Symbols as in Table 3.

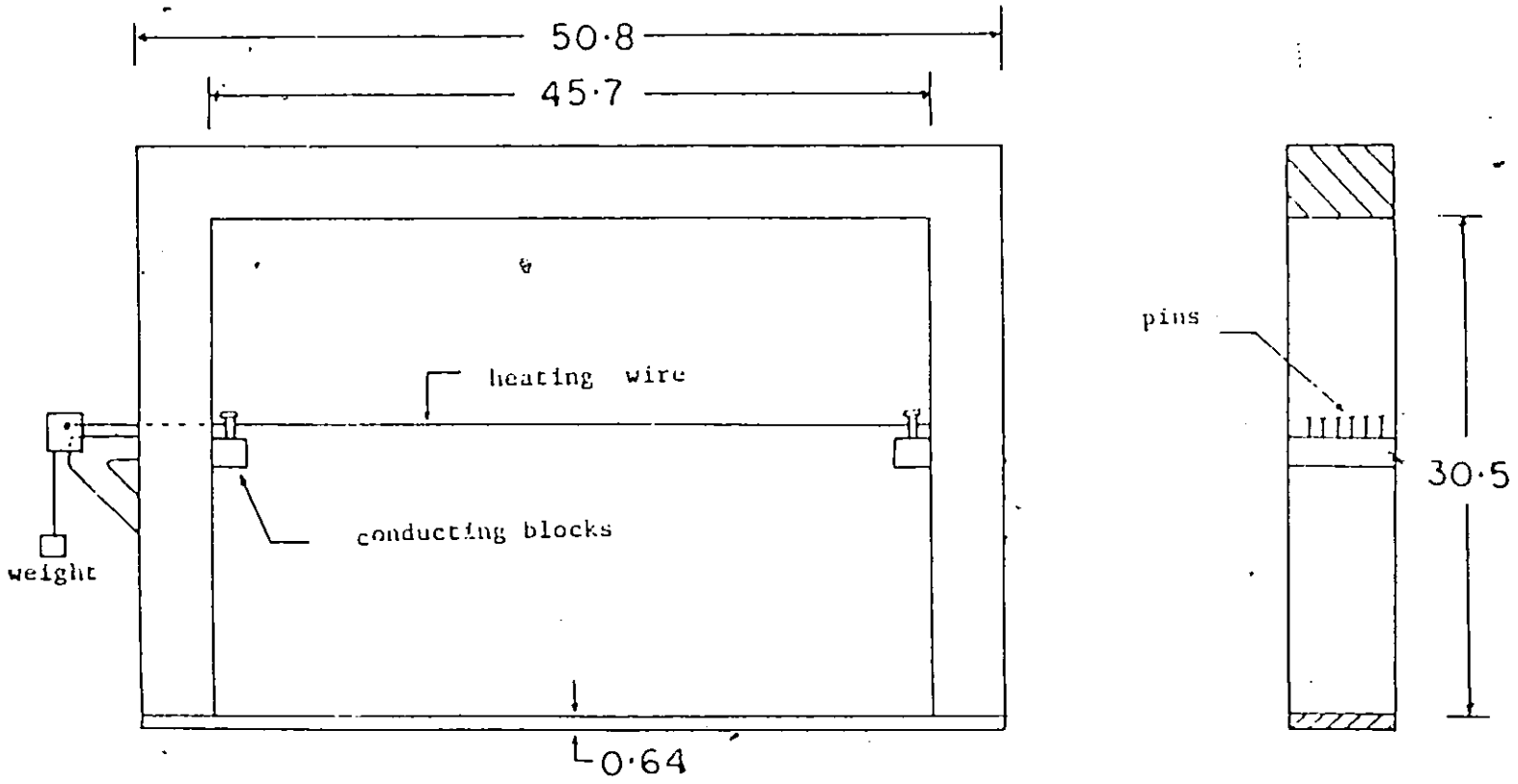

Figure 9.1. Sketch of the heating system. All dimensions in mm.

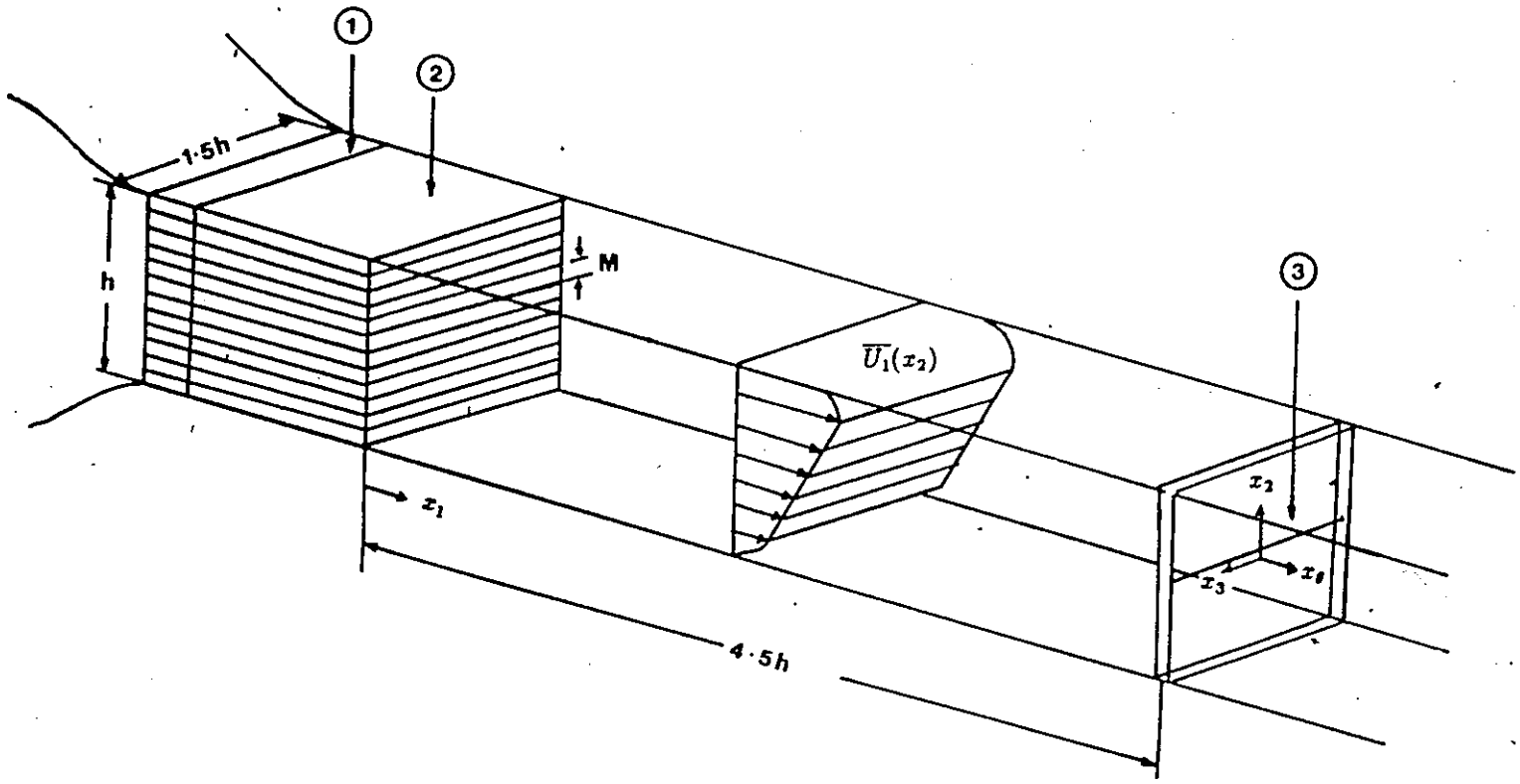

Figure 9.2. Sketch of the wind tunnel test section. (1) shear generator (2) flow seperator (3) heating source.

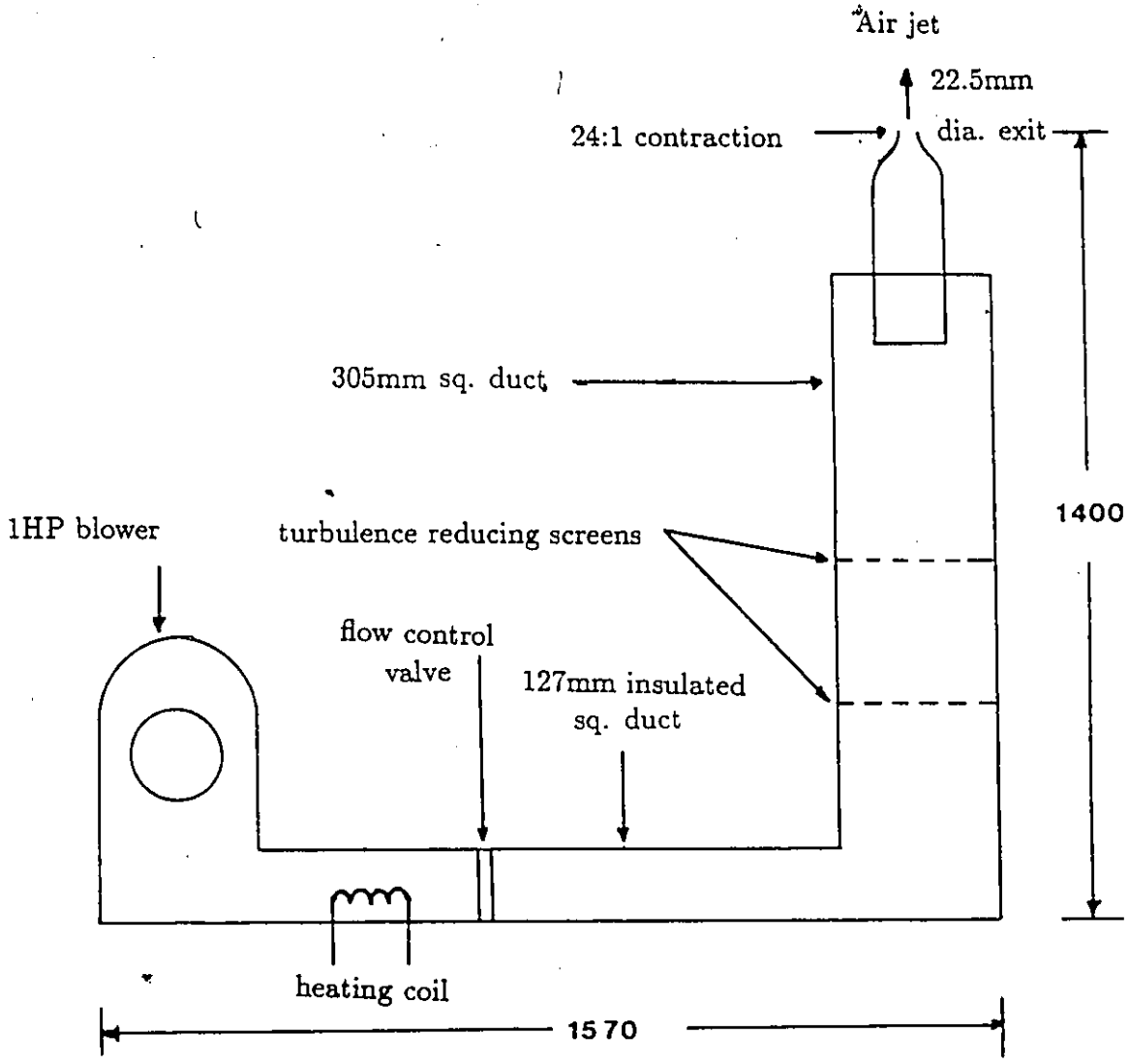

Figure 9.3. The calibration jet. All dimensions in mm.

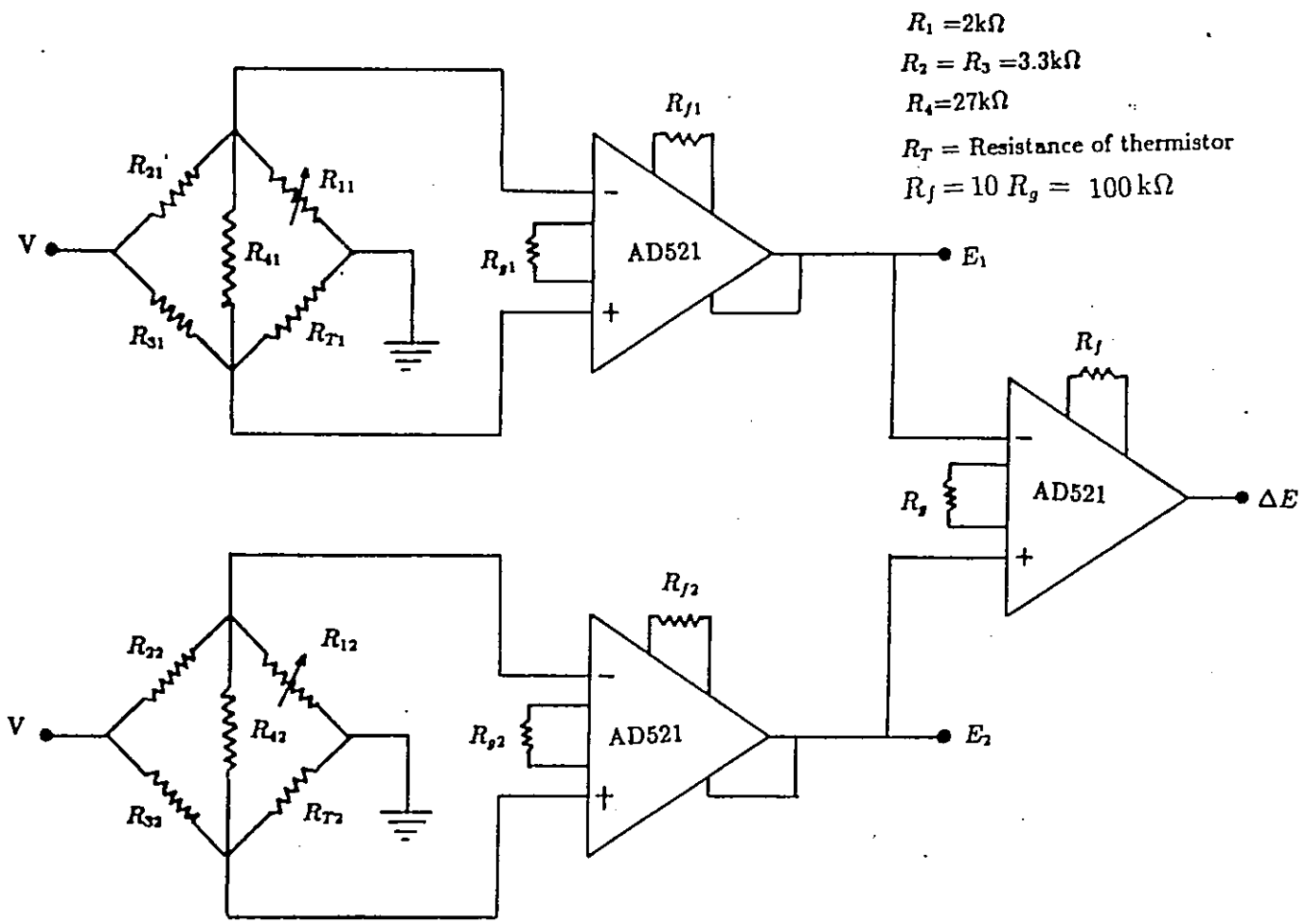

Figure 9.4. Thermistor circuit diagram.

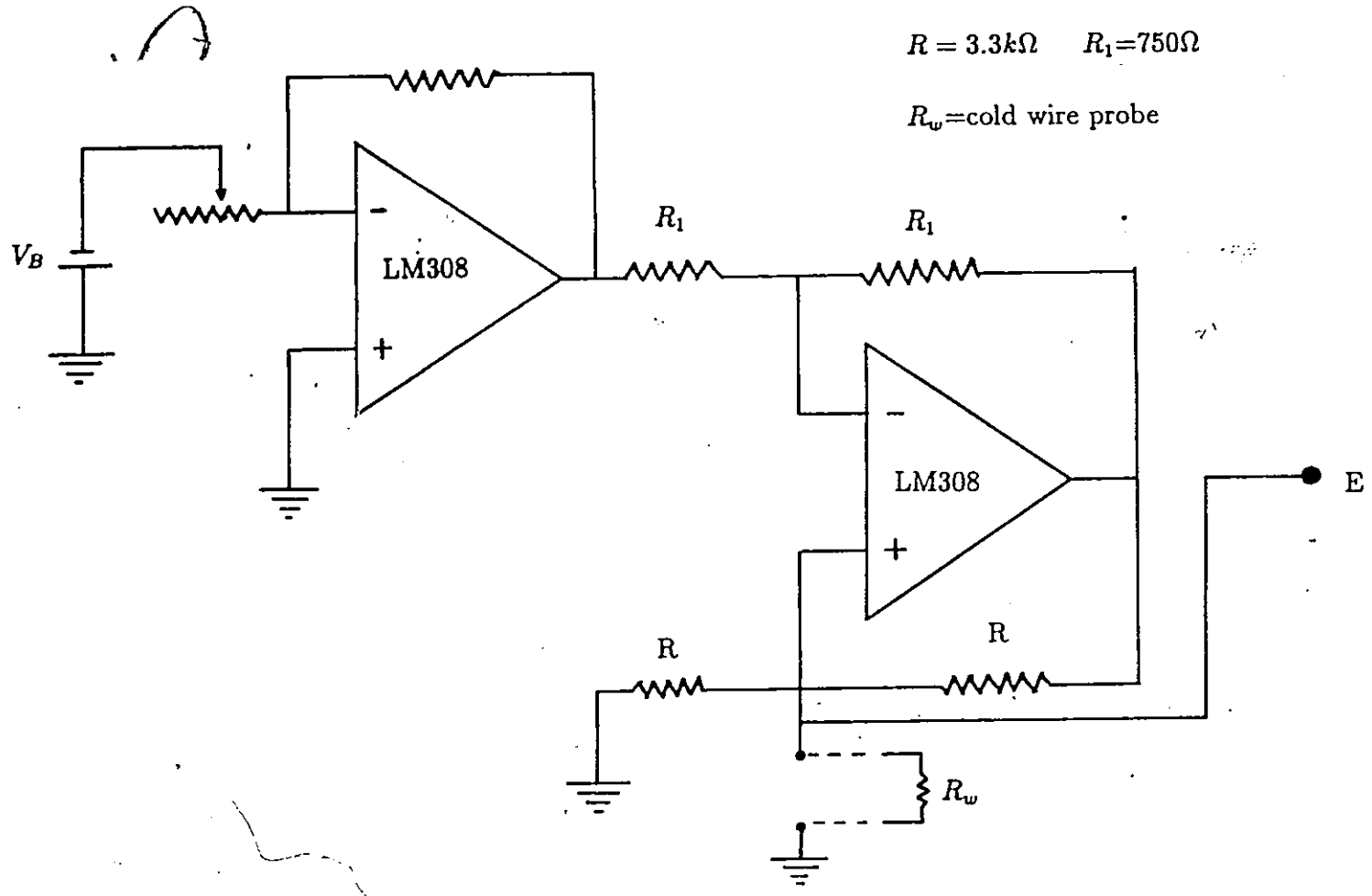

Figure 9.5. Constant current circuit diagram.

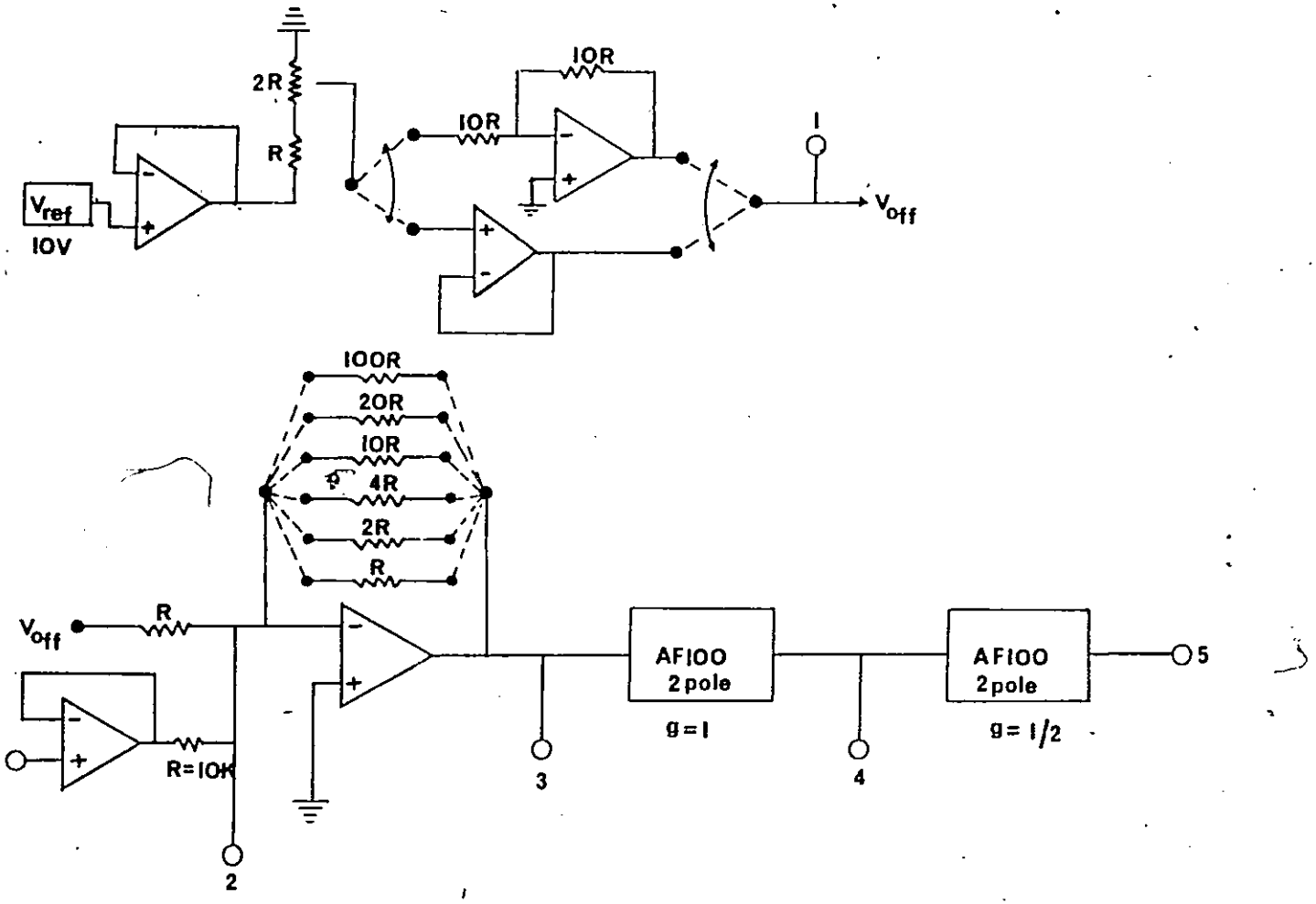

Figure 9.6. Analog signal conditioning circuit diagram. (Courtesy G.Holloway)

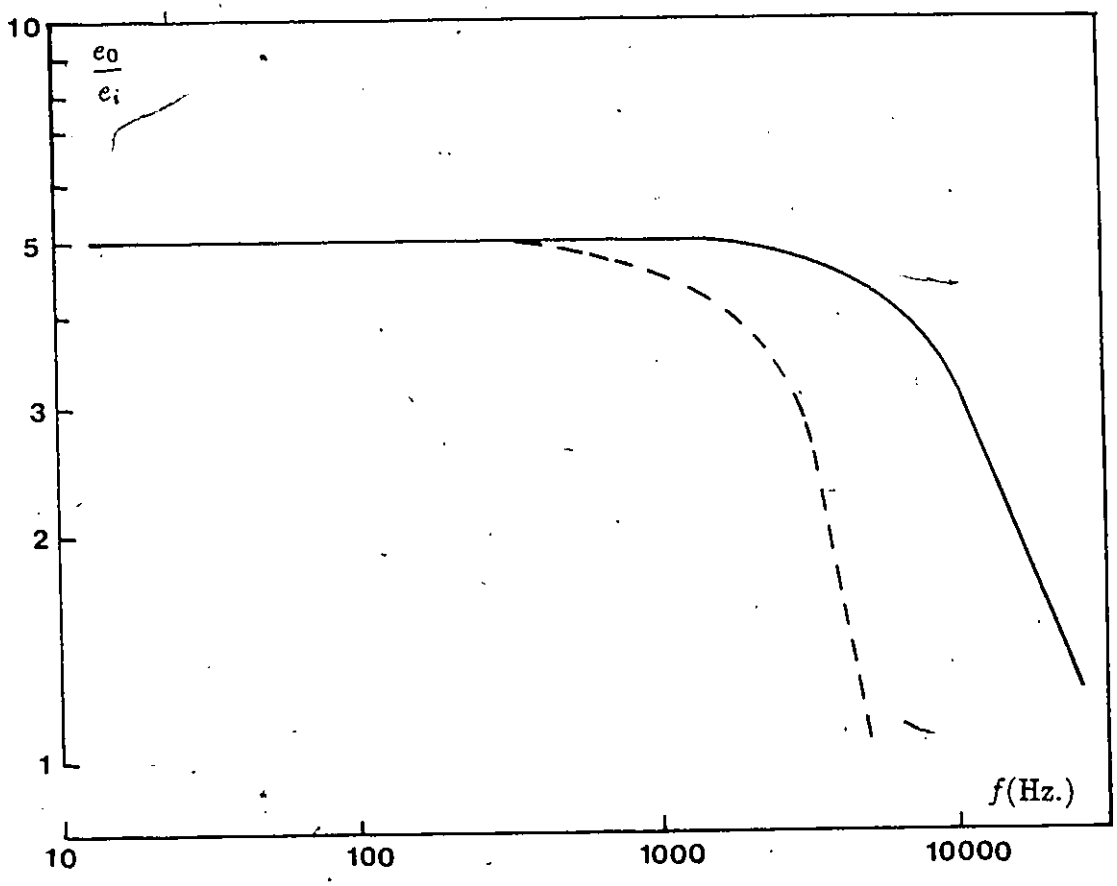

Figure 9.7. Frequency response of the analog signal conditioning circuit. Gain=5.0; 3dB cut-off : — — 3kHz, ——— 10kHz.

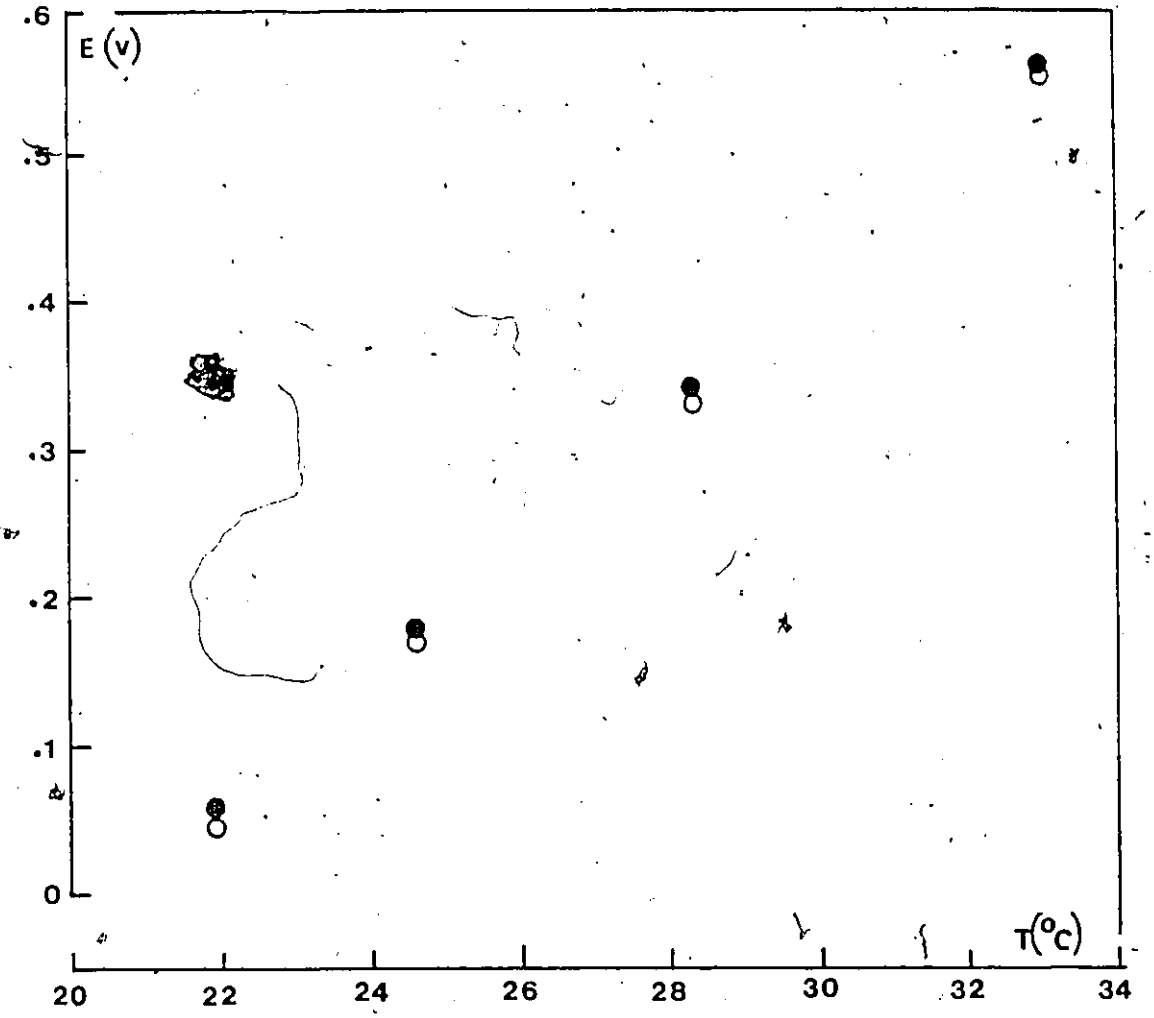

Figure 9.8. Typical thermistor calibration curves. o : reference thermistor, • : measuring thermistor.

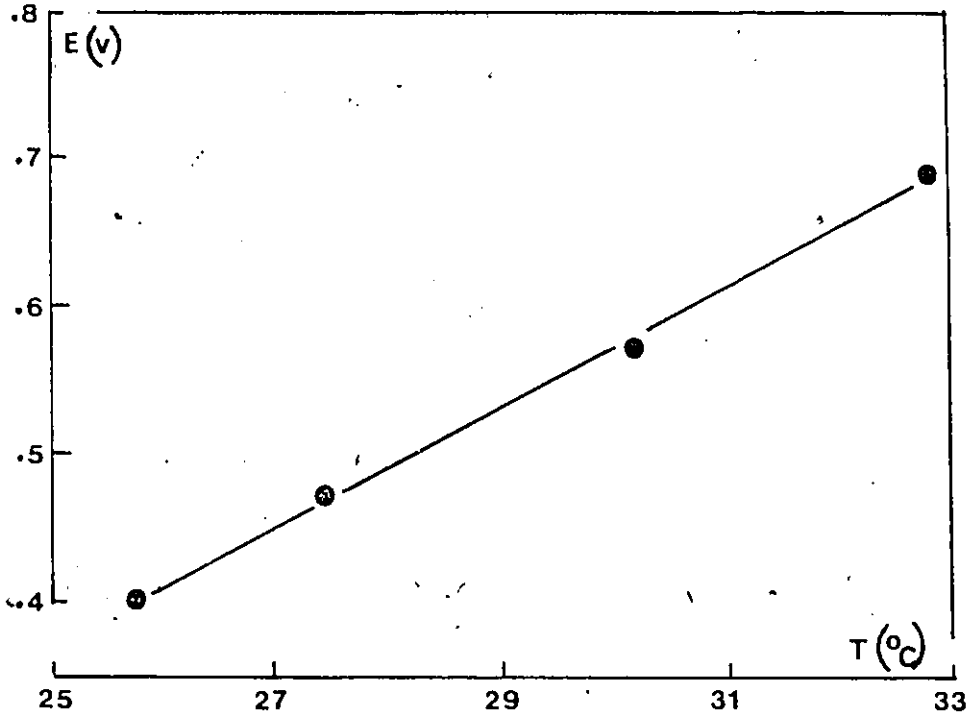

Figure 9.9. Typical cold-wire calibration curve.

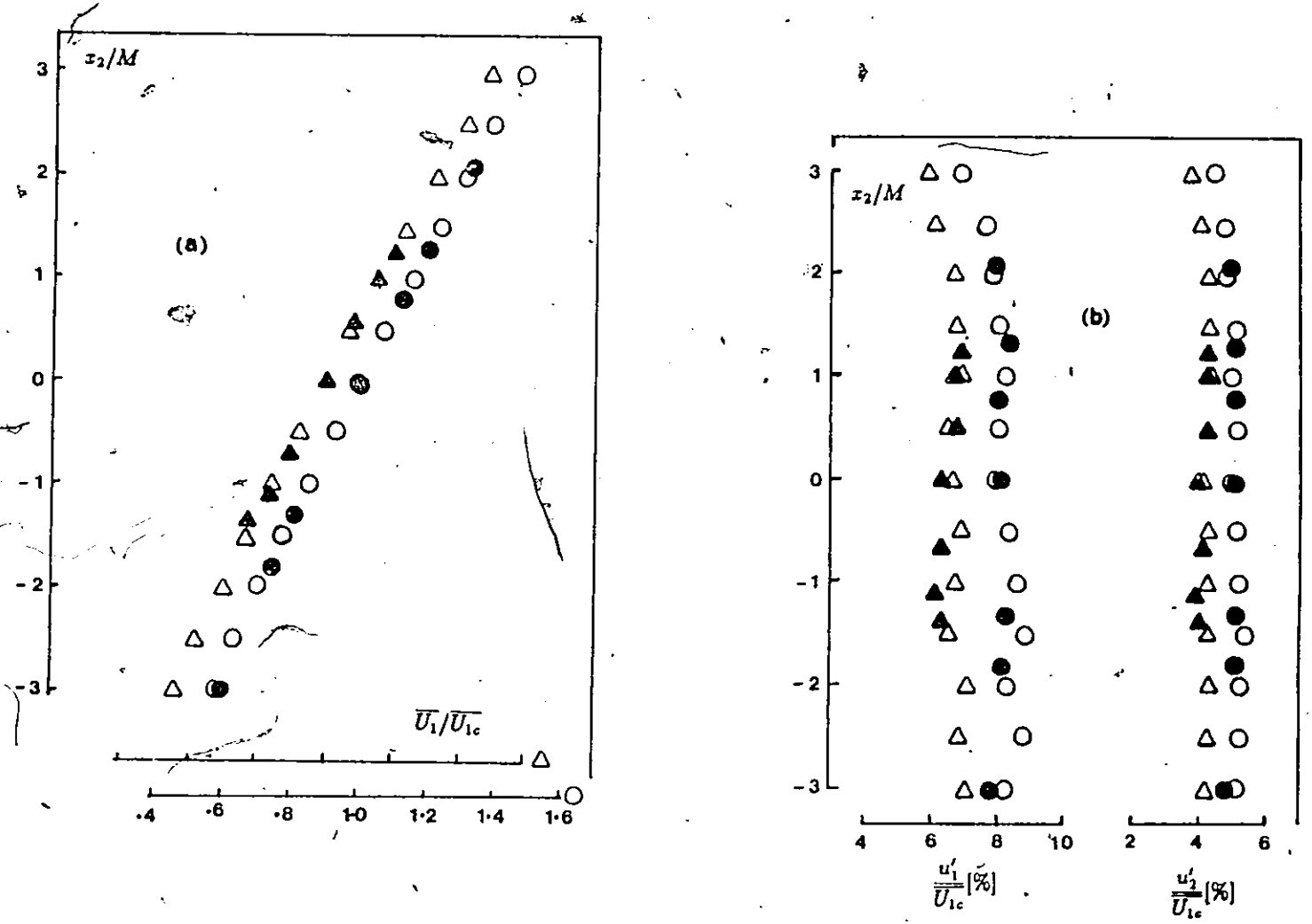

Figure 10.1. Transverse variation of (a) the mean velocity (b) the r.m.s. velocities; △, ▲ : $x_0/M = 48$, ○ ● :$x_0/M = 84.0$, $\overline{U}_{1c} = 7.8$m/s; solid symbols indicate the presence of a heated source.

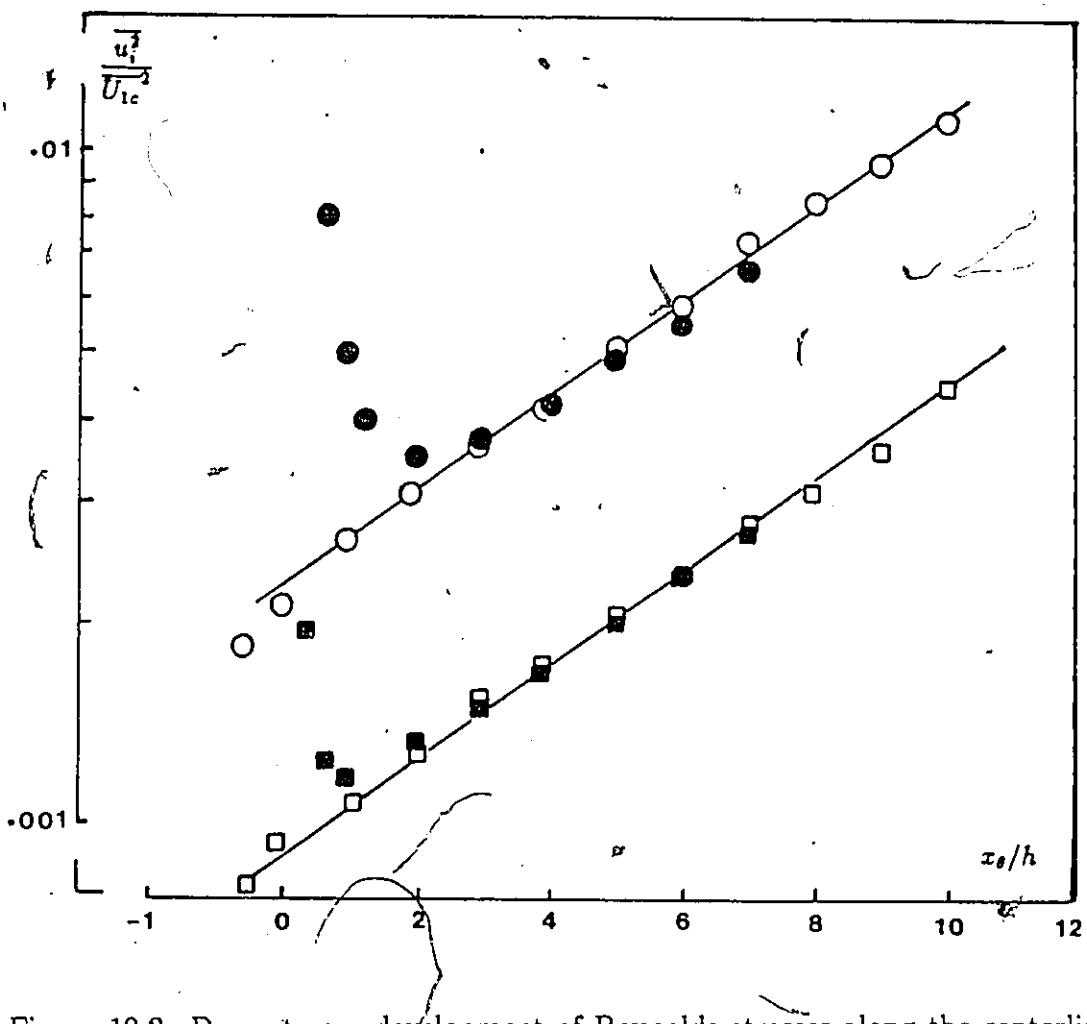

Figure 10.2. Downstream development of Reynolds stresses along the centerline; o : $\overline{u_1^2}$, □ : $\overline{u_2^2}$; $\overline{U}_{1c} = 7.8m/s$; solid symbols indicate the presence of a heated source.

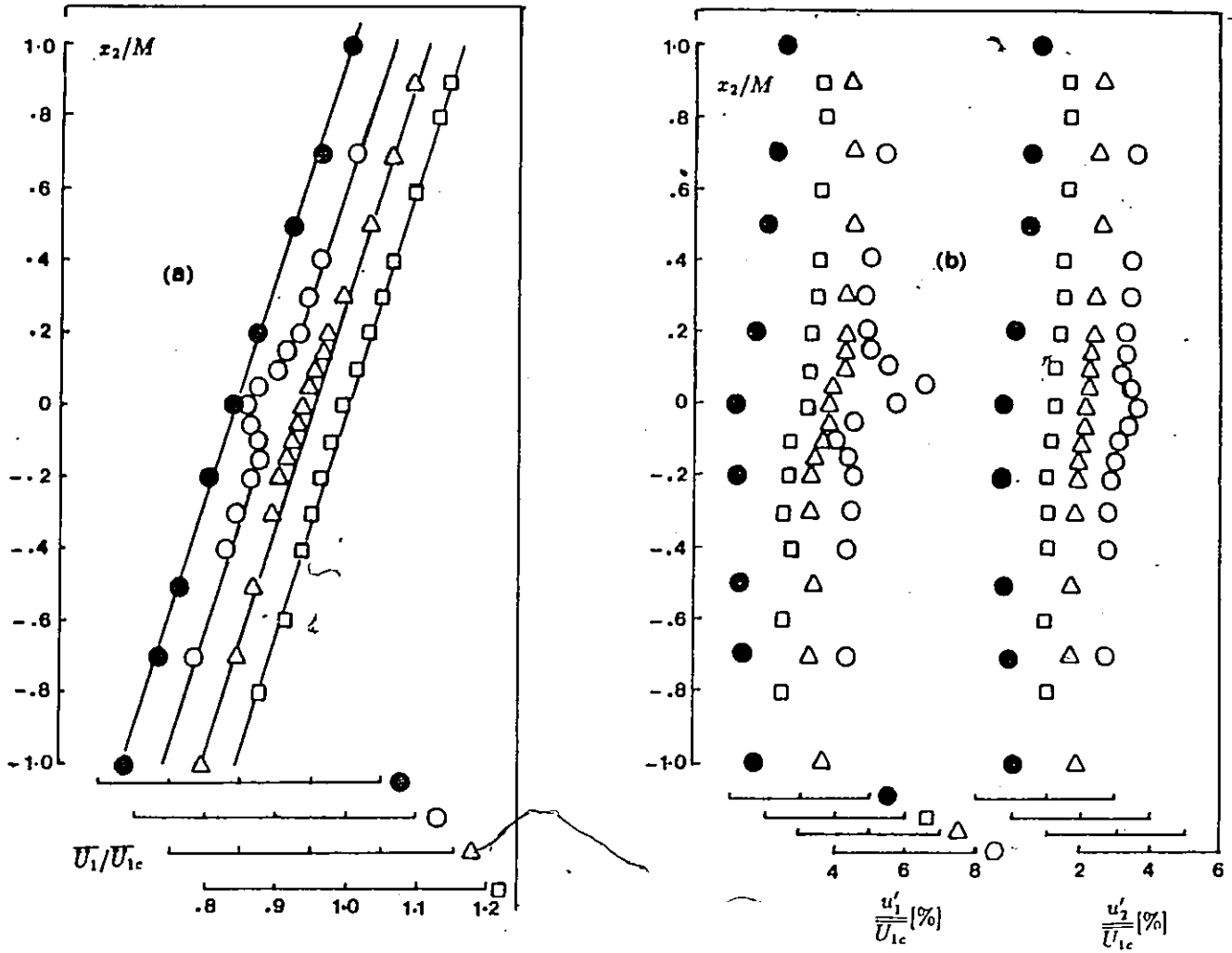

Figure 10.3 Transverse profiles downstream of the ribbon. (a) mean velocity (b) r.m.s. velocities. $x_0/M = 0.0$(•, without ribbon), 2.0 (o), 8.0 (△), 12.0 (□); $\overline{U}_{1c} = 7.85m/s$.

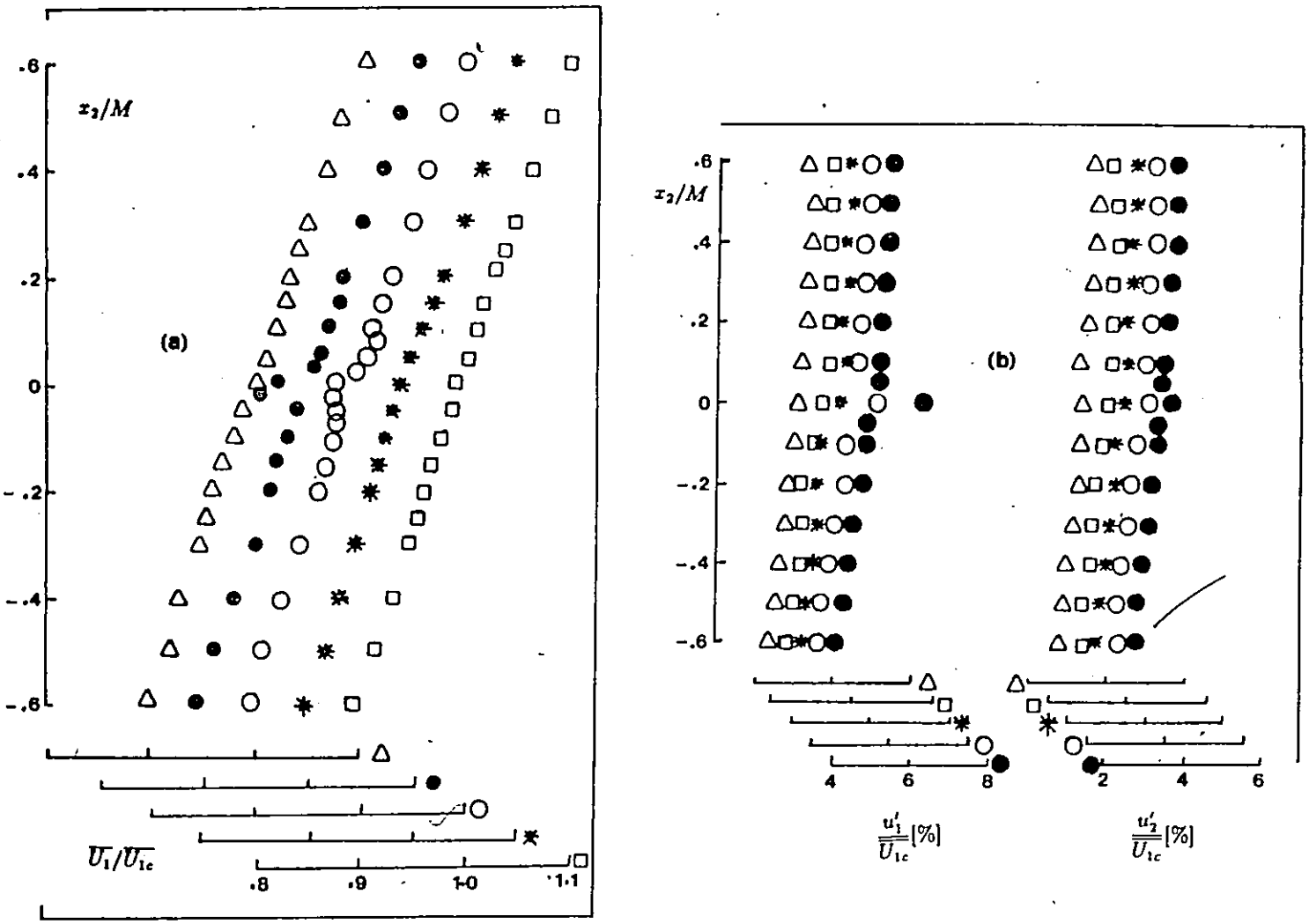

Figure 10.4. Transverse profiles downstream of the 0.051mm dia. wire. (a) mean velocity (b) r.m.s. velocities. $x_\theta/M = 6.0$ ($\triangle$, without wire), 0.25 ($\bullet$), 1.0 (o), 3.0 ($*$), 6.0 ($\square$); $\overline{U}_{1c} = 13.3$m/s.

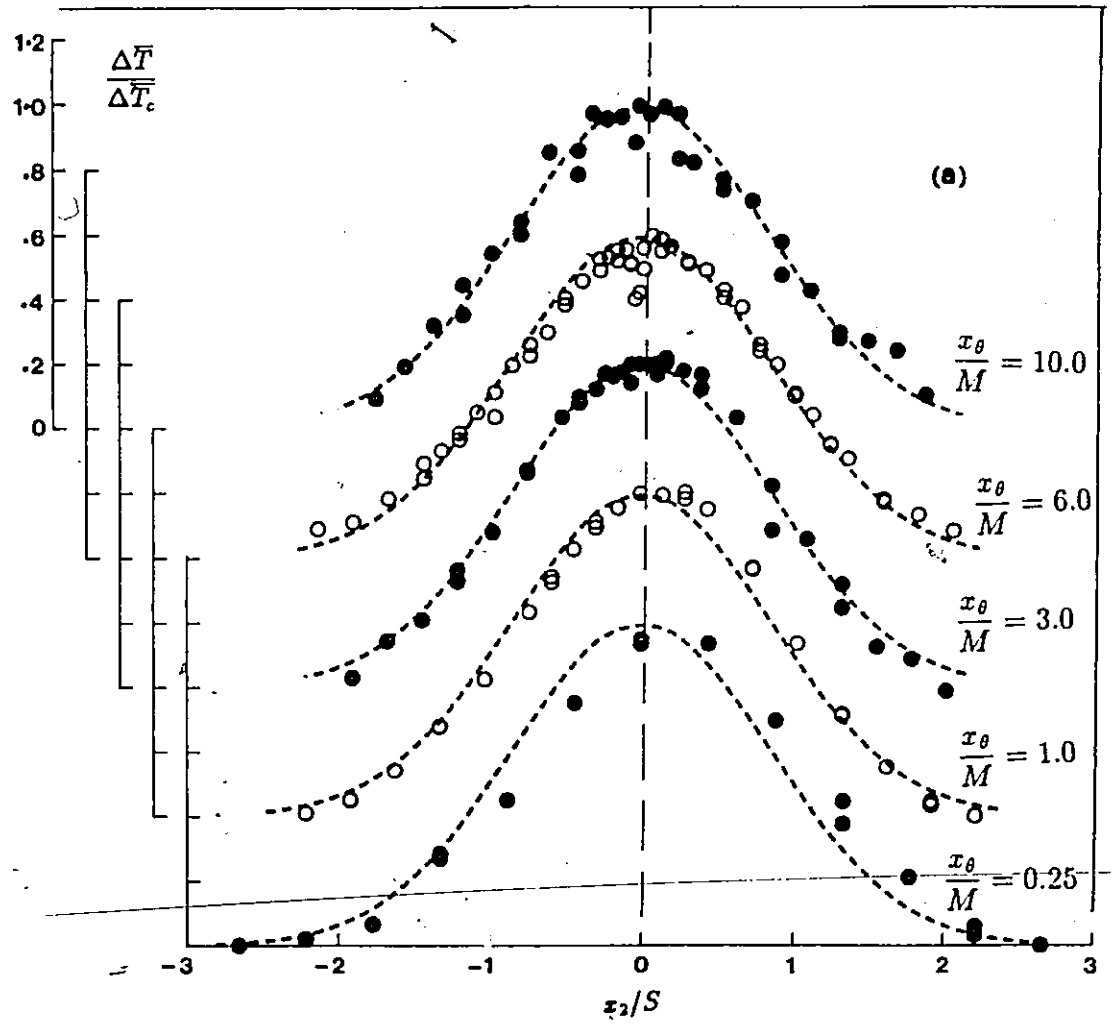

Figure 10.5. Transverse profiles of the mean temperature rise (a) downstream of 0.051mm dia. wire (b) downstream of ribbon.

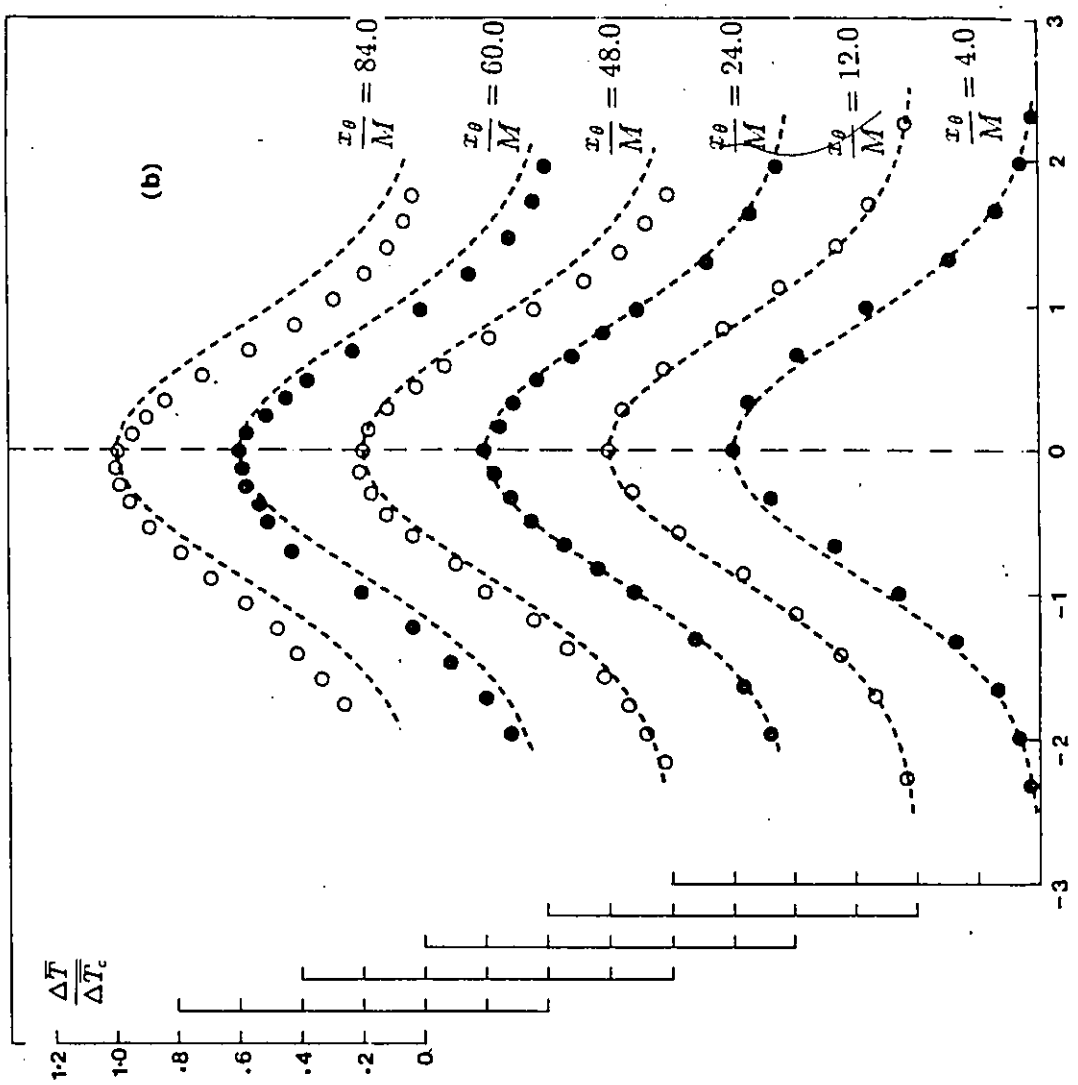

Figure 10.5. continued

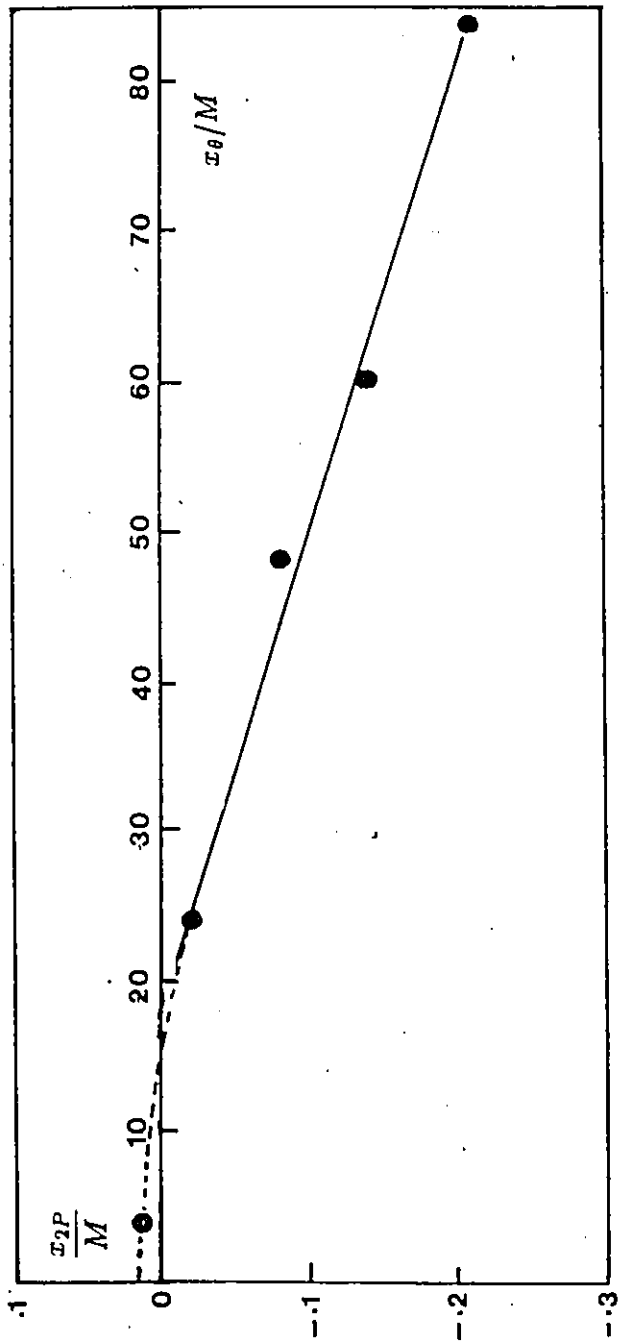

Figure 10.6. Locus of the peak mean temperature rise.

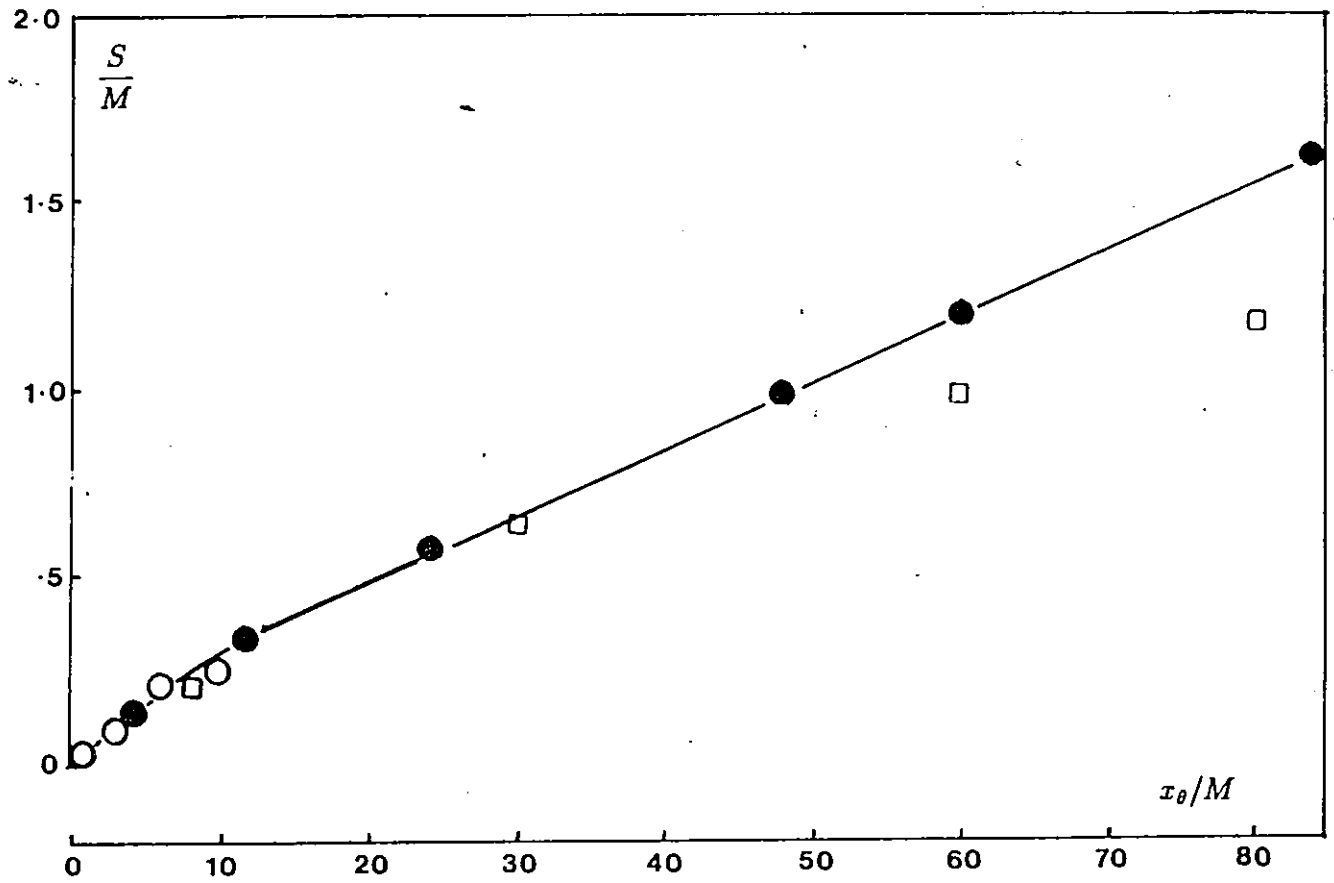

Figure 10.7. Downstream development of the half width of the mean temperature profile; o: 0.051mm dia. wire, • ribbon, □ Warhaft(1984).

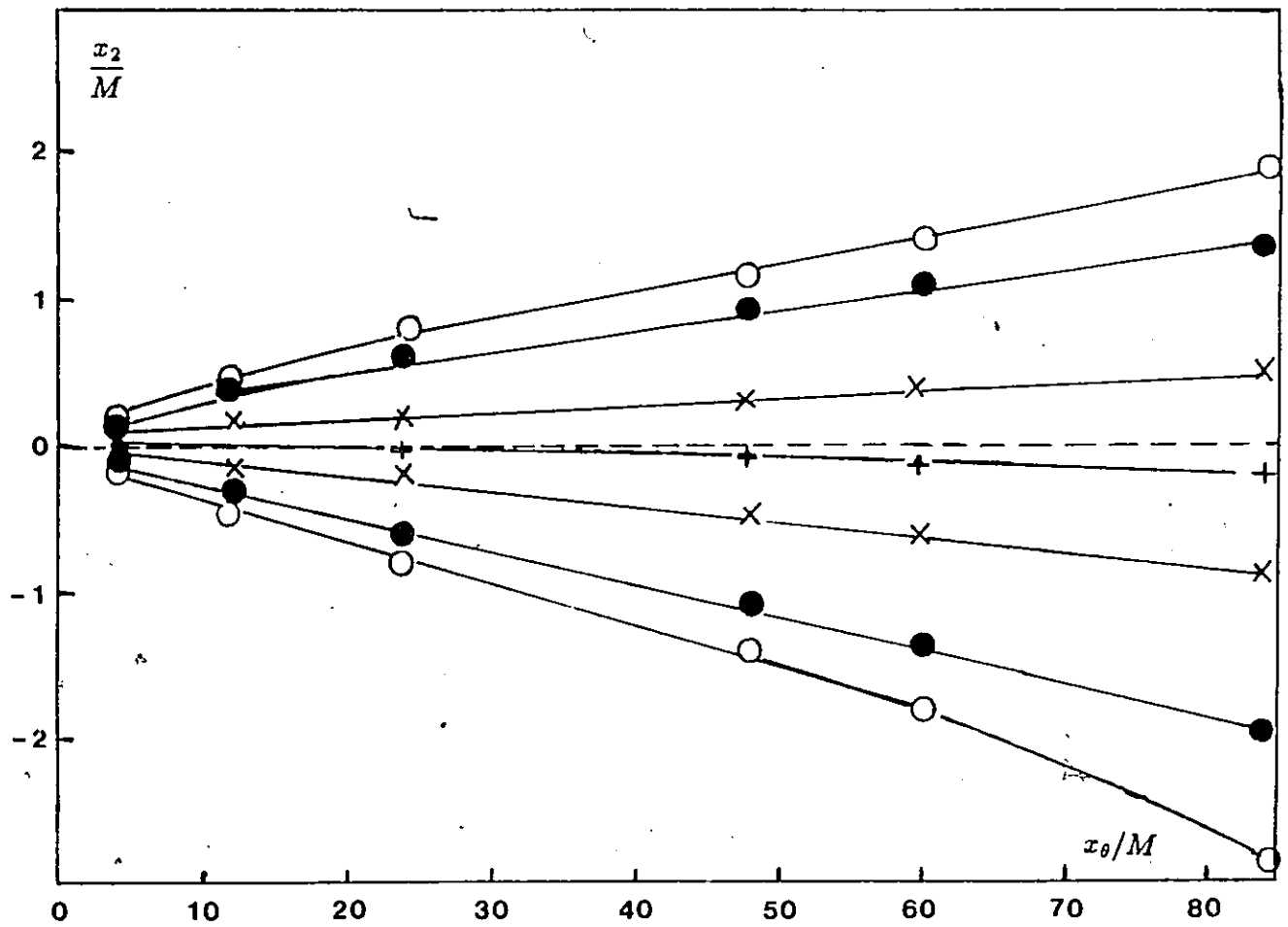

Figure 10.8. Locus of positions with $\Delta\overline{T}/\Delta\overline{T}_p = 1.0$ (+), 0.9 (×), 0.5 (•), 0.3 (○).

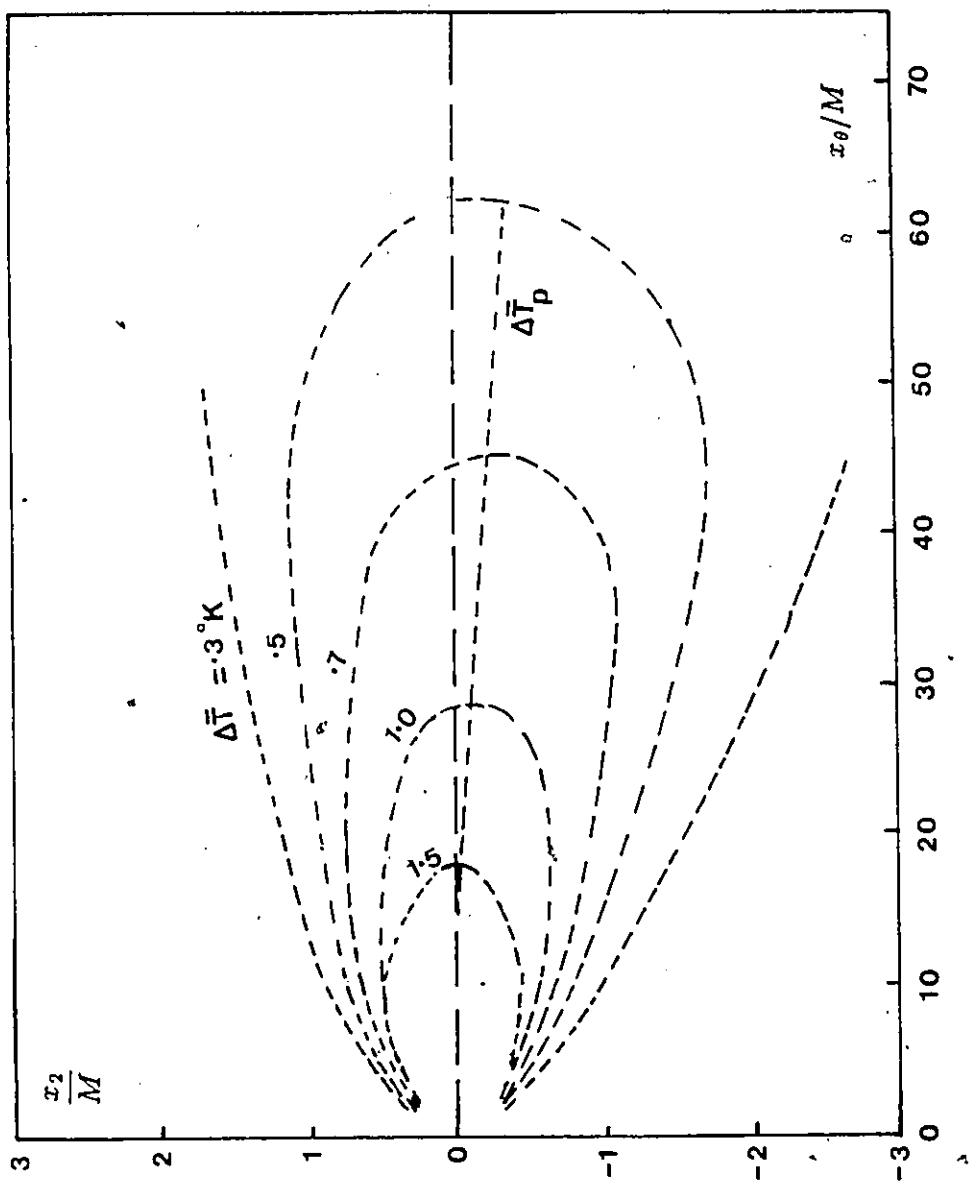

Figure 10.9 Mean isotherms on the tunnel centerplane.

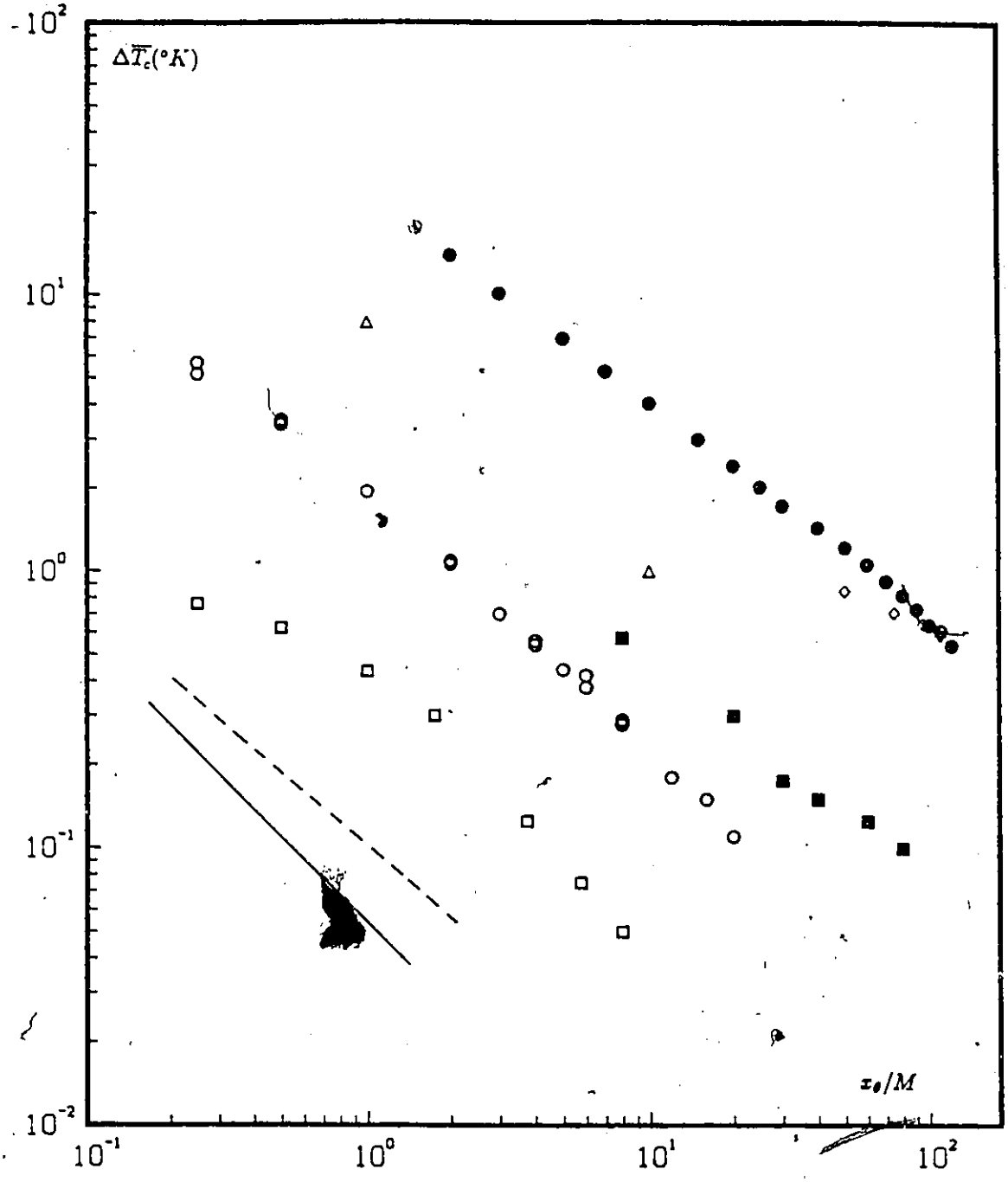

Figure 10.10. Downstream decrease of the centerline mean temperature rise; o : 0.051mm dia. wire, • : ribbon, △ : Stapountzis et al.(1986), □ Warhaft(1984) ($d_w = 0.025mm$), ■ Warhaft(1984) ($d_w = 0.127mm$) , ◇ : Tavoularis and Corrsin (1981 a); ——— n=1.0, — n=0.75.

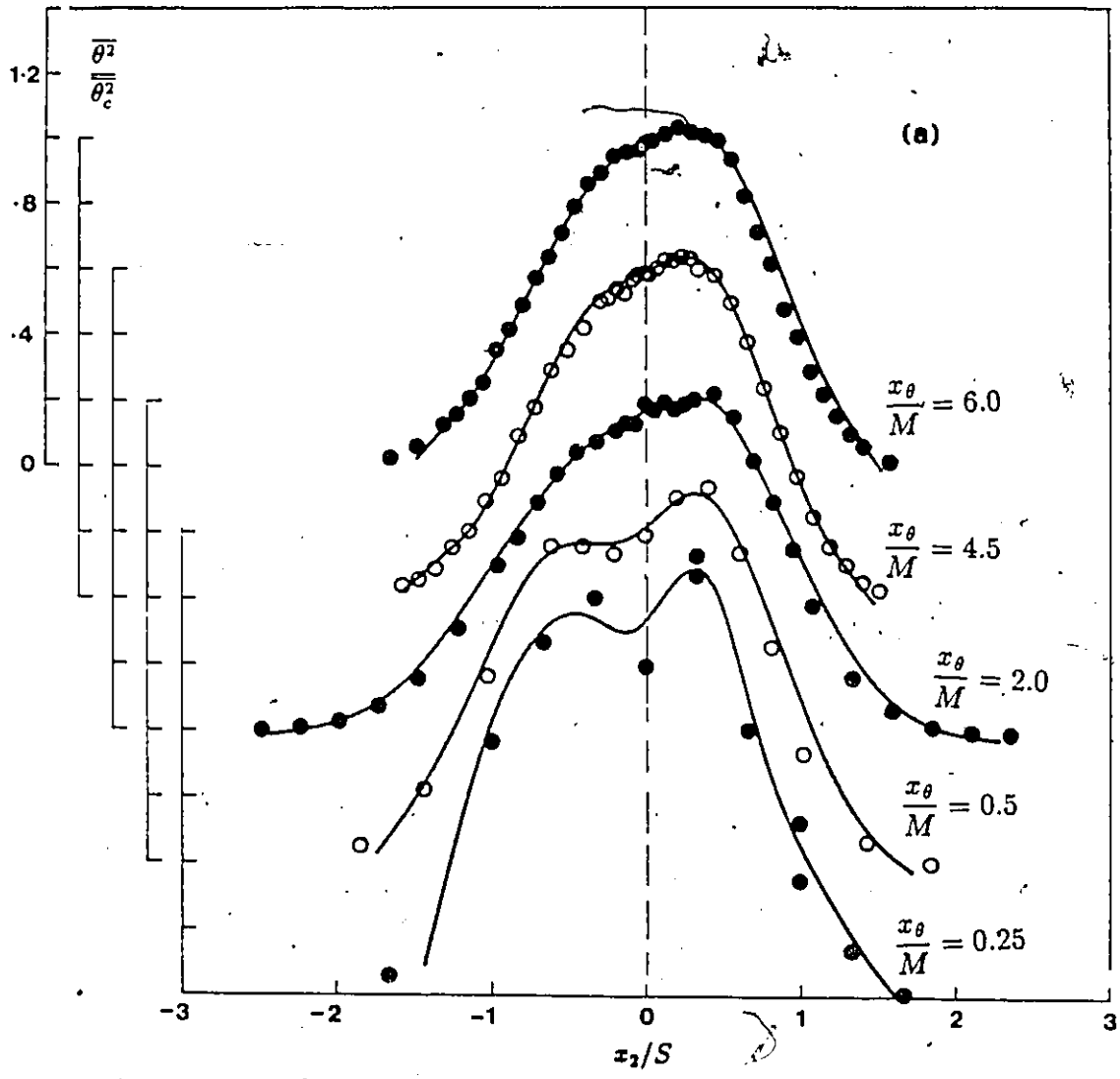

Figure 10.11. Transverse distribution of the mean square temperature fluctuations downstream of (a) 0.051mm dia. wire and (b) the ribbon

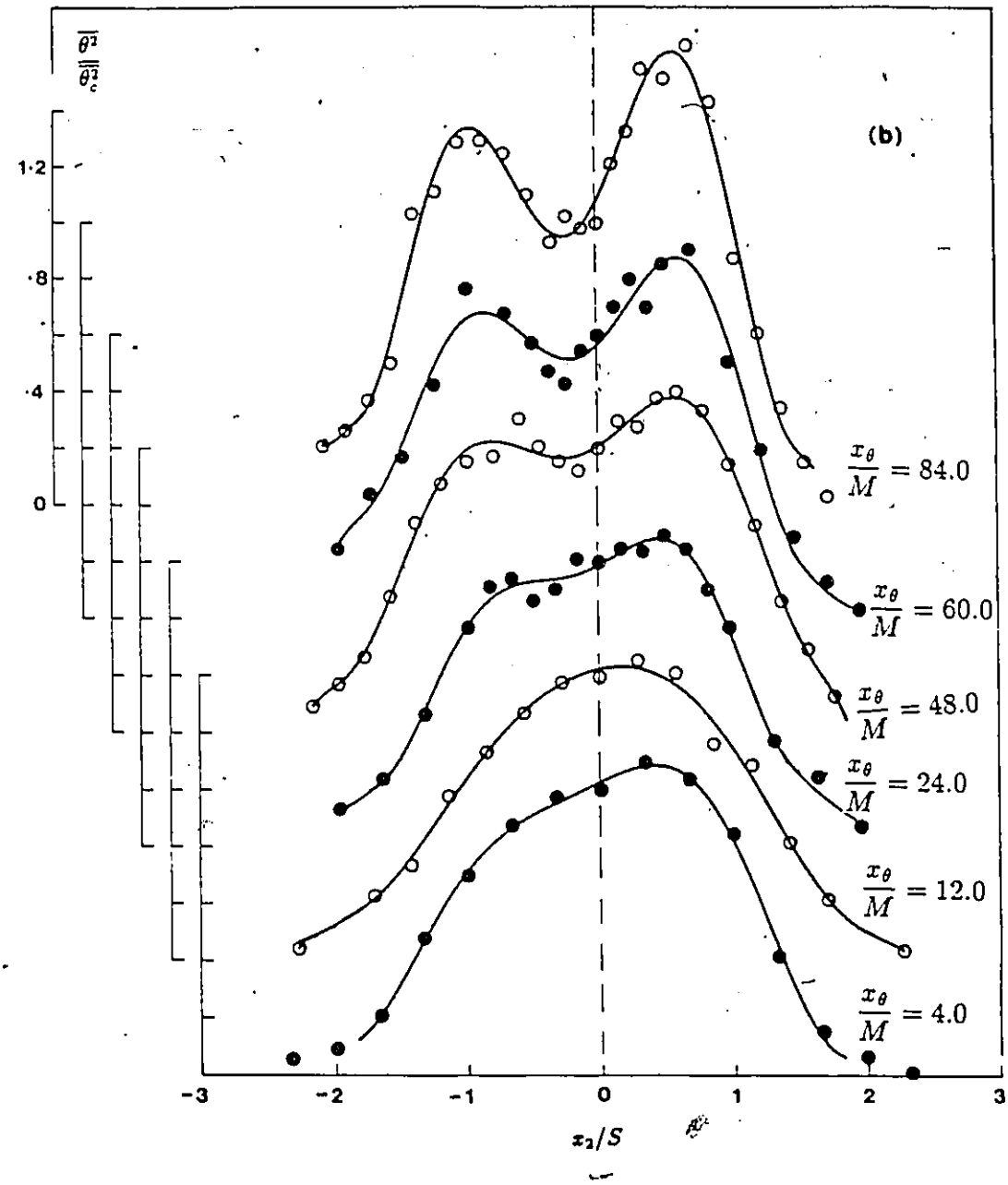

Figure 10.11. continued

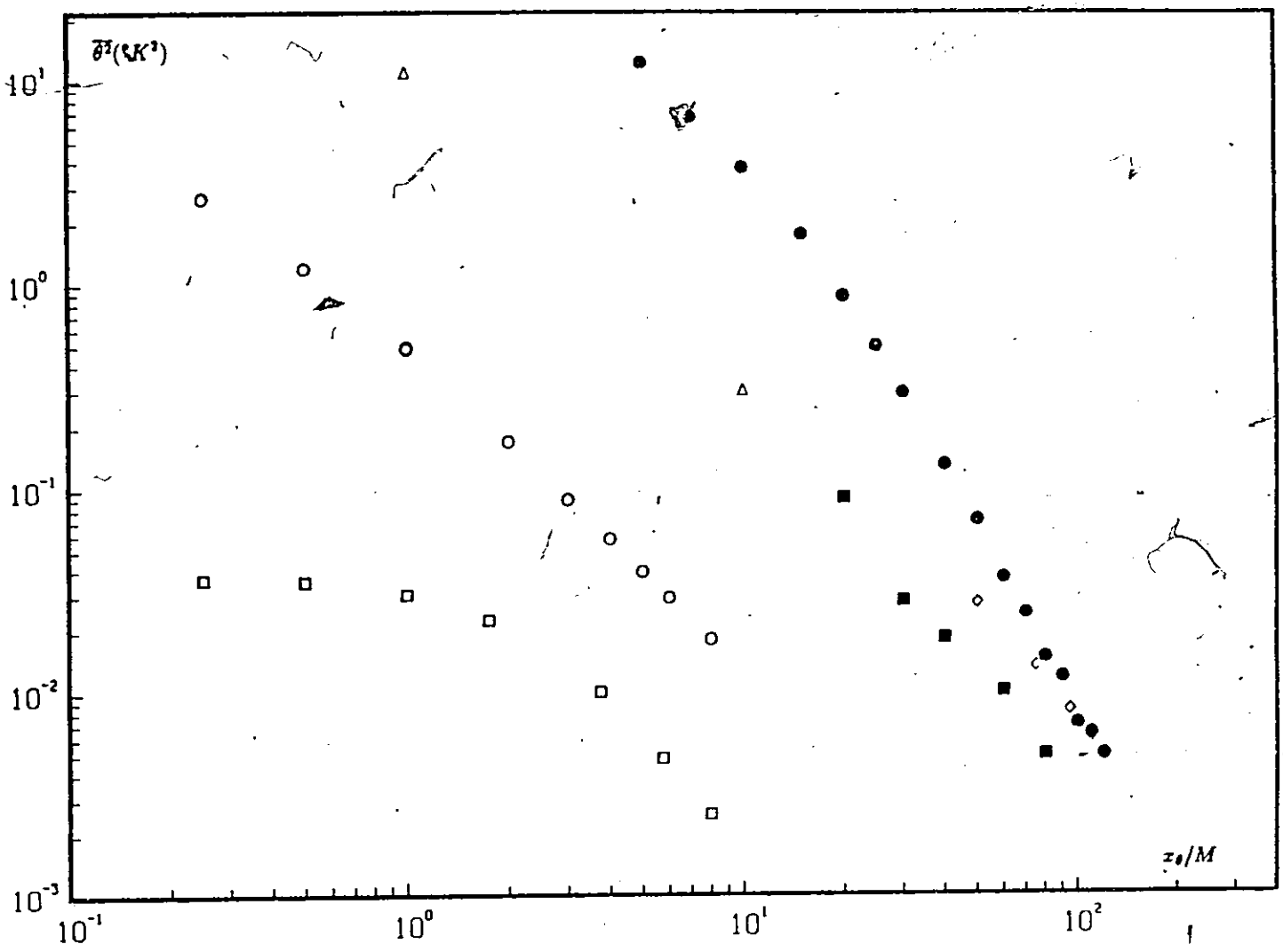

Figure 10.12. Downstream development of the centerline mean square temperature fluctuations. ○ : 0.051mm dia. wire, ● : ribbon, □($d_w = 0.025mm$), ■($d_w = 0.127mm$) : Warhaft(1984), △ : Stapountzis et al.(1986), ◇ : Tavoularis and Corrsin (1981 a).

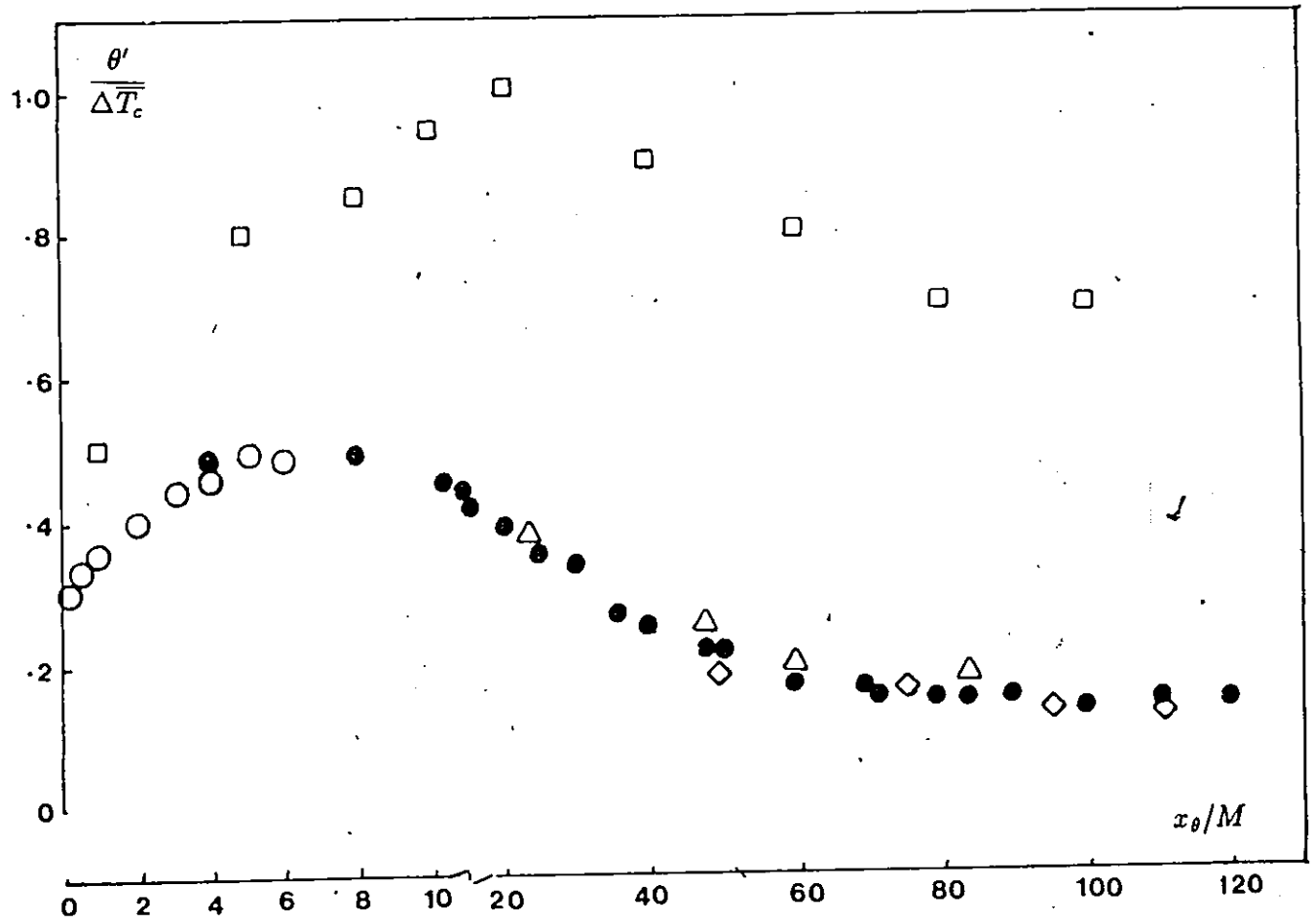

Figure 10.13. Downstream development of (a) $\theta'_c/\Delta\overline{T}_c$; ○ : 0.051mm dia. wire; • : ribbon □ : Warhaft(1984), ◇ : Tavoularis and Corrsin (1981a): (b) $\theta'_r/\Delta\overline{T}_c$; △ : ribbon.

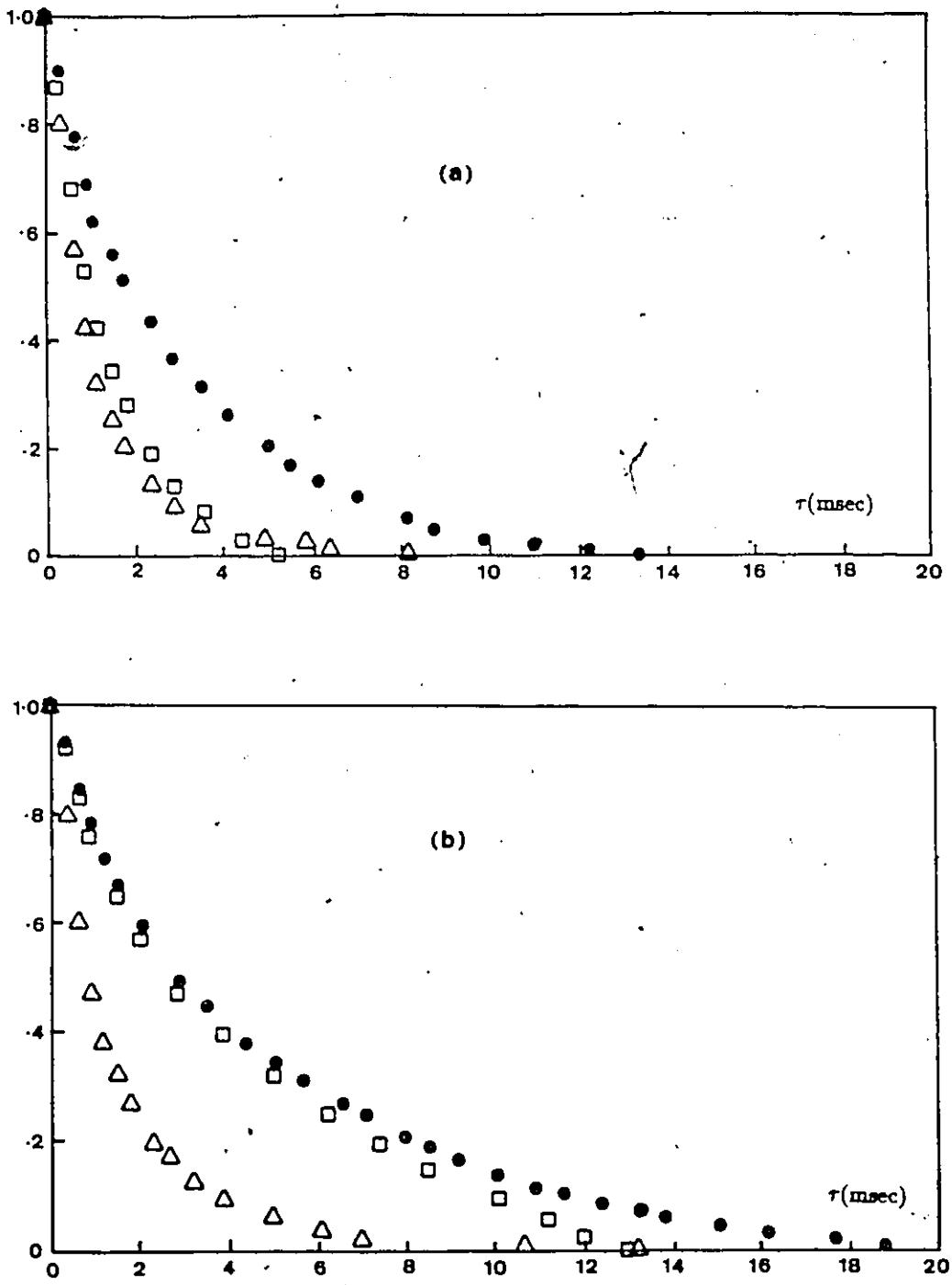

Figure 10.14. Autocorrelation functions along centerline at (a) $x_\theta/M = 72.0$ and (b) $x_\theta/M = 24.0$. • : $R_{11}(\tau)$, △ : $R_{22}(\tau)$, □ : $R_{\theta\theta}(\tau)$; $\overline{U}_{1c} = 7.85$ m/s.

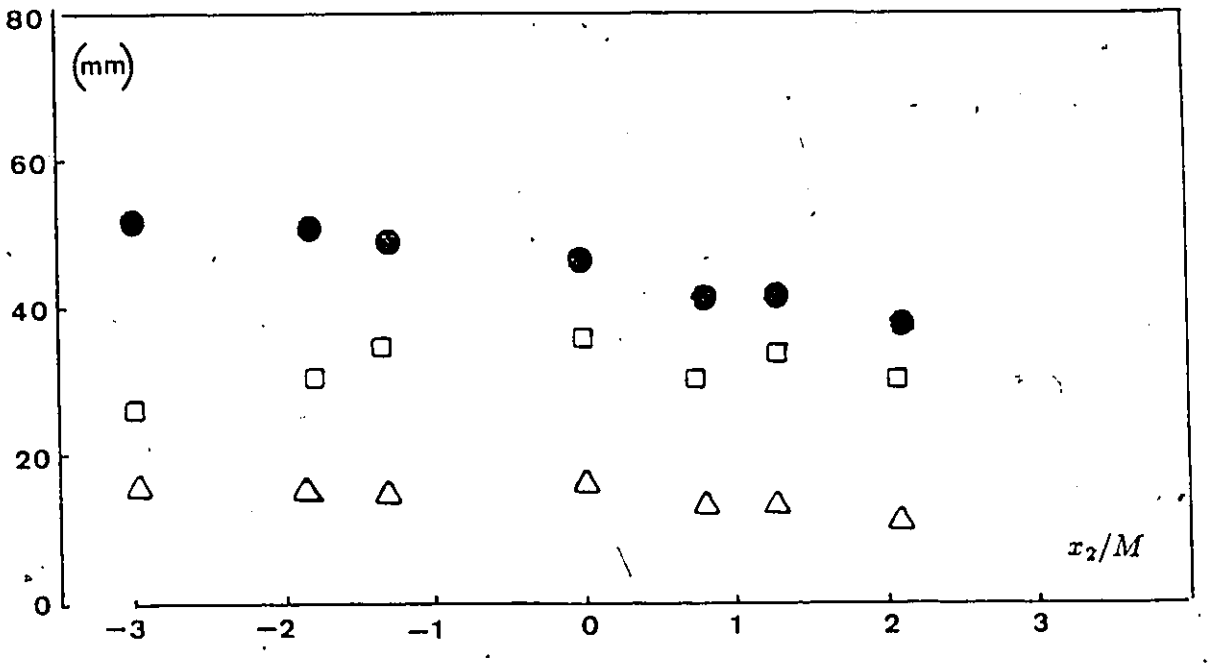

Figure 10.15. Transverse distribution of integral length scales at $x_\theta/M = 84.0$. ● : $L_{11,1}$, △ : $L_{22,1}$, □ : $L_{\theta\theta,1}$.

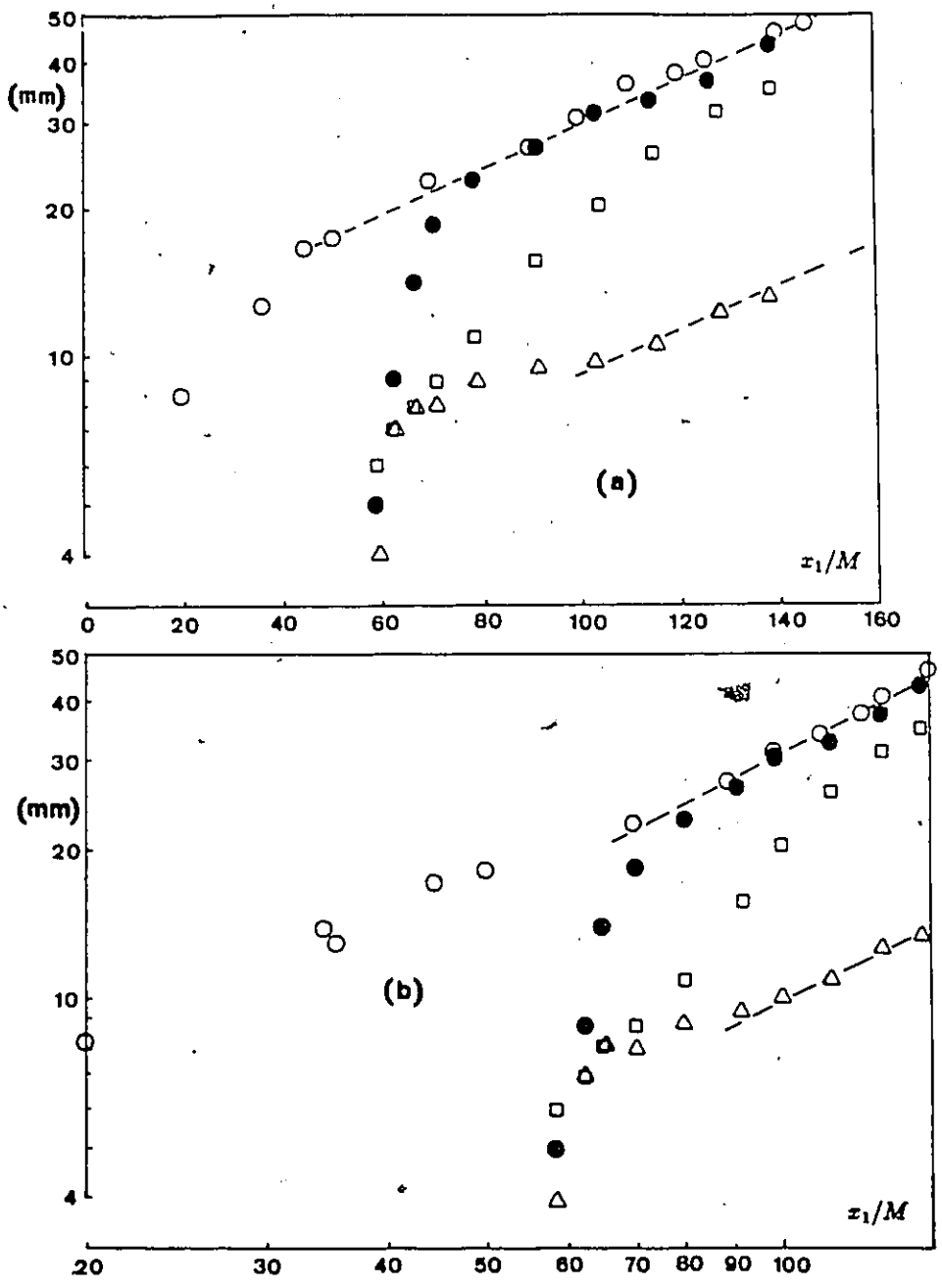

Figure 10.16. Downstream development of integral length scales along the center-line (a) in semi-logarithmic co-ordinates (b) in logarithmic co-ordinates; • : $L_{11,1}$, △ : $L_{22,1}$, □ : $L_{\theta\theta,1}$, ○ : $L_{11,1}$ from Part A (no heating source).

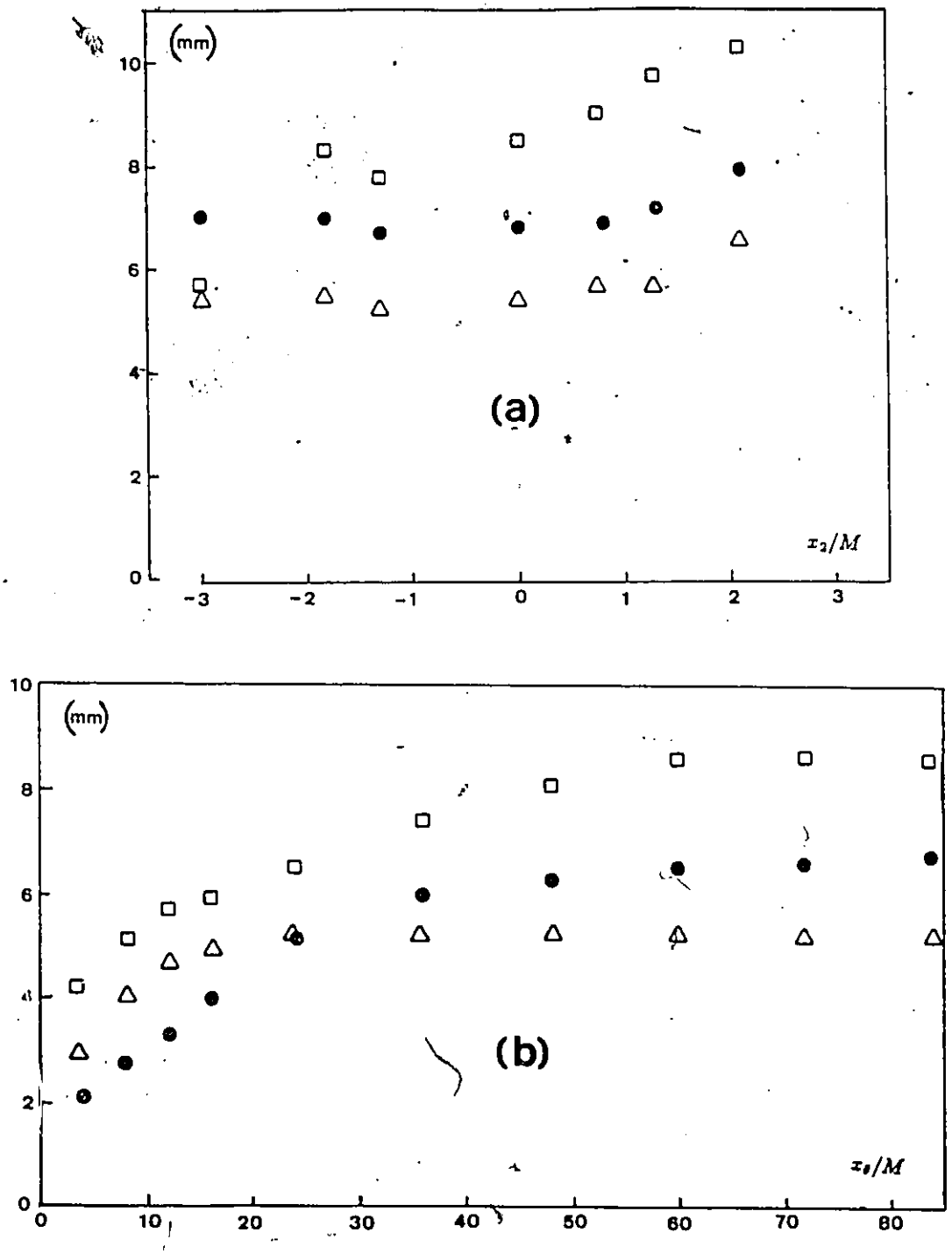

Figure 10.17. Measurements of the Taylor and Corrsin microscales. (a) transverse distribution at $x_\theta/M = 84.0$ (b) downstream development; • : λ_{11}, △ : λ_{21}, □ : $\lambda_{\theta 1}$.

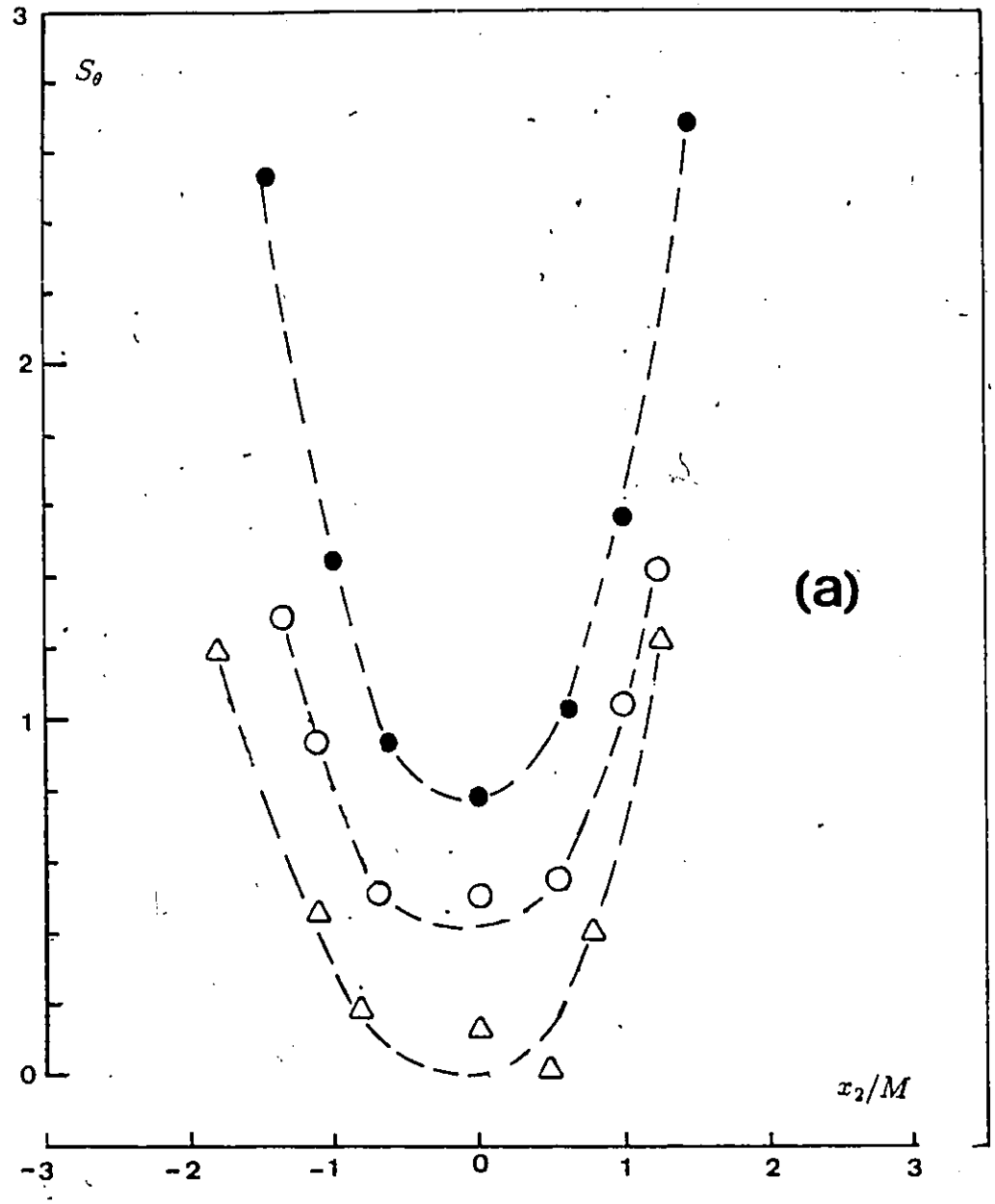

Figure 10.18. Measurements of skewness factors; (a) transverse distribution of S_θ; at $x_\theta/M = 24.0$ (•), 48.0 (○), 84.0 (△). (b) downstream (centerline) development of S_θ(•), S_{u_1}(○), S_{u_1}(△).

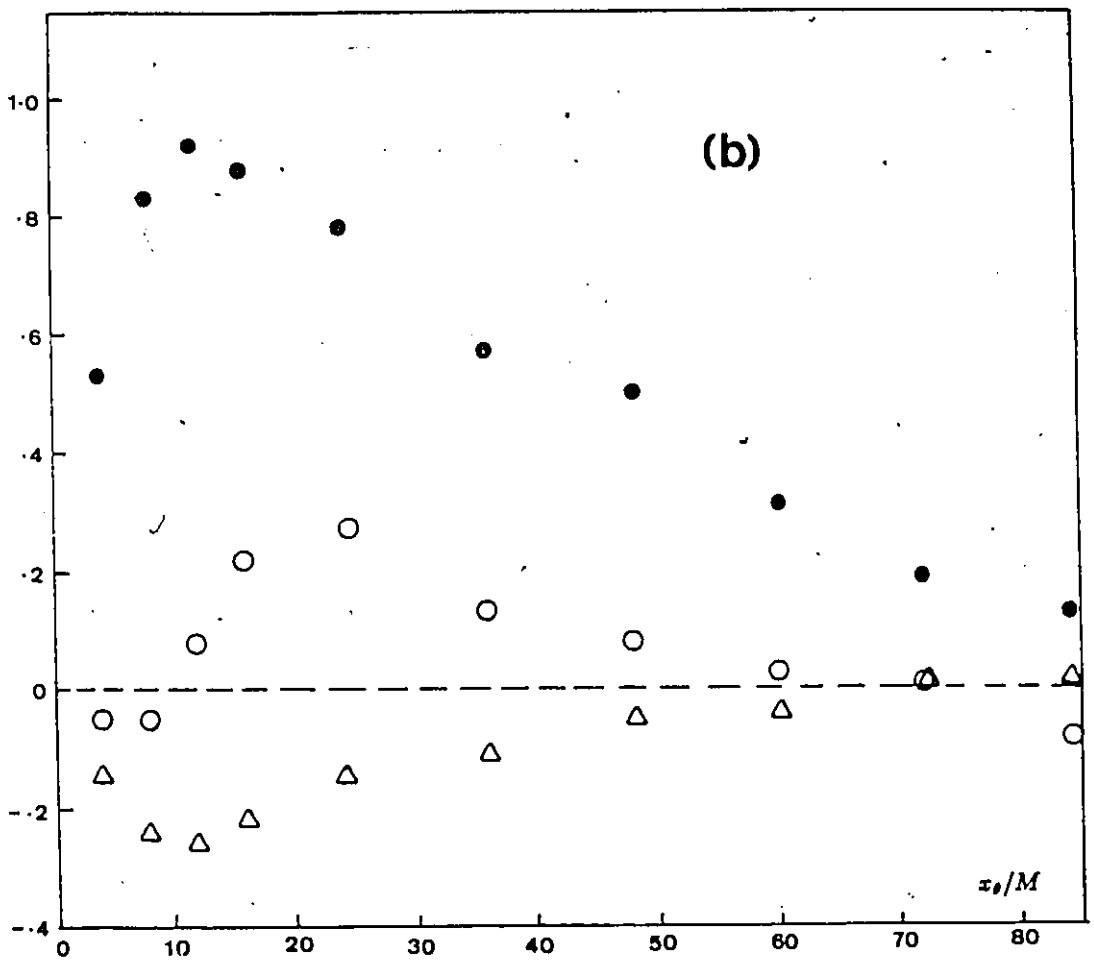

Figure 10.18. continued

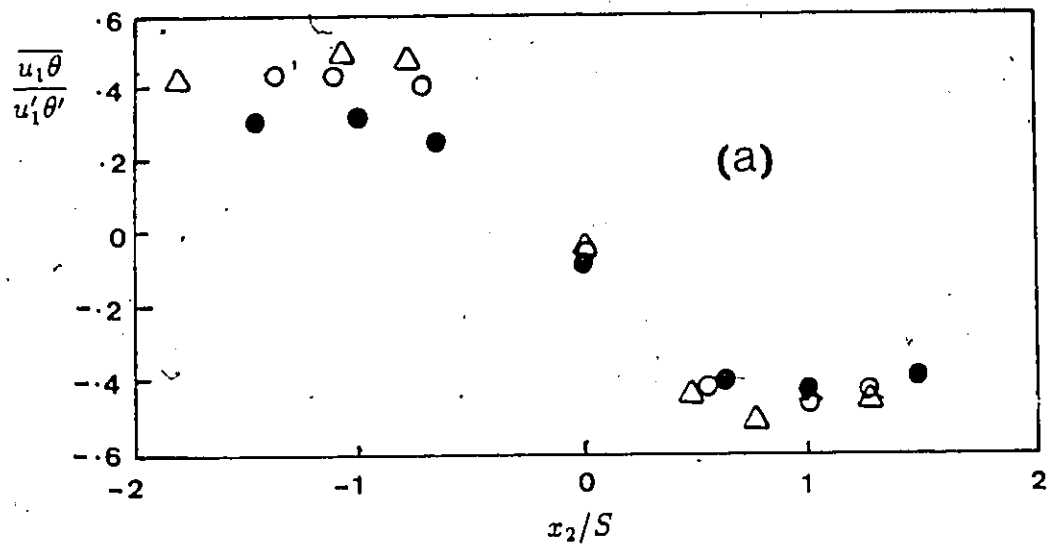

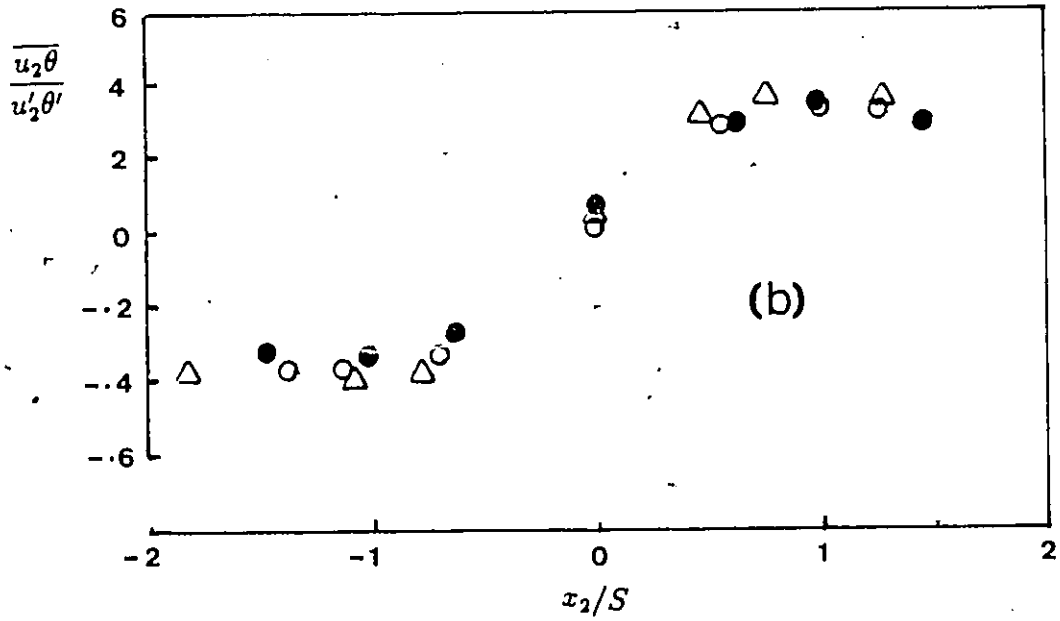

Figure 10.19 Transverse distribution of (a) $\overline{u_1\theta}/u_1'\theta'$ (b) $\overline{u_2\theta}/u_2'\theta'$; profiles at x_1/M = 24.0 (•), 48.0 (o), 84.0 (△).

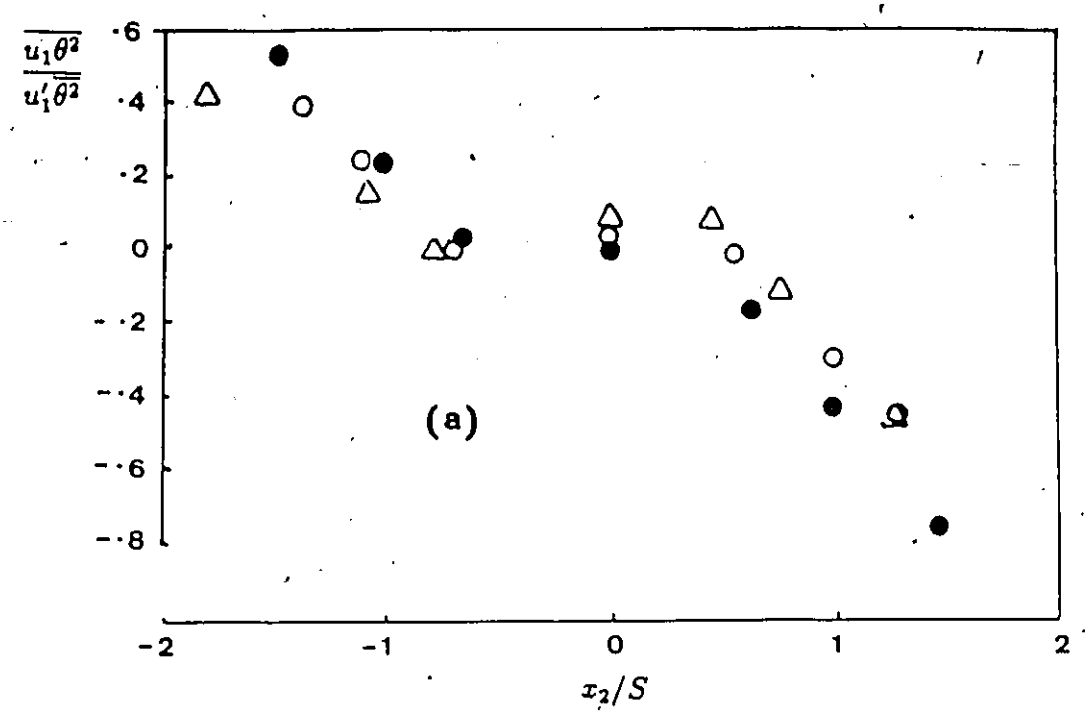

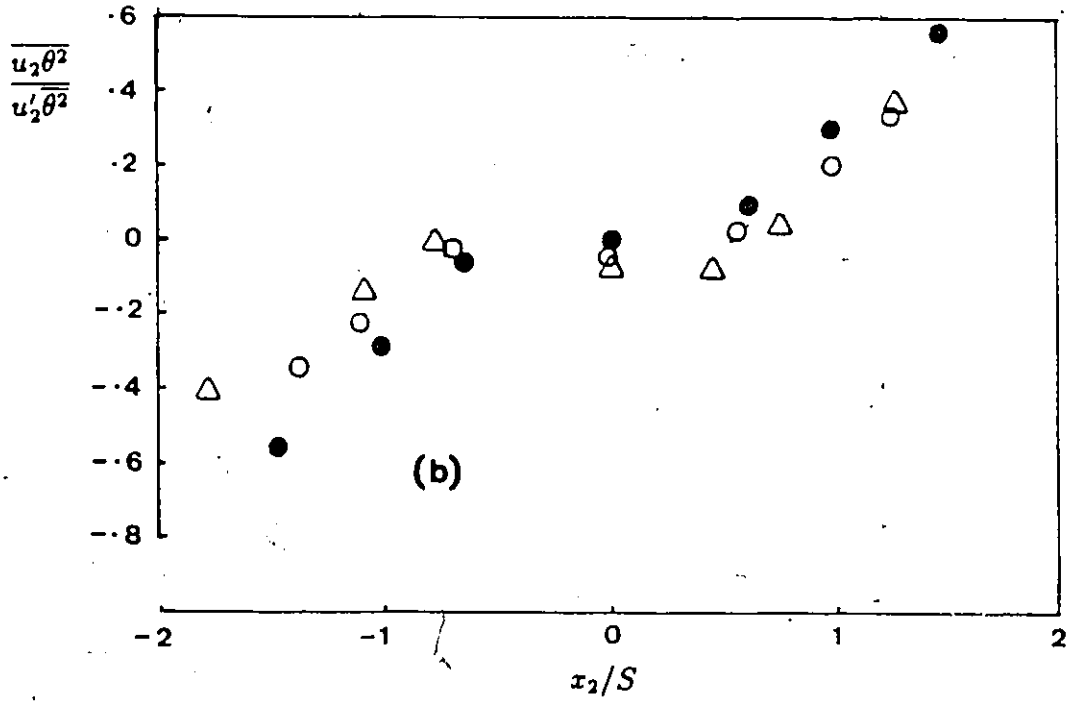

Figure 10.20. Transverse distribution of (a) $\overline{\theta^2 u_1}/\overline{\theta^2}u_1'$ (b) $\overline{\theta^2 u_2}/\overline{\theta^2}u_2'$. Symbols as in Figure 10.19.

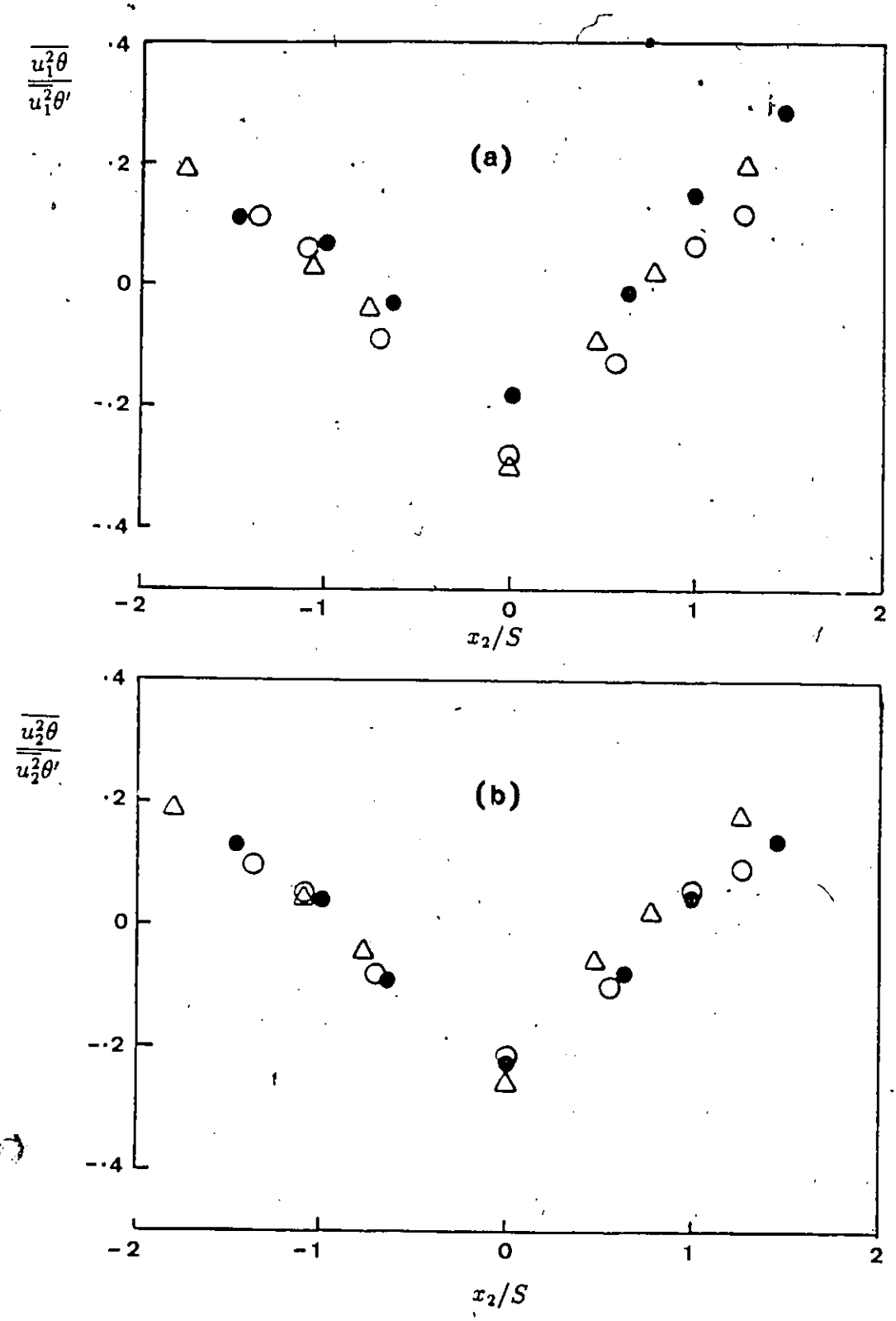

Figure 10.21. Transverse distribution of (a) $\overline{u_1^2\theta}/\overline{u_1^2\theta'}$ (b) $\overline{u_2^2\theta}/\overline{u_2^2\theta'}$. Symbols as in Figure 10.19.

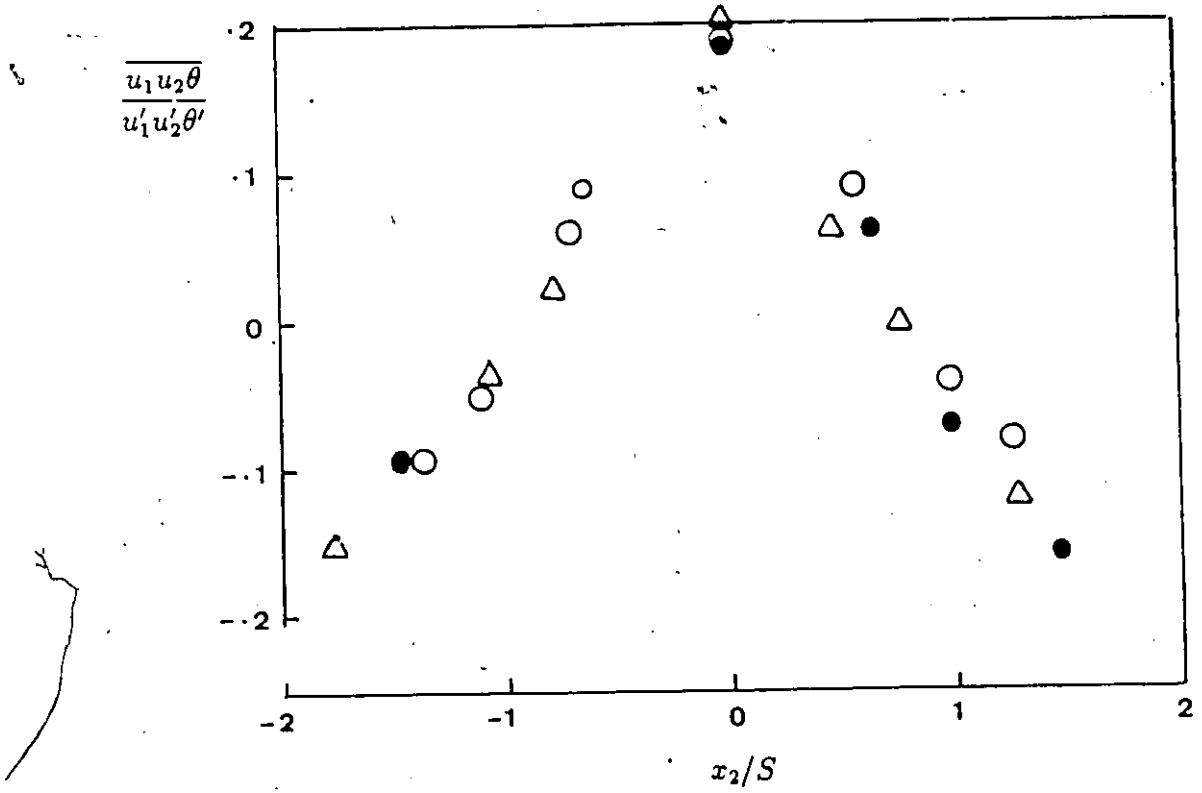

Figure 10.22. Transverse distribution of $\overline{u_1 u_2 \theta}/u_1' u_2' \theta'$. Symbols as in Figure 10.19.

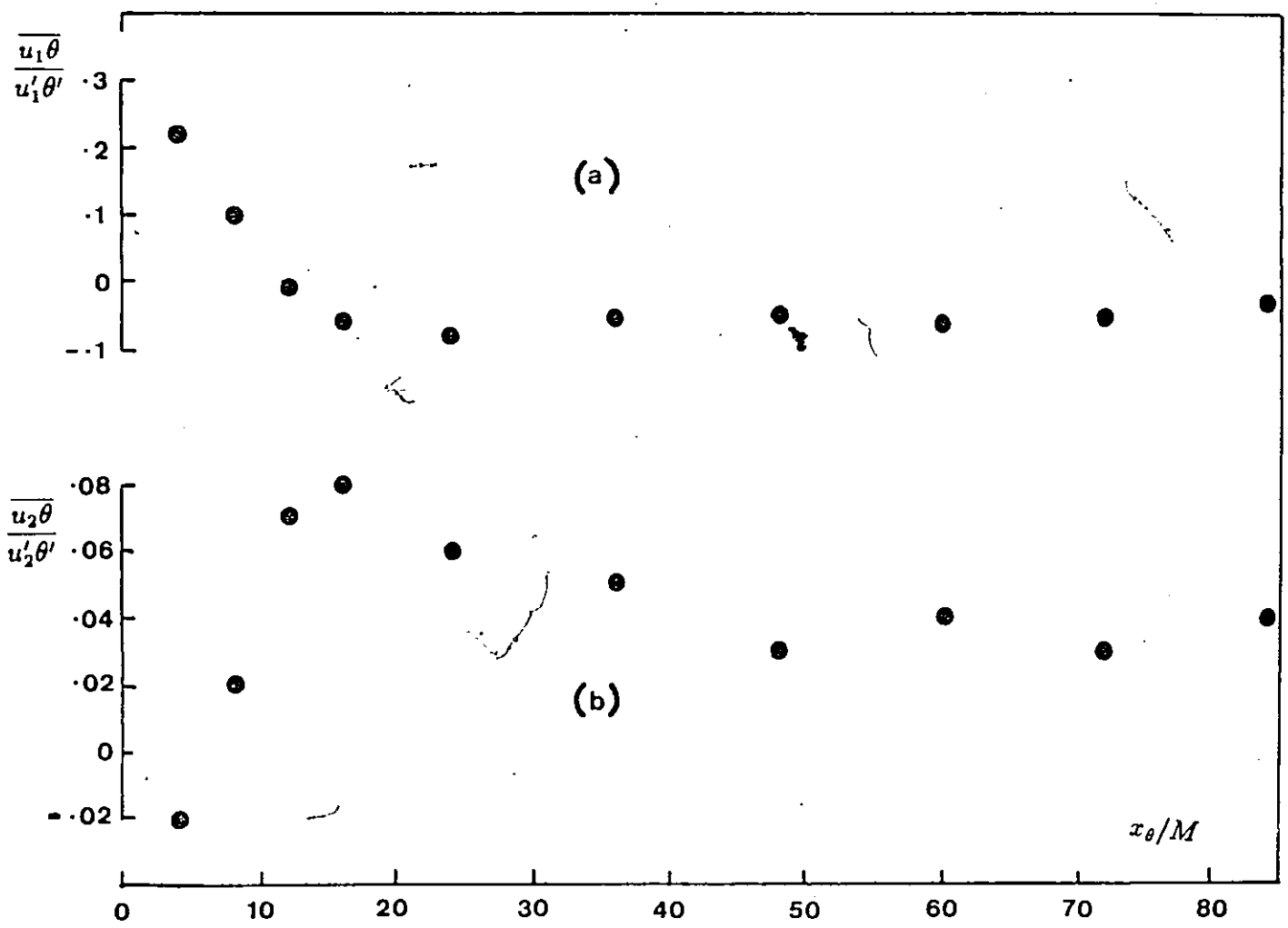

Figure 10.23. Downstream (centerline) development of temperature-velocity correlation coefficients.

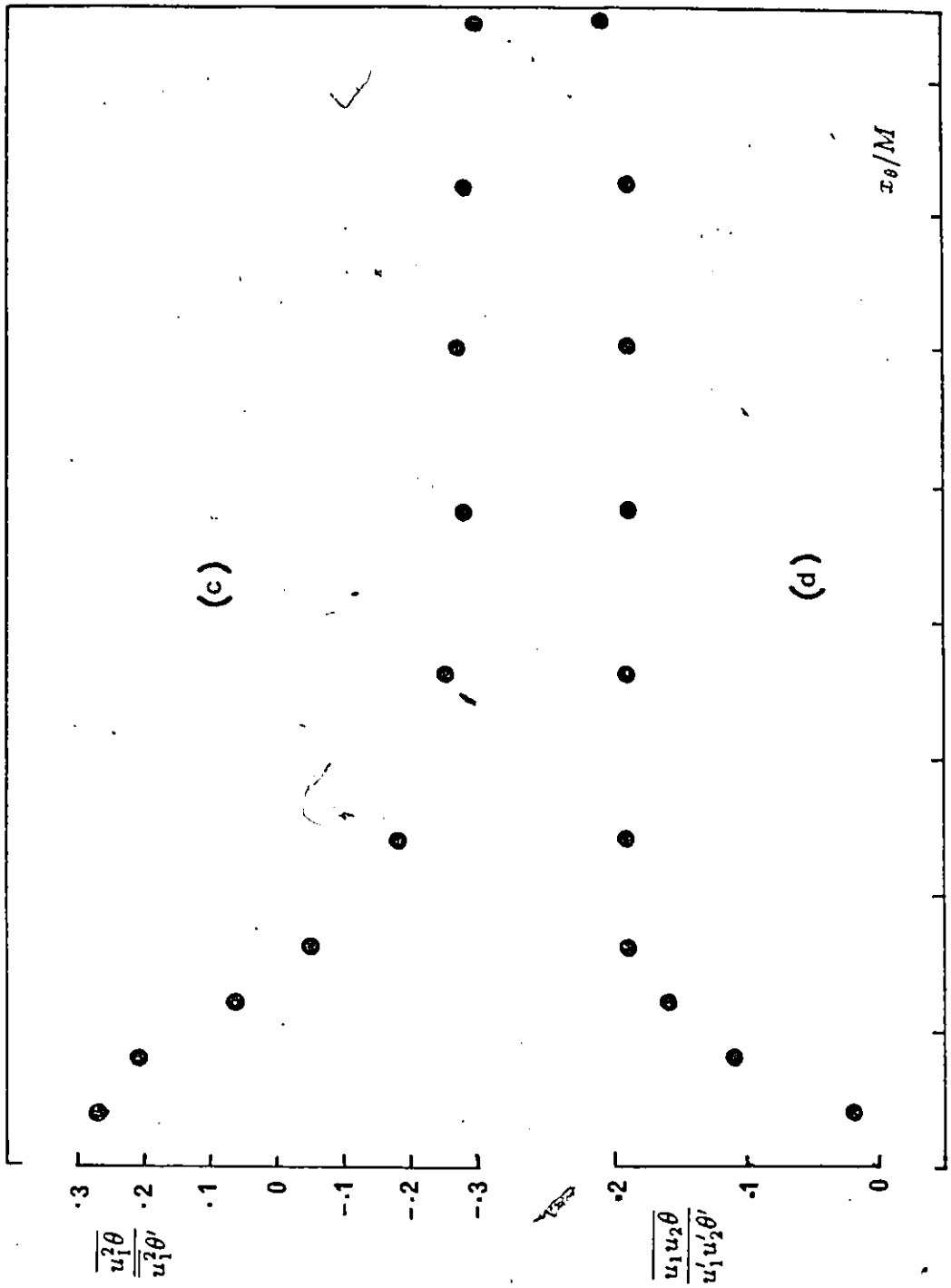

Figure 10.23. continued

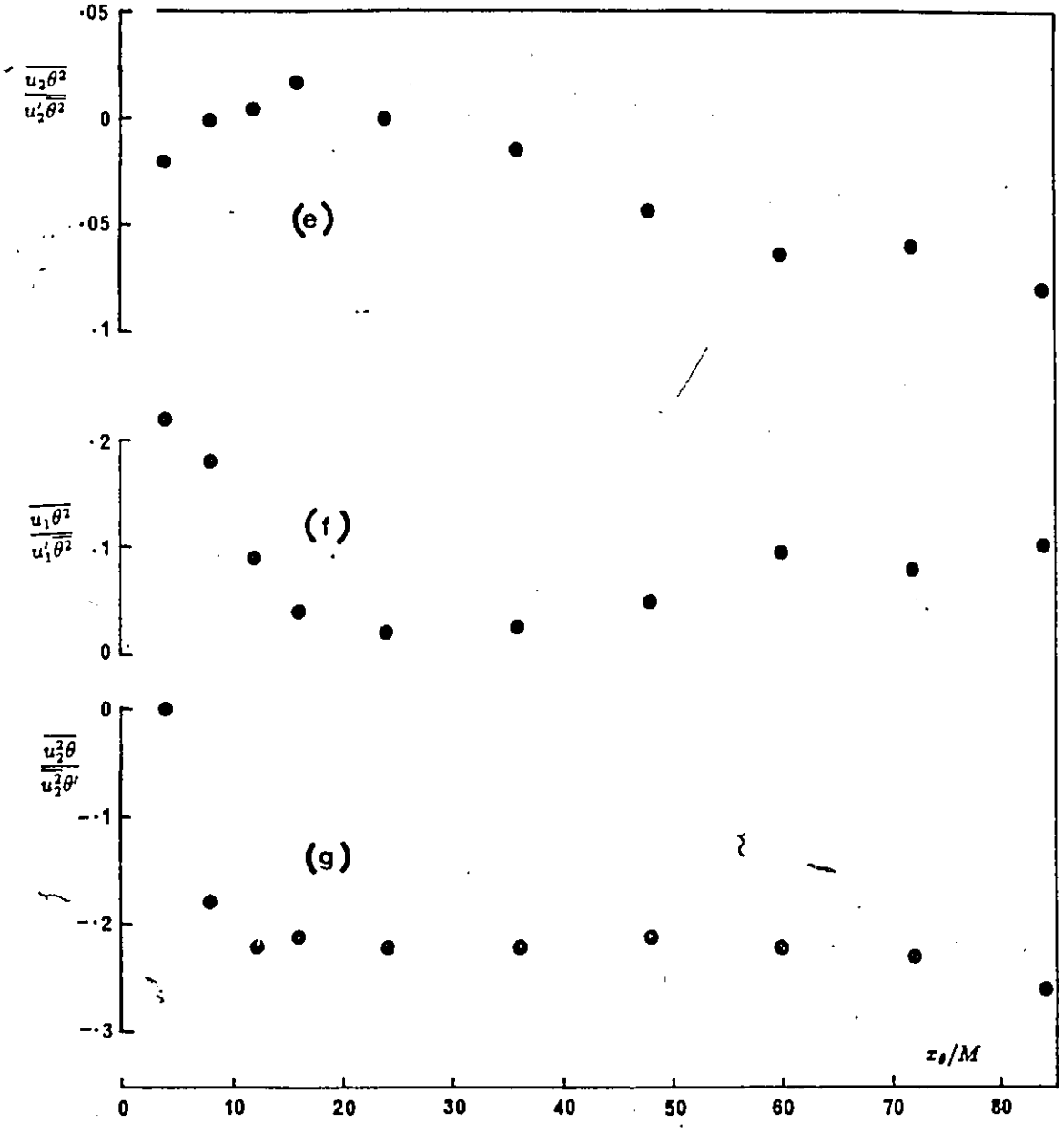

Figure 10.23. continued

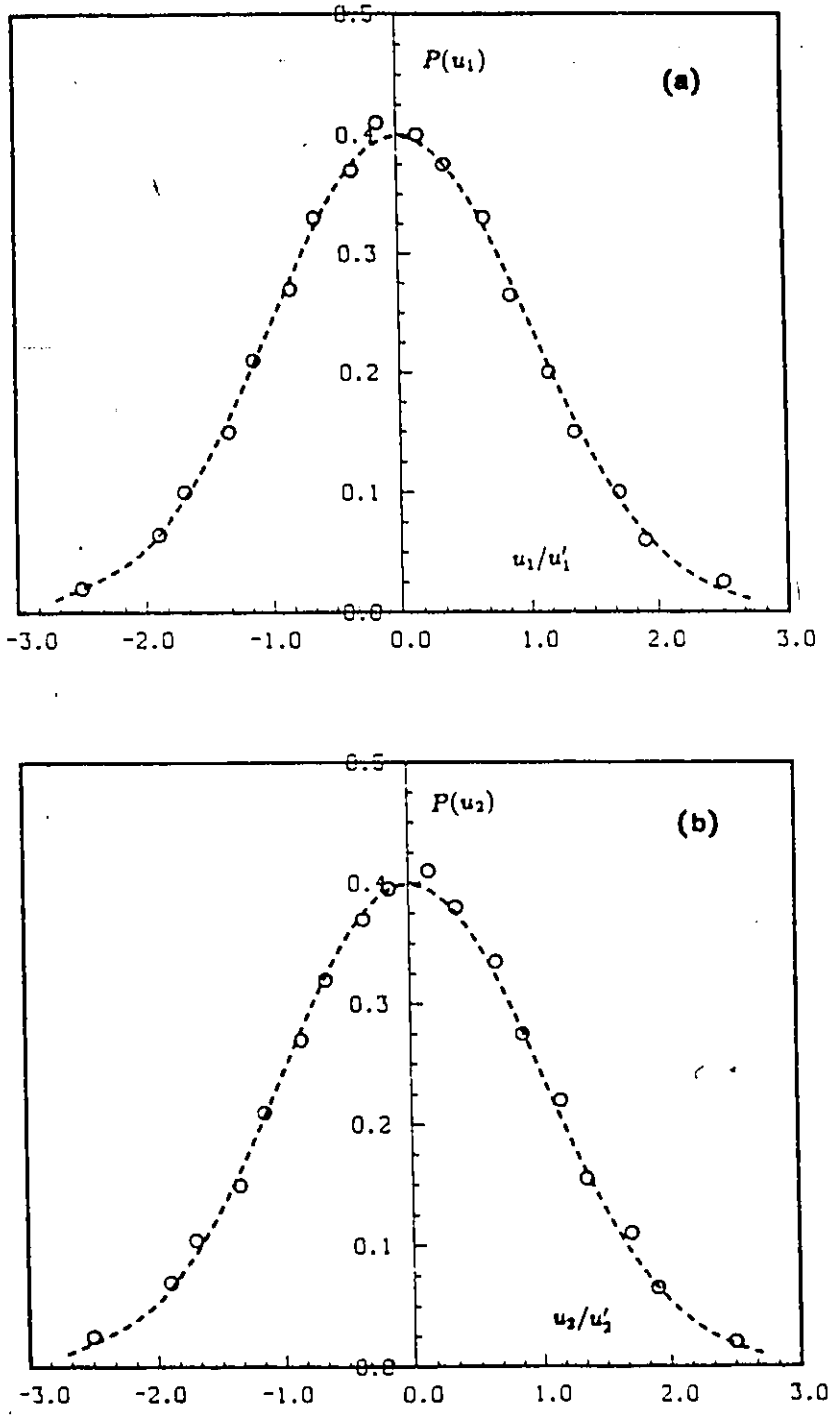

Figure 10.24. Probability density functions at $x_\theta/M = 84$, $x_2/M = 0.0$ (a) $P(u_1)$ (b) $P(u_2)$.

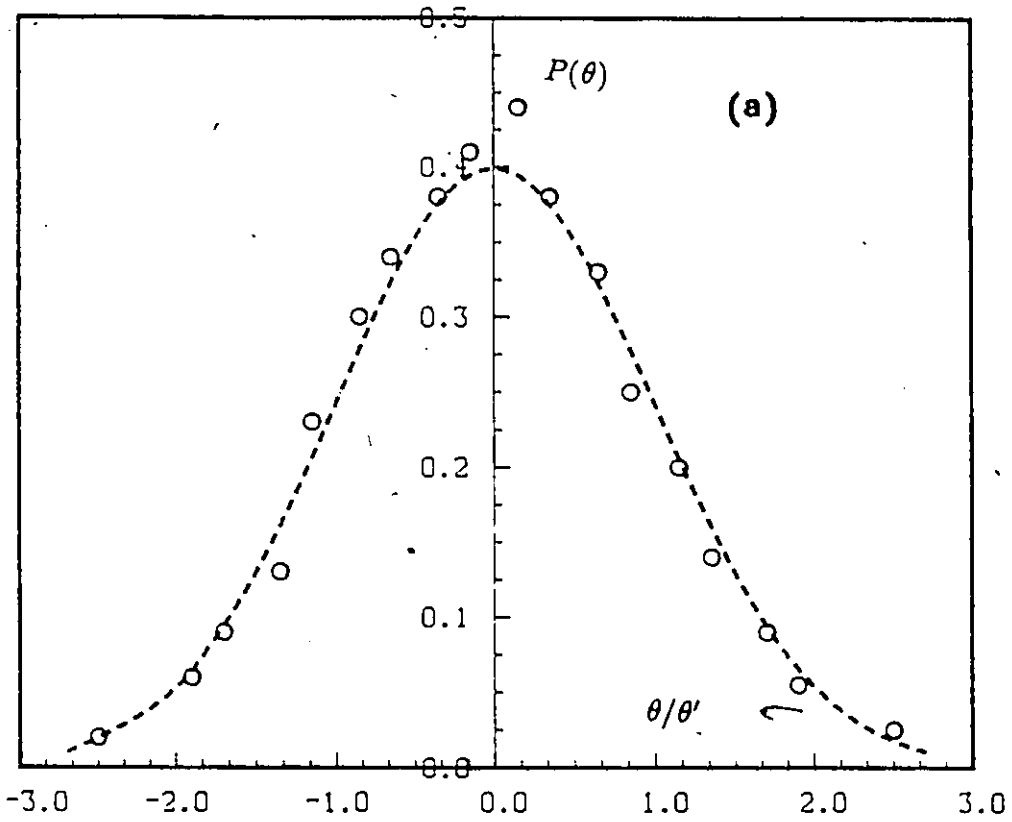

Figure 10.25. Probability density function of θ at $x_\theta/M = 84$ (a) $x_2/M = 0.0$ (b) $\bullet$: $x_2/M = 1.3$, $\circ$: $x_2/M = -1.8$ (c) $\bullet$ $x_2/M = 2.1$, $\circ$: $x_2/M = -3.0$

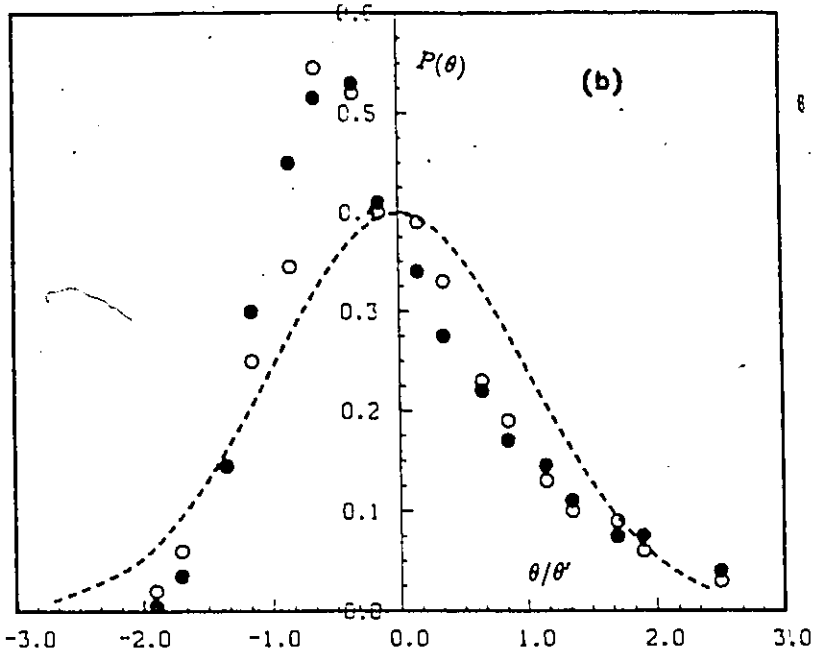

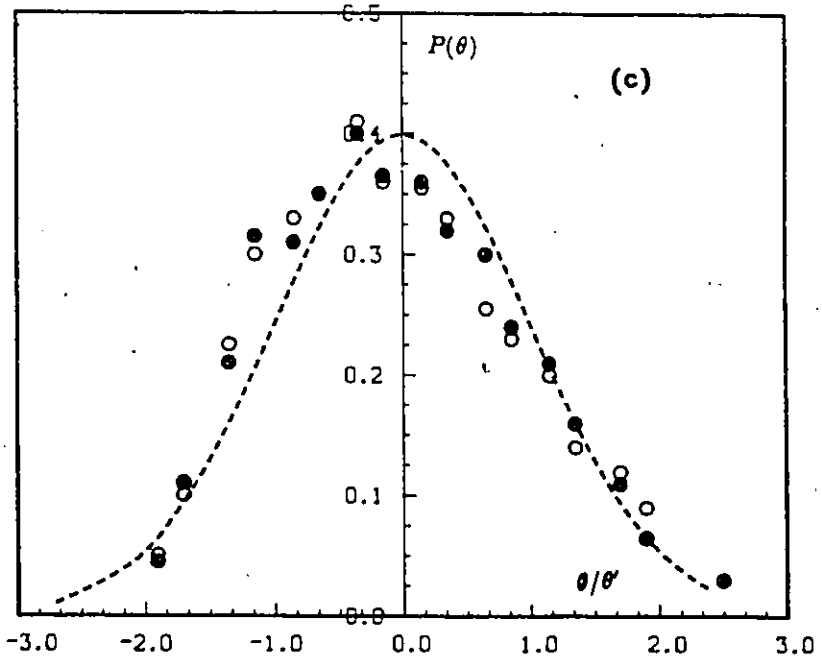

Figure 10.25. continued

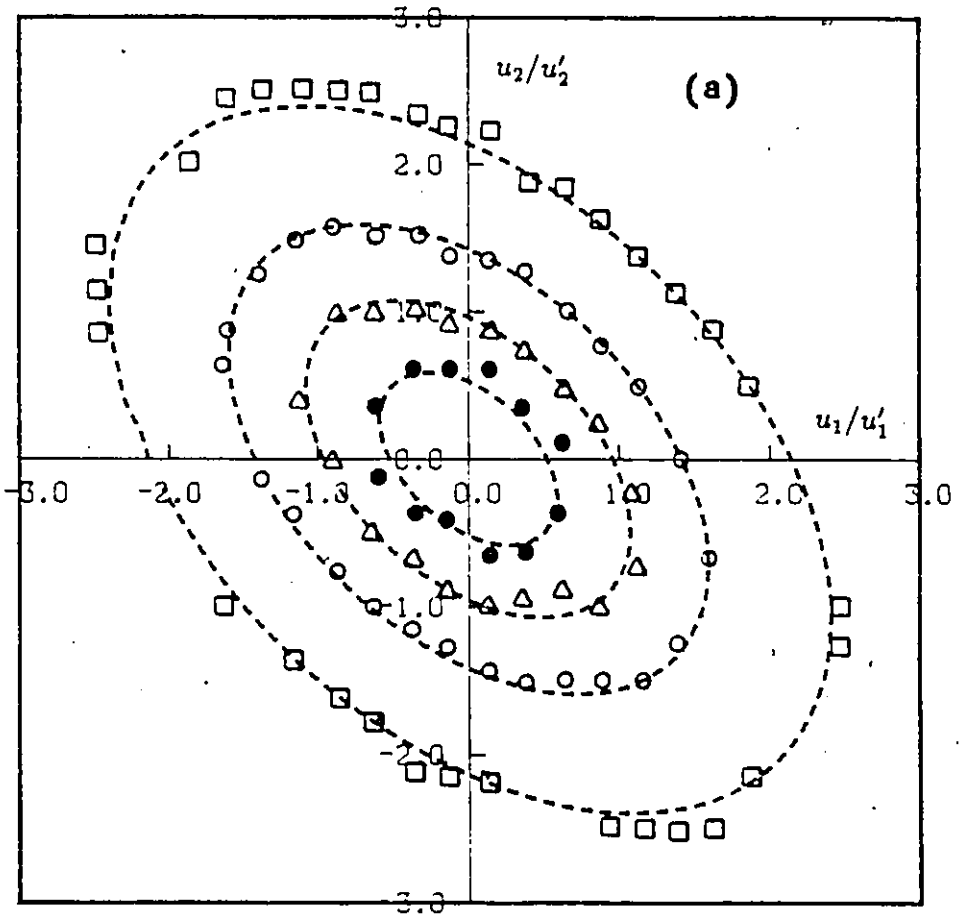

Figure 10.26. Isoprobability contours of u_1 and u_2 at $x_\theta/M = 84.0$; (a) $x_2/M = 0.0$ (b)$x_2/M = 2.1$; $\mathrm{P}(u_1, u_2) = \bullet : 0.15$, $\triangle : 0.1$, $\circ : 0.05$, $\square : 0.01$.

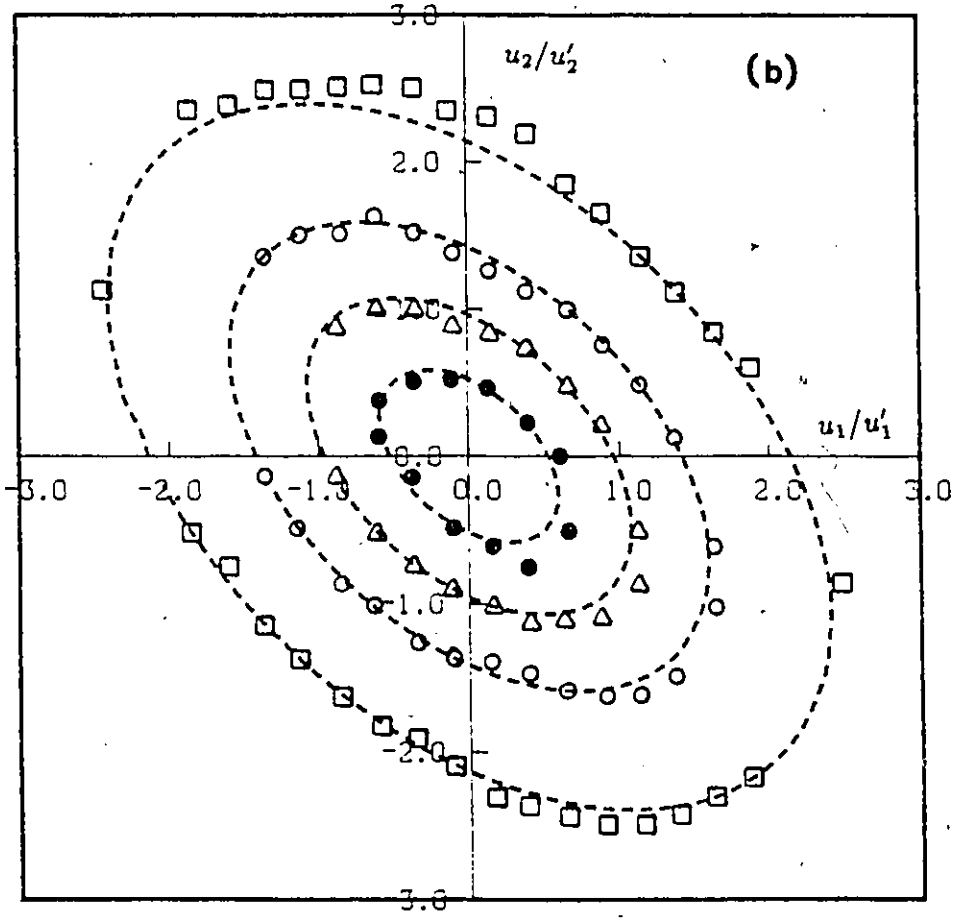

Figure 10.26. continued

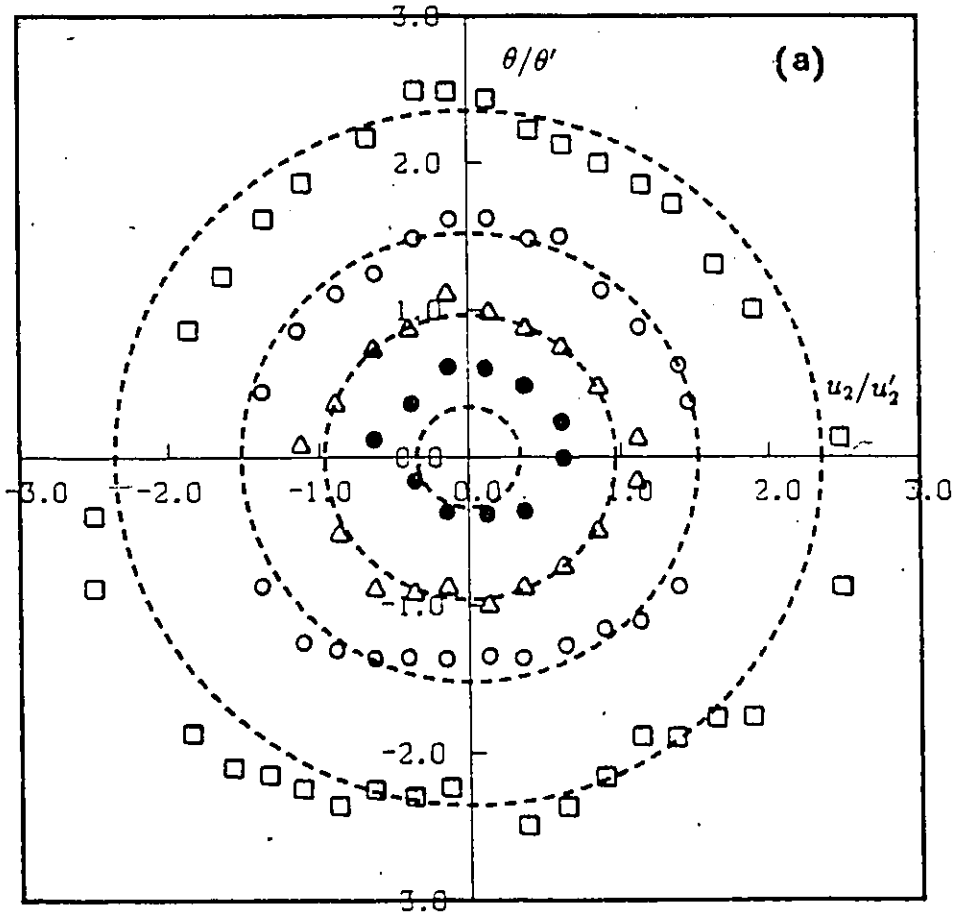

Figure 10.27. Joint probability contours of velocity components and temperature at $x_\theta/M = 84.0$; (a)P(u_2, θ) at $x_2/M = 0.0$ (b)P(u_2, θ) at $x_2/M = 2.1$ (c)P(u_2, θ) at $x_2/M = 2.1$ .Symbols as in Figure 27.

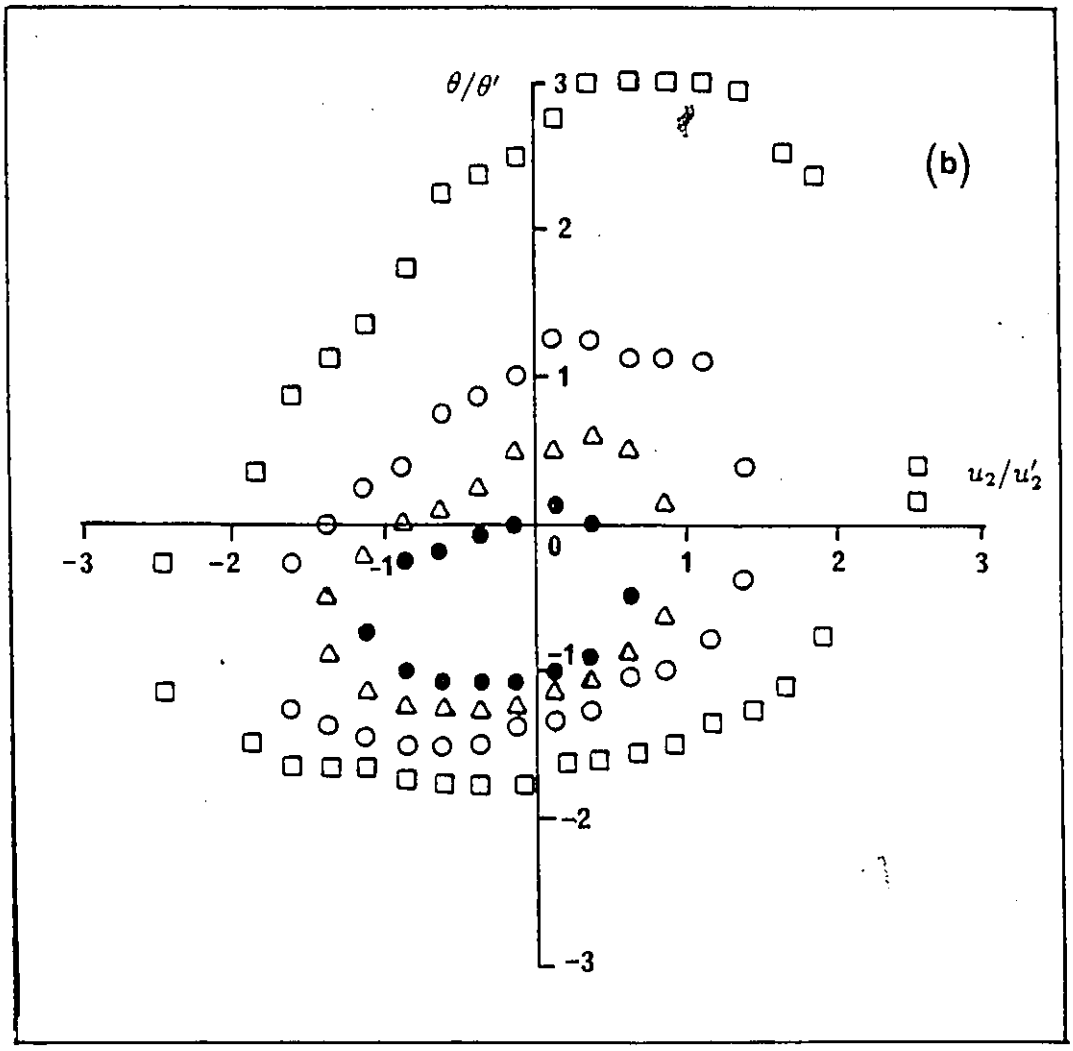

Figure 10.27. continued

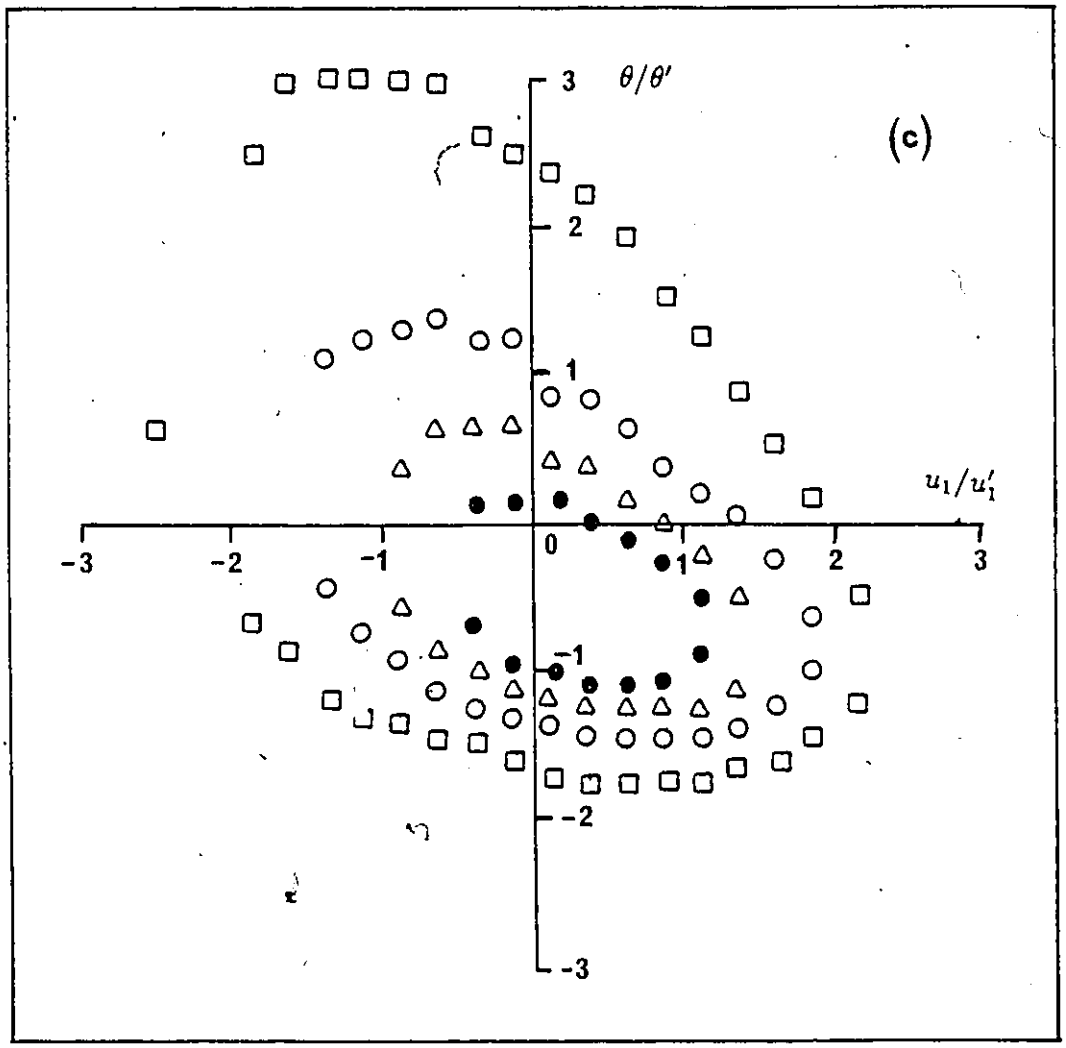

Figure 10.27. continued

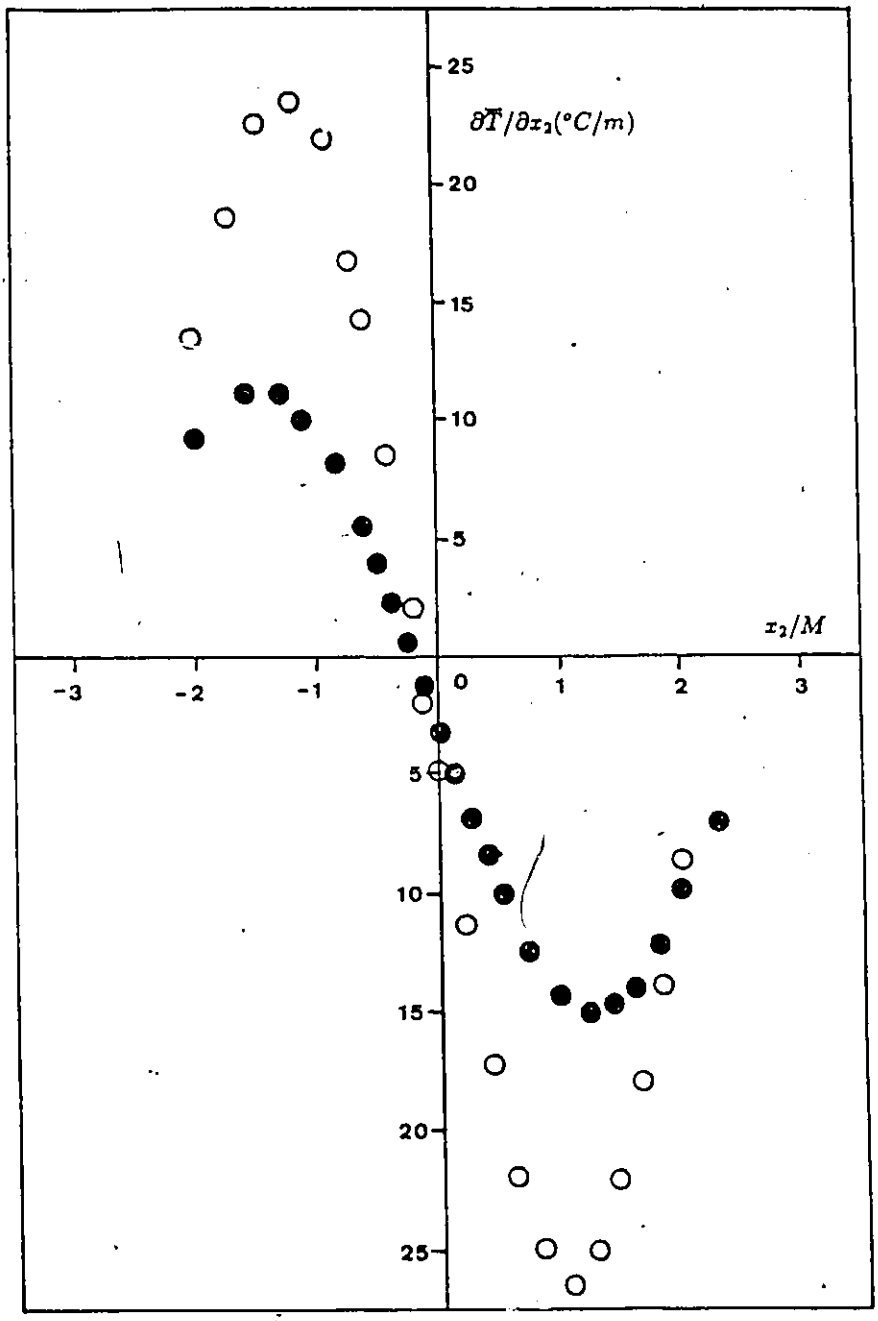

Figure 11.1. Transverse distribution of the mean temperature gradient computed by differentiating a fitted polynomial to the data of Figure 10.5 o : $x_\theta/M = 24.0$, • : $x_\theta/M = 84.0$.

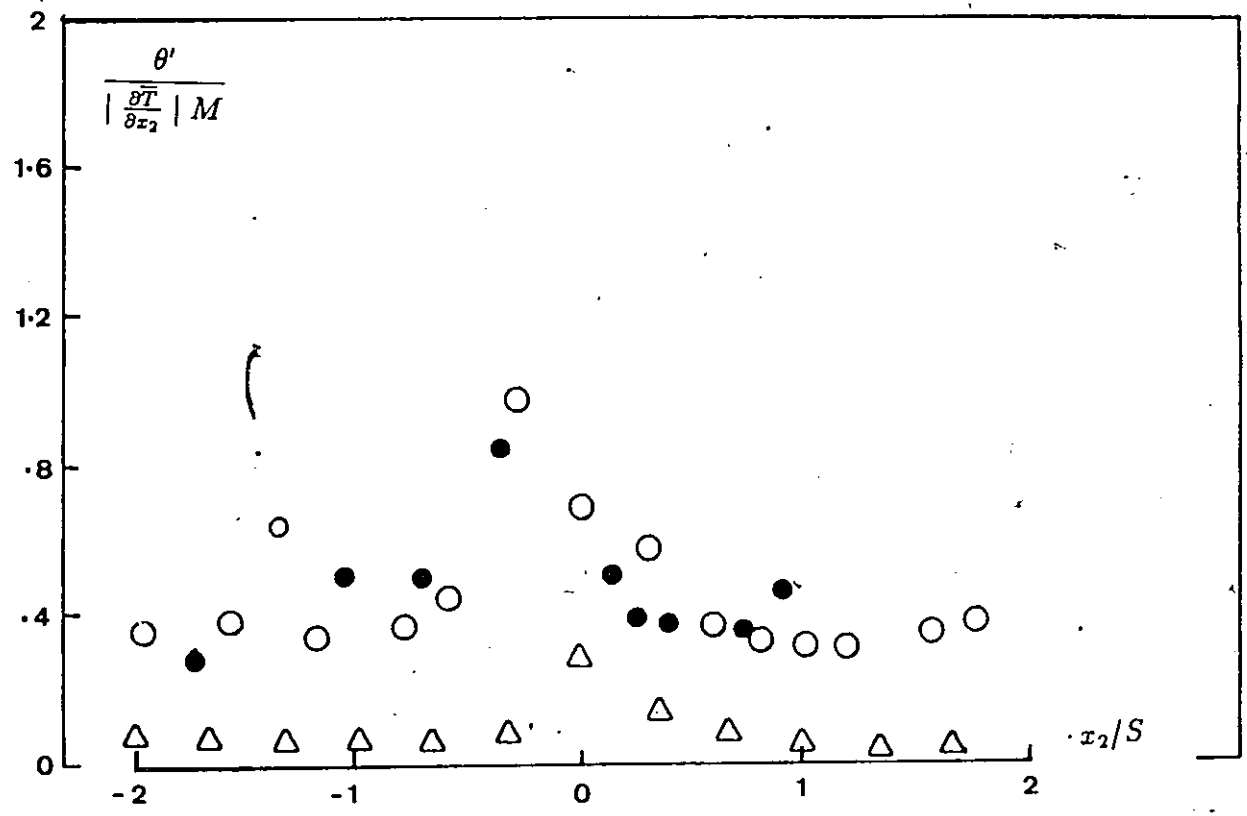

Figure 11.2. Transverse variation of the parameter $\theta'/(|\frac{\partial T}{\partial x_2}| M)$; $x_0/M = 4.0$ (△), 48.0 (○), 84.0 (●).

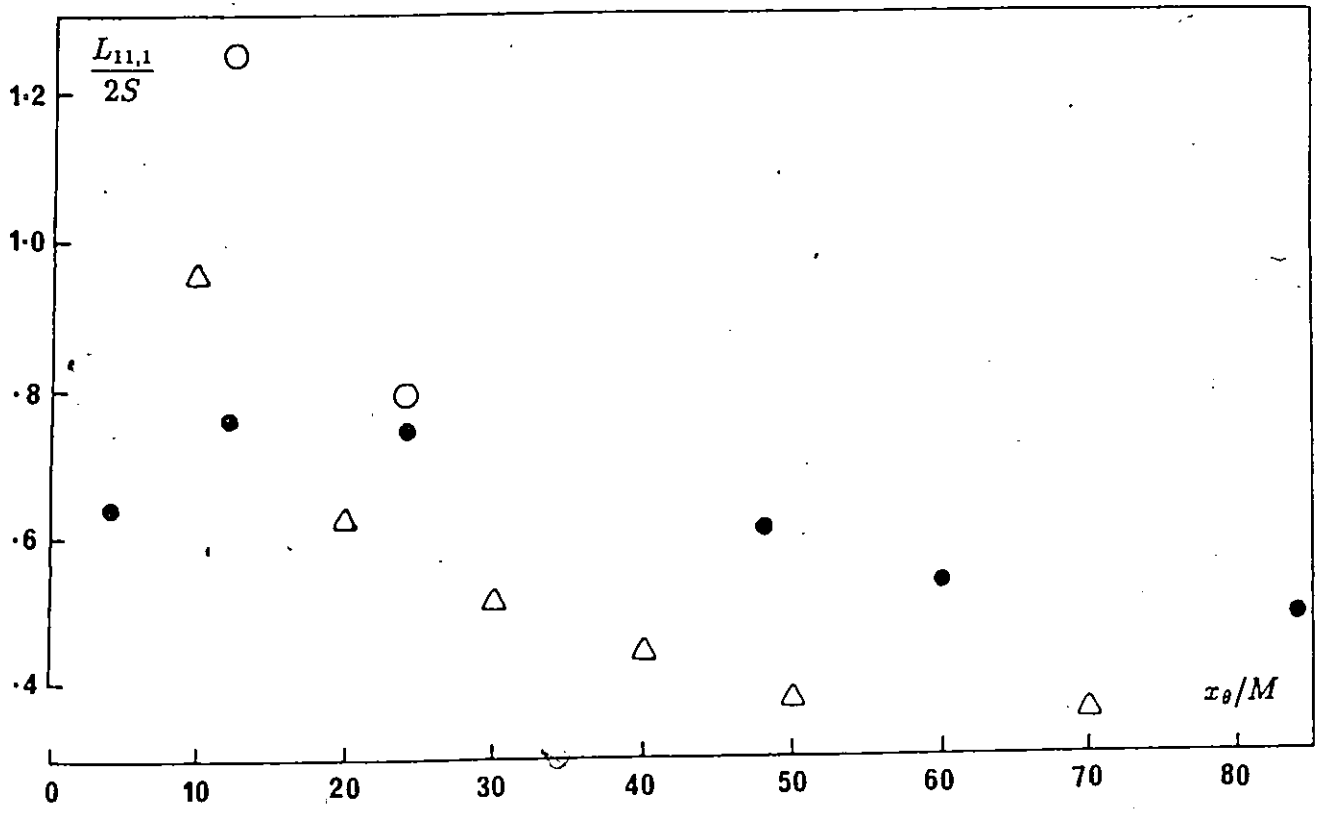

Figure 11.3. Downstream development of the ratio of velocity length scale to the total width of the mean temperature profile. o : scale measured without ribbon, • : scale measured with ribbon, △ : Warhaft (1984).

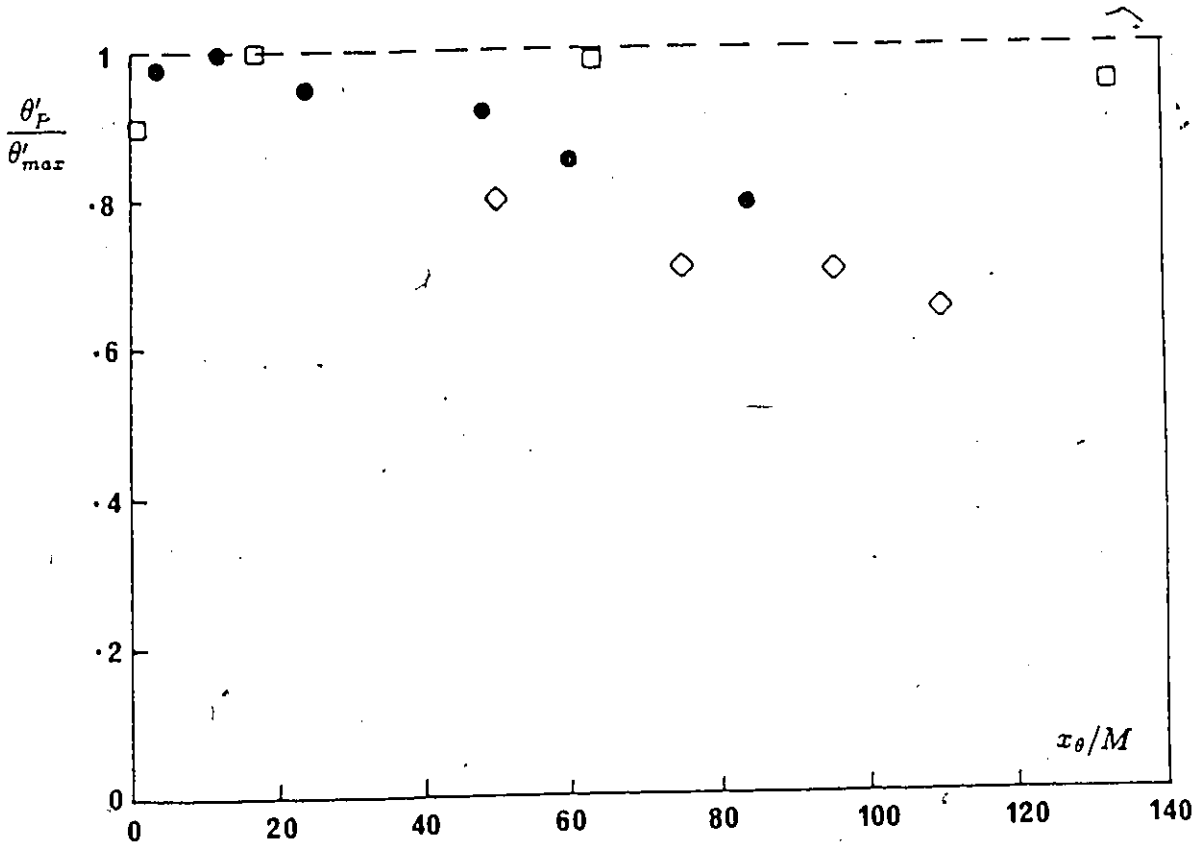

Figure 11.4. Downstream development of the ratio θ'_p/θ'_{max} (θ'_p is measured at the position of the mean temperature peak and θ'_{max} is the maximum value of the local θ' profile). • : present results, ◇ : Tavoularis and Corrsin (1981a),□ : Warhaft (1984).

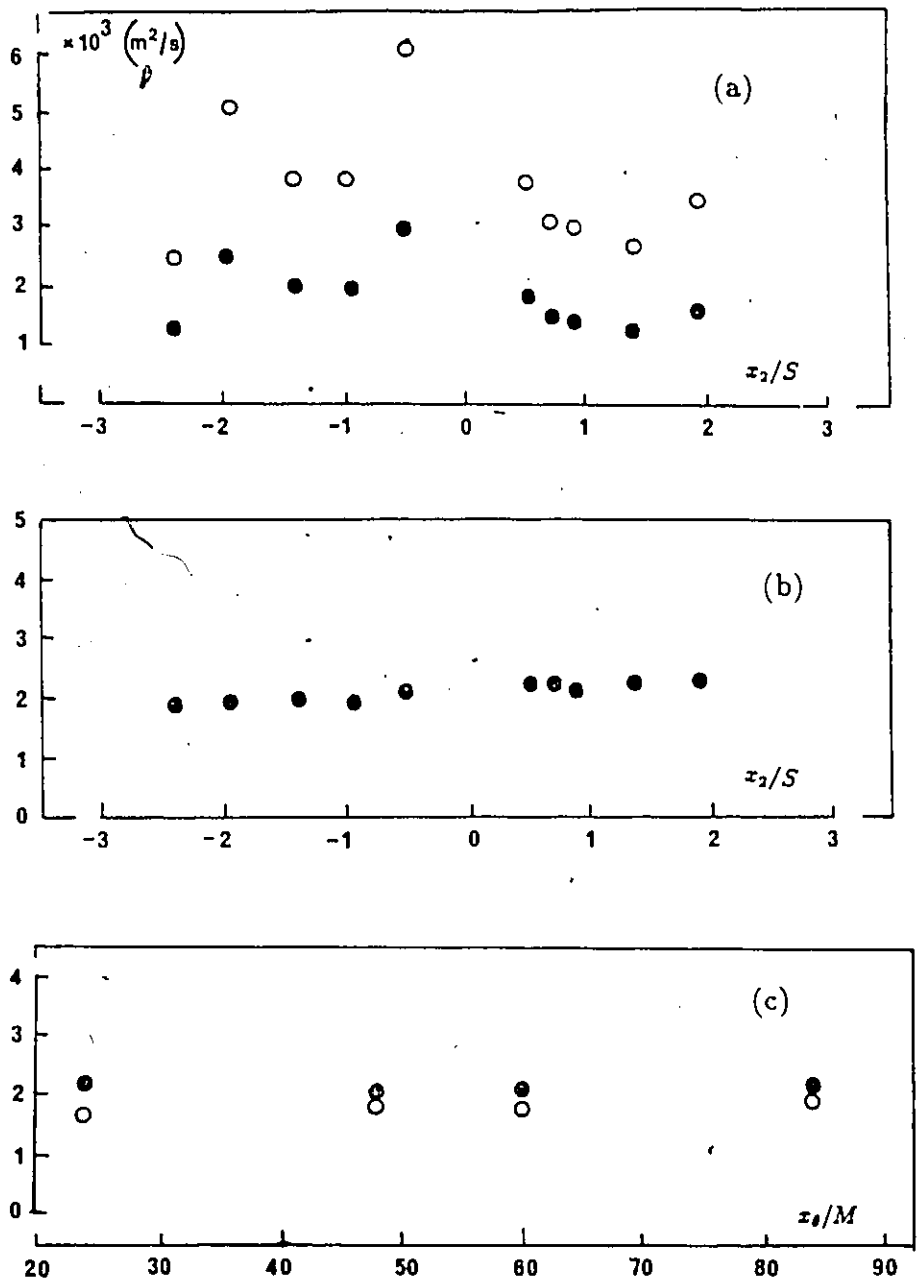

Figure 11.5. Distribution of the turbulent diffusivities and their ratio; (a) •: D_{22}, o: $-D_{12}$, $x_\theta/M = 84$ (b) $-D_{12}/D_{22}$, x_θ/M=84 (c) $-D_{12}/D_{22}$, o: x_2/S=-0.85, •: x_2/S=0.85.

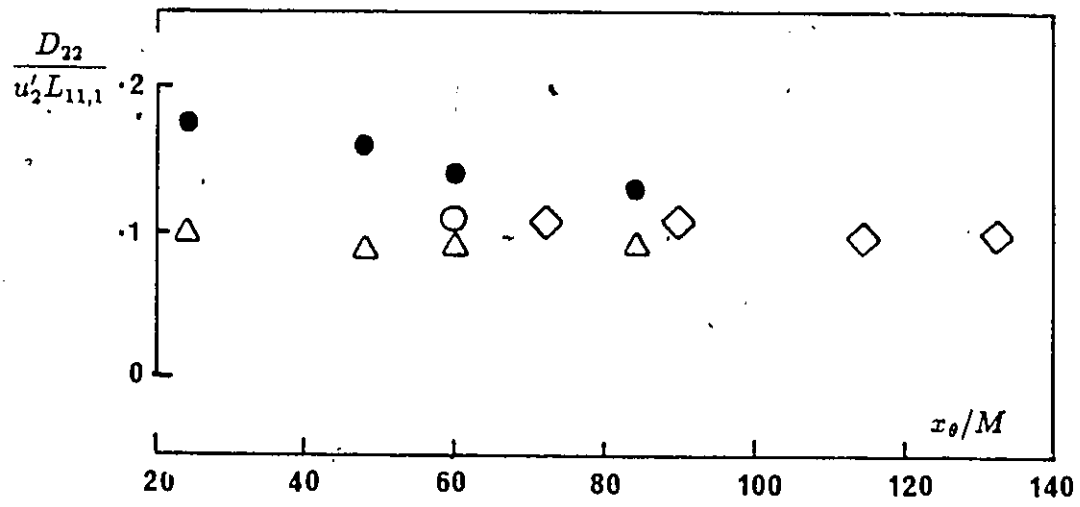

Figure 11.6. Downstream development of the ratio $D_{22}/(u_2' L_{11,1})$. present results : • (σ_T), △ (σ_T); ○ : Sreenivasan et al. (1981); ◇ : Tavoularis and Corrsin (1981a).

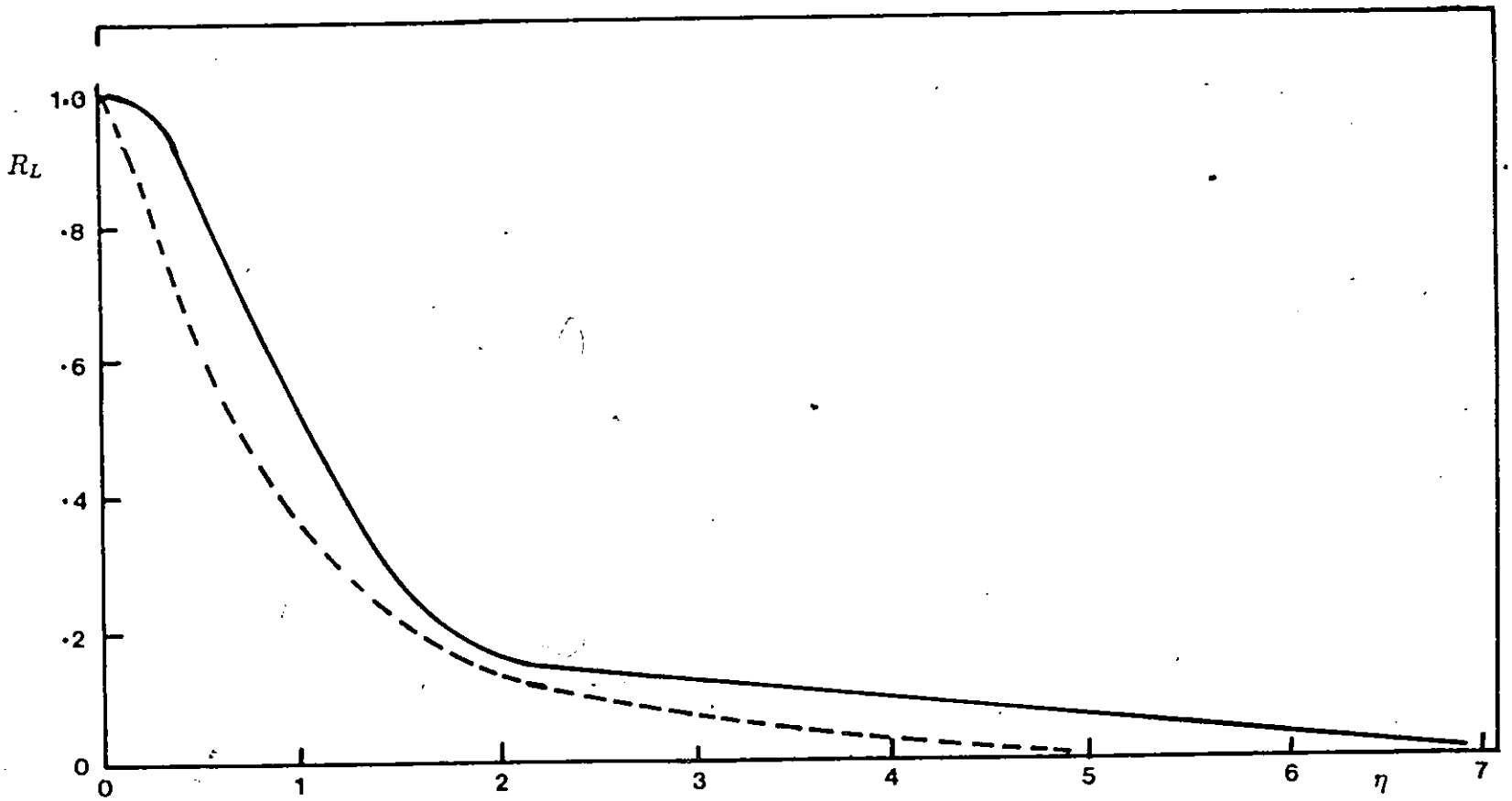

Figure 11.7 Lagrangian autocorrelation function estimated from dispersion measurements. — — Eulerian autocorrelation in a convected frame (Harris et al. 1977).